In-vitro and *in-silico* evaluation for phytochemicals and anti-diabetic potentials of *Trichodesma zeylanicum* ethanolic and ethyl acetate extracts

By

MANYUWA MANASE

18006683

Research Dissertation for the Master of Science Degree in Biochemistry

in the

DEPARTMENT OF BIOCHEMISTRY AND MICROBIOLOGY

FACULTY OF SCIENCE, ENGINEERING AND AGRICULTURE

UNIVERSITY OF VENDA

THOHOYANDOU, LIMPOPO PROVINCE, SOUTH AFRICA

Supervisor: Dr SC Tshidino-Vukeya

Co-supervisors: Prof NE Madala and Ms A-T Ramabulana

Submission date: 10 February 2025

© University of Venda

Declaration

I, Manase Manyuwa, student number 18006683, hereby attest that I have complied with the University's policies and rules applicable to postgraduate research to the best of my knowledge and belief. I admit to having read and comprehended said policies and rules. I certify that the research project I am submitting for the Master of Science in Biochemistry degree at the University of Venda is entirely original to me and has never been submitted elsewhere for a different degree. All sources have been properly cited and acknowledged.

Signature:  Date: 10 February 2025

© University of Venda

University of Venda
Creating Future Leaders

Abstract

Background: *Trichodesma zeylanicum* (Burm. f) R.Br. belongs to the Boraginaceae family. It is an annual shrub native to Australia, Africa, and Asia. This plant contains phytochemicals with antioxidant and anti-diabetic properties of interest to people with T2DM. The present study was aimed at an *in-vitro* and *in-silico* evaluation of phytochemicals and anti-diabetic potentials of ethyl acetate (EA) and ethanol extracts from the leaf, stem, and root of *T. zeylanicum.*

Materials and methods: *Trichodesma zeylanicum* was collected from Maungani village near the University of Venda. Its leaf, root, and stem were washed, dried in the shade, and ground into powder. Plant part powders were weighed separately and extracted using absolute EA and ethanol. Plant extract filtrates were concentrated using the rotary evaporator. Qualitative biochemical methods, including Thin-layer chromatography (TLC), were used for phytochemical and antioxidant analyses using ascorbic acid, gallic acid, and rutin as standards. The liquid chromatography quadrupole time of flight mass spectrometry (LC-qTOF-MS) technique was used for phytochemical analyses and identifications. *In-silico* α-amylase, α-glucosidase, and vascular endothelial growth factor receptor 2 (VEGFR2) inhibitory potentials of selected identified phytochemicals were screened using the Protein Data Bank available α-amylase, α-glucosidase, and VEGFR2 by molecular docking methods using acarbose and sorafenib as standard inhibitors.

Results: Known and unknown phytochemicals in EA extracts of all of *T. zeylanicum* organs were analysed and identified. In comparison to EA, it was commonly observed that ethanol showed its potential to extract more bioactive chemicals from *T. zeylanicum* root (59 mg), stem (58 mg) and leaf (67 mg) extracts, as both percentage yields are high. The DPPH radical scavenging activity of EA root, stem and leaf extracts exceeds that of ethanol plant extracts at low to high concentrations, with the EA leaf extract displaying superior radical scavenging activity of up to 70.259±2.029% at 40 µg/mL when compared to ascorbic acid (86.057±0.610%) [$p \leq 0.001$] at the same concentration**.** Although the ethanol radical scavenging activity of root, stem and leaf extracts was extremely low, the leaf extract radical scavenging activity was moderately promising. TPC in ethanol root (11.489±0.545 µg GAE/mg dried extract), stem (10.753±1.116 µg GAE/mg dried extract) and leaf (47.187±2.300 µg GAE/mg dried extract) extracts surpass the EA root (1.604±0.206 µg GAE/mg dried extract, $p \leq 0.001$), stem (2.280±0.844 µg GAE/mg dried extract, $p \leq 0.001$) and leaf (2.760±0.086 µg GAE/mg dried extract, $p \leq 0.0001$) extracts with ethanol leaf extract depicting significantly higher amount of the phenolic content compared to those of ethanol root and stem extracts ($p \leq 0.001$).

Among the selected compounds docked against two enzyme markers for diabetes and one protein for wound development, ligand 1A (4-[2,6-Dihydroxy-4-(6,7,8-trihydroxy-2-naphthyl) phenoxy]-3-hydroxy-7-(3,4,5-trihydroxyphenyl) naphthalene-1,2-dione) from EA root extract of *T. zeylanicum* showed the highest binding affinities when docked against α-amylase (-11,0 kcal/mol), α-glucosidase (-10,2 kcal/mol), and VEGFR2 (-9,6 kcal/mol) in comparison with acarbose (positive control) for α-amylase (-7.4 kcal/mol) and α-glucosidase (-7.8 kcal/mol), and sorafenib (positive control) for VEGFR2 (-8.1 kcal/mol) as inhibitors.

© University of Venda

The molecular networking displayed closely related human pancreatic α-amylases (AMY2A and AMY2B) and intestinal α-glucosidase (GAA) participating in the metabolism of carbohydrates, together with the involved interacting enzymes leading to T2DM, whereas the kinase VEGFR2 is not in association with these enzymes, although playing a role in wound formation from diabetic patients. Multiple sequence alignment data demonstrated the α-amylase, α-glucosidase and VEGFR2 fully conserved regions (Trp, Lys, Val, Pro, Gly, Ala, Gln, and Ser), which can support their role in digesting carbohydrates and wound formation.

Conclusion: Findings in this study demonstrated that the EA root extract of T. zeylanicum contains phytochemicals with anti-diabetic potentials associated with wound healing and antioxidants, suggesting that the root of this plant can serve as a source of phytochemicals with antidiabetic and wound healing properties. Cytotoxicity of ethanol and EA extracts from different organs of *T. zeylanicum*, molecular dynamic simulation (MD) and an *in-vitro* α-amylase and α-glucosidase inhibitory activity test are recommended for further research to validate and explore the findings of the molecular docking and safety and efficacy of these plant extracts.

Keywords: α-Amylase, α-glucosidase, *In-silico,* phytochemicals, *Trichodesma zeylanicum* extracts

© University of Venda

Dedication

From the deepest part of my heart, this work is dedicated to my unique parents, Mr M.F. Manyuwa. and Mrs L. Ndou. To my mother, Mrs L. Ndou, you have been the very anchor of my life and the non-partisan source of strength and love that has gotten me to this point. Through all the trials these years, your patience, sacrifices, and unwavering encouragement have carried me through some of the darkest days, reminding me of the power of resilience and kindness. You have been a significant role model, teaching me to dream big, get up after falling and keep trying, even when the path looked improbable. Each page of this book is imbued with your influence, courage, and the very love you put into everything you do. I am eternally grateful and grateful for all the efforts you have made to support my dreams.

To my father, Mr M.F. Manyuwa, the one who instilled in me the values of hard work, integrity, and resilience. Your wisdom, patience, and faith in me have been invaluable on my difficult path through the academic wilderness. Your confidence in my abilities lifts me out of despair, teaching me that I am often stronger than I might think. Thank you for always being beside me, guiding me, supporting me as I move forward, and showing me how to face life with strength and dignity. I owe this success to your constant support and presence.

To my biological siblings, Sandra, Busisiwe, Uhone, and Tshilidzi Smile Manyuwa, who have provided so much joy and relief through their love and laughter. Each of you has been a chapter in my upbringing, from which I derive pieces of who I am. Each of you, in your own way, has been a confidante, friend, and bastion of family ties. You motivate me to remain focused and to press on through your chronic reinforcement and encouragement. Thank you for always being there for my cheerleaders, where you would shed light and perspective into my life amidst hardships.

To my partner, Confidence Nembudani, who has been my anchor throughout this journey. This includes patience, understanding, and love. There cannot be anything more one can ask for, especially on the long nights and days offered by the entire process toward this goal. Thank you for your unyielding support, for every celebration around all respective achievements along the journey, and for helping me find balance in pursuing my dreams. One has always been the shoulder, the perspective, or the motivation through it all. This is as much your achievement as it is mine, and I am so grateful to have been able to walk this journey alongside you.

Each of you has played a unique and irreplaceable role in this accomplishment. This work is dedicated to you all with deep gratitude and love. Finally, I dedicate this discourse to God Almighty, the omnipotent, for he is the one who brought me to where I am today. He made it possible, for he made everything possible for me.

© University of Venda

Acknowledgements

First and foremost, I thank God for the life and health he granted me during these trying moments. I am also thankful to my supervisor, Dr S.C. Tshidino-Vukeya, for being the best and most understanding of the supervisors I could ask for, for sharing invaluable knowledge, skills, and insight, and for the exceptional guidance, patience, and insight throughout the course of my research. Besides, I owe profound respect to your expertise for the effort spent supporting me in developing my analytical skills and deepening my understanding of the subject. I sincerely appreciate the time devoted to supporting me and the many challenging discussions that tremendously shaped this achievement.

I owe a great debt of thanks to my co-supervisors, Ms A-T. Ramabulana and Prof. N.E. Madala, for their generous support and valuable, constructive comments, and most profound appreciation for the valuable supervision this work has received. All your support and guidance are much appreciated. Their multiple views and insightful comments greatly improved my work quality and rigour, and their encouragement kept me thoroughly motivated. I have been fortunate enough to draw on their knowledge and expertise. Their contribution to science is an inspiration: eternal thanks for having been under their supervision.

I am also grateful to Prof. T. VanRee of the Department of Chemistry for his input and English editing during the research proposal development stages. My immense gratitude to the laboratory technologies of the Department of Food Science and Technology (Dr O.P. Bamidele, Dr B. Nethathe, and Dr S.E. Ramashia) for the facilities, microwell-plate reader spectrophotometry, and technical assistance they provided for research. The staff at the laboratory were most helpful, and their expertise and willingness to assist played a significant role in carrying out the various experiments. Their support contributed significantly to the successful completion of this dissertation. Last but not least, I express my heartfelt gratitude to the Department of Biochemistry and Microbiology, Faculty of Science, Engineering, and Agriculture, with special mention to the University of Venda, for admitting me to this university in a highly engaging program. In the same breath, I compliment the help, care, and kindness that I received from my birth parents, siblings, and partner. They have always been with me through thick and thin in my endeavours. Their generosity with financing equally deserves mention, as it enabled me to undertake my research and rent places to stay.

© University of Venda

National conference attendance (abstract and poster presentation)

1. Manase Manyuwa, Ntakadzeni Edwin Madala, Anza-Tshilidzi Ramabulana, Shonisani Cathphonia Tshidino. (2024). *In-vitro* and *in silico* evaluation for phytochemicals and anti-diabetic potentials of extracts from different organs of *Trichodesma zeylanicum*. 28th SASBMB Congress. The Ranch, Protea Hotel. Polokwane, Limpopo province, South Africa, 07-10 July 2024 (abstract and poster).

2. Manase Manyuwa, Ntakadzeni Edwin Madala, Anza-Tshilidzi Ramabulana, Shonisani Cathphonia Tshidino. (2024). *In-vitro* and *in silico* evaluation for phytochemicals and anti-diabetic potentials of extracts from different organs of *Trichodesma zeylanicum*. UNIVEN research open day. UNIVEN research conference centre, Limpopo province, South Africa, 19 July 2024 (abstract and poster).

© University of Venda

Table of Contents

Declaration ii

Abstract iii

Dedication v

Acknowledgements vi

National conference attendance (abstract and poster presentation) vii

Table of Contents viii

List of Figures xii

List of Tables xv

List of abbreviations and symbols xvi

Chapter 1 1

1. Introduction and background of the study. 1

1.1. Diabetes mellitus. 1

1.2. Global description of *Trichodesma zeylanicum* (Burm.f) R.Br. 2

1.3. History, origin, and global distribution of *T. zeylanicum*. 3

1.4. Climate requirements (Ecology) of *T. zeylanicum.* 4

1.5. *Trichodesma zeylanicum* utilisation and antioxidant properties. 4

1.6. Importance of α-glucosidase and α-amylase in T2DM and their inhibition. 5

1.7. Vascular endothelial growth factor receptor 2 kinase. 6

1.8. The importance of LC-qTOF-MS, molecular docking, networking, and protein-protein sequence alignment in the evaluation of plant extracts with antioxidant and antidiabetic potentials. 7

1.9. Defining the research 8

1.9.1. Problem statement 8

1.9.2. Hypothesis 9

1.9.3. Aim of study 9

1.9.4. Objectives 9

Chapter 2 10

2. Methodology 10

2.1. Plant collection. 10

© University of Venda

University of Venda
Creating Future Leaders

2.2. Preparation of plant extract. 11
2.3. *In-vitro* phytochemical qualitative analysis through chemical tests. 12
2.3.1. Test for Steroids. 12
2.3.2. Test for terpenoids. 12
2.3.3. Test for coumarins. 12
2.3.4. Test for phenols. 12
2.3.5. Test for alkaloids. 12
2.3.6. Test for saponins (Foam test) 13
2.3.7. Test for tannins 13
2.3.8. Test for glycosides 13
2.3.9. Test for flavonoids 13
2.3.10. *In-vitro* qualitative phytochemical antioxidant analysis using TLC. 13
2.3.11. Phytochemicals fingerprinting on thin-layer chromatography. 14
2.4. Quantitative antioxidant assays 14
2.4.1. DPPH-radical scavenging assay 14
2.4.2 Determination of total phenolic content 15
2.5. *In-silico* phytochemical analysis and anti-diabetic potentials of EA and ethanol extracts from different organs of *T. zeylanicum* 16
2.5.1 LC-qTOF-MS analysis of EA and ethanol extracts from different organs of *T. zeylanicum* 16
2.5.2. Molecular docking (*In-silico*) of α-glucosidase, α-amylase and VEGRF2 against selected identified compounds. 17
2.5.3. Molecular networking procedure 17
2.5.4. Protein-protein sequence alignment 18
2.5.5. Statistical analysis 19
Chapter 3 20
3. Results and Discussion of EA and ethanol extracts from different organs of *T. zeylanicum* 20
3.1. Percentage yields of EA and ethanol extracts from *T. zeylanicum* (Burm. f) R. Br. root, stem, and leaf. 20
3.2. Qualitative phytochemical analysis of EA and ethanol extracts from different plant organs 21

© University of Venda

3.2.1. TLC chromatograms of EA and ethanol plant extracts visualised under normal light. 22

3.2.2. TLC chromatograms of EA and ethanol plant extracts visualised under long UV light. 24

3.2.3. TLC chromatograms of EA and ethanol plant extracts developed by vanillin-sulfuric acid, DPPH, and ferric chloride reagents. 26

3.2.4. Phytochemical tests 31

3.3. Quantitative phytochemical analysis of ethanol and EA extracts from different organs of *T. zeylanicum.* 35

3.3.1. Antioxidant potential of plant extract using DPPH-radical scavenging activity. 35

3.3.2. Total phenolic content of plant extracts 40

3.4. *In-silico* phytochemical analysis and anti-diabetic potentials of EA and ethanol extracts from different organs of *T. zeylanicum* 43

3.4.1. LC-qTOF-MS phytochemicals analysis of ethanol and EA extracts from different organs of *T. zeylanicum*. 43

3.4.2. Negative $[M-H]^-$ ionisation fragments identified by Sirius software. 46

3.4.3. LC-qTOF-MS chromatograms detected and identified compounds in EA and ethanol extracts from different organs of *T. zeylanicum*. 49

3.4.4. Molecular docking of α-amylase, α-glucosidase and VEGFR2 against selected identified compounds to assess their antidiabetic potentials. 51

3.4.4.1. Retrieved proteins (α-amylase, α-glucosidase, and VEGFR2 kinase) from the RCSB Protein Data Bank database for molecular docking. 51

3.4.4.2. Selected identified compounds in EA extracts from different organs of T. zeylanicum docked against α-amylase. 51

3.4.4.3. Selected identified compounds in EA extracts from different organs of T. zeylanicum docked against α-glucosidase 58

3.4.4.4. Selected identified compounds in EA extracts from different organs of T. zeylanicum docked against VEGFR2 62

3.4.4.5. Selected identified compounds in ethanol extracts from different organs of T. zeylanicum docked against α-amylase. 67

3.4.4.6. Selected identified compounds in ethanol extracts from different organs of T. zeylanicum docked against α-glucosidase 72

© University of Venda

University of Venda
Creating Future Leaders

3.4.4.7. Selected identified compounds in ethanol extracts from different organs of T. zeylanicum docked against VEGFR2 77

3.4.4.8. The molecular docking summary 81

3.4.5. Distribution of phytochemical compounds within the plant organs 82

3.4.6. Predicted biological protein-protein networks. 85

3.4.6.1. α-Amylase and α-glucosidase predicted biological protein-protein networks 85

3.4.6.2. VEGFR2 predicted biological protein-protein networks. 87

3.4.7. α-Amylase, α-glucosidase and VEGFR2 Multiple sequence alignment 89

3.5. Conclusion 91

3.6. Recommendations for the future studies 92

Chapter 4 94

4. List of References 94

4.1. References 94

© University of Venda

List of Figures

Figure 1.1: *Trichodesma zeylanicum* (Burm. f) R. Br plant……..……..3

Figure 1.2: Plant geographical distribution ……..…….3

Figure 2.1: *Trichodesma zeylanicum* (Burm. f) R.Br. different organs……..…..…..10

Figure 2.2: *T. zeylanicum* dried extract……...……..……..…...…..11

Figure 3.1: The percentage yields of ethanolic and EA extracts from different organs of *T. zeylanicum*……..21

Figure 3.2A: TLC chromatograms of EA plant extracts developed in four mobile phases, EMW (ethyl acetate: methanol: water), CEF (chloroform: ethyl acetate: formic acid), TAF (toluene: acetone: formic acid), and ED (ethyl acetate: dichloromethane) and visualised under normal light before spraying with detection reagents……..……..…..22

Figure 3.2B: TLC chromatograms of ethanol plant extracts developed in four mobile phases, EMW (ethyl acetate: methanol: water), CEF (chloroform: ethyl acetate: formic acid), TAF (toluene: acetone: formic acid), and ED (ethyl acetate: dichloromethane) and visualised under normal light prior spraying with detection reagents…….23

Figure 3.3A: TLC chromatograms of EA plant extracts developed in four mobile phases, EMW (ethyl acetate: methanol: water), CEF (chloroform: ethyl acetate: formic acid), TAF (toluene: acetone: formic acid), and ED (ethyl acetate: dichloromethane) and monitored under 365 nm long wave ultraviolet…….……25

Figure 3.3B: TLC chromatograms of ethanol plant extracts developed in four mobile phases, EMW (ethyl acetate: methanol: water), CEF (chloroform: ethyl acetate: formic acid), TAF (toluene: acetone: formic acid), and ED (ethyl acetate: dichloromethane) and monitored under 365 nm long wave ultraviolet……..…26

Figure 3.4A: TLC chromatograms of EA plant extracts developed in four mobile phases, EMW (ethyl acetate: methanol: water), CEF (chloroform: ethyl acetate: formic acid), TAF (toluene: acetone: formic acid), and ED (ethyl acetate: dichloromethane), with a different polarity that exhibits chemicals detected by Vanillin-sulfuric acid, DPPH reagent, and Ferric chloride……...……....27

Figure 3.4B: TLC chromatograms of ethanol plant extracts developed in four mobile phases, EMW (ethyl acetate: methanol: water), CEF (chloroform: ethyl acetate: formic acid), TAF (toluene: acetone: formic acid), and ED (ethyl acetate: dichloromethane), with a different polarity that exhibits chemicals detected by Vanillin-sulfuric acid, DPPH reagent, and Ferric chloride…….....28

© University of Venda

Figure 3.5: Percentage inhibition of DPPH radical scavenging activity of plant extracts. (A) ethyl acetate and (B) ethanol extracts from different organs of *T. zeylanicum*, which include leaf, stem, and root, using ascorbic acid as standard……..……...…..…..36

Figure 3.6A: Gallic acid standard curve ……40

Figure 3.6B: Total phenolic content comparison of ethanol and EA extracts from different organs of *T. zeylanicum*……42

Figure 3.7A: Typical LC-qTOF-MS chromatogram displaying phytochemical dispersion profiles in the ethyl acetate (EA) extract (2 mg/mL) of *T. zeylanicum* root, stem, and leaf, respectively……..…45

Figure 3.7B: Typical LC-qTOF-MS chromatogram displaying phytochemical dispersion profiles in the ethanol (E) extract (2 mg/mL) of *T. zeylanicum* root, stem, and leaf, respectively…….……...……46

Figure 3.8: The molecular structures of selected identified compounds from *T. zeylanicum* root, stem and leaf (A) ethyl acetate and (B) ethanolic extract that were docked against α-amylase, α-glucosidase, and VEGFR2……..……...……...50

Figure 3.9: Structural homolog depicting α-helices, β-strands, loops, and turns, active sites and the whole protein groups of the proteins used for molecular docking. (A) pancreatic α-amylase, (B) α-glucosidase, and (C) VEGFR2……...…….…….51

Figure 3.10: Molecular docking of α-amylase against (A) Acarbose, (B) Ligand 1A, (C) Ligand 2A, and (D) Ligand 3A……..……...53

Figure 3.11: Molecular docking of α-glucosidase against (A) Acarbose, (B) Ligand 1A, (C) Ligand 2A, and (D) Ligand 4A……...59

Figure 3.12: Molecular docking of VEGFR2 against (A) Sorafenib, (B) Ligand 1A, (C) Ligand 2A, and (D) Ligand 4A…….…….....64

Figure 3.13: Molecular docking of α-amylase against (A) Acarbose, together with (B) Ligand 7A, (C) Ligand 8A, and (D) Ligand 6A……..……...68

Figure 3.14: Molecular docking of α-glucosidase against (A) Acarbose, (B) Ligand 10A, (C) Ligand 8A, and (D) Ligand 9A……..…….....73

Figure 3.15: Molecular docking of VEGFR2 against (A) Sorafenib, (B) Ligand 6A, (C) Ligand 8A, and (D) Ligand 6A…….……79

Figure 3.16: Metabolites relative abundance of EA and ethanol extracts from different organs of *T. zeylanicum* …….....……83

© University of Venda

University of Venda
Creating Future Leaders

Figure 3.17: Protein-protein network focused on (A) the human pancreatic α-amylase (AMY2A) and (B) the intestinal α-glucosidase (GAA) and their networking enzymes…….…….……..86

Figure 3.18: The protein-protein network centred around VEGFR2 (KDR) and its networking enzymes…...88

Figure 3.19: Multiple sequence alignment display of human pancreatic α-amylase, intestinal α-glucosidase, and VEGRF2…….....91

© University of Venda

List of Tables

Table 2.1: Preparation of different concentrations of plant extracts and controls for the DPPH-scavenging assay……...…..15

Table 3.1: Phytochemicals tested in EA and ethanol root, leaf, and stem extracts of *T. zeylanicum*…….32

Table 3.2: % DPPH-scavenging activity of EA and ethanol root, stem, and leaf extracts of *T. zeylanicum*…..37

Table 3.3A: Metabolites separated by LC-qTOF-MS in negative ionization mode in *T. zeylanicum* EA root, stem, and leaf extracts……..…….....46

Table 3.3B: Metabolites separated by LC-qTOF-MS in negative ionization mode in *T. zeylanicum* ethanol root, stem, and leaf extracts……..….48

Table 3.4: The binding affinities of selected identified compounds in EA root, stem, and leaf extracts of *T. zeylanicum* with the highest binding affinity to the α-amylase and the interacting amino acid residues of the protein……..…..……..…....53

Table 3.5: The binding affinities of selected identified compounds in EA root, stem, and leaf extracts of *T. zeylanicum* with the highest binding affinity to the α-glucosidase and the interacting amino acid residues of the protein……...……..59

Table 3.6: The binding affinities of selected identified compounds in EA root, stem, and leaf extracts of *T. zeylanicum* with the highest binding affinity to the VEGFR2 and the interacting amino acid residues of the protein……...……64

Table 3.7: The binding affinities of selected identified compounds in ethanol root, stem, and leaf extracts of *T. zeylanicum* with the highest binding affinity to the α-amylase and the interacting amino acid residues of the protein……...68

Table 3.8: The binding affinities of selected identified compounds in ethanol root, stem, and leaf extracts of *T. zeylanicum* with the highest binding affinity to the α-glucosidase and the interacting amino acid residues of the protein……74

Table 3.9: The binding affinities of selected identified compounds in ethanol root, stem, and leaf extracts of *T. zeylanicum* with the highest binding affinity to the VEGFR2 and the interacting amino acid residues of the protein……...……79

Table 3.10: Summary of selected identified compounds in studied plant extracts with good binding affinities against all three docked proteins……..……81

© University of Venda

List of abbreviations and symbols

µg:	Microgram
µL:	Microlitre
Abs:	Absorbance
AMP:	Adenosine monophosphate
AMY:	α-Amylase
CEF:	Chloroform: ethyl acetate: formic acid
DM:	Diabetes mellitus
EA:	Ethyl acetate
ED:	Ethyl acetate: dichloromethane
EMW:	Ethyl acetate: methanol: water
EtOH:	Ethanol
FDA:	Food and Drug Administration
FGF:	Fibroblast Growth Factor
GAA:	Intestinal α-glucosidase
GAE:	Gallic Acid Equivalents
GAA:	Neutral α-glucosidase
GBE:	1,4-α-glucan branching enzyme
HDL:	High density lipoprotein
kV:	kilovolt
LC-qTOF-MS:	Liquid chromatography-quadrupole time-of-flight mass spectrometry
mg:	Milligram
mL:	Millilitre
MGAM:	Maltase glucoamylase
NaI:	Sodium iodide
nm:	Nanometre
NRP1:	Neuropilin-1
PDB:	Protein Data Bank
PDGFC:	Platelet-derived Growth Factor C
PECAM1:	Platelet and endothelial cell adhesion molecule 1
PPI:	Protein-protein interactions
PYGL:	Glycogen phosphorylase
RCSB:	Research Collaboratory for Structural Bioinformatics
RF:	Retention factor

© University of Venda

RMSD:	Root mean square deviation
RSA:	Radical scavenging activity
SI:	Sucrase-isomaltose
T. zeylanicum:	*Trichodesma zeylanicum* (Burm.f) R.Br
T1D :	Type 1 diabetes
T1DM:	Type 1 diabetes mellitus
T2D:	Type 2 diabetes
T2DM:	Type 2 diabetes mellitus
TAF:	Toluene: acetone: formic acid
TLC:	Thin-layer chromatography
UV:	Ultraviolet
VEGF:	Vascular endothelial growth factor
VEGFR:	Vascular endothelial growth factor receptor

© University of Venda

Chapter 1

1. Introduction and background of the study.

The global description, distribution, history, origin, climate requirements, utilization, and antioxidants of *T. zeylanicum* of the study are outlined in this chapter. Diabetes and the digestive (α-glucosidase and α-amylase) and wound-associated (VEGFR2) enzymes are detailed. The study's problem statement, hypothesis, aim, and objectives are also described.

1.1. Diabetes mellitus.

Diabetes mellitus (DM) is one of the oldest known diseases afflicting humanity. Its earliest account was found about three thousand years ago in Egyptian manuscripts (Ahmed, 2002). In 1936, an unambiguous distinction was made between Type 1 diabetes mellitus (T1DM) and Type 2 diabetes mellitus (T2DM). Over the past few decades, the number of DM cases has increased, mainly due to the continuous increase in the incidence of T2DM. T2DM was first recognised as a metabolic syndrome in 1988 (Patlak, 2002). Previously known as non-insulin-dependent diabetes, it is the most generic form of diabetes characterised by hyperglycaemia, impaired insulin synthesis, and secretion secondary to insulin resistance (Olokoba *et al*., 2012). It results from the interaction of genetic, environmental, and behavioural risk factors (Zimmet *et al*., 2001; Azevedo and Alla, 2008; Ripsin *et al*., 2009).

The incidence and prevalence of T2DM increase with age (Ahmad, 2013). Broadly, T2DM is categorized into two subsets: diabetic with obesity and diabetic without obesity. Diabetic patients with obesity usually develop mechanisms of resistance to endogenous insulin from alterations in cell receptors associated with fat distributed in the abdominal region. Non-obese T2DM is characterized by both post-receptor insulin resistance and a deficiency in insulin production and release (Robertson, 1995; Kahn, 1994). T1DM is anything but a misaligned control of glucose homeostasis obliterating the autoimmune destruction of the insulin-producing pancreatic β-cell, which progressively presages insulin deficiency, leading to hyperglycaemia (Katsarou *et al*., 2017). When this deficiency is sustained, it succumbs to progressively deteriorating metabolic derangements with accompanying worsening hyperglycaemia, diabetic ketoacidosis, starvation, and death (Katsarou *et al*. 2017). T1DM only constitutes around 10% of the world's diabetes cases; nonetheless, it occurs with increasing incidence many years earlier during life (Haller *et al*., 2005). While it can occur at any age, T1DM typically occurs in adolescents, peaking around puberty (Patterson *et al*., 2009). T1DM occurs with equal frequency in both sexes before puberty, with slightly more males affected by the disease during adolescence and young adulthood (Karvonen *et al*., 1997).

© University of Venda

Insulin is a peptide hormone secreted from the pancreatic islets of Langerhans β cells that acts like a key, unlocking a passage for glucose from food to enter the body's cells for energy production (Bliss, 1993). The body breaks down all carbohydrate foods into blood glucose, which insulin helps to transport into cells. In cases where the body cannot produce or use insulin effectively, blood glucose levels rise, a condition referred to as hyperglycaemia (Olokoba *et al*., 2012). Therefore, long-term high blood glucose levels are associated with damage to the body and failure of various organs and tissues (Mohamed *et al*., 2016). Effective practical approaches to prevent T2DM include changes in lifestyle, diet, weight control and the introduction of blood pressure and glucose level measures as the first line of defence proposed against T2DM (Ripsin *et al*., 2009). Failure of these measures in patients who demonstrate persistent hyperglycaemia and elevated glycated haemoglobin levels, oral anti-diabetes medications are used to mediate the subsequent management of diabetes mellitus for these specific patients (Dowarah and Singh, 2020).

Previous studies indicated that the *Trichodesma zeylanicum* contains phytochemicals with antioxidant and anti-diabetic properties, which is of interest to people with T2DM (Narendra *et al*., 2015). Many traditional uses of *T. zeylanicum* are astonishing in treating numerous ailments. The leaf and the root of *T. zeylanicum* have been heavily used by the local communities for treating wounds. In Malawi, the root are also used to treat diarrhoea. According to Gurib-Fakim *et al*. (1997), powdered root of *T. zeylanicum* are used externally on wounds and the skin for pain relief.

1.2. Global description of *Trichodesma zeylanicum* (Burm.f) R.Br.

Trichodesma zeylanicum is the scientific name for an annual plant that is an herb or shrub native to Africa, Asia, and Australia, known by the common names' *northern bluebell*, *camel bush*, and *cattle bush* [Figure 1.1] (Mosti *et al*., 2007; Abdelgawad *et al*., 2021). It is an upright, branching plant that can grow up to 1.5 meters tall. It is covered with stiff, densely packed hairs that give the plant a greyish hue. There are red spots on the young stem. The flowers are placed in a terminal inflorescence that is loosely branching (Mosti *et al*., 2007). They have a white centre and a pale blue funnel form. The fruit is a dry capsule disarticulating into four loculi, each containing a seed (Hyde *et al*., 2013). *Trichodesma* is a derivative of the Greek words-thrix or trikhos (hair) and desme (band or bundle) and refers to the twisted hairs or awns that arise at the termination of the anthers. The species name refers to the relatively narrow leaf (Retief *et al*., 2002).

The root is a deep taproot that is often lignified. The stem is firm, cylindrical, and covered with brittle hairs; it is light green with rose-coloured hues and dark red spots and is fleshy when young (Retief *et al*., 2002). The base quickly looks woody (Chidambaram *et al*., 2013). The leaf blade is elliptical, oblong, or narrowly oval (Figure 1.1). The base might be cordate or attenuated, while the apex can be acute or obtuse (Saboo *et al*., 2013). Root and leaf arrangement is important for treating the size and shape of each leaf because it does vary markedly depending on the distance of them to the axis of the inflorescence in relation to the distance of the leaf of the inflorescence.

© University of Venda



Figure 1.1: *Trichodesma zeylanicum* (Burm. f) R. Br plant (Retief *et al*., 2002).

In the initial instance, they are huge in size, measuring 6 to 15 cm in length and 1 to 5 cm in breadth (Hyde *et al*., 2013). Size diminishes towards the inflorescences or at the apex of the plant. The leaf are between 2 and 5 cm long (Figure 1.1). White stiff hairs, 0.5 to 0.8 mm long, with tuberculate bases, cover both sides. On the underside, there is a noticeable pinnate venation (Retief *et al*., 2002).

1.3. History, origin, and global distribution of *T. zeylanicum*.

Trichodesma zeylanicum was first described as *Borago zeylanica* Burm. f. in 1768 from Australia by Nicolaas Laurens Burman, and later transferred into genus *Trichodesma* to become *Trichodesma zeylanicum* (Burm. f.) R. Br. in 1810 by Robert Brown (Figure 1.1). The *T. zeylanicum* belongs to the Boraginaceae family under the Plantae kingdom, Boraginales order, *Trichodesma* genus and magnoliopsida class of the phylum Tracheophyta (Hyde *et al*., 2013).

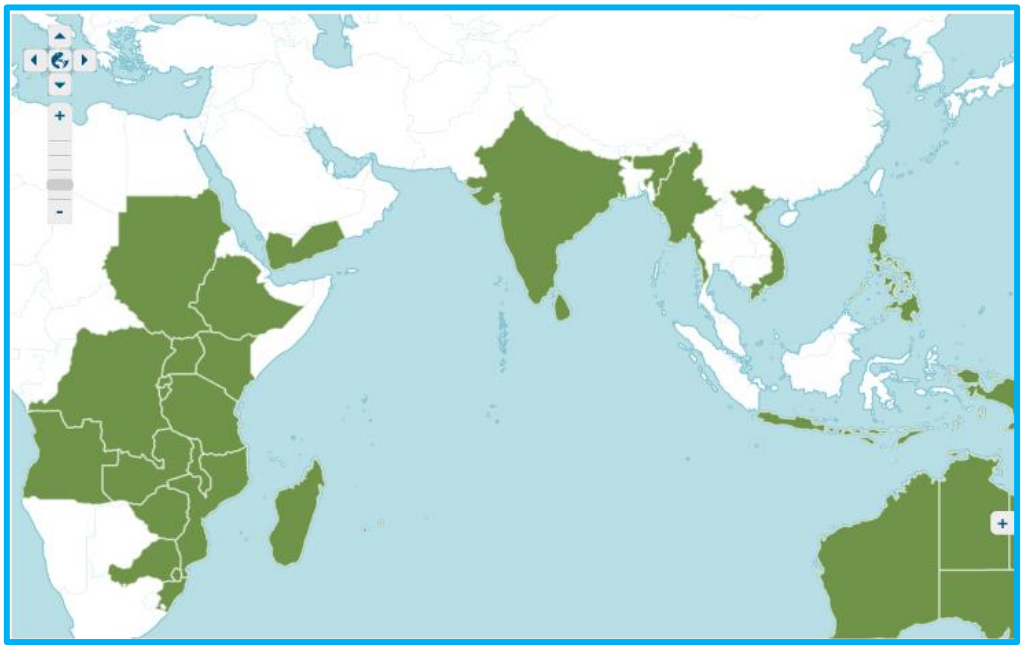


Figure 1.2: Plant geographical distribution (http://www.worldfloraonline.org/taxon/wfo-0000411041).

© University of Venda

The species of *T. zeylanicum* originated in various organs of Africa (Ethiopia, Kenya, Madagascar, Malawi, Mozambique, Namibia, South Africa, Sudan, Swaziland, Tanzania, Uganda, Zaire, Zambia, Zimbabwe) and Asia (India, the Philippines, Malaysia), and Australasia (Mauritius Australia and Fiji) also in East Africa, India, Southeast Asia, and the islands of the Indian Ocean (Comoros, Mayotte, Madagascar, Mauritius, Reunion, and Seychelles) (Mosti *et al*., 2007; Abdelgawad *et al*., 2021). In Comoros, *Trichodesma zeylanicum* thrives in open, exposed terrain, where it is seen near fields and the edges of roadways with an altitude of up to 400 m (Mosti *et al*., 2007; Abdelgawad *et al*., 2021). The weed is a significant element for rainfed crops in Madagascar. It is prevalent in the southwestern part, near the middle and western part, although it has, more recently, been reported in the highlands. The species has become established at low elevations and in arid regions of Mauritius. It is a ruderal plant that thrives on stony alluvial rivers and grows along highways, waste areas, and fallow areas (Abdelgawad *et al*., 2021). *Trichodesma zeylanicum* (Figure 1.1) grows on the island of Mayotte in open areas in the dry zone of the south of the island. On points, islands, and crops are where it is most prevalent. In Reunion, *Trichodesma zeylanicum* is a particularly prevalent species. It enjoys broad spaces with plenty of sunlight because it does best in dry areas (Mosti *et al*., 2007). The majority of where it is located are waste areas, roadside ditches, and fields. The island's most significant population is located on its western coast. In Seychelles, it grows in open areas and abandoned sites. It is rarely plentiful (Mosti *et al*., 2007).

1.4. Climate requirements (Ecology) of *T. zeylanicum.*

Trichodesma is a genus of perennial and annual herbs or subshrubs. *Trichodesma zeylanicum* is located across grasslands and woodlands along dry riverbeds as a common weed in both old and new cultivated land, pioneering the disrupted section along roadsides, well-drained sandy-gravel turf, poorly drained loam, or in rocky, well-drained soils, in full sun (Figure 1.1). It is common, and it is considered a weed of national significance. It occurs throughout Africa, ascending to 1700 m. (Mosti *et al*., 2007; Abdelgawad *et al*., 2021).

1.5. *Trichodesma zeylanicum* utilisation and antioxidant properties.

Traditionally, *Trichodesma zeylanicum* has been used to treat various diseases such as arthritis, fever, skin disease arthralgia, and dysentery [Figure 1.1] (Sharma *et al*., 2009). Each part of this plant has exhibited antioxidant, anti-inflammatory, analgesic, antipyretic, antibacterial, and antidiabetic action (Abdelgawad *et al*., 2021). The plant is sometimes harvested from the wild as a local source of food and medicine. The green leaf and root of this plant are chewed and made into a poultice applied to wounds, boils, and snakebites in Tanzania (Ngonda *et al*., 2014). Root are either chewed or, more traditionally, pounded, with the resulting extract used as a remedy for tuberculosis, stomachache, poisoning, and rheumatism. In Malawi, leaf and root are applied to treat wounds, while the root treat dysentery (Ngonda *et al*. 2014). In the Mascarene Islands, a decoction is used against fever and dysentery which are diuretics. Its powdered root is analgesic when used on wounds.

© University of Venda

In Zimbabwe and Comoros, the powdered form of dried leaf is utilized for infected wounds, while fresh leaf decoction is used to avert stillbirth. In South Africa, *T. zeylanicum* is said to allay pain and promote wound healing. In India and Sri Lanka, the plant is used against snakebite (Ngonda *et al*., 2013; Ngonda *et al*., 2014). They are used as an emollient in Tanzania, India, and Pakistan. Seed oil/flower essence is sold on the world market under the trade name called wild borage oil. Australia is the major producer, with Western Europe as the principal market (Ruffo *et al*., 2002). Trade quantity and value are unknown. Tanzania, Malawi, and Madagascar prepare eaten with vegetables, young leaf, and shoots (Ruffo *et al*., 2002). Camels consume this plant, but other livestock seem to avoid this plant (Ruffo *et al*., 2002). Previous studies indicated that *Trichodesma zeylanicum* plant contains phytochemicals with antioxidant and anti-diabetic properties of interest to people with T2DM (Narendra *et al*., 2015).

1.6. Importance of α-glucosidase and α-amylase in T2DM and their inhibition.

Elevated blood glucose levels are a hallmark of T2DM, which can result in major side effects such as cardiovascular disease, retinopathy, neuropathy, and nephropathy (Ch'ng *et al*., 2019). With a global death rate of 4.9 million, T2DM continues to be one of the most prevalent medical conditions, accounting for 90% of all cases of diabetes (Dona *et al*., 2010). Inhibiting the breakdown of dietary carbohydrates is one of the treatment strategies used to manage postprandial hyperglycaemia in T2DM. A crucial enzyme called pancreatic α-amylase in the digestive system converts dietary carbohydrates like starch into simpler monosaccharides (Vocadlo *et al*., 2008). These undergo additional degradation by α-glucosidases, resulting in absorbed glucose entering the bloodstream in the body (Peyrot des Gachons and Breslin, 2016). Furthermore, pancreatic α-amylase elevates the levels of blood glucose and postprandial hyperglycaemia (Kazeem *et al*., 2013).

Well-known pharmaceutical candidates for regulating and treating postprandial blood glucose increases are α-glucosidase and α-amylase inhibitors such as acarbose, voglibose, and miglitol (DeFronzo, 2004). New therapeutic methods are being investigated to regulate postprandial glucose levels because of the serious adverse effects of commercially available anti-diabetic medications. Studies are being conducted on medicinal plant extracts that inhibit α-glucosidase and α-amylase, which regulate blood glucose levels after meals. This makes α-glucosidase and α-amylase an exciting and innovative therapeutic target for treating T2DM (Sim *et al*., 2010). One possible strategy to stop dietary glucose absorption is using natural resources such as carbohydrate-digestive enzyme inhibitors, which have fewer side effects than synthetic drugs. Therefore, to help fight T2DM, researchers are looking into the α-glucosidase and α-amylase inhibitory activity of medicinal plants and their phytochemical constituents (Oyedemi *et al*., 2010). The size of starch molecules prevents them from passing through the blood-brain barrier. Nevertheless, glucose is essential for normal brain function.

© University of Venda

Thus, the complex starch molecule is broken down into simple sugar bits by the enzymes α-glucosidase and α-amylase to make it easier for the blood-brain barrier to process (Morris *et al*., 2011). The breakdown of excess starch into smaller sugar pieces causes levels of glucose in the blood to increase. According to Oboh *et al*. (2016), researchers are interested in developing potent α-glucosidase and α-amylase inhibitory substances after discovering that several enzymatic inhibiting agents, such as acarbose, miglitol, and voglibose, are effective at suppressing these enzymes. These inhibitors are promoted as potent therapeutic targets for managing medical conditions such as obesity and diabetes (Sales *et al*., 2012). According to Kazeem *et al*. (2013), these inhibitors transform the body's environment to reduce postprandial blood glucose levels and delay the breakdown of sugary foods. According to scientific research, acarbose is an anti-diabetic medication that suppresses the α-glucosidase and α-amylases (Agarwal, 2016).

1.7. Vascular endothelial growth factor receptor 2 kinase.

The family of receptor protein tyrosine kinases known as Vascular endothelial growth factor receptors (VEGFRs) are crucial for controlling tumour-induced angiogenesis (Salimi *et al.*, 2022; Wang *et al*., 2024). VEGFR inhibitors are used extensively to manage various tumours (Kabrun *et al*., 1990). However, the practical applicability of existing VEGFR inhibitors is hampered to some degree by their possible toxicity and poor clinical efficacy (Wang *et al*., 2024). Thus, it is necessary to create innovative tactics to enhance clinical results and reduce the harmful effects of VEGFR inhibitors. One significant way that tumours encourage development and propagation is by angiogenesis, which is the creation of new arteries from pre-existing vasculature (Kerbel *et al*., 2002; Wang *et al*., 2024). The primary effector of VEGF-mediated proliferation of cells and a key player in tumour angiogenesis is vascular endothelial growth factor receptor 2 kinase (VEGFR2) (Salimi *et al.*, 2022). The extracellular portion, a small transmembrane domain, and a tyrosine kinase domain comprise the type III transmembrane kinase receptor known as VEGFR2 (Holmes *et al*., 2007). When VEGF/VEGFR2 binds, downstream signalling is activated. As a result, VEGFR2 is strongly auto-phosphorylated as a tumour develops (Xia *et al*., 2014; Kajal *et al*., 2019).

Considering its function, VEGFR2 has been recognized as an ideal target for developing new inhibitors that will prevent angiogenesis (Vailhé *et al*., 2001; Al-Sanea *et al*., 2021). Consequently, stopping the VEGFR2 signalling pathway has been seen as a key and appealing target for anti-angiogenesis therapy in the fight against cancer (Xia *et al*., 2014; Kajal *et al*., 2019). To date, the Food and Drug Administration (FDA) has licensed some medications for VEGFR2 inhibition, including sorafenib, pazopanib, axitinib, regorafenib, and lenvatinib (Kang *et al*.,2018; Modi and Kulkarni *et al*., 2019). The effectiveness of cancer treatment may be diminished by adverse effects and drug resistance linked to the usage of anticancer medications (Kang *et al*.,2018; Modi and Kulkarni *et al*., 2019). Therefore, it is very desirable to find and create new medications, preferably have better efficacy and fewer adverse reactions, but this is an exceedingly difficult and complex problem (Kang *et al*.,2018; Modi and Kulkarni *et al*., 2019; Xia *et al*., 2014).

© University of Venda

1.8. The importance of LC-qTOF-MS, molecular docking, networking, and protein-protein sequence alignment in the evaluation of plant extracts with antioxidant and antidiabetic potentials.

Liquid chromatography combined with quadrupole time-of-flight mass spectrometry (LC-qTOF-MS) is a powerful analytic instrument to determine and characterize the complex phytochemical composition of plant extracts. It provides highly resolved, precise mass measurements to allow precise identification of known and novel compounds at even minute concentrations (Ramabulana *et al*., 2021). Its capability to provide detailed fragmentation patterns aids in the elucidation of the structures of bioactive molecules which is crucial to relate the activity of certain compounds to observed biological activities, like antioxidant and antidiabetic effects (Tan *et al*., 2020). The totality of powerful techniques in the identification of bioactive compounds is followed by molecular docking, which has a significant role in the prediction and representation of the interactions between plant-derived phytochemicals and target proteins. Molecular docking modelling predicts the binding affinity and orientation of bioactive compounds to their active sites in key targets involved, for instance, in glycaemic control, such as α-amylase and α-glucosidase (Ibrahim *et al*., 2015). This computational strategy further gives suggestions as to how these bioactive compounds could inhibit or modulate the activity of these enzymes, and their possible therapeutic mechanisms would thus be the subject of discussion at the molecular level (Ibrahim *et al*., 2015).

Protein-protein (PPI) analysis adds another dimension, exploring how modulation of target proteins by plant-derived compounds may affect wider cellular networks. PPI analysis helps to identify a critical hub of proteins and the signalling cascades involved for instance, in the oxidative stress response and insulin signalling pathways (Szklarczyk *et al*., 2025). Understanding these interactions will allow the researchers to predict potential synergistic effects, any overlooked reactions, and their eventual effect on metabolic health. By understanding these interactions, researchers can predict potential synergistic effects, off-target interactions, and the overall impact of plant extracts on metabolic health (Sim *et al*., 2010). Together, these methodologies form a running framework whereby an elaborate analysis of plant extracts with antioxidant and antidiabetic potentials can bridge the areas of interest from phytochemistry, bioinformatics, and pharmacology.

Finally, protein-protein sequence alignment is a critical bioinformatics tool in evaluating plant extracts with antioxidant and antidiabetic potentials since it helps in elucidating the conserved regions, active sites, and structural motifs of target proteins such as α-amylase and α-glucosidase (Vasistha *et al*., 2025). The amino acid sequences of these proteins from distinct species are compared to explore functional likenesses, thereby assessing the evolutionary conservation of these proteins as well as the meaning within their functions for which plant-based compounds exert their effects (Zhang *et al*., 202). Additionally, the alignment will help ascertain active binding sites for different phytochemicals which will facilitate molecular docking studies in drug discovery along with detection of disease-specific mutations or variants such as diabetes. Thus, protein sequence alignment increases the ability to predict protein-ligand interactions, elucidate biological pathways, and optimize the therapeutic potential of bioactive compounds in plant extracts.

© University of Venda

1.9. Defining the research

1.9.1. Problem statement

Currently, one of the emerging fields in contemporary biomedical sciences is the study of diabetes and the substances that promote wound recovery (Salimi *et al.*, 2022; Wang *et al*., 2024). There is a wealth of knowledge among traditional healers worldwide regarding lesser-known wild plants that can be used to treat burns, wounds, and diabetes (Galiano *et al*., 2004; Kumar *et al*., 2007). The surprising range of diseases that *T. zeylanicum* has been used to cure traditionally suggests that more scientific investigation into the plant's potential medical benefits is needed. According to earlier research, *T. zeylanicum* has anti-diabetic effects which is of interest to individuals with T2DM (Narendra *et al*., 2015). It has been discovered that *T. zeylanicum* contains antioxidants that shield cells and tissues from damaging free radicals produced when our bodies utilise oxygen (Adelakun *et al*., 2009). According to Greenhalgh (2003), Many diabetics experience wounds that heal slowly, poorly, or never at all, and occasionally an opportunistic infection may appear. The activity of white blood cells is hampered by diabetes because it affects how the body makes or reacts to the hormone insulin when blood glucose levels are consistently elevated (Salimi *et al.*, 2022; Wang *et al*., 2024). Accordingly, the body is less equipped to combat bacteria and seal bleeding wounds when the white blood cells are not functioning properly (Greenhalgh, 2003). In addition to impairing circulation, uncontrolled diabetes can make it more difficult for the body to supply nutrients to wounds by slowing down blood flow (Salimi *et al.*, 2022; Wang *et al*., 2024). Consequently, the wounds might not recover or heal slowly (Dinh *et al*., 2011).

Numerous herbs are employed to cure injuries in Malawi. The communities have long used the leaf and root of *T. zeylanicum* to cure injuries. The leaf are consumed as vegetables, but the roots are used to manage diarrhoea. According to Gurib-Fakim *et al*. (1997), the pulverised roots of *T. zeylanicum* are administered externally as an analgesic to wounds and skin. Additionally, it has been discovered that this plant has a low concentration of the poisonous alkaloids supinine (O'Kelly *et al*., 1961). Despite this finding, most of the knowledge regarding *T. zeylanicum's* medicinal value comes from cultures in Africa, Asia, and Australia (Kumar *et al*., 2007), where the plant is accepted as effective and used to cure various illnesses. The plant's phytonutrients may lower the incidence of diabetes, injuries, cancer, and other illnesses like hypertension. Still, additional research must be conducted to fully understand how phytochemicals work and how they can prevent these conditions (Adelakun *et al*., 2009).

Measuring and analysing the antioxidant and phytochemical characteristics of *T. zeylanicum* root, stem, and leaf ethanol and EA extracts are essential to determining the chemicals that may be responsible for the plant extracts' anti-diabetic and antioxidant capabilities. Since Narendra *et al*. (2015) reported that *T. zeylanicum* had anti-diabetic effects, which is of interest to people with T2DM, their research was conducted outside South Africa.

© University of Venda

Developing plant extracts that can treat diabetes, and its related wounds is still crucial to enhancing people's lives by using readily available, less expensive traditional medicinal plants as a substitute for synthetic medications that are known to have a variety of negative effects. However, phytochemicals contained in these medicinal plant extracts are known, while some remain to be elucidated and studied against the selected diabetes markers. The present study aims to *in-vitro* and *in-silico* evaluate phytochemicals and anti-diabetic potentials of the ethanolic and EA extracts of *Trichodesma zeylanicum* found in South Africa, Limpopo province, Vhembe district.

1.9.2. Hypothesis

The ethanol and ethyl acetate (EA) extracts of *T. zeylanicum* root, stem and leaf contain phytochemicals with antioxidant activity, and α-glucosidase, α-amylase, and VEGFR2 inhibitors.

1.9.3. Aim of study

The study's primary goal was to analyse phytochemicals and evaluate the anti-diabetic potential of ethanol and EA extracts of *T. zeylanicum* root, stem, and leaf *in-vitro* and *in-silico.*

1.9.4. Objectives

- ✓ To extract molecules with phytochemical properties from the *Trichodesma zeylanicum* (Burm.f) R.Br. root, stem and leaf using ethanol and EA.
- ✓ To qualitatively evaluate various phytochemicals in ethanol and EA extract from the *T. zeylanicum* root, stem and leaf using TLC methods.
- ✓ To *in-vitro* estimate the antioxidant activity and total phenolic content in ethanol and EA extracts of *T. zeylanicum* root, stem and leaf using biochemical quantitative methods.
- ✓ To identify phytochemicals in ethanol and EA extract from the *T. zeylanicum* root, stem and leaf using LC-qTOF-MS.
- ✓ To *in-silico* study and evaluate α-glucosidase, α-amylase and VEGFR2 inhibitory potentials of selected identified phytochemicals in ethanol and EA extract of *T. zeylanicum* root, stem and leaf using molecular docking methods.
- ✓ To create impartial and protein-protein interactions that incorporate functional and physical interactions using a STRING network.
- ✓ To identify similarities in structure or functions among α-glucosidase, α-amylase and VEGFR2 enzymes using protein sequences comparison through multiple sequence alignment by ClustalW.

© University of Venda

Chapter 2

2. Methodology

This chapter summarises the materials utilised and the experimental procedures to extract metabolites from *T. zeylanicum* root, stem and leaf using ethanol and EA extraction solvents. Metabolite identification methods such as liquid chromatography, quadrupole time of flight mass spectrometry (LC-qTOF-MS), and inhibitory methods such as *in-silico* molecular docking are summarised in this chapter.

2.1. Plant collection.

Trichodesma zeylanicum (Burm.f) R.Br. was collected from the neighbourhood of the University of Venda at a village called Maungani (GPS coordinates: 22.98027° S, 30.42907° E), in Limpopo province, Vhembe district, South Africa, after the project was granted ethical clearance by the Faculty Research Ethics Committee (FREC) of the Faculty of Science, Engineering and Agriculture, University of Venda (Ethical clearance certificate number: FSEA/23/BMY/26). The whole plant specimen was submitted to the UNIVEN herbarium for identification by Prof. Peter Tshisikhawe (specimen voucher number SCTV01). Briefly, *T. zeylanicum* was separated from other plants through its morphological characteristics (Figure 2.1A). The plant was dug and pulled from the soil to be removed with the intact root safely. The lower dried leaves of the plant were removed. The *T. zeylanicum* root and fresh leaves were cut off and separated from the stem. These three different plant organs were washed with distilled water separately and blotted on a paper towel (Figures 2.1A-C). After being allowed to dry at room temperature, the plant root, fresh leaf, and stem were ground into a powder in a blender.



Figure 2.1: *Trichodesma zeylanicum* (Burm. f) R.Br. different organs. **(A)** Whole plant with leaf, **(B)** root, and **(C)** stem (Own image, May 2023)

© University of Venda

2.2. Preparation of plant extract.

Ethanol and EA extracts of *T. zeylanicum* root, stem, and leaf were prepared following the procedure reported by Tshidino and Montsho (2017). Using a weighing scale, 10 g of the dried, ground-up root, stem, and leaf were weighed separately and transferred to clean, labelled 500 mL sample storage bottles with lids. Each 500 mL sample storage bottle was filled with 100 mL of ethanol and 10 g of the ground-up root, stem, and leaf, which were mixed thoroughly. After being wrapped in foil, the storage bottles were placed on a small orbital shaker (LASEC STUART, Poland, EU) and shaken at 130 rpm for three (3) hours. The samples were filtered using Whatman filter paper number 1 (diameter 150 mm) and collected in clean, labelled 500 mL storage bottles. After being securely sealed, the sample storage bottles were put in the refrigerator. The remainder of the plant residues in storage bottles were mixed with 100 mL of ethanol extraction solvent. After covering the mixture with foil was put on the same shaker and shaken at the same speed overnight. After filtering with a Whatman filter paper, the mixture was placed in 500 mL storage bottles with the initial filtrates. The filtrates of the combined ethanol extract were transferred into a round-bottom flask that had been weighed. To eliminate ethanol, the plant extracts were concentrated for 15 minutes at 78°C in a rotary evaporator (DüZGüNES 2003; Bnyan *et al*., 2019). The dried extracts were kept in the round-bottom flask below in Figure 2.2.

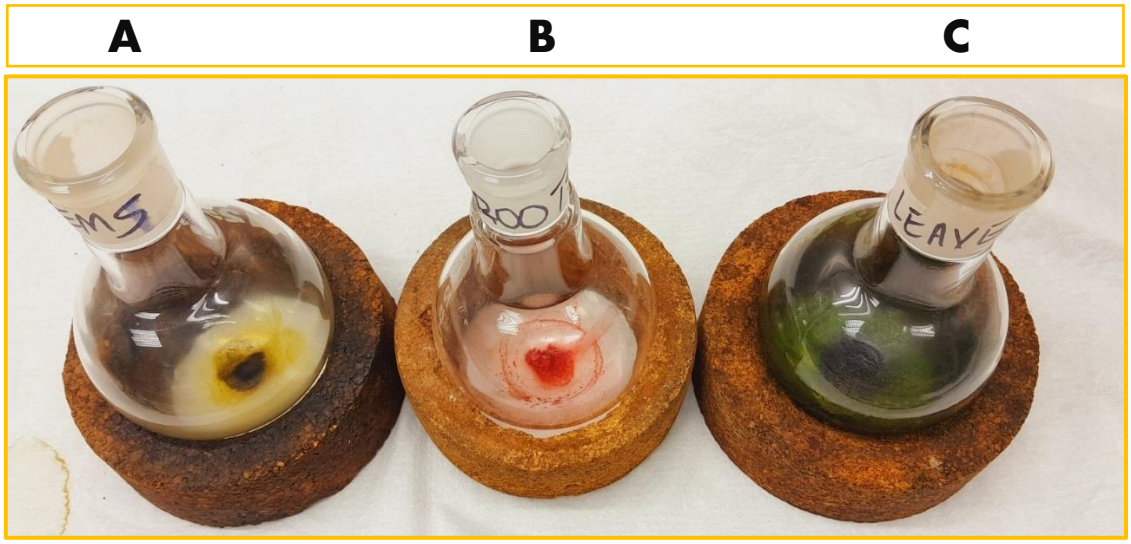


Figure 2.2: *T. zeylanicum* dried extract. (A) stem, (B) root, and (C) leaf (Own image, July 2023).

The round-bottom flask containing the sample was put inside a fume hood to evaporate the remaining ethanol. The dried samples were weighed on a weighing balance to determine the plant extract yield using the gravimetric method (Alamgir *et al*., 2018). The small volumes of ethanol were added into the flask containing root, stem, and leaf concentrated extracts to dissolve them, and they were kept in 1,5 mL Eppendorf tubes as aliquots (2 mg and 10 mg) in a -20°C freezer for further phytochemical analysis. The same procedure was followed for plant extraction using EA, except that plant extracts were concentrated in a rotary evaporator at

© University of Venda

77,1°C to remove EA. EA plant extracts were stored in 1,5 mL Eppendorf tubes as aliquots (2 mg and 10 mg) in a -20°C freezer for further phytochemical analysis.

2.3. *In-vitro* phytochemical qualitative analysis through chemical tests.

2.3.1. Test for Steroids.

Ethanol and EA root, stem, and leaf extracts of *T. zeylanicum* (2 mg) were dissolved separately in 1 mL of their respective extraction solvent to a 2 mg/mL concentration. A mixture of 250 µL sulfuric acid and 250 µL chloroform was added to the extract solution (245 µL) to observe the presence of the steroids (Pandey *et al*., 2014). Thereafter, blue-green, pinkish, yellowish-brown, or reddish-brown colours were anticipated in both EA and ethanol extracts, which indicates the presence of steroids (Iqbal *et al*., 2015; Zulkifli *et al*., 2012).

2.3.2. Test for terpenoids.

Root, stem, and leaf extracts (2 mg) were dissolved separately in 1 mL of their respective extraction solvent to a 2 mg/mL concentration. The extract solution (245 µL) was mixed with 250 µL chloroform and 150 µL sulfuric acid to observe the presence of terpenoids (Ayoola *et al*., 2008). A reddish-brown colour was anticipated in ethanol and EA extracts, indicating the presence of terpenoids (Das *et al*., 2014; Iqbal *et al*., 2015).

2.3.3. Test for coumarins.

Root, stem, and leaf extracts (2 mg) were dissolved separately in 1 mL of their respective extraction solvent until a concentration of 2 mg/mL. 375 µL of 10% sodium hydroxide (NaOH) was combined with 245 µL of the extract solution to observe the presence of coumarins (Skehan *et al*., 1990). A yellowish colour was expected in observation, indicating coumarins' presence (Ali *et al*., 2018; Le *et al*., 2021).

2.3.4. Test for phenols.

Root, stem, and leaf extracts (2 mg) were dissolved separately in 1 mL of their respective extraction solvent up to a 2 mg/mL concentration. A solution of root, stem, and leaf extract (245 µL) was mixed with 245 µL of 5% ferric chloride solution, and three drops were added to observe the presence of phenols (Joshiet *et al*., 2018). Thereafter, blue, violet, green, and reddish-brown colours were anticipated in EA and ethanol extracts, implying the presence of phenolic chemicals. Without phenolic chemicals, the mixture solution remains yellow (Archana *et al*., 2012; Khanam *et al*., 2015).

2.3.5. Test for alkaloids.

Root, stem, and leaf extracts (2 mg) were dissolved separately in 1 mL of their respective extraction solvent to a 2 mg/mL concentration. Six drops of the Dragendorff reagent were added to 245 µL of root, stem, and leaf extract to observe the presence of the alkaloids (Pandey *et al*., 2014). In the presence of the alkaloids, orange and orange-red colours were expected in observation in EA and ethanol extracts, which designates the presence of alkaloids (Arya *et al*., 2012; Kancherla *et al*., 2019).

© University of Venda

2.3.6. Test for saponins (Foam test)

Root, stem, and leaf extracts (2 mg) were separately diluted to a concentration of 2 mg/mL in 1 mL of their respective extraction solvent. Distilled water (300 µL) was added to 245 µL of root, stem, and leaf extract. The test tubes were placed in hot water for 10 minutes. Thereafter, the mixture was shaken vigorously for a 15-minute period. A few drops of olive oil were dispensed to observe the presence of saponins. The persistence of foam produced after 15 minutes implies the existence of saponins (Tepal, 2016).

2.3.7. Test for tannins

Root, stem, and leaf extracts (2 mg) were each dispersed in 1 mL of their respective extraction solvent to a 2 mg/mL concentration. Three drops of a solution containing 5% ferric chloride were introduced into 245 µL of root, stem, and leaf extract solution to observe the presence of tannins (Joshiet *et al*., 2018). Thereafter, a greenish-black or dark blue colour was anticipated to confirm the existence of tannins in both EA and ethanol extracts. Furthermore, in the absence of tannins and phenolic chemicals, the mixture solution remains yellow (Ali *et al*., 2018).

2.3.8. Test for glycosides

Root, stem, and leaf extracts (2 mg) were separately diluted in 1000 µL of their respective extraction solvent to reach a 2 mg/mL concentration. Approximately 1 mL of sulfuric acid was dispensed into the tubes containing 245 µL of root, stem, and leaf extract solution to observe the existence of glycosides. A reddish-brown was anticipated in the presence of glycosides (Khanam *et al*., 2015).

2.3.9. Test for flavonoids

Root, stem, and leaf extracts (2 mg) were diluted separately to a 2 mg/mL concentration in 1 mL of their respective extraction solvent. 245 µL of root, stem and leaf extract solution was exposed to a small amount of ferric chloride solution. The solution's intense green, blackish-red, or dark brown colour was expected to confirm the presence of flavonoids (Pooja and Vidyasagar, 2016).

2.3.10. *In-vitro* qualitative phytochemical antioxidant analysis using TLC.

The ethanol and EA extracts of *T. zeylanicum* (Burm.f.) R.Br. root, stem and leaf were subjected to TLC studies following the procedure outlined by Gujjeti and Mamidala (2013). Using scissors, 20 x 20 cm TLC silica gel 60 F254 plates (Germany) measuring 10 cm in length and 5 cm in width were cut. 1 cm from the bottom, the plates were gently marked with a pencil. Using a micropipette, the plant extracts (10 µL) were spotted on the pencil-marked bottom line of the TLC plates. The positive standards (2 µL, 1mg/mL) of rutin, gallic acid, and ascorbic acid were used in this study. Four polarity-varying mobile phases, CEF (chloroform: ethyl acetate: formic acid; 10:8:2; v/v/v), EMW (ethyl acetate: methanol: water; 20:2,7:2; v/v/v), TAF (toluene: acetone: formic acid; 9:18:3; v/v/v) and ED (ethyl acetate: dichloromethane; 9:20,7; v/v, were employed to develop the chemicals spotted on the TLC plate.

© University of Venda

Following the compound's development, the plates were taken out and air-dried for roughly 15 minutes. The DPPH reagent was sprayed onto the prepared TLC plates to observe the phytochemical antioxidant components in the ethanol and EA extracts of *T. zeylanicum* root, stem, and leaf. The fume hood was used when applying the spray reagents to the TLC plates.

2.3.11. Phytochemicals fingerprinting on thin-layer chromatography.

As described in section 2.3.10, the TLC plates were prepared and developed. Before and during the application of developing reagents, the produced TLC plates were viewed and monitored under UV light at 365 nm long-wave ultraviolet (Biradar and Rachetti, 2013). The plates were sprayed with DPPH reagent for visualising phytochemical antioxidant activity, with ferric chloride for visualising phenols and with Vanillin-sulfuric acid-sulfuric acid reagent to detect a wide range of phytochemicals, including flavonoids, phenolic compounds, and alkaloids. After spraying the developed TLC plates with vanillin-sulfuric acid-sulfuric acid reagent, compounds were visualised by incubating the TLC plates at 110°C in the PROLAB incubator for about 15 minutes. A pencil was used to circle the compounds that were visualised. The movement of the active compounds was expressed by the retention factor [RF] (Bate-Smith *et al*., 1950). $\text{Retention factor} = \frac{d\ solute}{d\ solvent}$, wherein D Solute is the distance travelled by the solute and D Solvent is the distance travelled by the solvent.

2.4. Quantitative antioxidant assays

2.4.1. DPPH-radical scavenging assay

The plant extracts were examined for their ability to scavenge DPPH radicals in the manner previously reported (Tshidino and Montsho, 2017; Yurchenko *et al*., 2020), using 0.004% (w/v, 100 mM) DPPH (Sigma-Aldrich, Germany) prepared in absolute ethanol. Pure ethanol was used as a negative control for ethanol plant extracts, EA was used as a negative control for EA plant extracts, and ascorbic acid was used as a positive control for both experiments. Briefly, 10 mg/mL of the stock solutions (plant extracts and positive control) were prepared in ethanol (EtOH) for ethanol plant extracts, whereas 0 mg/mL of the stock solutions (plant extracts and positive control) were prepared in EA for EA plant extracts. In contrast, the positive control was prepared in ethanol for the EA extracts. The determined volumes of the solvents and stock solutions were then added to 1.5 mL microcentrifuge tubes to dilute them into various concentrations ranging from 100-1000 µg/mL, as shown in Table 2.1.

© University of Venda

Table 2.2: Preparation of different concentrations of plant extracts and controls for the DPPH-scavenging assay (Tshidino and Montsho, 2017).

Control/plant extract Concentrations (µg/mL)	**10 mg/mL Plant extract or ascorbic acid stock solution (µL)**	**Respective extraction solvent (µL)**	**Final concentration (µg/mL)**
0	0	1000	0
100	10	990	5
200	20	980	10
400	40	960	20
600	60	940	30
800	80	920	40
1000	100	900	50

Chronologically, (10 µL) of the blank, followed by the ethanol and EA plant extracts ranging from 0-1000 µg/mL, and the ascorbic acid ranging from 0-1000 µg/mL, were added in triplicate into the wells of a 96-microwell plate (Table 2.1). The prepared 0.004% DPPH (190 µL) was added to the blank, and the solutions were placed into the 96-microwell plate using the multi-channel pipette and mixed gently. The mixes were incubated at room temperature in the dark for half an hour. Furthermore, the mixtures were shaken (300 rpm) before reading the absorbance using the microplate reader. The resultant solution's absorbance was measured at the wavelength (λ) of 520 nm with a 96-microwell plate reader (BMG Labotech Lansec). The data were presented as the mean and standard deviation (SD) following analysis. Three iterations of the experiment were conducted. The following formula was used to determine the free radical scavenging activity: DPPH-radical scavenging activity (RSA) = $\frac{Abs\ of\ control - Abs\ of\ sample}{Abs\ of\ control}$ x 100, where: Abs of control is the absorbance without samples, and Abs of sample is the absorbance of the test sample. The results were presented as the averages of three separate analyses.

2.4.2 Determination of total phenolic content

The total amount of phenols in the ethanolic and EA extracts of *T. zeylanicum* was estimated using the Folin-Ciocalteau method described by Singleton and Rossi (1965). Briefly, 1 mg/mL of Gallic acid stock solution was prepared in Ethanol. Ethanol plant extract (10 mg/mL) was prepared in ethanol, whereas EA plant extract (10 mg/mL) was prepared in EA. The ethanol stock solutions were diluted 5x, whereas the EA stock solutions were diluted 10x, except that the leaf extract was diluted 25x. A total of 7.5 µL of the blanks, standard and diluted plant extracts were pipetted in triplicate into a 96-microwell plate, starting with the blanks. The diluted (10x) Folin reagent was prepared in distilled water and covered with foil.

© University of Venda

The diluted Folin-Ciocalteau reagent (120 µL) and distilled water (54 µL) were added to the blanks and the solutions into the 96-microwell plate using the multi-channel pipette. The plate was gently shaken to combine the solutions, and it was then allowed to sit at room temperature for 5 minutes in the dark. Thereafter, 75% sodium carbonate (120 µL) was added to the wells and gently mixed at medium continuous speed for 1 minute. Then, the mixture was allowed to sit at room temperature for half an hour in the dark. The 96-microwell plate was subjected to the microplate reader (BMG Labotech Lansec). Furthermore, the mixture was shaken at 300 rpm before reading the absorbance using the microplate reader at the wavelength (λ) of 765 nm. The experiment was repeated three times. Gallic acid dilutions were used as a standard for calibration. The total phenolic contents were expressed as µg Gallic Acid Equivalents (GAE) per milligram dried plant extract (µg GAE/mg dried extract) following the method utilised by Singleton and Rossi (1965).

2.5. *In-silico* phytochemical analysis and anti-diabetic potentials of EA and ethanol extracts from different organs of *T. zeylanicum*

2.5.1 LC-qTOF-MS analysis of EA and ethanol extracts from different organs of *T. zeylanicum*

Ethanol and EA plant extracts phytochemical analyses were conducted on a liquid chromatography - quadrupole time-of-flight tandem MS instrument (LCMS-9030 qTOF, Shimadzu Corporation, Kyoto, Japan), with a Shim-pack Velox C18 column (100 mm × 2.1 mm with the particle size of 2.7 µM) (Shimadzu Corporation, Kyoto, Japan) was used. The column oven was set to 55°C, and the analytes were separated over a 53-minute binary gradient, as described by Ramabulana *et al*. (2021). The chromatographic eluents were further analysed in both positive and negative modes using the qTOF high-definition mass spectrometer under the following circumstances: Heat block temperature of 400°C, detector voltage of 1.8 kV, interface voltage of 4.0 kV, nebulization and 3 L/min of dry gas flow, 280°C for the DL temperature, and 42°C for the flight tube temperature. Using sodium iodide (NaI) as a calibration solution allowed for the monitoring of high mass accuracy. Additionally, samples were generated in three biological duplicates and will be examined in triplicate (for each biological replication), as stated in Ramabulana *et al*. (2021). The analytical system was examined using blank samples (50% aqueous methanol) for background contamination, interferences, or sample carryovers. The batch was started and finished with injections of quality control (QC, pooled) samples to guarantee system equilibration. To track and address changes in the instrument response, the sample selection was made at random, and the QC sample was examined after every fifth injection. The data was subjected to SIRIUS for annotation.

A fingerprinting method called SIRIUS CSI-FingerID predicts chemical fingerprints by using the MS^2 spectra and the fragmentation trees produced by SIRIUS as input (Duhrkop *et al*., 2015). According to Duhrkop *et al*. (2015), CSI: FingerID, a multiple kernel learning (MKL) technique coupled with support vector machines (SVMs), was utilized for annotation predictions.

© University of Venda

According to Shen *et al*. (2014), SVMs were used to predict whether a specific property will be present in the fingerprint of an unknown molecule. Each dataset pair's similarities were calculated using multiple fragmentation tree kernels and various spectrum kernels. After that, the embedded data was examined for patterns using statistics, geometry, and linear algebra (Hofmann *et al*., 2008). Since Sirius employs CSI: FingerID as a web service, no local computer resources are needed for computations. To distinguish between compounds that display a specific fingerprint feature and those that do not, SVMs are trained on kernel similarities. CSI: FingerID and FingerID (Heinonen *et al*., 2012) were contrasted. CSI: FingerID employed fragmentation trees to estimate the fragmentation. The trees were defined as directed graphs, with the formulas of the parent molecule's sub-molecules at the other nodes and the candidate molecular formula at the root node (Dührkop *et al*., 2014).

2.5.2. Molecular docking (*In-silico*) of α-glucosidase, α-amylase and VEGRF2 against selected identified compounds.

The molecular docking learning was conducted to assess the *in-silico* binding affinities of selected identified phytochemicals in ethanol and EA extracts from the root, stem, and leaf of *T. zeylanicum* against α-glucosidase, α-amylase, and VEGFR2. The docking was done based on the approach outlined by (Ibrahim *et al*., 2015). Acarbose and sorafenib were utilised as reference compounds. In short, the RCSB Protein Data Bank database (https://www.rcsb.org/) was utilised to retrieve and preserve the homologous models of the enzymes VEGRF2, α-glucosidase, and α-amylase in PDB format. The enzymes were purified by eliminating undesirable components (water, heteroatoms) using the Discovery Studio visualizer software. The finished protein containing the active site was supplemented with polar hydrogen atoms and stored as a PDB file. Several molecular structures, or ligands, were obtained from PubChem (https://pubchem.ncbi.nlm.nih.gov/) (Kim *et al*., 2021). The PyRx Virtual screening tool was employed to dock proteins and ligands. After being reduced, the ligands were changed to AutoDock ligands. Additionally, molecular docking computations were performed using AutoDock Vina Wizard (Morris *et al*., 2009). A blind docking technique was employed to anticipate a protein's ligand binding location (Dallakyan and Olson, 2015). The following grid coordinates were used to create a grid box: x = 7.9088 A, y = 60.4522 A, and z = 19.7871 A for the centre, and x = 67.2453 A, y = 72.6154 A, and z = 56.8457 A for the dimensions, with an exhaustiveness of 8. The generated grid box encapsulated the whole protein surface, enabling sufficient binding site identification. The protein structure was combined with ligand conformations with the greatest docking grade and RMSD = 0.0 A using Discovery Studio. The PDB format was then saved for additional analysis (Pettersen *et al*., 2004).

2.5.3. Molecular networking procedure

α-Glucosidase, α-amylase, and VEGFR2 were subjected to STRING (Search Tool for the Retrieval of Interacting Genes/Proteins) (https://string-db.org/) for the molecular networking procedure as outlined (Szklarczyk *et al*., 2025).

© University of Venda

STRING predicted protein-protein interactions by integrating together multiple sources of evidence, including experimental data, computational predictions, and knowledge from existing literature. From curated databases of experimentally validated PPIs, STRING aggregated known interactions. These include data from high-throughput experiments like yeast two-hybrid assays, affinity purification-mass spectrometry, or co-immunoprecipitation. STRING included computationally predicted interactions based on gene co-expression patterns, phylogenetic co-occurrence, and gene fusion events, which point to a functional relation if two separate genes in one species appear as a single fused gene in another. Included were interactions inferred from text mining, scanning the scientific literature for co-mentions of proteins within relevant contexts. STRING considers functional associations based on pathways, shared protein domains, and genetic linkages. Each of these sources of interaction was assigned a confidence score that specifies its prediction confidence level. Afterwards, STRING integrated them into a network in which nodes represented proteins and edges represented interactions, the interpretation of which was driven by their thickness or confidence level. By sorting through such a multitude of data types, STRING could present a more global, probabilistic interaction model.

2.5.4. Protein-protein sequence alignment

α-Amylase was subjected to ClustalW (https://www.genome.jp/tools-bin/clustalw) for multiple sequence alignment with α-glucosidase and VEGFR2 using the method employed by (Vasistha *et al*., 2025). ClustalW performed multiple sequence alignment (MSA) using a progressive alignment approach that follows a three-step process: (a) sequence comparison, (b) guide tree construction, and (c) progressive alignment. ClustalW calculates pairwise sequence similarities using a PAM and BLOSUM scoring matrix, typically through a global alignment algorithm. This distance matrix, consisting of the pairwise distances, later became the basis for constructing a guide tree via the neighbour-joining method. The guide tree led to the alignment order. The two most closely related sequences were aligned first, with progressively divergent sequences incorporated laterally through the tree about them. In this way, the process progressively aligns the two most similar sequences, adding additional sequences or existing alignments according to the tree structure. For the alignment, ClustalW assigned position-specific gap penalties, whereby a gap in a conserved region received a greater penalty than in variable regions, to enhance the accuracy of the alignment. The sequence weights were also integrated so that the influence of the overrepresented sequences would be restricted. The further a sequence moved, the less important it would become in giving undue emphasis to its dataset during the entire procedure, in which ClustalW iterative adjustments of gap penalties refined the alignment, given all alignments for consistency. This results in an alignment in which homologous residues are aligned across all input sequences, enabling downstream analyses of phylogenetic tree construction, motif discovery, and evolution studies.

© University of Venda

2.5.5. Statistical analysis

Results are reported as mean ± standard deviation (SD). The comparisons between groups were established with repeated measures two-way analysis of variance (ANOVA), followed by post hoc analysis, followed by Tukey test using GraphPad Prism version 10.4.1 (627). *P*-values <0.05 were identified as statistically significant.

© University of Venda

Chapter 3

3. Results and Discussion of EA and ethanol extracts from different organs of *T. zeylanicum*.

This chapter presents a detailed discussion of the data obtained from *T. zeylanicum* ethanol and EA extracts. Every outcome was acquired using the techniques that were employed. Various tables and figures demonstrate the outcomes of each objective of the study.

The primary aim in the present study was to assess phytochemicals and analyse the anti-diabetic potentials of EA and ethanol extracts from *T. zeylanicum* root, stem, and leaf *in-vitro* and *in-silico*. Furthermore, this was achieved by *in-silico* investigation and evaluation of inhibitory potentials of selected identified phytochemicals in EA and ethanol extracts of *T. zeylanicum* root, stem and leaf against α-glucosidase, α-amylase and VEGFR2. Every outcome was acquired using the techniques that were employed. Various tables and figures demonstrate the outcomes of each methodology and goal.

3.1. Percentage yields of EA and ethanol extracts from *T. zeylanicum* (Burm. f) R. Br. root, stem, and leaf.

Following the rotary evaporator procedure, the plant extract yield was calculated by deducting the masses of the round-bottom flasks containing the plant organ extracts from the masses of the flasks without the extracts (Alamgir *et al*., 2018). Under the ethanol solvent, the root extract exhibited a mass of 0,59 g (590 mg), the stem extract exhibited a mass of 0,58 g (580 mg), and the leaf extract exhibited a mass of 0,67 g (670 mg). Under EA solvent, the root extract showed a mass of 0.1 g (100 mg), the stem extract showed a mass of 0.1 g (100 mg), and the leaf extract showed a mass of 0.26 g (260 mg). Briefly, 10 g of pulverised, weighed ethanol and EA plant root, stem, and leaf extracts served as the theoretical starting materials. The following formula was used to express the extraction percentage yield: Percentage (%) yield = $\frac{Actual\ yield}{Theoretical\ Yield}\ x\ 100$,wherein the actual yield refers to the quantity of product achieved from a chemical reaction, while the theoretical yield denotes the greatest possible quantity of product that might be produced according to stoichiometric calculations (Alamgir *et al*., 2018). In the case of ethanol root, stem, and leaf extracts, the percentage yields were 5,9% (59 mg), 5,8% (58 mg), and 6,7% (67 mg), respectively, as presented below. In contrast to EA extracts, the root and stem extracts exhibited a percentage yield of 1% (10 mg), while the leaf extract exhibited a percentage yield of 2,6% (26 mg) as presented (Figure 3.1). These findings are in agreement with the previous study that reported a high ethanol percentage yield (18%) in comparison with the EA percentage yield (12%) of fresh dry *C. zeylanicum* extracts (Adarsh *et al*., 2020).

© University of Venda

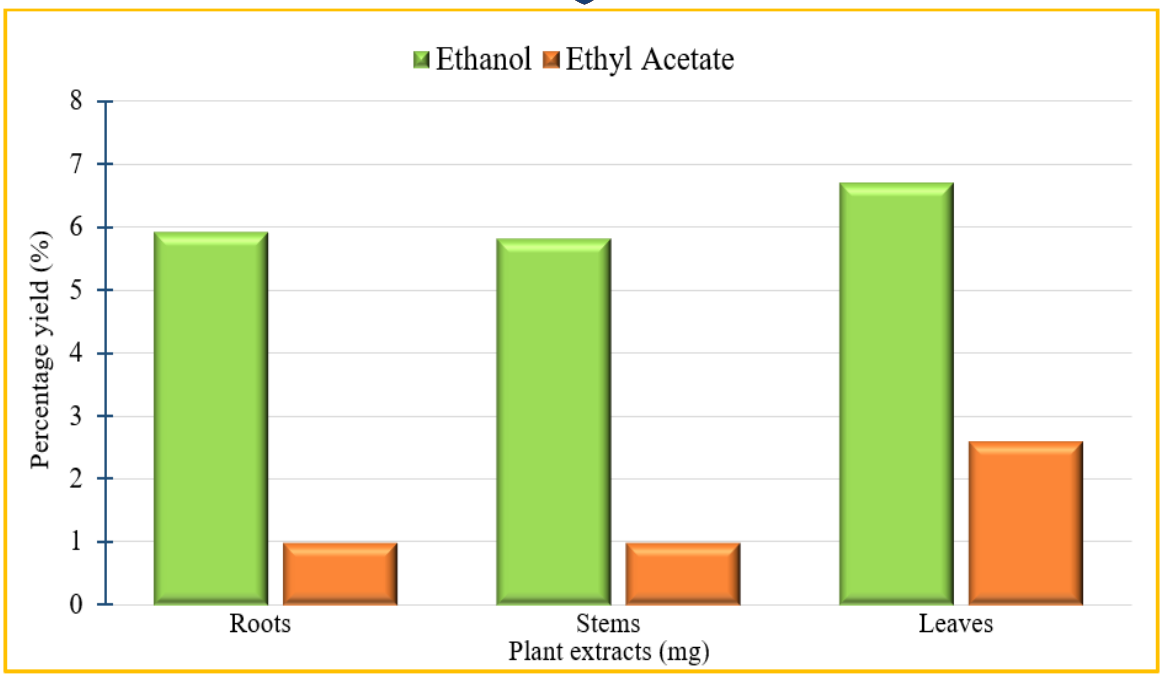


Figure 3.1: The percentage yields of ethanolic and EA extracts from different organs of *T. zeylanicum*.

The extractions were not done in triplicate due to the nature of the data being collected, the experiment being conducted and the available resources. Furthermore, the results were not suitable for statistical analysis. In comparison to the EA solvent, it was commonly observed that ethanol solvent showed its potential to extract more bioactive chemicals from *T. zeylanicum* root, stem, and leaf extracts, as both percentage yields are high. As previously reported, ethanol is an effective solvent for extracting a wide range of compounds because it is miscible with water and can dissolve polar and nonpolar molecules (Lefebvre *et al*., 2021). Due to its moderate polarity, ethanol is regarded as a highly effective solvent for the extraction of a variety of plant phytochemicals, mainly phenolic compounds such as flavonoids and phenolic acids, because it can dissolve both polar and non-polar compounds found within the plant tissue (Lefebvre *et al*., 2021). Given that the ethanol and EA leaf extracts had high percentage yields, the leaf contained more phytochemicals than the other plant organs. While the stem and leaf were extracted with ethanol, yielding nearly identical percentages, those extracted with EA showed the same percentage yields. However, ethanol extracted more phytochemicals from all three plant organs when compared with EA (Figure 3.1).

3.2. Qualitative phytochemical analysis of EA and ethanol extracts from different plant organs

The thin-layer chromatography was used to analyse the phytochemicals in EA and ethanol extracts from *T. zeylanicum* organs. The bioactive phytochemicals migrated differently according to their polarity when four distinct developing mobile phases were employed. Phytochemical tests are of immense importance in the estimation of bioactive compounds present in plants that possess medicinal applications. These tests helped in discovering naturally occurring antioxidants (phenols) and other therapeutic agents (terpenoids, saponins, glycosides, flavonoids, steroids, coumarins, alkaloids, and tannins), which find application in pharmaceuticals.

© University of Venda

3.2.1. TLC chromatograms of EA and ethanol plant extracts visualised under normal light.

Overall, the mobile phases, ED and CEF, respectively, showed a higher capacity for migrating and displaying the metabolites than the other prepared mobile phases before the plates were sprayed with visualising reagents, shown in Figure 3.2A. The phytochemicals extracted from *T. zeylanicum* employing ethanol and EA as extraction solvents were analysed using thin-layer chromatography after developing them in four mobile phases with varying polarities (Figures 3.2A and B). The findings are unique since no study has been conducted that shows TLC chromatograms of ethanol and EA leaf, stem, and root extract of *T. zeylanicum.* The *T. zeylanicum* plant is of interest as there are few ancient studies done. Thus, the findings of *T. zeylanicum* EA and ethanol extracts are serving as a novel.

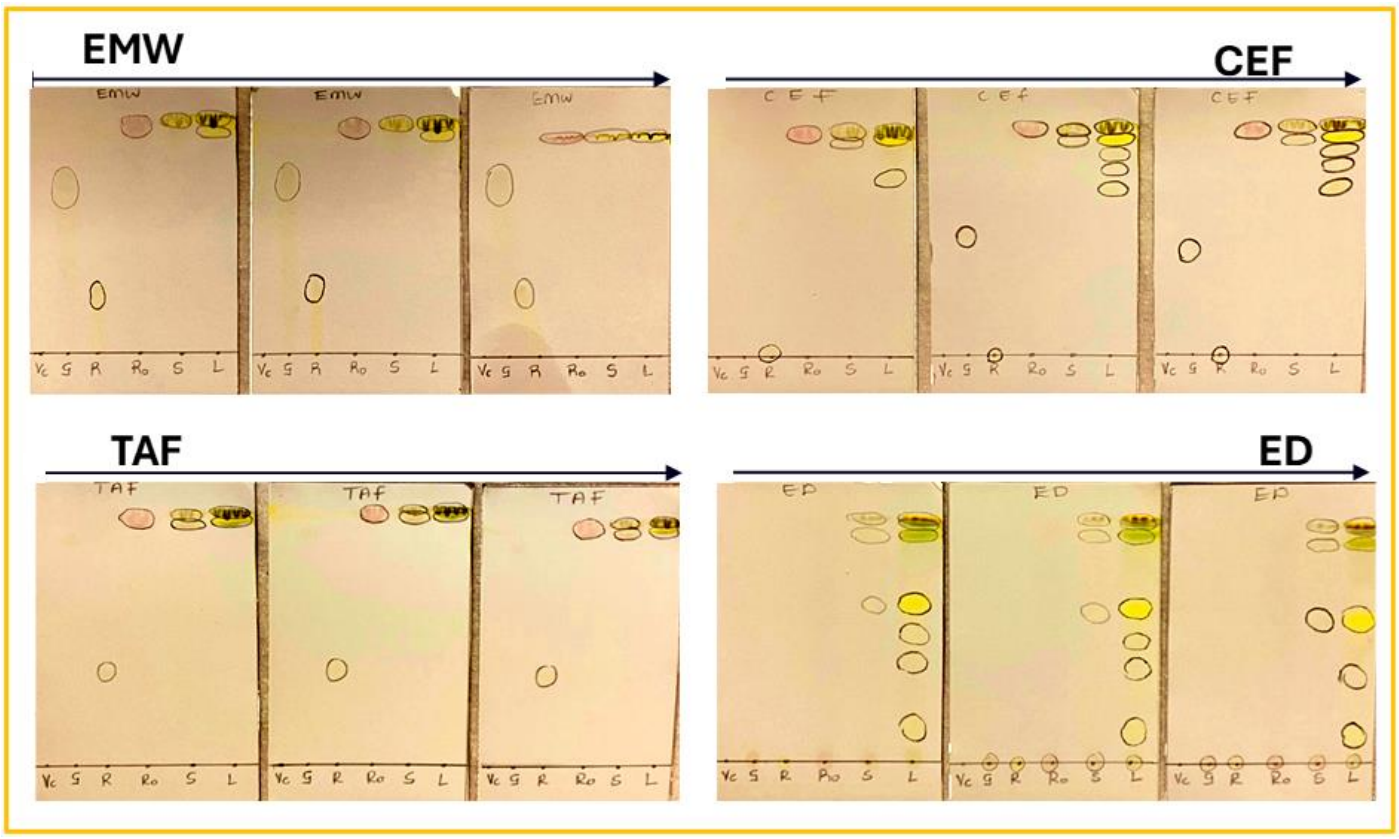


Figure 3.2A: TLC chromatograms of EA plant extracts developed in four mobile phases, EMW (ethyl acetate: methanol: water), CEF (chloroform: ethyl acetate: formic acid), TAF (toluene: acetone: formic acid), and ED (ethyl acetate: dichloromethane) and visualised under normal light before spraying with detection reagents. Vc (Vitamin C/Ascorbic Acid); G (Gallic acid); R (Rutin); Ro (Root extract); S (Stem extract); L (Leaf extract).

© University of Venda

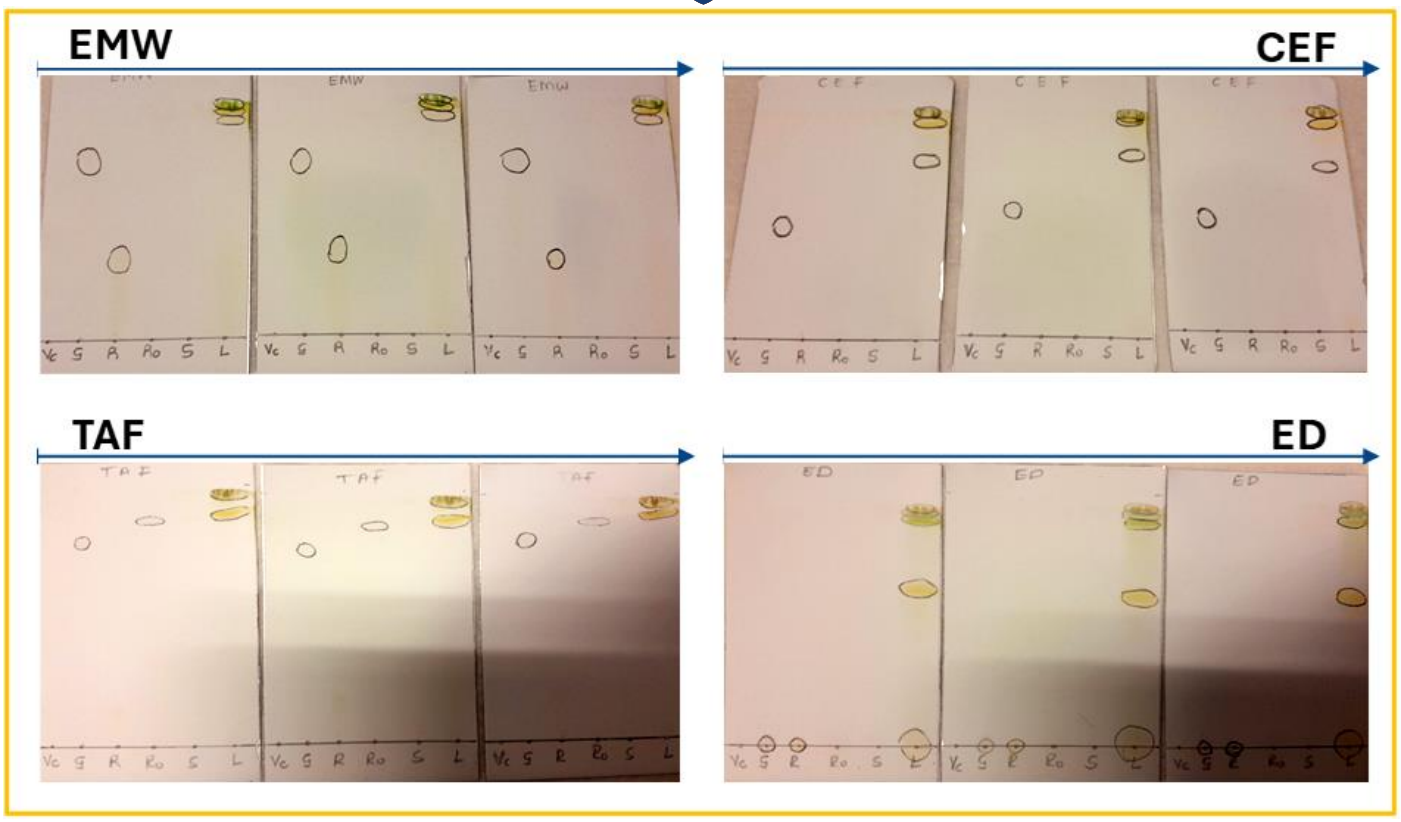


Figure 3.2B: TLC chromatograms of ethanol plant extracts developed in four mobile phases, EMW (ethyl acetate: methanol: water), CEF (chloroform: ethyl acetate: formic acid), TAF (toluene: acetone: formic acid), and ED (ethyl acetate: dichloromethane) and visualised under normal light prior spraying with detection reagents. Vc (Vitamin C/Ascorbic Acid); G (Gallic acid); R (Rutin); Ro (Root extract); S (Stem extract); L (Leaf extract).

For the EA plant extracts (Figure 3.2A), considering that more migrating metabolites are often found in the mobile phases ED and CEF, the foregoing data confirm that the EA leaf extract contains a higher number of phytochemicals than the EA extracts from other plant organs (Figures 3.2A, 3.2B, 3.4A and 3.4B). Compared to the other mobile phases, the ED mobile phase developed more compounds from the EA leaf extract when visualised under normal light before spraying with reagents (Figure 3.2A). The EA leaf extract colour representation in mobile phases is similar, especially on ED and CEF, demonstrating the extraction's dependability (Figure 3.2A). ED mobile phase is described as moderately polar, while both solvents have polar characteristics. EA is slightly more polar than dichloromethane (Mol *et al*., 2003). The presence of multiple hydroxyl groups (-OH) is responsible for the polarity of gallic acid (the phenolic), rutin (a flavonoid), and ascorbic acid (butenolide), thus explaining their solubility in polar solvents such as water; however, rutin has much lower solubility in water than the other two compounds (Seal *et al*., 2016). So, despite its extremely promising potential, ED was unable to migrate the controls due to the polarity. Therefore, the compounds found do not represent either of the controls used in this study, and this further suggests the compounds are nonpolar. Additionally, several compounds were examined following the spot detection technique employed (Figure 3.4A).

© University of Venda

Under ethanol solvent (Figure 3.2B), as anticipated, the mobile phases EMW and TAF appear to have migrated a greater number of nonpolar chemicals found in the ethanol leaf extract, which are coloured green, yellow, and light yellow, respectively, from the top to bottom. The same was observed with TAF, except that just two yellow-noted chemicals were detected in the ethanol leaf extract. According to Kagan *et al*. (2014), compounds such as alkenes, alkynes, and some carbonyl compounds exhibit these colours. Compared to the other mobile phases, the ED mobile phase transported more compounds from the ethanol leaf extract, and it also moved the polar leaf extract. The ethanolic leaf extract colour representation in both mobile phases is similar, demonstrating the extraction's dependability. Remarkably, the mobile phases only appeared to have moved the ethanol leaf extract, except in TAF, which also migrated the ethanol root extract. Of the four mobile phases considered, ED has demonstrated the ability to move and exhibit more plant compounds before the application of spot detection techniques (Figures 3.2A and B). Despite its extremely promising potential, ED was able to migrate the controls. Therefore, the compounds observed under normal light do not appear to represent either of the controls (Figures 3.2A and B).

3.2.2. TLC chromatograms of EA and ethanol plant extracts visualised under long UV light.

Figures 3.3A and B display the comparative TLC profile of EA and ethanol extracts under the 365 nm long-wave ultraviolet light used to observe and monitor the various substances that, aside from the other lights, may be spotted under the impact of ultraviolet light alone. The 365 nm long-wave ultraviolet was also used to view the compounds' fluorescence and the colours they display (Figures 3.3A and B).

On EA extracts, Figure 3.3A, considering that when compared to the reagents applied, vanillin-sulfuric acid showed the greatest potential for picking established compounds, it was generally noticed that throughout the mobile phases (EMW, CEF, TAF and ED) the compounds displayed the same fluorescence, rutin being lime green (Figure 3.3A). Upper EA root, stem and leaf compounds exhibited purple, pink, and dark pink, respectively. On DPPH, controls remained yellowish except on the ED mobile phase, wherein its fluorescence is blue surf. The upper EA compound colour fluorescence presented pink to red on EA stem and leaf extracts, whereas on the root, it is yellowish, as shown in Figure 3.3A. On DPPH-CEF, there was a noticeable compound from EA leaf extract, which displayed a blue surf colour, unlike other compounds on DPPH, which appeared to be like gallic acid on ED, which can imply that the compound can probably be similar to gallic acid (Figure 3.3A). Under the ferric chloride reagent, the controls remained blackish, whereas the upper compounds' hue fluorescence was noticed to be pinkish to reddish on the EA stem and leaf extract (Figure 3.3A). The findings concur with those that Shandukani *et al*. (2018) had previously published (Figure 3.3A). The findings are unique since no study has been conducted that shows TLC chromatograms of ethanol and EA leaf, stem, and root extract of *T. zeylanicum.*

© University of Venda

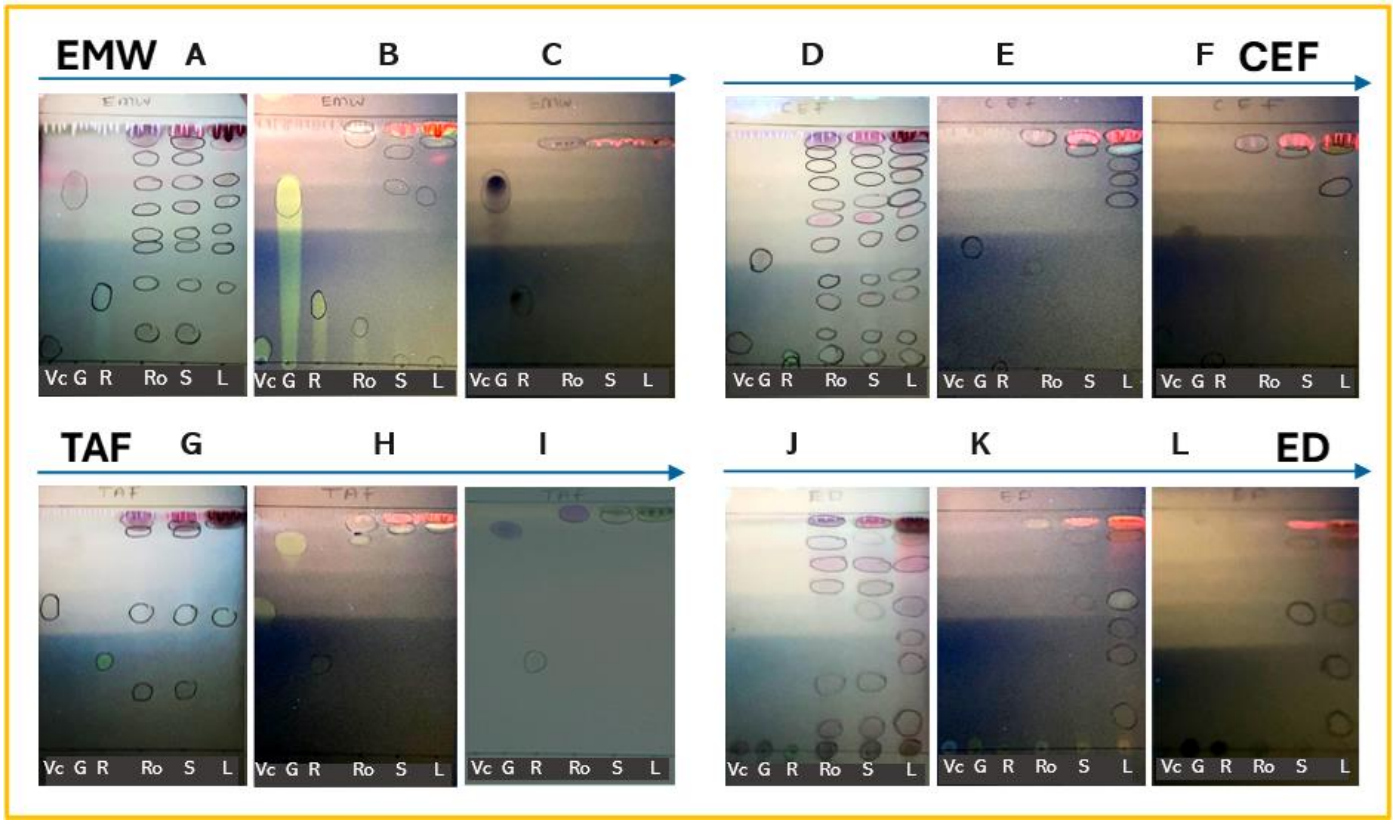
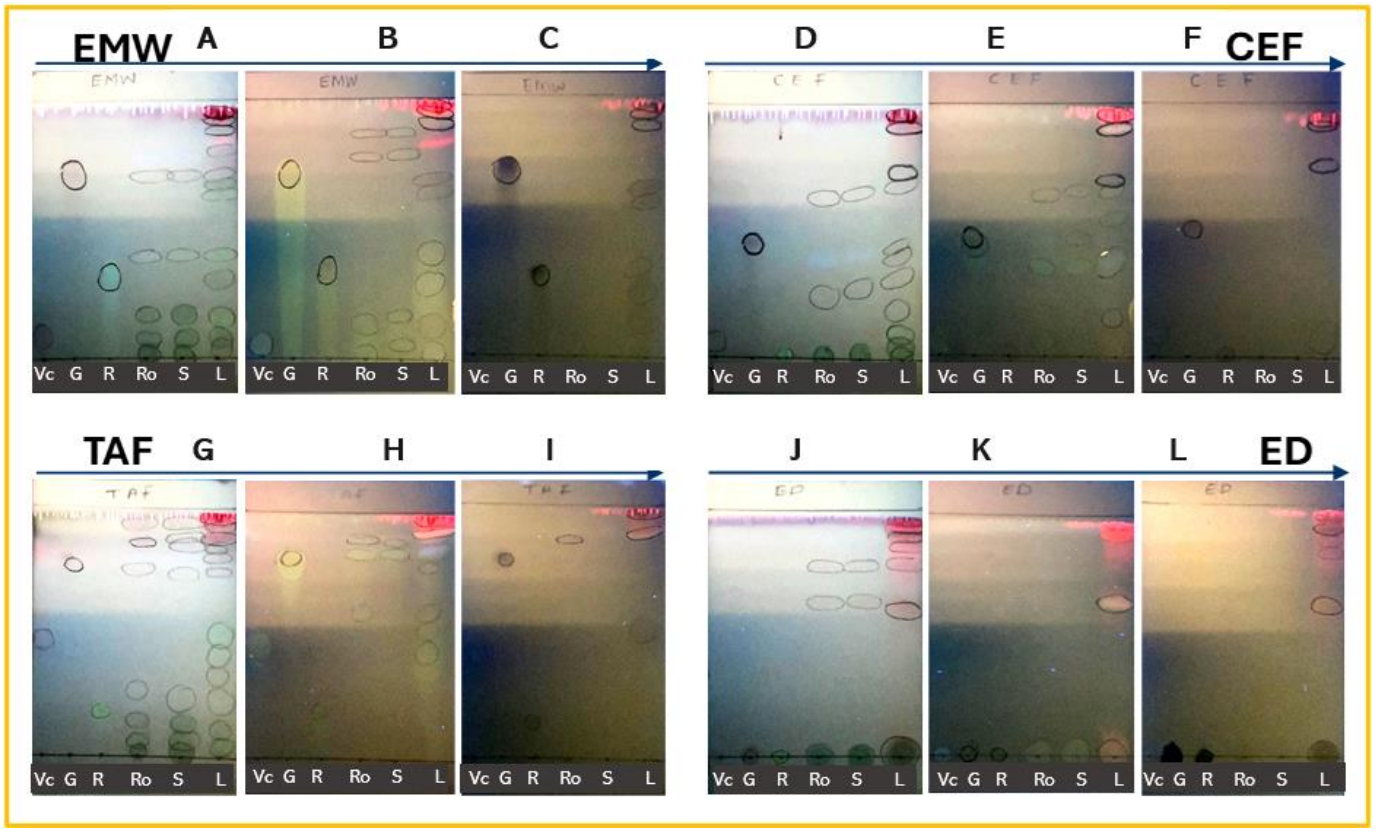


Figure 3.3A: TLC chromatograms of EA plant extracts developed in four mobile phases, EMW (ethyl acetate: methanol: water), CEF (chloroform: ethyl acetate: formic acid), TAF (toluene: acetone: formic acid), and ED (ethyl acetate: dichloromethane) and monitored under 365 nm long wave ultraviolet. Vc (Vitamin C/Ascorbic Acid); G (Gallic acid); R (Rutin); Ro (Root extract); S (Stem extract); L (Leaf extract).



© University of Venda

Figure 3.3B: TLC chromatograms of ethanol plant extracts developed in four mobile phases, EMW (ethyl acetate: methanol: water), CEF (chloroform: ethyl acetate: formic acid), TAF (toluene: acetone: formic acid), and ED (ethyl acetate: dichloromethane) and monitored under 365 nm long wave ultraviolet. Vc (Vitamin C/Ascorbic Acid); G (Gallic acid); R (Rutin); Ro (Root extract); S (Stem extract); L (Leaf extract).

In ethanol plant extracts, Figure 3.3B, vanillin was generally noticed throughout (EMW, CEF, TAF and ED), the compounds displayed the same fluorescence, rutin being lime green except on EMW, it was blue surf (Figure 3.3B). Most of the compounds, especially from ethanol leaf extract, exhibited pinkish to reddish colour, whereas some exhibited sky blue to lime green colour. A pinkish unmarked ethanol leaf extract's compounds from the top were noticed under 365 nm long wave ultraviolet on EMW, which was not detected and circled prior to UV light (Figure 3.3B). The same applies to CEF; two unmarked blue surf ethanol root and stem extract compounds were detected after subjection to UV light. Throughout (EMW, CEF, TAF and ED) on DPPH, controls remained yellowish except on the ED Mobile phase, wherein its hue fluorescence is blue surf (Figure 3.3B). Most upper compounds' hue fluorescence presented pinkish to reddish on ethanol leaf extract, whilst some exhibited orange to yellowish. A pinkish unmarked compound was detected on EMW after the plate was subjected to UV light (Figure 3.3B). On the ferric chloride chemical test, the controls remained blackish, whereas the upper compounds' hue fluorescence was noticed to be pinkish on ethanol leaf extract, shown in Figure 3.3B.

3.2.3. TLC chromatograms of EA and ethanol plant extracts developed by vanillin-sulfuric acid, DPPH, and ferric chloride reagents.

Various spraying reagents, namely DPPH, vanillin-sulfuric acid, and ferric chloride, were employed to visualise the developed phytochemicals on the TLC plates as a bioactive chemical detection approach (Figures 3.4A and B**)**. In the presence of the polar developing solvent EMW, both controls, ascorbic acid, gallic acid and rutin, were established simultaneously with the chemicals indicated by circles on the TLC Plates (Figure 3.4A). Overall, under the vanillin-sulfuric acid reagent, eight compounds from the EA root and leaf extract were detected, whereas nine were detected from the EA stem extract, displaying few distinct colours, whilst most displayed the same colour. The plant's organs' extract movement and colours were comparable, demonstrating that the compounds were distributed amongst the plant organs. The control ascorbic acid and gallic acid displayed a grey colour, whereas rutin displayed a yellow colour, and this suggested that the plant's organ extract probably contained all the standards because they showed colours that were comparable to the control. This could probably suggest that the plant contains phenolic, flavonoids and butanolides class of compounds (Sawant *et al*., 2010) as depicted below in Figure 3.4A. The findings are unique since no study has been conducted that shows TLC chromatograms of ethanol and EA leaf, stem, and root extract of *T. zeylanicum.*

© University of Venda

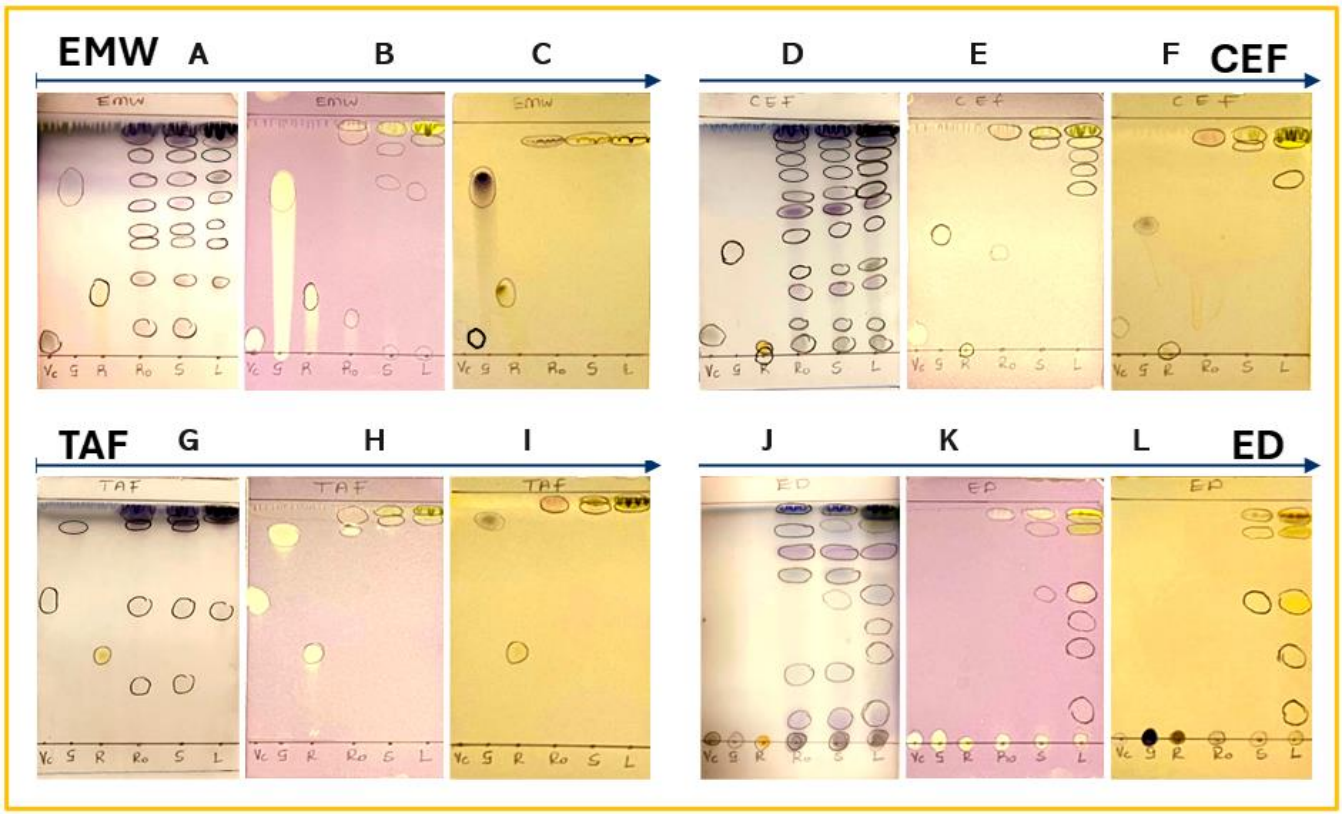
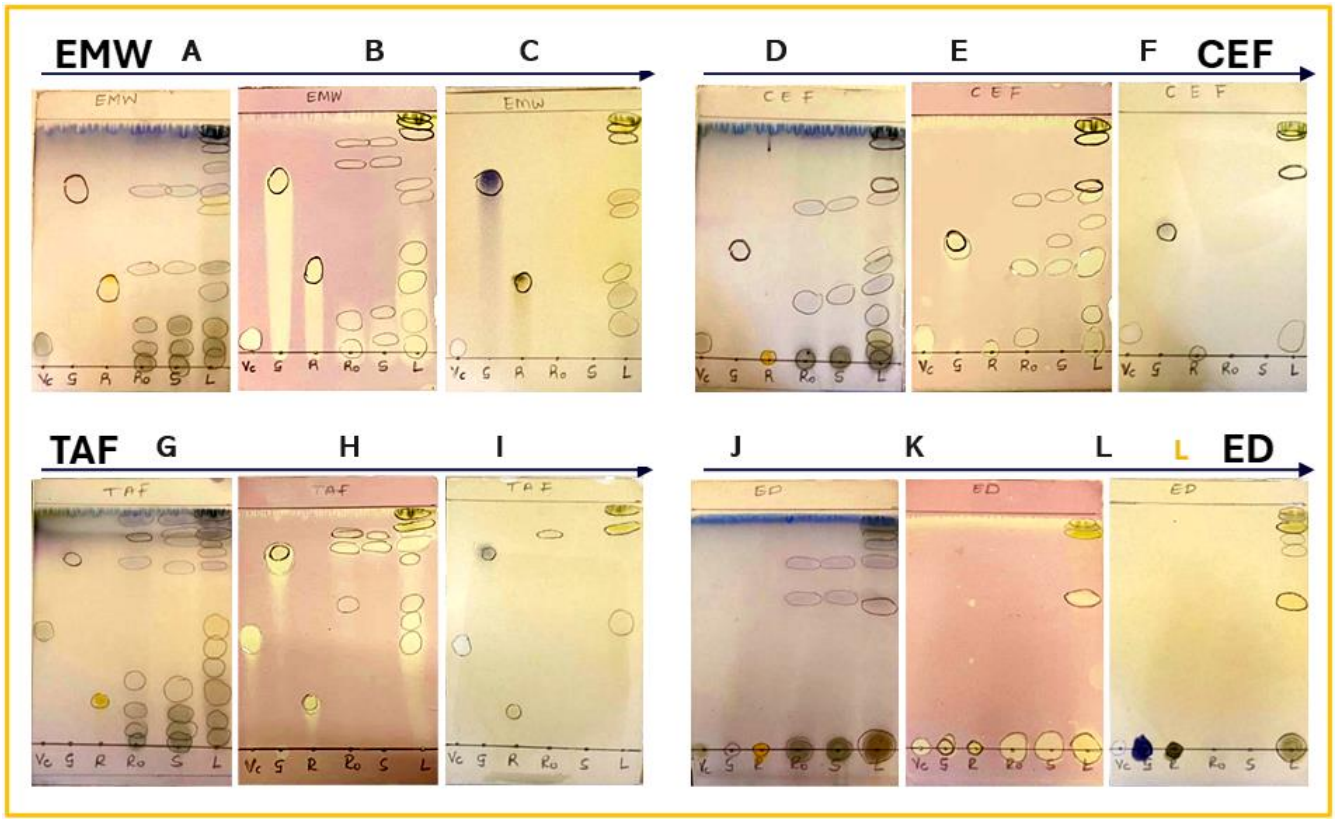


Figure 3.4A: TLC chromatograms of EA plant extracts developed in four mobile phases, EMW (ethyl acetate: methanol: water), CEF (chloroform: ethyl acetate: formic acid), TAF (toluene: acetone: formic acid), and ED (ethyl acetate: dichloromethane), with different polarity that exhibit chemicals detected by vanillin-sulfuric acid (A, D, G and J), DPPH reagent (B, E, H and K), and ferric chloride (C, F, I, and L). Vc (Vitamin C/Ascorbic Acid); G (Gallic acid); R (Rutin); Ro (Root extract); S (Stem extract); L (Leaf extract).



© University of Venda

Figure 3.4B: TLC chromatograms of ethanol plant extracts developed in four mobile phases, EMW (ethyl acetate: methanol: water), CEF (chloroform: ethyl acetate: formic acid), TAF (toluene: acetone: formic acid), and ED (ethyl acetate: dichloromethane), with a different polarity that exhibits chemicals detected by Vanillin-sulfuric acid (A, D, G and J), DPPH reagent (B, E, H and K), and Ferric chloride (C, F, I and L) respectively. Vc (Vitamin C/Ascorbic Acid); G (Gallic acid); R (Rutin); Ro (Root extract); S (Stem extract); L (Leaf extract).

On the TLC plates for the DPPH scavenging test (Figure 3.4A), the mobile phase EMW demonstrated less promise for migrating and exhibiting the bioactive antioxidant chemicals. Both controls developed and displayed a yellowish colour. The EA root extract revealed three metabolites, whereas the EA stem and leaf extracts presented four compounds. Under the yellowish ferric chloride reagent, both controls migrated together with the compounds detected from the EA root, stem, and leaf extracts, of which each exhibited one developed compound. vanillin-sulfuric acid has demonstrated a greater capacity to recognize the resultant chemicals on the polar silica gel layered on the plate on the mobile phases EMW, CEF, TAF and ED (Figure 3.4A).

Under the intermediate mobile phase CEF (Figure 3.4A), the two controls (Ascorbic acid and gallic acid) both migrated; however, only rutin remained stationary on the origin spotting baseline. Vanillin-sulfuric acid reagent revealed eleven developed chemicals for the root, the stem, and the leaf extract. Ascorbic acid and gallic acid presented a grey colour, whereas stationary rutin exhibited a yellow colour (Figure 3.4A). The migration patterns of the plant organ extracts were similar; the plant component extracts migrated in comparable ways. As a result, they presented the same colour in the sense that the bottom and second bottom ones exhibited a grey colour, and the third from the bottom exhibited a purple colour, respectively (Figure 3.4A). Moreover, this validates the presence of ascorbic acid and gallic acid in the plant extracts as they possess the greyest colour. Although the EA leaf extract exhibited green nonpolar chemicals spotted mostly at the top of the TLC plate, which hence validates the plant organs' variations.

The DPPH reagent demonstration displayed less of promise for detecting and exhibiting the antioxidant bioactive chemicals in all the mobile phases (EMW, CEF, TAF and ED). Interestingly, both controls and plant extracts presented similar colours as previously reported on EMW (Figure 3.4A). On the mobile phase CEF, five compounds (5) were spotted from the EA leaf extract. Only rutin control remained stationary, although the ascorbic acid moved less. Ferric chloride depicted the control patterns as the same, except for the colours presented. The plant's chemicals spotted were few, with the EA root extract displaying a distinctive purple colour. On CEF, vanillin-sulfuric acid demonstrated a higher potential for identifying the resultant chemicals, as shown above in Figure 3.4A.

© University of Venda

The nonpolar mobile phase TAF demonstrated reduced compound migration in comparison to EMW and CEF (Figure 3.4A). It was observed that ascorbic acid did not migrate when exposed to ferric chloride (Figure 3.4A). Four developed compounds from the root, five from the stem, and three from leaf extracts were selected by the vanillin-sulfuric acid reagent. The extracts shared components from plant sections in terms of similar colours and contain ascorbic acid and gallic acid (Figure 3.4A). The DPPH demonstrated the nonpolar phytochemical antioxidants from both plant organs that migrated to the solvent front. The mobile phase ED was unable to migrate the controls, as they were detected on the stationary spotting phase. However, the vanillin-sulfuric acid reagent, on the other hand, did an outstanding task of clearly presenting the colour and movement pattern of the phytochemicals. Remarkably, the two plant sections exhibit the identical purple colour of the phytochemicals ranked third from the top, which corresponds to the same plant properties (Figure 3.4A). While the leaf displayed eight spots, the root and stem only reported seven.

For the bioactive compounds that were extracted via ethanol detection (Figure 3.4B), the same spraying reagents utilised on EA were used. Both controls, ascorbic acid, gallic acid, and rutin, developed alongside the compounds indicated by circles on the TLC plate when the polar developing solvent EMW was present (Figure 3.4B). Considering the observed phytochemicals, five compounds from the root and stem extracts and twelve from the leaf extract were found when the vanillin-sulfuric acid reagent was employed, as presented in Figure 3.4B. Similar movement patterns and colours were observed in the root and stem, indicating that the same chemical composition or distribution of compounds among the plant components is shared by them. Taking colour into consideration, rutin possessed a golden colour, while the control chemicals, ascorbic acid and gallic acid, appeared greyish in hue. While most extracts demonstrated a greyish colour similar to ascorbic acid and gallic acid, the leaf extract produced two yellow chemicals that, given their colour, are equivalent to rutin. Given that their colours resembled those of the controls, it was implied that the plant extracts included the standards (Figure 3.4B).

On the DPPH reagent, both controls developed and displayed a yellowish colour (Figure 3.4B). The root was revealed to be the most plant part with excess metabolites, with nine metabolites exhibited, whereas the leaf and stem presented four compounds (Figure 3.4B). The root and stem registered similar movement patterns and colours, suggesting that they share the same chemical composition or demonstrating that the antioxidant compounds were distributed amongst the plant organs. On the yellowish ferric chloride reagent, both controls migrated together with the compounds detected from the ethanol leaf extract only. The ethanol root and stem extract compounds were not detected. Remarkably, the gallic acid presented a dark black or grey colour, and the ascorbic acid presented a white colour (Figure 3.4B). vanillin-sulfuric acid and DPPH, when considered together with all the spraying reagents under EMW, have demonstrated greater potential for displaying their respective phytochemicals.

© University of Venda

Under the intermediate mobile phase CEF (Figure 3.4B), the two controls (Ascorbic acid and gallic acid) both migrated; however, only rutin remained stationary on the origin spotting baseline. vanillin-sulfuric acid reagent revealed three detected chemicals for the ethanol root and the stem extracts, whereas the ethanol leaf extract registered excess compounds. While immobile rutin displayed a yellow colour, ascorbic acid and gallic acid revealed a grey colour (Figure 3.4B). The plant constituent extracts travelled in similar ways, as seen by similarities in migration patterns and colours of the extracts from the root and stem. As a result, they presented the same colour in the sense that the bottom ones exhibited a greyish colour and the second from the bottom exhibited a purple colour, respectively (Figure 3.4B). On DPPH reagent, interestingly, both controls and plant extracts presented similar colour as previously noticed on EMW. Excess compounds were spotted in the ethanol leaf extract. Only rutin control remained immobile, although the ascorbic acid moved less. Except for colour presentation, ferric chloride illustrated the control patterns as identical to the prior CEF. There were hardly any compounds found in the plant, and few were detected in the ethanol leaf extract. On mobile phase CEF, vanillin-sulfuric acid and DPPH, respectively, demonstrated a higher potential for identifying their respective resultant chemicals (Figure 3.4B).

The nonpolar mobile phase TAF demonstrated that vanillin-sulfuric acid, DPPH, and ferric chloride bioactive chemicals migrated in diverse ways according to their polarities (Figure 3.4B). On vanillin-sulfuric, ethanol root, stem and leaf extracts and standards migration varied noticeably. Nonetheless, it was observed that the controls in both vanillin-sulfuric acid, DPPH and ferric chloride migrated in the same fashion, validating the experiment reliability as they were all subjected to the same mobile phase TAF (Figure 3.4B). When exposed to vanillin-sulfuric acid, the ethanol leaf extract registered more metabolites than the ethanol root and stem extracts. The migratory patterns varied in all the plant (root, stem, and leaf) extracts. When exposed to ferric chloride, only one compound was reported from the ethanol root extract and three from the ethanol leaf extract, whereas the stem extract did not register any compound detected by ferric chloride (Figure 3.4B). The findings are unique since no study has been conducted that shows TLC chromatograms of ethanol and EA leaf, stem, and root extract of *T. zeylanicum.*

The mobile phase ED demonstrated reduced compound migration compared to EMW, CEF and TAF, respectively (Figure 3.4B). ED could not migrate the controls as they were detected steadily in the stationary spotting phase. The ethanol root and stem extract registered the same number of detected compounds with the same migration pattern and colours, which strongly suggests the distribution and sharing of compounds within the plant parts (Figure 3.4B). However, on DPPH and Ferric chloride, the mobile phase ED was unable to migrate the root and stem, and the spraying reagents could not display other developed metabolites. The DPPH only displayed its respective antioxidant compounds from ethanol leaf extract, whereas the stem and root extracts showed no antioxidant compound movement. All the controls remained stationary at the spotting phase. Ferric chloride registered its respective phenolic compounds in ethanol leaf extract, while stem and root extracts, together with the controls, remained stationary (Figure 3.4B).

© University of Venda

3.2.4. Phytochemical tests

The results of phytochemical screening of *T. zeylanicum* EA and ethanol plant extracts are shown in Table 3.1. Observing colour changes served as the basis for the qualitative study of phytochemicals. The phytochemical analysis of *T. zeylanicum* reveals significant variations in compound presence across EA root, stem, and leaf extracts, each showing unique concentrations of different bioactive substances. These terpenoids are moderately present in the EA root, stem, and leaf extract, where they present a yellowish-brown colour in the root and stem and a green colour in the leaf extracts (Table 3.1). Adarsh *et al*. (2020) confirm the presence of terpenoids from *C. zeylanicum* EA extract. They have also been found to improve insulin sensitivity and lower blood glucose levels, with additional anti-inflammatory effects, which are imperative in the management of complications related to diabetes (Ghasemzadeh *et al*., 2018). Another important phytochemical, saponins, was found to be present in all EA plant organs in appreciable amounts, as they produced white precipitates or the development of stable foam, maintaining the same colour.

Saponin inhibits the enzymes that convert disaccharides into monosaccharides, lowering the rise in blood glucose (Oishi *et al*., 2007; El Barky *et al*., 2017). T1D and T2D patients benefit greatly from this medication, which also helps to avoid postprandial elevated blood sugar levels. Moreover, it has been demonstrated that bitter melon saponin stimulates the liver to store glycogen and the islets of Langerhans to secrete insulin (Zhu *et al*., 2012; Barkey *et al*., 2017). Furthermore, bitter melon saponin may improve peripheral glucose oxidation in erythrocytes and adipocytes, decrease hepatic gluconeogenesis, and enhance hepatic glycogen production (El Barky *et al*., 2017; Hamissou *et al*., 2013). Additionally, they have been shown to lower blood glucose levels by increasing plasma insulin levels, releasing insulin from the pancreas, and rejuvenating insulin activity. They are also well-recognised for their capability to lower cholesterol (Metwally *et al*., 2012). In addition, saponin can prevent the circulation from producing glucose (Tian *et al*., 2005). Innovative studies have shown that they frequently appear consistently in therapeutic plants (Das *et al.*, 2020).

Flavonoids serve as antioxidants and are highly present as intense green in the EA leaf extract. In contrast, they are slightly present in EA stem and root extracts as essentially colourless to light yellow, which may be due to the absence of anthocyanins (Table 3.1). Essential data from animal and cell models demonstrated that dietary flavonoids or flavonoid-rich extracts can reduce the symptoms of diabetes mellitus and prevent T2DM. Dietary flavonoids reduce blood glucose levels by preserving pancreatic β-cells, triggering insulin signalling, encouraging the pancreas to release insulin, and blocking enzymes that metabolise carbohydrates (Xiao, 2022). This high flavonoid concentration aligns with observations in other plants where flavonoids combat oxidative stress, especially in the foliage (Del Río *et al*., 2021). Beneficial antioxidants called phenols are abundant in EA leaf extract and may help lower blood glucose and block the activity of α-amylase and other important enzymes involved in the metabolism of carbohydrates (Kumar *et al*., 2019). EA stem and root extracts are slightly less concentrated, which may be due to lower phenolic content, as shown below in Table 3.1.

© University of Venda

Table 3.1: Phytochemicals tested in EA and ethanol root, leaf, and stem extracts of *T. zeylanicum*.

Extraction solvent	Plant organ extract	Terpenoids	Saponins	Glycosides	Flavonoids	Steroids	Phenols	Coumarins	Alkaloids	Tannins
Ethyl acetate	**Root**	+	+++	-	+	++	+	+++	+++	-
	Stem	+	+++	-	+	++	+	+++	+++	-
	Leaf	+	+++	-	+++	+++	+++	-	-	+++
Ethanol	**Root**	+++	++	+++	+	+++	+	+	-	-
	Stem	+++	++	+++	++	+++	+	-	+++	-
	Leaf	+	++	-	+++	+++	+++	-	-	+++

+ (Slightly present); ++ (Moderately present); +++ (Highly present); - (Absent/undetected)

Coumarins and alkaloids are highly concentrated in EA root and stem extracts (Table 3.1). Coumarins were present in yellowish in the EA root and stem extracts (Ali *et al*., 2018; Le Thi *et al*., 2021). They are known for effects such as anti-inflammatory, anticoagulant, antihypertensive, anticonvulsant and antioxidant activity (Flores-Morales *et al*., 2023). As previously reported, coumarins significantly induce AMP-activated protein kinase, which is favourable for preventing and treating T2DM (Ranđelović *et al*., 2021). Alkaloids exhibited an orange colour in EA root and stem extract, while leaf extract showed a blackish-green tint (Table 3.1), aligning with alkaloid storage in root structures for defence purposes. The alkaloidal components have been discovered to reduce the degree of insulin resistance (Behl *et al*., 2022). Anti-diabetic alkaloids effectively combat hyperglycaemia by encouraging glucose uptake and glycogen production (Tang *et al*., 2017). Prior research demonstrated alkaloids exhibit antidiabetic effects by inhibiting enzymes [α-amylase, α-glucosidase, aldose reductase, and dipeptidyl peptidase-IV] (Adhikari, 2021).

© University of Venda

Lastly, tannins are highly concentrated in EA leaf extract (Table 3.1) because they have been shown to improve glucose absorption and, hence, lower blood sugar levels, thereby minimising the incidence of diabetes (Sun *et al*., 2020*;* Song *et al*., 2018). According to *in-vivo* research, kaki-tannin stopped type 2 diabetic mice given a high-fat diet from experiencing increases in plasma total cholesterol, non-HDL cholesterol, triglycerides, and insulin. Additionally, kaki-tannin consumption stimulated the genes involved in cholesterol metabolism and inhibited fatty liver (Matsumoto and Yokoyama, 2012; Sieniawska, 2015). Steroids were highly or particularly abundant in EA leaf extract, showing an intense green hue, whereas they were moderately present in EA root and stem extracts, both displaying a yellowish-brown hue (Table 3.1). It is also known that steroids inhibit glucose uptake in muscles and adipose tissues, meaning that more glucose will be found circulating in the blood; this indicates that the body becomes more resistant to insulin, and hence, more insulin will be required to shuttle the glucose into the cells (Prabhakar *et al*., 2024). All the plant organs (EA root, stem, and leaf extract) tested negative for glycosides (Table 3.1). However, a colour change was observed, although not in the anticipated colours.

Under ethanol extracts, the phytochemical analysis of *T. zeylanicum* reveals significant variations in compound presence across root, stem, and leaf extracts, each showing unique concentrations of different bioactive substances. Terpenoids are highly present in ethanol root and stem extract, with only a slight presence in the leaf extract (Table 3.1). The ethanol root and stem extracts produced a reddish-brown colour, while the leaf extract was greenish black (Das *et al*., 2014; Iqbal *et al*., 2015). Terpenoids are associated with antimicrobial and anti-inflammatory properties. According to some research, they are crucial for controlling diabetic complications because they increase insulin sensitivity and lower blood glucose levels (Ghasemzadeh *et al*., 2018). This discovery is consistent with previous results that show their presence not only at higher concentrations in roots but also in sections other than leaves due to their essential role in plant defence mechanisms (Ali *et al*., 2020).

All plant organs (ethanol root, stem, and leaf extract) showed a moderate presence of saponins indicated by white precipitates or foam development, uniformly across root, stem, and leaf extract, with a constant colour observed (Table 3.1). Saponins are reported for their role in reducing cholesterol levels and providing antifungal properties (Metwally *et al*., 2012). Additionally, it has been mentioned that saponin prevents the glucogenesis process in the blood (Tian *et al*., 2005). Recent research supports the belief that they regularly occur all over medicinal plants (Das *et al*., 2020). Their even distribution over different plant organs corresponds with other findings where saponins are distributed within other medicinal plants to protect against possible colonisation by microbial agents (Rai *et al*. 2021). Glycosides are seen mainly in the ethanol root and stem extract, but not in the leaf extract (Table 3.1). The ethanol root extract was reddish-purple; the ethanol stem extracts were reddish-brown in colour, and the ethanol leaf extract was greenish black (Table 3.1). Glycosides are related to antioxidant properties and can help prevent consumption by herbivores.

© University of Venda

Glycosides were reported to occur in several plant organs (ethanol root and stem extract), and this is consistent with reports on their defence and therapeutic functions, including antioxidant and cardioprotective activities (Mekonnen *et al*., 2018). Flavonoids are most noticeable in ethanol leaf extract, giving it a dark green hue, while ethanol stem extract exhibited a brownish hue (Table 3.1). It appeared that the lowest concentration of these flavonoids was found in the ethanol root extract. Flavonoids are vital for plant tissues, especially leaves, to protect against oxidative stress because they are vitamins linked to antioxidant activity (Del Río *et al*., 2021). This assertion is consistent with earlier studies on the topic, which showed that leaves frequently absorb flavonoids to fend off oxidative damage and UV radiation (Kumar *et al*., 2017).

Steroids were widely distributed in ethanol root, stem, and leaf extracts, exhibiting greenish-black in the leaf and reddish-brown in the root and stem extracts (Iqbal *et al*., 2015; Zulkifli *et al*., 2012). Steroids are essential for cell structure and defence and are frequently concentrated in leaves to withstand environmental stress. This distribution matches findings in other plants where steroids aid in strengthening leaf cell walls (Ghasemzadeh *et al*., 2018). As previously mentioned, steroids are believed to prevent the body's muscles and fat from absorbing glucose, which causes it to circulate in the bloodstream. This lowers the body's sensitivity to insulin, necessitating additional insulin to get the glucose into the cells (Prabhakar *et al*., 2024).

Phenols show a slight presence in ethanol root and stem extracts, which may be due to low phenolic content, whereas they show a high presence in ethanol leaf extract (Table 3.1). They are well-recognised for their antioxidant properties, which probably help lower blood sugar and oxidative stress and block the activity of α-amylase and other important enzymes involved in the metabolism of carbohydrates (Kumar *et al*., 2019). Their presence in ethanol leaf extract is consistent with research that highlighted the function of phenols as potent defence molecules in plant tissues actively engaged in photosynthesis (Nguyen *et al*., 2019). The reddish-brown ethanol root extract has a small amount of coumarins, whereas the stem and leaf extracts have none at all (Table 3.1). Alkaloids are highly present in ethanol stem extract, with an observed yellowish-orange colour (Table 3.1). By encouraging the synthesis of glycogen and the ingestion of glucose, they effectively combat hyperglycaemia (Tang *et al*., 2017). Tannins are absent in ethanol root and stem extract but highly present in leaf extract, showing an intense green colour (Table 3.1). Tannins decrease blood sugar levels by improving glucose absorption, which lowers the incidence of diabetes (Sun *et al*., 2020*;* Song *et al*., 2018). The above results are consistent with those previously reported by Mwambyale (2021). These findings align with a previous study by Darsh *et al*. (2020), which found similar phytochemicals in dry *C. zeylanicum* ethanol and EA extracts.

© University of Venda

3.3. Quantitative phytochemical analysis of ethanol and EA extracts from different organs of *T. zeylanicum.*

3.3.1. Antioxidant potential of plant extract using DPPH-radical scavenging activity.

DPPH is frequently used to evaluate an antioxidant's capacity to scavenge free radicals (Gulcin and Alwasel, 2023). The reduction of absorbance results from antioxidants present in the plant extracts donating an electron or a hydrogen atom to the DPPH radical, converting it into its non-radical form, DPPH-H. When an antioxidant is added, a DPPH solution will turn from purple to yellow, preventing the free radical from escaping and neutralising it. Higher percentage inhibition refers to the extract's capability to scavenge free radicals, manifesting greater antioxidant activity. The antioxidant activity is represented as an inhibition percentage at a specific concentration, indicating how effectively each extract can neutralise free radicals. The statistical analysis of DPPH-scavenging activities of EA and ethanol extracts of *T. zeylanicum* root, stem, and leaf tested from 0 to 50 µg/mL are presented below in Table 3.3.

In all ranges of concentrations, the standard (ascorbic acid) showed the highest radical scavenging activity that increased continuously from about 56.553±2.249% at 5 µg/mL to about 95.445±0.430% at 50 µg/mL (Figure 3.5A). Its great antioxidant capacity is reflected in the steady increase of the ascorbic acid beyond that of all plant extracts, as exhibited (Figure 3.5A). In the EA leaf extract, a high scavenging activity of about 68.712±3.083% at 5 µg/mL ($p \leq 0.001$) compared to ascorbic acid (56.553±2.249%) and a decrease in scavenging activity of 54.982±1.739% at 10 µg/mL ($p \leq 0.05$) with rapid increase up to 50 µg/mL ($p \leq 0.001$) was noticed, displaying statistical significance when compared to the ascorbic acid, beyond which the activity remained consistent from 40 µg/mL (70.259±2.029%) ($p \leq 0.001$) up to 50 µg/mL (70.221±2.393%) with a fluctuation between 60% and 65% (Figure 3.5A and Table 3.2). Thus, the above observation indicates that the EA leaf extract shows a high to moderate antioxidant activity that reaches a plateau at higher concentrations (Figure 3.5A and Table 3.2).

The antioxidant activity of the both ethanol and EA leaf extract was highest at 40 µg/mL, with EA leaf extract scavenging activity of 70.259±2.029% showing statistical significance when compared to ethanol leaf extract (21.896±4.103%) at the same concentration ($p \leq 0.001$) and this inhibition of DPPH radicals expressed that EA leaf extract contains a significant amount of antioxidant compounds which donate electrons to neutralize free radicals. A high percentage of inhibition reflected the leaf extract's high free radical scavenging ability. This agrees with the present findings that leaf extracts have the highest total phenolic content (Figure 3.6B) since phenolic compounds are renowned for their antioxidant properties. Therefore, the high antioxidant activities observed suggest that leaf extracts may be highly capable of reducing oxidative stress and are useful in protecting biological systems against oxidative damage. Leaf extracts could be highly valuable in developing natural antioxidant products such as skincare formulations.

© University of Venda

Given their high antioxidant activity, leaf extracts are prime candidates for creating natural antioxidant supplements, functional foods, or skincare products that protect against oxidative damage. The above results are in accordance with the previously reported findings. While antiproliferative and anticancer activity has not yet been identified, it was noted that the EA fraction of EA leaf extract possesses antioxidant potential (Swetha *et al*., 2020)

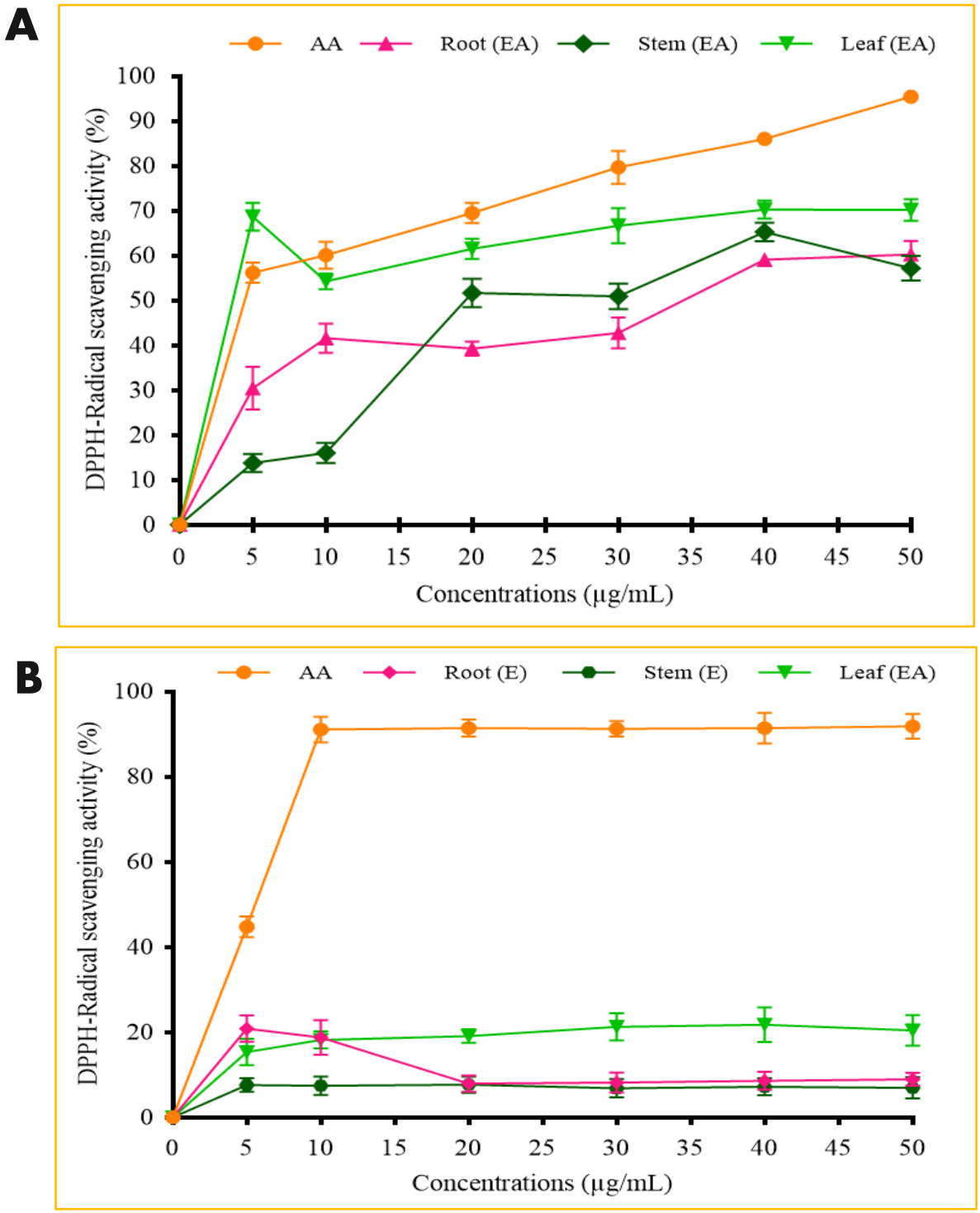


Figure 3.5: Percentage inhibition of DPPH radical scavenging activity of plant extracts. **(A)** ethyl acetate and **(B)** ethanol extracts from different organs of *T. zeylanicum*, which include leaf, stem, and root, using ascorbic acid as a standard.

© University of Venda

Table 3.2: Statistical analysis of % DPPH-scavenging activity of EA and ethanol root, stem, and leaf extracts of *T. zeylanicum*

Control or plant extract final concentration (µg/mL)	Ascorbic acid DPPH inhibition (%)	Ethyl acetate plant extracts			Ascorbic acid DPPH inhibition (%)	Ethanol plant extracts		
		Leaf	Stem	Root		Leaf	Stem	Root
0	0.000±0.000	0.000±0.000	0.000±0.000	0.000±0.000	0.000±0.000	0.000±0.000	0.000±0.000	0.000±0.000
5	56.553±2.249	68.712±3.083***	13.745±1.998$^{***\ ###}$	30.088±4.831$^{***\ ###}$	44.196±2.413	15.782±3.099$^{**\ ¥¥¥¥}$	7.647±1.640$^{**\ ##}$	20.894±3.115$^{**\ #}$
10	60.097±3.014	54.982±1.739*	16.989±2.246$^{***\ ###}$	42.932±3.294$^{***\ #}$	91.141±3.000	17.292±2.049$^{***\ ¥¥¥}$	7.288±2.225$^{***\ #}$	18.798±4.104***
20	68.875±2.288	60.905±2.308**	51.570±3.216$^{**\ ##}$	39.391±1.586$^{***\ ##}$	91.446±1.979	19.658±1.585$^{***\ ¥¥¥}$	7.692±1.921$^{***\ #}$	7.975±1.930$^{***\ ##}$
30	79.743±3.697	66.741±3.921***	50.177±2.814$^{**\ ##}$	47.795±3.452$^{***\ ##}$	91.921±1.798	21.122±3.190$^{***\ ¥¥¥}$	6.891±2.197$^{***\ ##}$	8.227±2.373$^{***\ ##}$
40	86.057±0.610	70.259±2.029***	65.544±2.057***	59.105±0.895$^{***\#}$	91.446±3.606	21.896±4.103$^{***\ ¥¥¥¥}$	7.190±1.999$^{***\ ##}$	8.624±2.078$^{***\ ##}$
50	95.445±0.430	70.221±2.393***	57.725±2.790$^{***\ ##}$	60.258±3.017$^{***\#}$	91.853±2.931	20.393±3.575$^{***\ ¥¥¥¥}$	6.928±2.533$^{***\ #}$	8.952±1.470$^{***\ ##}$

* = significantly different from ascorbic acid (control) and plant extracts of the respective solvent, $p \leq 0.05$ (*), $p \leq 0.01$ (**), $p \leq 0.001$ (***), $p \leq 0.0001$ (****); $^{\#}$ = significantly different from leaf extract of the respective solvent and other plant extracts (root and stem extracts), $p \leq 0.05$ ($^{\#}$), $p \leq 0.01$ ($^{\#\#}$), $p \leq 0.001$ ($^{\#\#\#}$), $p \leq 0.0001$ ($^{\#\#\#\#}$) and $^{¥}$ = significantly different from leaf extracts of the two respective solvents, $p \leq 0.05$ ($^{¥}$), $p \leq 0.01$ ($^{¥¥}$), $p \leq 0.001$ ($^{¥¥¥}$), $p \leq 0.0001$ ($^{¥¥¥¥}$).

© University of Venda

The initial DPPH radical scavenging activity of ethyl acetate (EA) stem extract was lower proceeding 13.745±1.998% ($p \leq 0.001$) at 5 µg/mL, 16.989±2.246% ($p \leq 0.001$) at 10 µg/mL and rapidly increased to 51.570±3.216% ($p \leq 0.01$) by 20 µg/mL, displaying a high statistical significance when compared to ascorbic acid and the EA leaf extract at the same concentrations. Then it displayed some fluctuation peaking at 20 µg/mL (51.570±3.216%) to 50 µg/mL (57.725±2.790%), where it displayed statistical difference when compared to ascorbic acid ($p \leq 0.001$) and EA leaf extract ($p \leq 0.01$) (Figure 3.5A and Table 3.2). This fluctuation observed after 20 µg/mL indicates that the level of antioxidant capacity may not continuously improve with increased EA stem extract dosages. The moderate antioxidant activity was exhibited by the EA stem extract, with about 65.544±2.057% inhibition at 40 µg/mL (Figure 3.5A and Table 3.2). EA stem extract showed no statistical significance when compared to the EA leaf extract 40 µg/mL (Figure 3.5A and Table 3.2). Even though it is moderate, it may contribute to the overall antioxidant capacity in combination with other plant organs. The EA stem extract can be less favoured for antioxidant activities, but it can be screened for various bioactive compounds. While less active, the addition of stem could be made for those desiring whole-plant extracts.

The lowest antioxidant activities were observed for the EA root extract, starting from about 30.088±4.831% at 5 µg/mL ($p \leq 0.001$) when compared to ascorbic acid and EA leaf extract and fluctuating throughout, reaching about 60.258±3.017% at 50 µg/mL with high statistical significance when compared to ascorbic acid ($p \leq 0.001$) and less statistical significance when compared to EA leaf extract ($p \leq 0.05$) (Figure 3.5A and Table 3.2). It was generally noticed that even though EA root extract improved with higher concentration, it was not as effective as EA leaf and stem extract against DPPH radicals. The lowest antioxidant activity was exhibited by the EA root extract, with an inhibition of about 60.258±3.017% at 50 µg/mL. It follows, therefore, that EA root extract is fairly concentrated with antioxidant compounds and exhibits a high capacity in the neutralisation of free radicals, though less compared with that exhibited by EA leaf and stem extracts. This activity in the EA root extract could be due to specific phenolic compounds or other antioxidants contributing to this activity. They may still contribute to the reduction of oxidative stress and hence may be of therapeutic benefit. Root could be combined with leaf to formulate products where moderate antioxidant activity is desired. With moderate activity, root extracts can be used in formulations requiring a balanced antioxidant effect or where specific root-derived compounds are desired.

In Figure 3.5B, the ethanol qualitative analysis, nearly 100% of radical scavenging activity was observed from 10 µg/mL (91.141±3.000%) all the way to 50 µg/mL (91.853±2.931%) for standard (ascorbic acid). This elevated level remains till all concentrations range from 10-50 µg/mL (Figure 3.5B and Table 3.2). This indicates that the reference or standard antioxidant's capacity to scavenge free radicals is superior to the average. A plateau occurs after the conventional antioxidant's 91.141±3.000% at 10 µg/mL radical scavenging activity, which continues to be approximately or around 91% even when concentrations increase to 50 µg/mL.

© University of Venda

This indicates that the standard approaches its maximal efficacy early on and has good antioxidant potential even at low concentrations.

The ethanol leaf extract's activity and statistical significance commences at around 15.782±3.099% when tested at a concentration of 5 µg/mL ($p \leq 0.01$) when compared to ascorbic acid and progressively rises to about 21.896±4.103% ($p \leq 0.001$) at 40 µg/mL when compared to EA leaf extract (Figure 3.5B and Table 3.2). Moderate antioxidant potential is shown by the steady but sluggish increase in radical scavenging activity at higher doses. At all concentrations between 5 and 50 µg/mL, the ethanol leaf extract exhibits an average radical scavenging activity ranging between 15.782±3.099%–20.393±3.575% exhibiting a high statistical significance when compared to EA extract at 40 and 50 µg/mL ($p \leq 0.001$) (Figure 3.5B and Table 3.2). Although this extract's antioxidant activity is lower than the standard, it consistently demonstrates radical scavenging, indicating that *T. zeylanicum* leaf has moderate antioxidant qualities and may contain moderate amounts of compounds with antioxidant properties, such as flavonoids or phenolics. Although not as effective as the standard, they are rich in antioxidant components such as flavonoids, phenolic acids, and terpenoids that contribute to moderate scavenging action, and their steadiness indicates that they have the potential to be a natural antioxidant at higher dosages. Its continuous medium activity suggests an antioxidant effect that may endure for a prolonged period at various dosages, making it potentially appropriate for use as a natural antioxidant supplement and in food preservation.

The ethanol root extract reaches a peak of 20.894±3.115% activity at 5 µg/mL ($p \leq 0.01$) when compared to ascorbic acid and ($p \leq 0.05$) when compared to ethanol leaf extract, but then decreases all the way to around 8.952±1.470% at 50 µg/mL ($p \leq 0.001$) when compared to ascorbic acid and ($p \leq 0.01$) when compared to ethanol leaf extract (Figure 3.5B and Table 3.2). Greater quantities of ethanol root extract suggest a diminished antioxidant ability at higher ethanol root extract concentrations. The ethanol root extract displays relatively high activity, reaching a peak of 20.894±3.115% at 5 µg/mL ($p \leq 0.01$) followed by 18.798±4.104% at 10 µg/mL ($p \leq 0.001$) when compared to ascorbic acid, after which the activity remains relatively at a range between 7.975±1.930%-8.952±1.470% in higher concentrations between 20-50 µg/mL respectively (Figure 3.5B and Table 3.2). There is no statistical difference at 10 µg/mL when compared to ethanol leaf extract. The less attenuated activity clearly demonstrates that the ethanol root has a weak antioxidant effect when compared to other organs of the plant and with a standard. Although the peaks start to drop slightly at around 10-20 µg/mL, from there on it remains very stable and flat. Compared to those in the ethanol leaf extract and standard, it appears that the bioactive antioxidant chemicals in the ethanol root are either less prevalent or less efficient in scavenging free radicals. The slight peak observed at low concentrations indicates that certain root constituents have antioxidant action, but their effect is not strong or sustained. The ethanol root extract's low activity may indicate that it has fewer or weaker free radical scavenging chemicals.

© University of Venda

The ethanol stem extract showed the lowest activity of all plant organs in about a range between 7.647±1.640% at 5 µg/mL and high statistical significance ($p \leq 0.01$) when compared to both ascorbic acid and ethanol leaf extract to 6.928±2.533% at 50 µg/mL ($p \leq 0.001$) when compared to ascorbic acid and less statistical difference ($p \leq 0.01$) when compared to ethanol leaf extract. For all the concentrations tested, the ethanol stem extract showed the lowest activity of all plant organs (Figure 3.5B and Table 3.2). This shows that the ethanol stem extract has an incredibly low antioxidant activity in contrast to the plant organs' ethanol leaf and root extracts that were evaluated and remained flat at all tested dosages or concentrations. The stem extract displayed a high statistical difference at 10, 20, 30 and 40 µg/mL ($p \leq 0.001$) with a decrease in scavenging activity. The fact that the ethanol stem extract of *T. zeylanicum* exhibits the lowest antioxidant potential could be indicative of either the fact that the ethanol stem extract does not contain significant amounts of potent antioxidants, or the compounds present in the stem are inefficient in quenching the free radicals in the DPPH assay. Uniform low activities, regardless of the used concentrations, show that the antioxidant activity of the stem is not concentration-dependent and remains minimal. Ethanol stem extract had the least antioxidant capacity, implying that either the levels of antioxidant compounds in this part were lower or that ethanol was not an effective extractor for such compounds.

3.3.2. Total phenolic content of plant extracts

The strong linear relationship ($R^2 = 0.9954$) between absorbance at 765 nm and gallic acid concentration confirms the accuracy and reliability of the assay for determining phenolic compounds (Figure 3.6A). The equation y = 0.627x directly calculates unknown phenolic concentrations by measuring absorbance and interpolating within the standard curve. As phenolic compounds exhibit antioxidant properties, their quantification will be necessary to establish plant-based products' nutritional, medicinal, and functional properties.

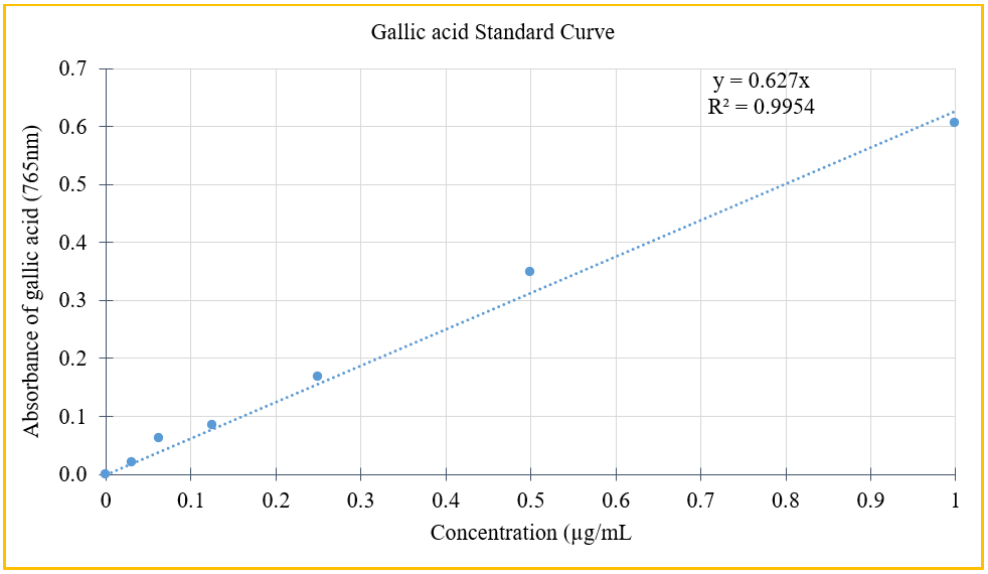


Figure 3.6A: Gallic acid standard curve.

© University of Venda

This standard curve is widely used in pharmacology and environmental studies to evaluate antioxidant capacity and study the impact of processing on bioactive compounds (Kalpoutzakis *et al*., 2023). In this study, A gallic acid standard curve is used to quantify total phenolic content in a sample by comparing the absorbance of a test solution to a known concentration of gallic acid (Figure 3.6A). The findings are unique since no study has been conducted that shows TPC chromatograms of ethanol and EA leaf, stem, and root extract of *T. zeylanicum*.

The findings demonstrate the insight distribution of the phenolic compounds in ethanolic and EA extracts from different organs of *T. zeylanicum*. The phenolic contents in EA extracts of leaf, stem and root are consistently lower compared with the ethanol extracts of these three plant organs (Figure 3.6B). The influence of solvent choice on the extraction of phytochemicals for various purposes is distinctly influenced by the extraction of certain compounds depending on their polarities. Ethanol, being a more polar solvent, ends up carrying the broadest spectrum of these phytochemicals with it as compared to EA (Figure 3.6B).

Regardless of the solvent used, the ethanol and EA leaf extract of *T. zeylanicum* consistently show the highest phenolic content, suggesting that they are a key part of the plant for applications requiring phenolic compounds, as shown below in Figure 3.6B. Interestingly, the leaves of *T. zeylanicum* can be harvested without uprooting the plant to be used for antidiabetic studies and the development of its possible drugs from ethanol and EA plant extracts. Additionally, ethanol leaf extract was also shown to contain more phytochemicals with antioxidant activity, which may be phenolics, as revealed by TLC plates developed with DPPH reagent and by the DPPH quantitative test as discussed above (Figure 3.4B). The findings are unique since no study has been conducted that shows TLC chromatograms of ethanol and EA leaf, stem, and root extract of *T. zeylanicum.*

Ethanol leaf extract has the highest amount of phenolics at approximately 47.520±2.300 µg GAE/mg dried extract, displaying a very high statistical significance ($p \leq 0.0001$) when compared to EA leaf extract and a statistical difference ($p \leq 0.001$) when compared to the ethanol root and stem extract (Figure 3.6B). The relatively high concentration suggests that leaves are the richest source of phenolic compounds linked to high antioxidant action (Chen *et al*., 2020; Mazhar *et al*., 2022). Antioxidants neutralise free radicals and unstable molecules, which cause oxidative stress and lead to cellular damage, ageing, and diseases like cancer (Saboo *et al*., 2014). With such a high concentration of phenolics, the ethanol leaf extract of *T. zeylanicum* is expected to have powerful antioxidant properties, hence adding substantial value to nutraceutical products during supplement formulation to reduce oxidative stress and promote general health (Chen *et al*., 2020). The ethanol extracts from leaves can be added to cosmetics industries in skin care products, acting against free radicals, preventing ageing, and healing because of their antioxidant nature (Gălbău *et al*., 2024).

© University of Venda

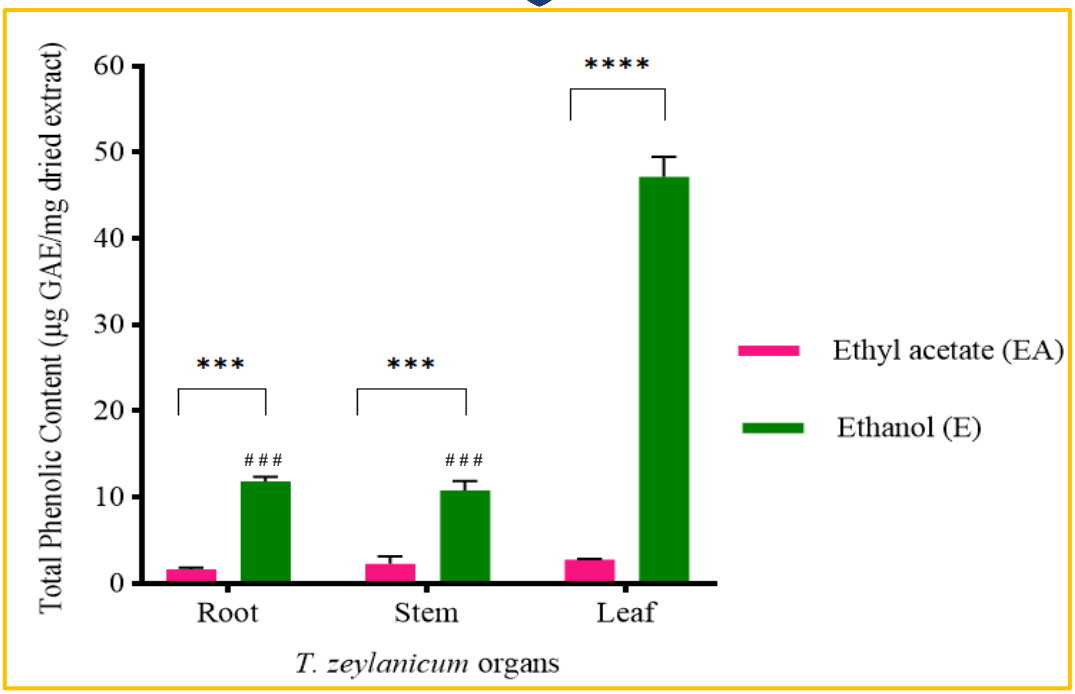


Figure 3.6B: Total phenolic content comparison of ethanol and EA extracts from different organs of *T. zeylanicum*. * = significantly different from root, leaf and stem extract of different extraction solvents, $p \leq 0.05$ (*), $p \leq 0.01$ (**), $p \leq 0.001$ (***), $p \leq 0.0001$ (****); and # = significantly different from ethanol leaf extract when compared to ethanol leaf and root extracts, $p \leq 0.05$ (#), $p \leq 0.01$ (##), $p \leq 0.001$ (###), $p \leq 0.0001$ (####).

EA leaf extract showed lower TPC (2.761±0.086 µg GAE/mg dried extract) when compared to the ethanol leaf extract (47.520±2.300 µg GAE/mg dried extract) with $p \leq 0.0001$ statistical significance (Figure 3.6B). However, its total phenolic content was higher than that observed in the EA root and stem extracts, with no statistical difference. This means among the EA organs of the plant evaluated, leaves were the richest in phenolic compounds and might, therefore, have the highest antioxidant potential since the phenolic content is associated with antioxidant activity (Mazhar *et al*., 2022). The relatively high phenolic content in the EA leaf extract suggests that EA is still effective in extracting phenolics from this plant organ. This could also be why leaves still show the highest content due to their higher natural abundance in these kinds of compounds when compared with other plant organs (Chen *et al*., 2020). The leaf extract of *T. zeylanicum* continues to stand out as a rich source of phenolics, regardless of the extraction solvent. However, ethanol is known to extract a larger quantity efficiently as it extracts more phenolics in all three plant organs (Figure 3.6B). This confirms that leaves remain the best target for antioxidant-rich extracts as presented.

It follows that the EA root extract has a lower TPC (1.604±0.206 µg GAE/mg) in comparison with the ethanol root extract (11.849± 0.545 µg GAE/mg) with a high statistical significance ($p \leq 0.001$). This lower phenolic content aligns with the lower antioxidant activity in the root extract (Figure 3.5A), as phenolic compounds are a major contributor to radical scavenging capacity. However, it may still be helpful in applications for which less potent activity is beneficial. For example, in traditional medicine, it is not uncommon to find the root of several plant species valued for their mild therapeutic action (Ozioma *et al*., 201).

© University of Venda

In this respect, the EA root extract of *T. zeylanicum* could be investigated further for specific anti-diabetic or anti-inflammatory activity, which can support less concentrated formulations in medicinal products. Low root phenolic content shows that EA does not effectively extract the phenolics from this plant organ (Figure 3.6B). Other phenolics less soluble in EA might be present in the root tissue.

The amount of phenolic present in the ethanolic stem extract is approximately 10.753±1.116 µg GAE/mg dried extract, a moderate concentration compared to the ethanol leaf extract with a high statistical significance ($p \leq 0.001$). When compared to EA stem extract, the ethanolic stem extract TPC is statistically and significantly high ($p \leq 0.001$) (Figure 3.6B). There is still a considerable amount of phenolics in the ethanol stem extract, which shows that they might also contribute to antioxidant activity, even though the ethanol leaf extract is more critical in that view. The extracts from the ethanol stem extract might be one of the potential secondary sources of antioxidant-rich extracts that could be useful in applications in functional foods. The moderate contents of phenolic compounds evidenced that these ethanol stem extracts may be considered for anti-diabetic and antioxidant formulations in the pharma industry. The EA stem extract contains a phenolic content of about 2.280±0.844 µg GAE/mg, which, although somewhat significantly lower compared to the leaf extract of the same solvent ($p \leq 0.001$), still retains quite a good amount of phenolics that contribute to its antioxidant attributes. The stem has a high phenolic content in EA extraction, which is moderately high, just like in the trend observed with ethanol extraction (Figure 3.6B). It indicates that the phenolics of the stem of this plant are somewhat soluble in polar and medium-polarity solvents. The EA stem extracts might still be helpful in formulations for which antioxidant activity is desired, but clearly, they are less potent than the ethanol leaf extracts. The findings are unique since no study has been conducted that shows TPC chromatograms of ethanol and EA leaf, stem, and root extract of *T. zeylanicum.*

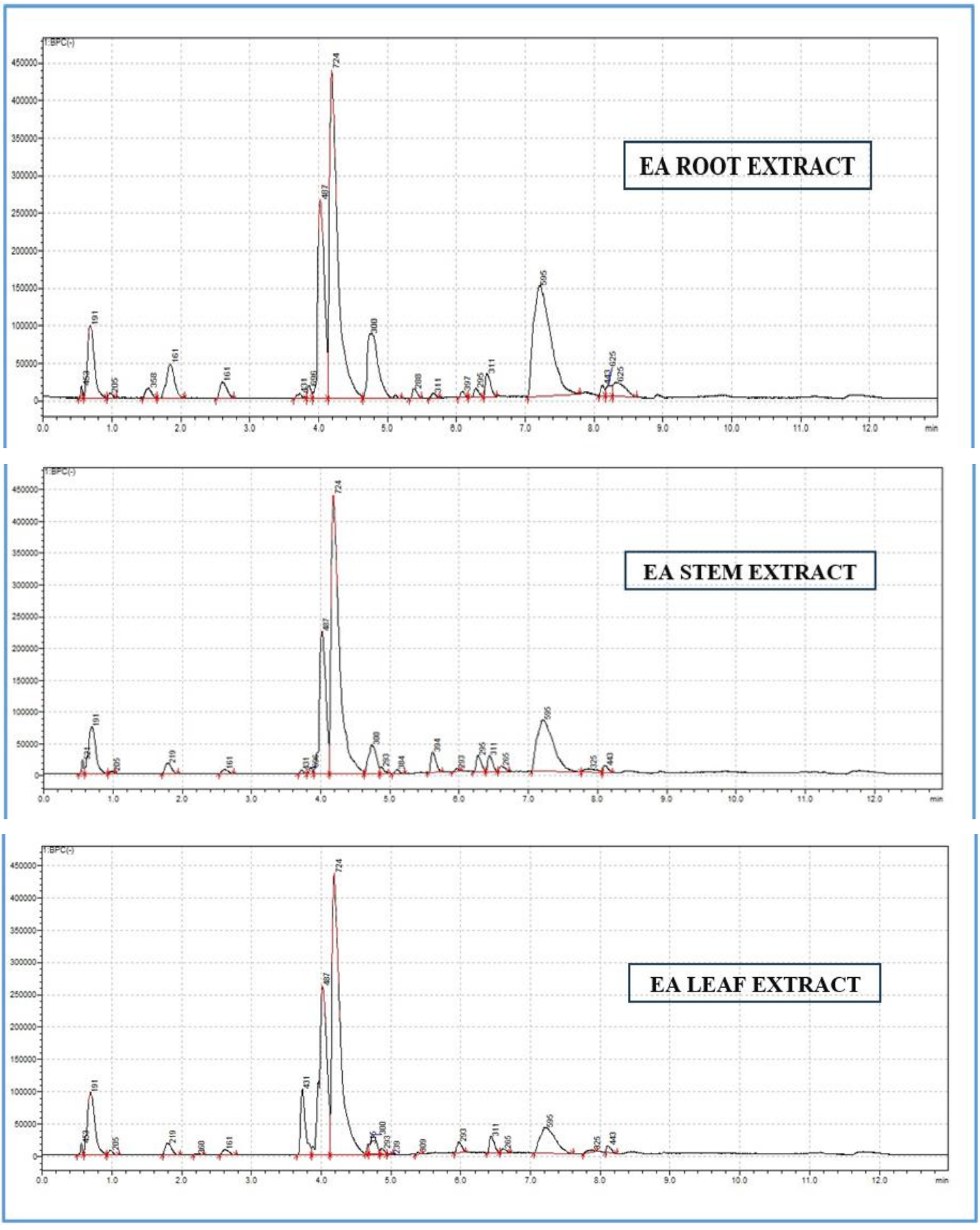
3.4. *In-silico* phytochemical analysis and anti-diabetic potentials of EA and ethanol extracts from different organs of *T. zeylanicum*

3.4.1. LC-qTOF-MS phytochemicals analysis of ethanol and EA extracts from different organs of *T. zeylanicum*.

A plot of the peak intensities of ions in a sample versus their retention time (Figures 3.7A and B). The chromatograms provide an identification and quantification of the compounds in a sample (Figures 3.7A and B). The LC-qTOF-MS chromatograms for the ethyl acetate (EA) and ethanol (E) extracts of root, stem, and leaf of *T. zeylanicum* show generally similar phytochemical profiles with remarkable variations in both the composition and areas under the given peaks in the chromatograms (Figures 3.7A and B). Possibly, some of the peaks could represent the distribution of the active compounds across the plant organs. The chromatograms show large peaks that elute at distinct retention times, which represent important phytochemicals, with the ethanol and EA leaf extracts having the greatest peak intensities, usually suggesting a higher concentration of certain bioactive compounds (Figures 3.7A and B).

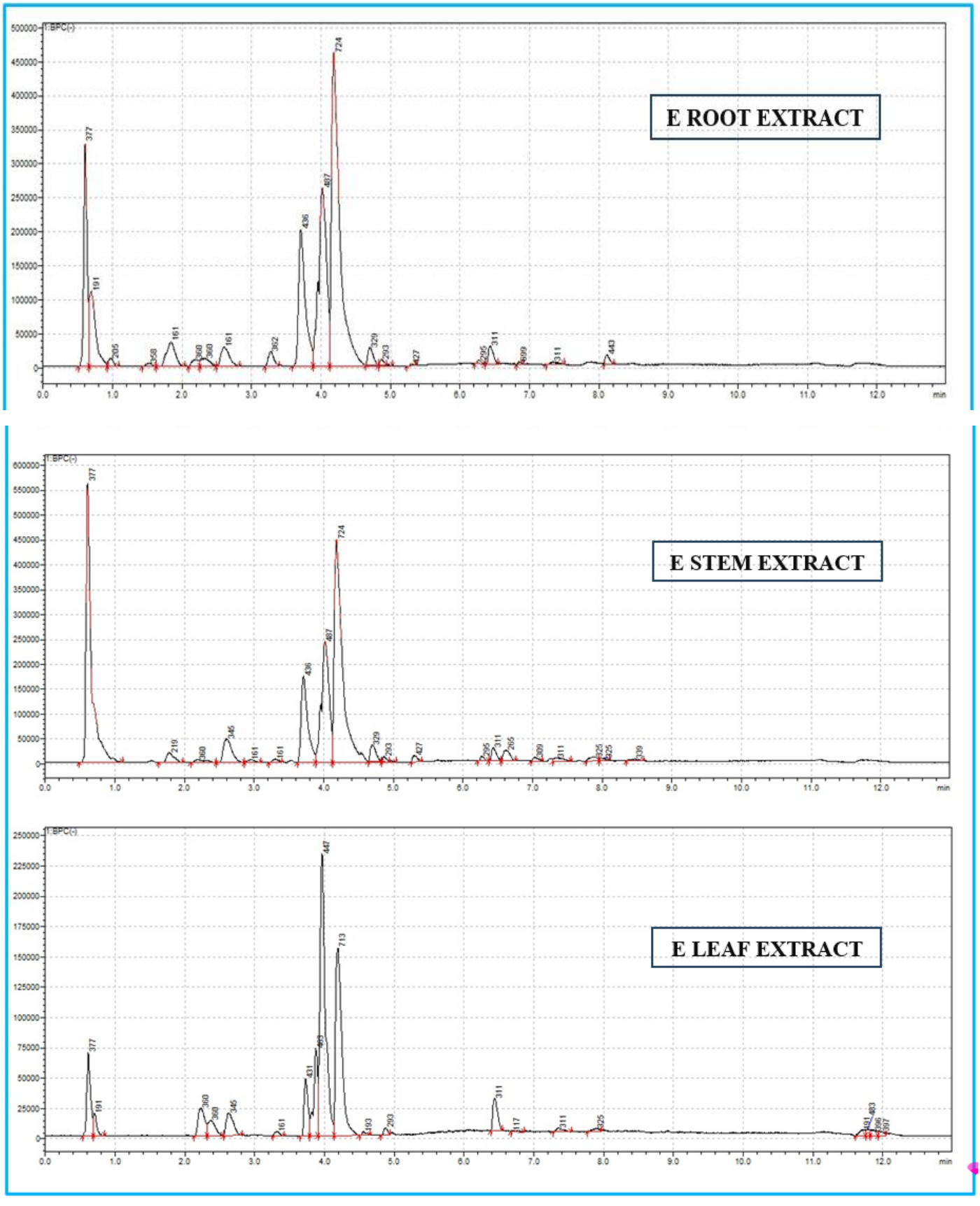
© University of Venda

We found that the ethanol and EA stem and root extracts were remarkably similar in terms of their profiles, with lower peak intensities, suggesting that the compounds are in lesser abundance. The higher concentrations of the active bio-compounds in the ethanol and EA leaf extract may have increased medicinal or biological efficacy in relation to the stem and leaf extracts of both solvents as depicted (Figures 3.7A and B).



© University of Venda

Figure 3.7A: Typical LC-qTOF-MS chromatogram displaying phytochemical dispersion profiles in the EA (EA) extract (2 mg/mL) of *T. zeylanicum* root, stem, and leaf, respectively. The Y-axis indicates the absorbance in AU units, while the X-axis represents the elution time in minutes.



© University of Venda

Figure 3.7B: Typical LC-qTOF-MS chromatogram displaying phytochemical dispersion profiles in the ethanol **(E)** extract (2 mg/mL) of *T. zeylanicum* root, stem, and leaf, respectively. The Y-axis indicates the absorbance in AU units, while the X-axis represents the elution time in minutes.

3.4.2. Negative [M-H] $^{-}$ ionisation fragments identified by Sirius software.

Mass spectral data were obtained in ESI (-) mode. Metabolites from the chromatogram (Figures 3.7A and B) were identified in Tables 3.3A and B. Previous studies validated the identification of the compounds in Tables 3.3A and B (Abdelgawad *et al*., 2021; Altemimi *et al*., 2017; Chrzanowska *et al*., 2024; Malik *et al*., 2023; Sykłowska *et al*., 2023). The chemicals that were found confirmed the presence of the compounds listed in Tables 3.3A and B. While some chemicals were discovered, others were not because their metabolites could not be detected. Some of the compounds that displayed their potential as inhibitors include 4-[2,6-Dihydroxy-4-(6,7,8-trihydroxy-2-naphthyl) phenoxy]-3-hydroxy-7-(3,4,5-trihydroxyphenyl) naphthalene-1,2-dione (Isochromanequinones), Capronor (17-hydroxysteroids), SCHEMBL6844198 (Hexoses), 3,5,6,7-tetrahydroxy-2-(3-methoxyphenyl)-8aH-chromen-8a-yl (methoxybenzenes), 5-Hydroxy-4-oxo-2-(2,3,4-trimethoxy-5-sulfophenyl) chromene-8-sulfonic acid (anthraquinones), Geshoidin (Hexoses) and 2-[2-(2-prop-2-enoyloxyethynoxy)-4-[(E)-2-[4-(2-prop-2-enoyloxyethynoxy)-3-prop-2-enoylperoxyphenyl] ethenyl] phenoxy] ethynyl prop-2-enoate (Anthracenes) (Tables 3.3A and B).These tables (Tables 3.3A and B) show all those metabolites identified from *T. zeylanicum* ethyl acetate root extracts using LC-qTOF-MS in negative ionization.

Table 3.3A: Metabolites separated by LC-qTOF-MS in negative ionization mode in *T. zeylanicum* EA root, stem, and leaf extracts.

EA ROOT EXTRACT					
Peak number	**[M-H] $^{-}$ fragments (Da)**	**Retention time (Min)**	**Molecular formula**	**Tentative identification**	**Classification**
1	724	0,55	$C_{18}H_{14}O_{23}S_4$	Uknown	Sulfobenzoic acid
2	300	4,47	$C_{16}H_{13}O_6$	3,5,6,7-tetrahydroxy-2-(3-methoxyphenyl)-8aH-chromen-8a-yl	Methoxybenzenes
3	487	4,74	$C_{18}H_{16}O_{12}S_2$	5-Hydroxy-4-oxo-2-(2,3,4-trimethoxy-5-sulfophenyl) chromene-8-sulfonic acid	Anthraquinones
4	288	5,38	$C_{16}H_{17}O_5$	Uknown	Naphthoquinones
5	397	6,09	$C_{21}H_{18}O_8$	5,4'-Diacetoxy-3,7-dimethoxyflavone	7-O-methylated flavonoids
6	311	6,44	$C_{21}H_{28}O_2$	Capronor	17-hydroxysteroids
7	595	7,22	$C_{32}H_{20}O_{12}$	4-[2,6-Dihydroxy-4-(6,7,8-trihydroxy-2-naphthyl) phenoxy]-3-	Isochromanequinones

© University of Venda

				hydroxy-7-(3,4,5-trihydroxyphenyl) naphthalene-1,2-dione	
8	311	7,34	$C_{17}H_{28}O_3S$	4-Undecylbenzenesulfonic acid	Benzenesulfonic acids and derivatives
9	625	8,32	$C_{34}H_{26}O_{12}$	2,2',4,4'-Tetrahydroxy-5,5',7,7'-tetramethoxy-3,3'-dimethyl-1,1'-bianthraquinone	Naphthols and derivatives
10	625	8,35		Uknown	Naphthols and derivatives
EA STEM EXTRACT					
1	300	4,73	$C_{16}H_{13}O_6$	3,5,6,7-tetrahydroxy-2-(3-methoxyphenyl)-8aH-chromen-8a-yl	Methoxybenzenes
2	293	4,87	$C_{17}H_{26}O_4$	Gingerol	Gingerols
3	384	5,10	$C_{20}H_{17}O_8$	CID 100969270	O-methylated flavonoids
4	595	7,21	$C_{32}H_{20}O_{12}$	2-[2-(2-prop-2-enoyloxyethynoxy)-4-[(E)-2-[4-(2-prop-2-enoyloxyethynoxy)-3-prop-2-enoylperoxyphenyl] ethenyl] phenoxy] ethynyl prop-2-enoate	Anthracenes
5	311	7,34	$C_{17}H_{28}O_3S$	Undecylbenzenesulfonic acid	Benzenesulfonic acids and derivatives
6	325	7,87	$C_{18}H_{30}O_3S$	4-Dodecylbenzenesulfonic acid	Benzenesulfonic acids and derivatives
EA LEAF EXTRACT					
1	724	0,56	$C_{16}H_6O_{33}$	Uknown	Hydrolysable tannins
2	300	4,74	$C_{16}H_{13}O_6$	CID 131834329	Benzenediols
3	293	4,88	$C_{17}H_{26}O_4$	Gingerol	Gingerols
4	595	7,19	$C_{32}H_{20}O_{12}$	2-[2-(2-prop-2-enoyloxyethynoxy)-4-[(E)-2-[4-(2-prop-2-enoyloxyethynoxy)-3-prop-2-enoylperoxyphenyl] ethenyl] phenoxy] ethynyl prop-2-enoate	Naphthopyranones
5	311	7,34	$C_{17}H_{28}O_3S$	Undecylbenzenesulphonic acid	Benzenesulfonic acids and derivatives
6	325	7,89	$C_{18}H_{30}O_3S$	4-Dodecylbenzenesulfonic acid	Benzenesulfonic acids and derivatives
7	431	7,91	$C_{25}H_{38}O_6$	3-Hexadecoxycarbonylphthalic acid	p-Hydroxybenzoic acid alkyl esters

© University of Venda

Table 3.3B: Metabolites separated by LC-qTOF-MS in negative ionization mode in *T. zeylanicum* ethanol root, stem, and leaf extracts.

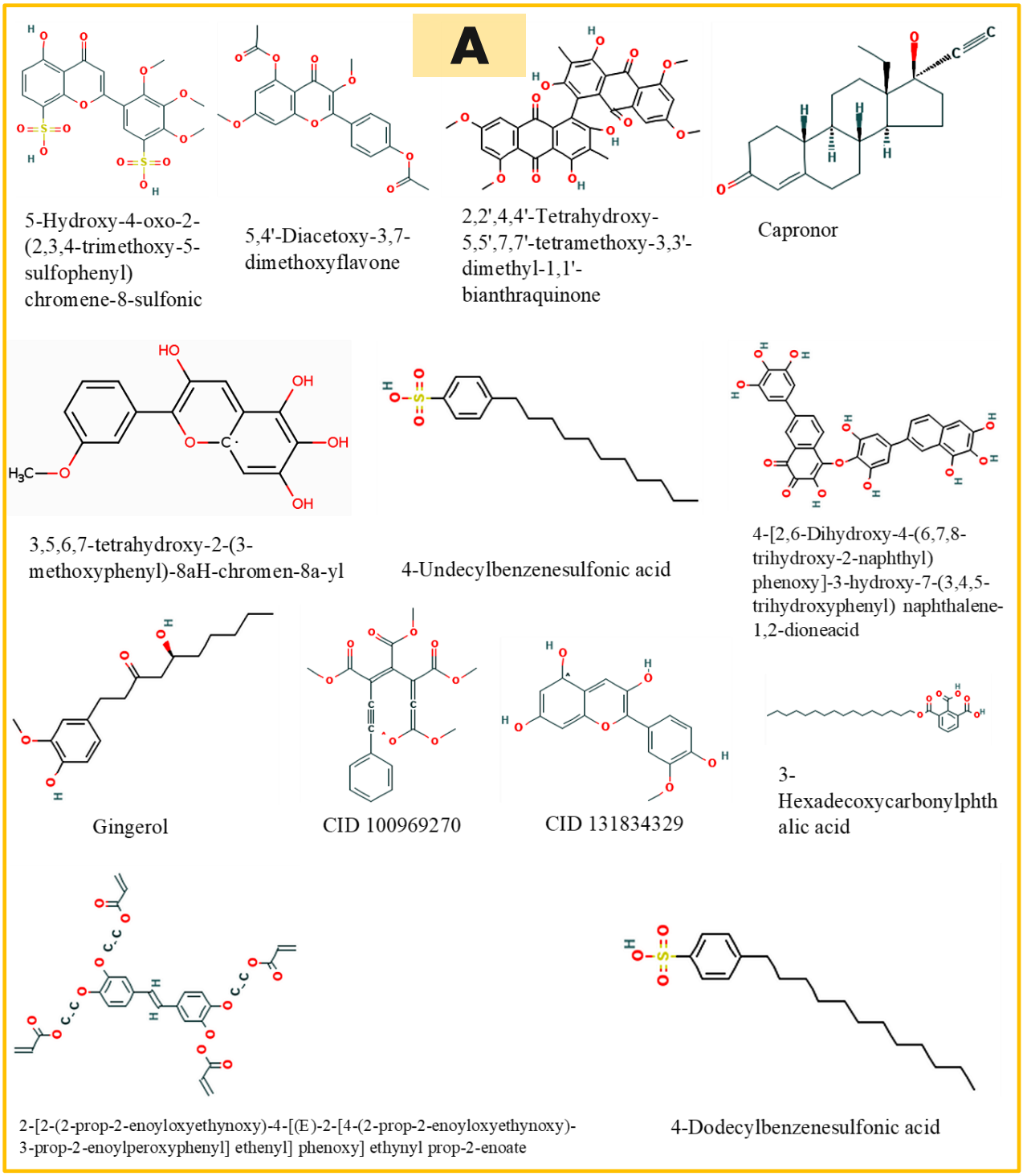
ETHANOL ROOT EXTRACT					
Peak number	**[M-H]$^-$ fragments (Da)**	**Retention time (Min)**	**Molecular formula**	**Tentative identification**	**Classification**
1	377	0,60	$C_{18}H_{18}O_9$	Geshoidin	Hexoses
2	436	3,70	$C_{27}H_{33}O_5$	CID 58879477	4-hydroxyflavonoids
3	329	4,71	$C_{18}H_{34}O_5$	Pinellic acid	Lineolic acids and derivatives
4	293	4,87	$C_{17}H_{26}O_4$	Gingerol	Fatty alcohols
5	295		$C_{17}H_{28}O_3S$	Undecylbenzenesulfonic acid	Benzenesulfonic acids and derivatives
6	311	6,43	$C_{21}H_{28}O_2$	Capronor	17-hydroxysteroids
7	311	7,34	$C_{17}H_{28}O_3S$	Undecylbenzenesulphonic acid	Benzenesulfonic acids and derivatives
8	443	8,11	$C_{19}H_{40}O_{11}$	Methoxytricosaethylene glycol	Fatty acyl glycosides of mono- and disaccharides
ETHANOL STEM EXTRACT					
1	377	0,61	$C_{18}H_{18}O_9$	SCHEMBL6844198	Hexoses
2	427	0,69	$C_{23}H_8O_9$	Uknown	1-hydroxy-2-unsubstituted benzenoids
3	360	2,21	$C_{13}H_{29}O_{11}$	Uknown	Alkyl glycosides
4	345	2,60	$C_{16}H_{26}O_8$	1,4-Butylene glycol diadipate	lipids and lipid-like molecules
5	436	3,71	$C_{27}H_{33}O_5$	CID 58879477	6-prenylated flavanones
6	329	4.69	$C_{18}H_{34}O_5$	Pinellic acid	Lineolic acids and derivatives
7	293	4,86	$C_{17}H_{26}O_4$	Gingerol	Gingerols
8	311	6,43	$C_{17}H_{28}O_3S$	C11-Linear alkyl benzene sulfonate	Benzenesulfonic acids and derivatives
9	311	7,34	$C_{17}H_{28}O_3S$	Undecylbenzenesulphonic acid	Benzenesulfonic acids and derivatives
10	325	7,89	$C_{18}H_{30}O_3S$	4-Dodecylbenzenesulfonic acid	Benzenesulfonic acids and derivatives
11	339	8,47	$C_{19}H_{32}O_3S$	Tridecylbenzenesulphonic acid	Benzenesulfonic acids and derivatives
ETHANOL LEAF EXTRACT					
1	447	3,96	$C_{21}H_{20}O_{11}$	Trifolin	Flavonoid-3-O-glycosides
2	293	4,88	$C_{17}H_{26}O_4$	Gingerol	Gingerols

© University of Venda

3	311	6,43	$C_{21}H_{28}O_2$	Capronor	17-hydroxysteroids
4	311	7,35	$C_{17}H_{28}O_3S$	Undecylbenzenesulphonic acid	Benzenesulfonic acids and derivatives
5	325	7,92	$C_{18}H_{30}O_3S$	4-Dodecylbenzenesulfonic acid	Benzenesulfonic acids and derivatives

3.4.3. LC-qTOF-MS chromatograms detected and identified compounds in EA and ethanol extracts from different organs of *T. zeylanicum*.

The LC-qTOF-MS chromatograms portray the chemical structures of some of the isolated target compounds from EA and ethanol root, stem, and leaf extracts of *T. zeylanicum* (Figures 3.8A and B).



© University of Venda

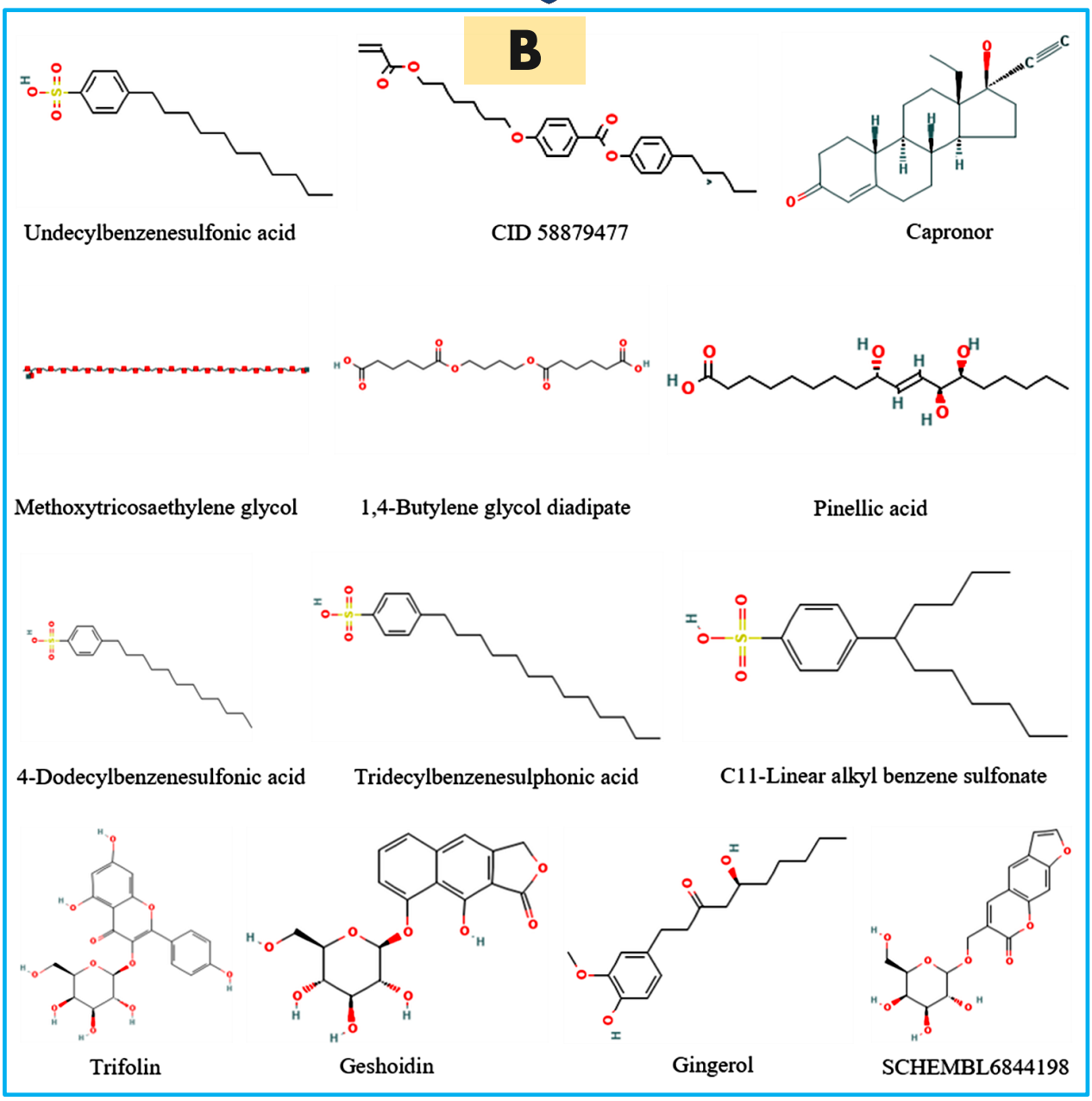


Figure 3.8: The molecular structures of selected identified compounds from *T. zeylanicum* root, stem, and leaf **(A)** ethyl acetate and **(B)** ethanolic extract that were docked against α-amylase, α-glucosidase, and VEGFR2.

The extracts are classified into two major divisions, the first one with EA root, stem, and leaf extract (A) and the second one with ethanol root, stem, and leaf extract (B) (Figures 3.8A and B). The ethanolic extract compounds include undecylbenzenesulfonic acid, CID 58879477, Capronor, Methoxytricosaethylene glycol, 1,4-butylene glycol diadipate, pinellic acid, 4-dodecylbenzenesulfonic acid, tridecylbenzenesulphonic acid, C11-linear alkyl benzene sulfonate, trifolin, geshodin, gingerol, and SCHEMBL6844198 (Figure 3.8B). These adsorption studies considered the principal enzymes α-amylase, α-glucosidase, and VEGFR2 kinase. This study expresses the profiles which highlight the possible biological activity of these compounds through *in-silico* molecular docking (Figure 3.10, Figure 3.11, Figure 3.12, Figure 3.13, Figure 3.14, and Figure 3.15), especially regarding the inhibition of diabetic and wound-related enzymes in therapeutic prospects.

© University of Venda

3.4.4. Molecular docking of α-amylase, α-glucosidase and VEGFR2 against selected identified compounds to assess their antidiabetic potentials.

The selected identified compounds were docked against α-amylase, α-glucosidase and VEGFR2 to study the antidiabetic properties of ethanol and EA extracts from different organs of *T. zeylanicum* associated with antioxidant activity and wound healing using acarbose and sorafenib as controls.

3.4.4.1. Retrieved proteins (α-amylase, α-glucosidase, and VEGFR2 kinase) from the RCSB Protein Data Bank database for molecular docking.

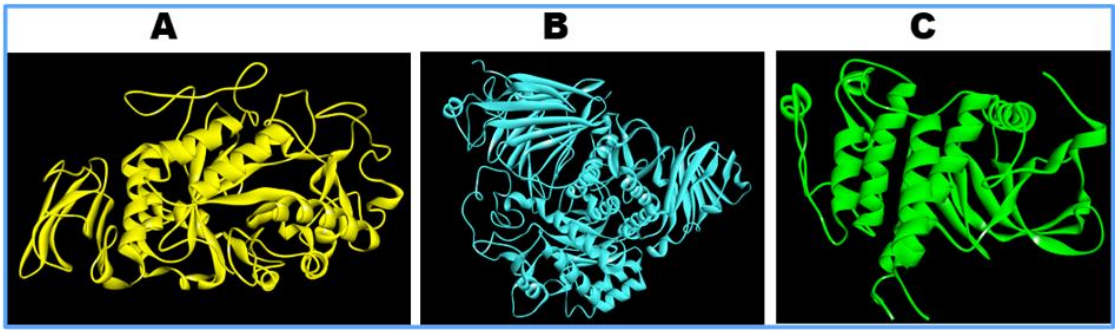


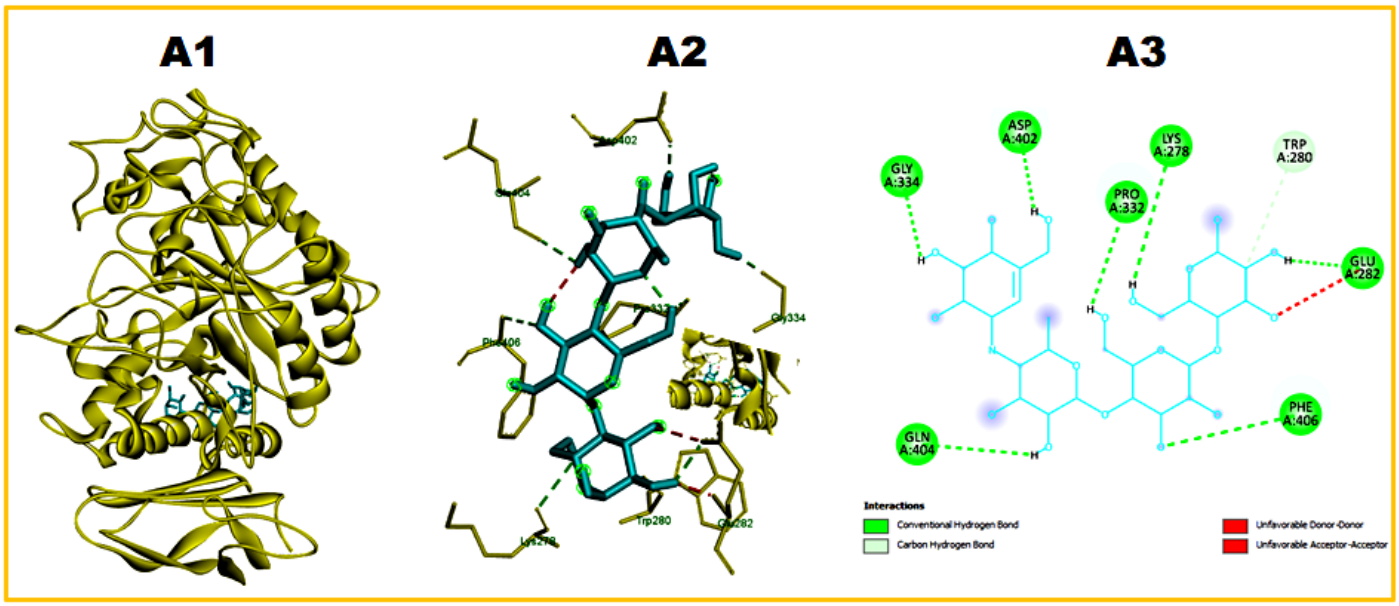
Figure 3.9: Structural homolog depicting active sites and the whole protein groups of the proteins used for molecular docking. (**A**) pancreatic α-amylase, (**B**) α-glucosidase, and (**C**) VEGFR2.

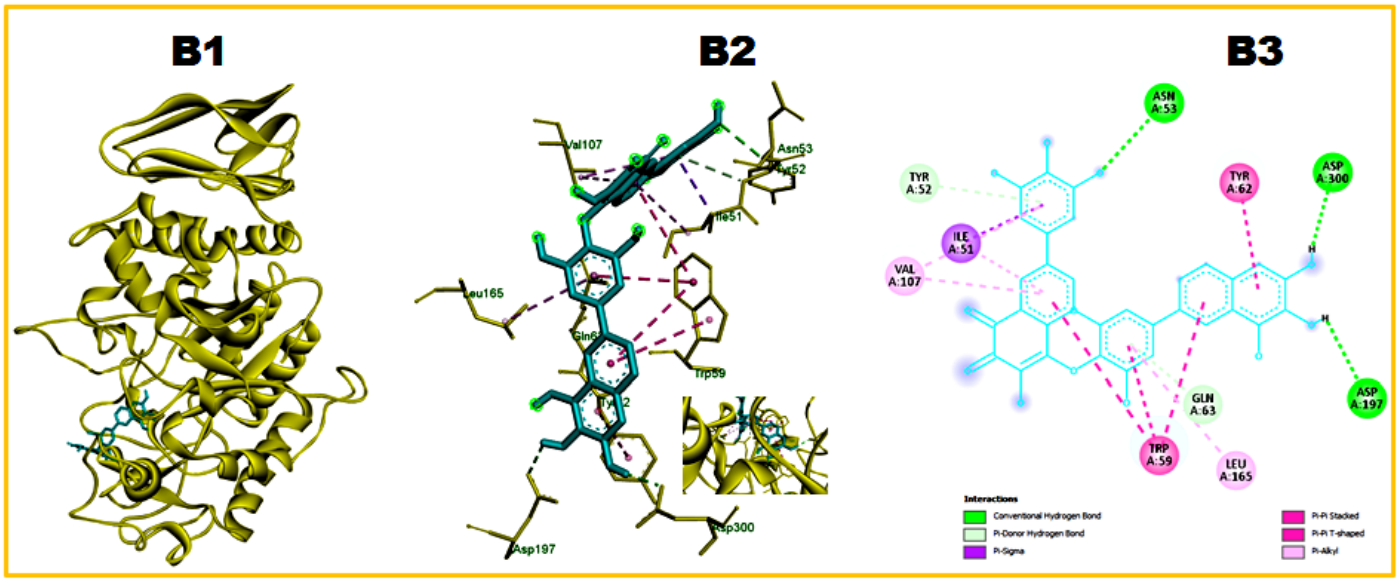
3.4.4.2. Selected identified compounds in EA extracts from different organs of *T. zeylanicum* docked against α-amylase.

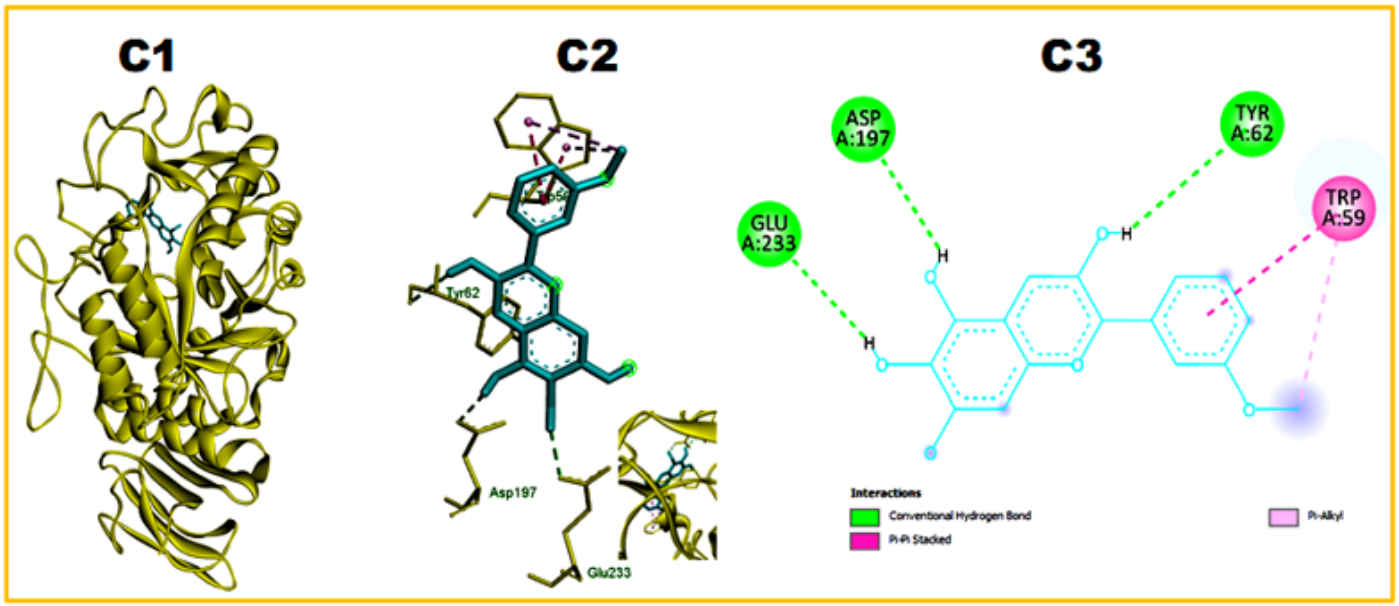
The structural homologue of the enzyme α-amylase that was recovered shows α-helices, β-strands, twists and loops, active sites, and entire protein groups (Figure 3.9A) were subjected to docking (Figure 3.10A) with acarbose and the inhibiting compounds identified from the EA plant extract (Table 3.3A). Table 3.4 shows the association affinities obtained from PyRx's docking of many ligands. Acarbose is a recognized α-amylase inhibitor, and it has been widely confirmed that it adheres to the active site and forms seven conventional hydrogen bonds with amino acids Gly334, Asp402, Pro332, Lys278, Glu282, Gln404 and Phe406; a single carbon-hydrogen bond by Trp280; a single unfavourable Donor-Donor by Glu282, and a single unfavourable acceptor-acceptor by Glu282. Additionally, it interacted with distant amino acid residues through Van der Waals interactions. Interestingly, Glu282 interacted with the ligand and registered two different bonds, as depicted in the first structure (Figure 3.10A). The amino acid residues that facilitated the overall binding of the protein-ligand complex are the ones that formed the conventional hydrogen bonds. The overall docking grade for the above interaction is -7.4 kcal/mol (Table 3.4). These findings comply with the previously reported results by Radzuan *et al*. (2024) and Nada *et al*. (2024). After binding to the active region of the α-amylase, acarbose showed that it might function as a competitive inhibitor (Figure 3.10A). Although the acarbose-α-amylase complex binding affinity in this study is high and following more recent studies mentioned above, in comparison with the previously reported findings (Zahra *et al*., 2024), the affinity is too low, whereas the findings reported by Baccari *et al*. (2024) were high.

© University of Venda

Interestingly, all these findings are comparable as the affinities are in close range, validating the present study's reliability with those of the positive controls.







© University of Venda

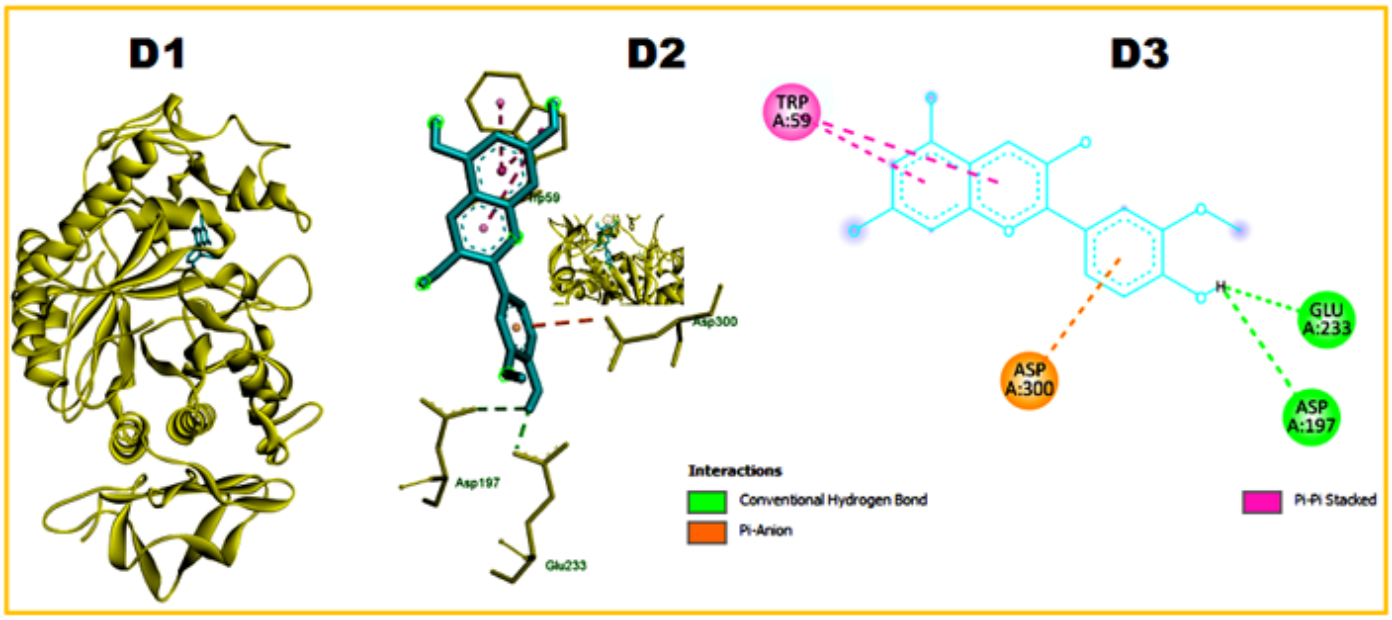


Figure 3.10: Molecular docking of **α-amylase** against **(A) Acarbose**, **(B) Ligand 1A, (C) Ligand 2A, and (D) Ligand 3A**. (A1–D1) depicts the active site of the α-amylase, (A2–D2) demonstrate the zoomed-in interaction site of the enzyme and ligands; (A3–D3) display the interacting amino acid residues of the α-amylase.

Table 3.4: The binding affinities of selected identified compounds in EA root, stem, and leaf extracts of *T. zeylanicum* with the highest binding affinity to the α-amylase and the interacting amino acid residues of the protein.

ligand	Ligand name/code and plant part	Molecular formula	Binding affinity (kcal/mol)	Rmsd /Ub	Rmsd /Ib	Interacting residues of the protein and their positions
Positive control	Acarbose	$C_{25}H_{43}NO_{18}$	-7,4	0	0	Gly334, Asp402, Pro332, Lys278, Gln404, Phe406, Glu282 and Trp280
Ligand 1A	4-[2,6-Dihydroxy-4-(6,7,8-trihydroxy-2-naphthyl) phenoxy]-3-hydroxy-7-(3,4,5-trihydroxyphenyl) naphthalene-1,2-dione (EA root extract)	$C_{32}H_{20}O_{12}$	-11,0	0	0	Asn53, Asp300, Asp197, Tyr52, Gln63, Ile51, Tyr62, Trp59, Val107, and Leu165
Ligand 2A	3,5,6,7-tetrahydroxy-2-(3-methoxyphenyl)-8aH-chromen-8a-yl (EA stem extract)	$C_{16}H_{13}O_6$	-7,9	0	0	Glu233, Asp197, Tyr62 and Trp59
Ligand 3A	CID 131834329 (EA leaf extract)	$C_{16}H_{13}O_6$	-8,2	0	0	Glu233, Asp197, Asp300 and Trp59

© University of Venda

Ligand 2A	3,5,6,7-tetrahydroxy-2-(3-methoxyphenyl)-8aH-chromen-8a-yl (EA root extract)	$C_{16}H_{13}O_6$	-79	0	0	Glu233, Asp197, Asp 300, and Trp59
Ligand 5A	2,2',4,4'-Tetrahydroxy-5,5',7,7'-tetramethoxy-3,3'-dimethyl-1,1'-bianthraquinone (EA root extract)	$C_{34}H_{26}O_{12}$	-8.6	0	0	Thr163, Asp300, His201, Gly306, Leu165, Ala307, Ile235, Trp59, and His305
Ligand 6A	Capronor (EA root extract)	$C_{21}H_{28}O_2$	-8.6	0	0	Asp300, Trp59, Tyr62, Ala198, and Leu162
Ligand 4A	2-[2-(2-prop-2-enoyloxyethynoxy)-4-[(E)-2-[4-(2-prop-2-enoyloxyethynoxy)-3-prop-2-enoylperoxyphenyl] ethenyl] phenoxy] ethynyl prop-2-enoate (EA stem extract)	$C_{32}H_{20}O_{12}$	-7.5	0	0	Gln63, Trp59 and Tyr62
Ligand 4A	2-[2-(2-prop-2-enoyloxyethynoxy)-4-[(E)-2-[4-(2-prop-2-enoyloxyethynoxy)-3-prop-2-enoylperoxyphenyl] ethenyl] phenoxy] ethynyl prop-2-enoate (EA leaf extract)	$C_{32}H_{20}O_{12}$	-7.5	0	0	Gln63, Trp59 and Tyr62

The molecular homologue of the enzyme α-amylase that was recovered shows α-helices, β-strands, twists and loops, active sites, and entire protein groups (Figure 3.9A) were subjected to docking (Figure 3.10B) with the inhibiting compounds identified from the ethanol root extract of *T. zeylanicum* (Table 3.3A). Multiple ligands docking by PyRx provided the binding affinities (Table 3.4). Ligand A (4-[2,6-Dihydroxy-4-(6,7,8-trihydroxy-2-naphthyl) phenoxy]-3-hydroxy-7-(3,4,5-trihydroxyphenyl) naphthalene-1,2-dione) from EA root extract demonstrated the outstanding binding energy compared to other plant root phytochemicals docked with (Figure 3.10B). The compound was bound to the enzyme by six interactions presented above. It was widely confirmed that it forms three typical hydrogen bonds when it attaches to the α-amylase's active site with amino acids Asn53, Asp300, and Asp197; two Pi-donor hydrogen bonds by Try52 and Gln63; a single Pi-sigma interaction by Ile51; two Pi-alkyl interactions by Val107 and Leu165. Appealingly, the two amino acid residues Tyr62 and Trp59 registered two different interactions, namely Pi-Pi stacked and Pi-Pi T-shaped; moreover, amino acid residue Trp59 formed three Pi-Pi stacked and Pi-Pi T-shaped interactions at once from different ligand atom positions as depicted above (Figure 3.10B). The chemical also bonded with distant amino acid residues through Van der Waals interactions. The amino acid residues facilitating the protein-ligand complex's overall binding are Asn53, Asp300 and Asp197. In comparison with the α-amylase positive inhibitor, altogether, this interaction has a total docking score of −11,0 kcal/mol, whereas the control binding

© University of Venda

energy was low at -7,4 kcal/mol (Table 3.4). The compound 4-[2,6-Dihydroxy-4-(6,7,8-trihydroxy-2-naphthyl) phenoxy]-3-hydroxy-7-(3,4,5-trihydroxyphenyl) naphthalene-1,2-dione validated its capacity to function as a competitive inhibitor by binding to the active site of the α-amylase (Figure 3.10B) with greater binding energy, hence it can be considered as a drug candidate. Interestingly, this compound has not been reported as an inhibitor; hence, these findings are novel.

The very same structural homologue of the α-amylase that was recovered displays the entire protein groups, loops, turns, α-helices, and β-strands (Figure 3.9A), and was subjected to docking (Figure 3.10C) with the inhibiting compounds identified from the EA stem extract of *T. zeylanicum* (Table 3.3A). Multiple ligands docking by PyRx provided the binding affinities (Table 3.4). Ligand 2A (3,5,6,7-tetrahydroxy-2-(3-methoxyphenyl)-8aH-chromen-8a-yl) from EA stem extract demonstrated the outstanding binding energy compared to other plant stem phytochemicals docked with (Figure 3.10C). The compound was bound to the enzyme by three different interactions as presented above. It was widely confirmed to connect with the α-amylase's active region and create three conventional hydrogen bonds with amino acids Glu233, Asp197, and Tyr62; a single Pi-Pi stacked and Pi-alkyl interaction by the same amino acid residue Trp59 (Figure 3.10C). Additionally, the chemical is associated with distant amino acid residues through Van der Waals interactions. The amino acid residues facilitating the protein-ligand complex's overall binding are Tyro62, Aspa197 and Glu233. In comparison with the α-amylase positive inhibitor, ultimately, the docking rating for this relationship is -7.9 kcal/mol, whereas the control binding energy was low at -7,4 kcal/mol (Table 3.4). The compound 3,5,6,7-tetrahydroxy-2-(3-methoxyphenyl)-8aH-chromen-8a-yl has been established to function as a competitive inhibitor by binding to the active domain of the α-amylase and can be considered as a drug candidate. The most remarkable part of this compound is that it has also not been reported as an inhibitor; hence, these findings are novel.

The identical structural homologue of the α-amylase that was recovered displays the entire protein groups, loops, turns, α-helices, and β-strands (Figure 3.9A) and was subjected to docking (Figure 3.10D) with the inhibiting compounds identified from the plant's EA leaf extract (Table 3.3A). Multiple ligands docking by PyRx provided the binding affinities (Table 3.4). Ligand 3A (CID 131834329) from EA leaf extract demonstrated outstanding binding energy compared to other plant leaf phytochemicals docked. The compound was bound to the enzyme by the three interactions presented above. It was broadly demonstrated that it forms two conventional hydrogen bonds from the same ligand hydrogen atom by amino acids Glu233 and Asp197. The same amino acid residues were reported to form the same conventional hydrogen bond. It also interacted via a single Pi-Anion interaction by amino acid Asp300, and two Pi-Pi stacked interactions by the same amino acid residue Trp59 (Figure 3.10D). The molecule also engaged with distant amino acid residues through Van der Waals attractions. The amino acid residues facilitating the protein-ligand complex's overall binding are Glu233 and Asp197. In comparison with the α-amylase positive inhibitor, thoroughly, this interaction has a −8,2 kcal/mol overall docking grade, whereas the control binding energy was low at -7,4 kcal/mol (Table 3.4).

© University of Venda

The compound CID 131834329 established its competence to function as a competitive inhibitor by adhering to the α-amylase's active site. Hence it can be considered as a drug candidate. The most remarkable part of this compound is that it also has not been reported as an inhibitor; hence, these findings are novel.

The EA root extract, Ligand 2A (3,5,6,7-tetrahydroxy-2-(3-methoxyphenyl)-8aH-chromen-8a-yl) molecule had a binding affinity of -7.9 kcal/mol, which was higher than that of the reference medication, acarbose (-7.4 kcal/mol) when bound to pancreatic α-amylase. Their binding affinities were provided by a variety of docked ligands based on PyRx (Table 3.4). Trp59 engaged in Pi-alkyl and Pi-stacking interactions with the ligand. The ligand's position in the binding pocket is stabilised by these hydrophobic or aromatic stacking interactions. The conventional hydrogen bond between Glu233, Asp197, and Asp300 appears to assist in anchoring the ligand in the binding pocket. Both aspartate and glutamate are negatively charged residues that frequently participate in acid-base catalysis or create hydrogen bonds to maintain the transition state of enzyme processes. Additionally, the chemical used Van der Waals interactions to form bonds with distant amino acid residues. Ligand 2A demonstrated its ability to function as an inhibitor when binding to the active site of the α-amylase, manifesting a bigger binding energy (-7.9 kcal/mol) (Table 3.4). Therefore, the molecule can be considered a potential anti-diabetic medication. Ligand 2A also demonstrated its ability to block by binding to the α-amylase's binding site with a considerably greater binding energy. Surprisingly, no report exists in the literature on this compound's mode of inhibition.

The EA root extract, Ligand 5A (2,2',4,4'-Tetrahydroxy-5,5',7,7'-tetramethoxy-3,3'-dimethyl-1,1'-bianthraquinone) presented its ability to have activity against the pancreatic α-amylase role in diabetes formation (Table 3.4). Trp59 interacted via Pi-Pi T-shaped, Pi-Pi stacked and Pi-sigma. Tryptophan forms aromatic stacking interactions with the ligand’s aromatic ring, stabilising it in the binding pocket. Tryptophan seemed to provide hydrophobic and spatial orientation for the ligand, consistent with prior experimental results. The side chains of Thr163 and Asp300 interacted through a typical hydrogen bond. A strong hydrogen bond is created between the aspartate with a functional group on the ligand, which pulls the ligand toward a critical catalytic or stabilising site in the enzyme. There are also interactions involving hydrogen bonding where threonine supports the interaction of the ligand, showing that this residue may also interact in a polar manner with the hydroxyl or carbonyl group of the ligand. Besides that, Histidine residues His101, His201, and Gly306 interacted through carbon-hydrogen bonds. The contribution of the histidine is a mix of polar and aromatic interactions. These residues often play a catalytic or structural role, and their involvement in binding implies that the ligand interacts with critical parts of the enzyme. Leu165, Ala307 and Ile235 Isoleucine Interacted via Alkyl and Pi-alkyl interactions. These hydrophobic residues interact with the ligand’s non-polar regions, helping to stabilise the binding through van der Waals forces. The chemical also bonded with distant amino acid residues through Van der Waals interactions. The amino acid residues that facilitated the overall binding of the protein-ligand complex are Thr163 and Asp300.

© University of Venda

With a binding energy of -8.6 kcal/mol, this ligand shows strong potential to bind effectively to α-amylase when compared to Acarbose (-7.4 kcal/mol), as shown in Table 3.4. Strong binding may reduce enzyme activity, supporting its role as an inhibitor.

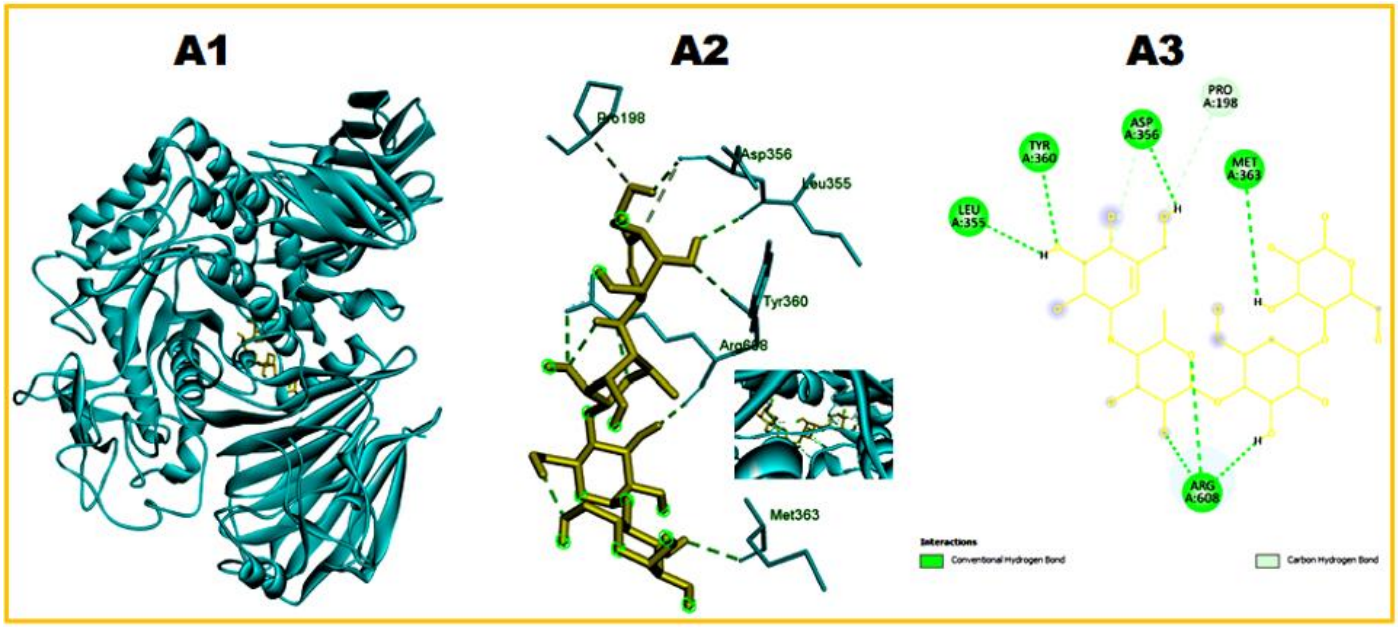
Another EA root extract, Ligand 6A (Capronor), was bound to pancreatic α-amylase, exerting anti-diabetic potential through stronger binding energy (-8.6 kcal/mol) in comparison with the positive control acarbose [-7.4 kcal/mol] (Table 3.4). Asp300 makes conventional hydrogen bonding interactions. The Aspartate forms a hydrogen bond with the ligand, anchoring it firmly within the active site. Since aspartate is often part of the catalytic triad in enzymes, this interaction may block substrate binding or enzymatic activity, suggesting competitive inhibition. Tyr62, Leu162, Ala198, and Trp59 Interacted via Alkyl and Pi–Alkyl. These residues interact with hydrophobic regions of the ligand, adding to the overall stability of the ligand-enzyme complex. Tryptophan interacts with the ligand's hydrophobic regions, likely stabilising it through stacking or nonpolar interactions. This interaction ensures proper orientation of the ligand in the binding pocket. This docking result suggests that Capronor is a strong candidate for α-amylase inhibition, with significant hydrogen bonding (Asp300) and hydrophobic interactions (Tyr62, Leu162, Ala198, and Trp59). Additionally, it has also been found that Van der Waals interactions assign a considerable role to the far-away few amino acid residues. The amino acid residue involved in the overall binding of the protein-ligand complex was Asp300. The binding energy measured at -8.6 kcal/mol supports its potential for acting as an effective inhibitor (Table 3.4). Furthermore, refining its hydrophobicity and polar properties could enhance it as a more auspicious candidate for therapeutic applications, regulating carbohydrate digestion.

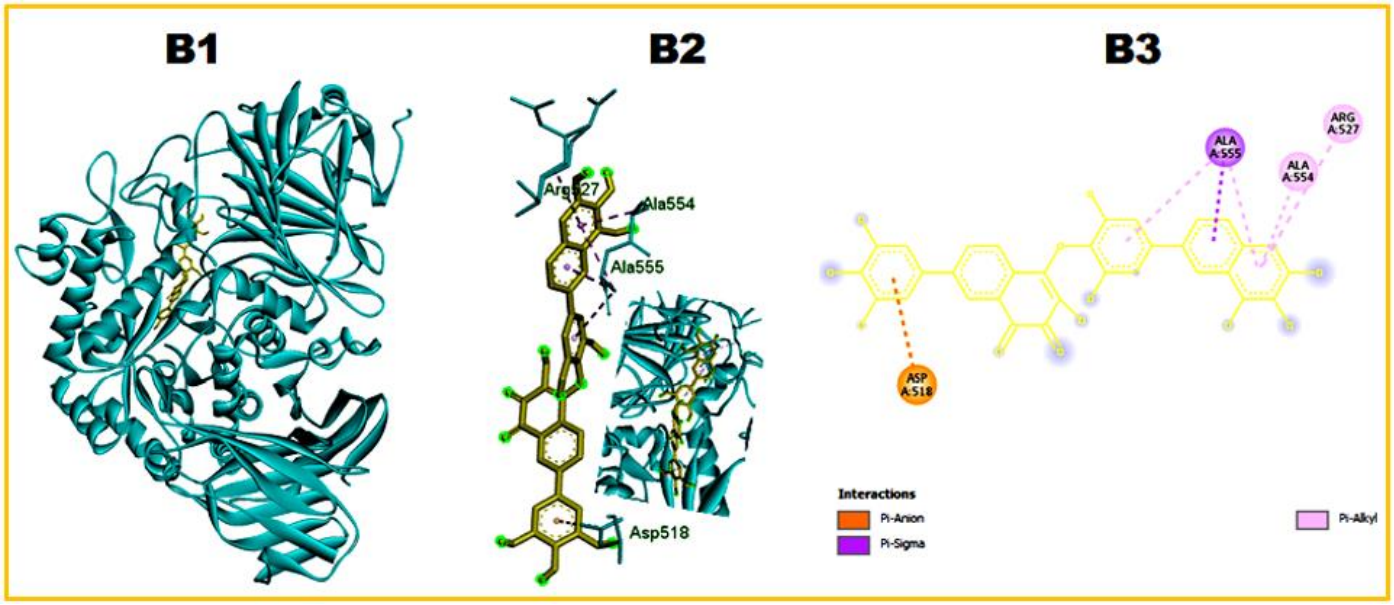
EA stem and leaf extract, Ligand 4A (2-[2-(2-prop-2-enoyloxyethynoxy)-4-[(E)-2-[4-(2-prop-2-enoyloxyethynoxy)-3-prop-2-enoylperoxyphenyl] ethenyl] phenoxy] ethynyl prop-2-enoate) was both bound to pancreatic α-amylase via two types of interactions, Pi-Donor hydrogen bond by Gln63. This is a stabilising interaction where the aromatic system interacts with the hydrogen-donating group of the amino acid residue. The polar Gln63 makes a considerable contribution to ligand binding via this interaction by virtue of its polar nature. Aromatic-residue Pi-Pi-stacked interactions by Trp59 and Tyr62 with the ligand's aromatic ringed system are critically essential to balancing out the hydrophobic and aromatic nature of the ligands in the binding pocket. The binding pocket's likely hydrophobic aromatic nature is supported by the presence of aromatic residues Tyr62 and Trp59. Polar Gln63 takes part in the binding pocket, giving it polarity. As a result, the pocket shows a balance between hydrophobic and polar areas, allowing polar interactions to occur. The ligand's ability to engage in strong aromatic interactions makes it a promising candidate, particularly for targets where such interactions are critical. Compared to the α-amylase positive inhibitor, the overall docking grade for this connection is -7,5 kcal/mol, whereas the control binding energy was low at −7,4 kcal/mol (Table 3.4).

© University of Venda

3.4.4.3. Selected identified compounds in EA extracts from different organs of *T. zeylanicum* docked against α-glucosidase.

The α-glucosidase (Figure 3.9B) was also subjected to docking with the control acarbose, as shown below in Figure 3.11A, and the inhibiting compounds identified from the plant organs extract (Table 3.3A). Multiple ligands docking by PyRx provided the binding affinities as depicted below in Table 3.5. The well-known acarbose, the α-glucosidase inhibitor, was typically confirmed by association with the active site, creating seven conventional hydrogen bonds with amino acids Leu355, Tyr360, Asp356, Met363, and remarkably, Arg608 interacted with acarbose and presented three conventional hydrogen bonds shown (Figure 3.11A); a single carbon-hydrogen bond by Pro198.





© University of Venda

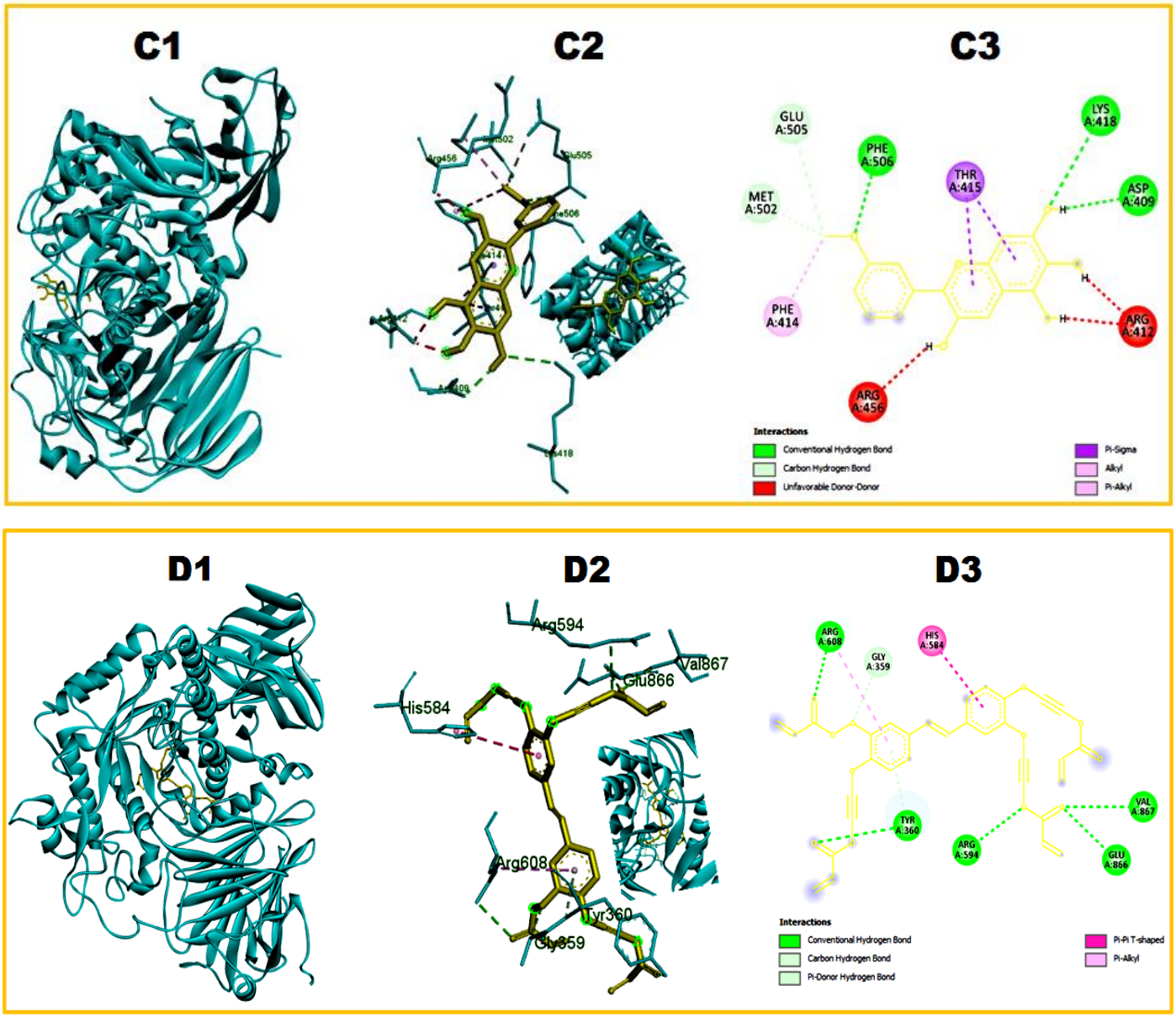


Figure 3.11: Molecular docking of **α-glucosidase** against (A) **Acarbose**, **(B) Ligand 1A, (C) Ligand 2A, and (D) Ligand 4A.** (A1–D1) depicts the active site of the α-glucosidase, (A2–D2) demonstrate the zoomed-in interaction site of the enzyme and ligands; (A3–D3) display the interacting amino acid residues of the α-glucosidase.

Table 3.5: The binding affinities of selected identified compounds in EA root, stem, and leaf extracts of *T. zeylanicum* with the highest binding affinity to the α-glucosidase and the interacting amino acid residues of the protein.

ligand	Ligand name/code and plant part extract	Molecular formula	Binding affinity (kcal/mol)	Rmsd /Ub	Rmsd /Ib	Interacting residues of the protein and their positions
Positive control	Acarbose	$C_{25}H_{43}NO_{18}$	-7,8	0	0	Leu355, Tyr360, Asp356, Met363, Arg608 and Pro198

© University of Venda

Ligand 1A	4-[2,6-Dihydroxy-4-(6,7,8-trihydroxy-2-naphthyl) phenoxy]-3-hydroxy-7-(3,4,5-trihydroxyphenyl) naphthalene-1,2-dione (EA root extract)	$C_{32}H_{20}O_{12}$	-10,2	0	0	Asp518, Ala555, Ala554, and Arg527
Ligand 2A	3,5,6,7-tetrahydroxy-2-(3-methoxyphenyl)-8aH-chromen-8a-yl (EA stem extract)	$C_{16}H_{13}O_6$	-7,5	0	0	Phe506, Lys418, Asp409, Glu505, Met502, Arg456, Arg412, Thr415 and Phe414.
Ligand 4A	2-[2-(2-prop-2-enoyloxyethynoxy)-4-[(E)-2-[4-(2-prop-2-enoyloxyethynoxy)-3-prop-2-enoylperoxyphenyl] ethenyl] phenoxy] ethynyl prop-2-enoate (EA leaf extract)	$C_{32}H_{20}O_{12}$	-7,8	0	0	Arg608, Tyr360, Arg594, Val867, Glu866, Gly359, and His584

The molecule further engaged with distant amino acid residues through Van der Waals attractions. The amino acid residues that facilitated the overall binding of the protein-ligand complex are bound by conventional hydrogen bonds, shown in Figure 3.11A. Altogether, the acarbose and α-glucosidase interaction has a total docking score of −7.8 kcal/mol (Table 3.5). Previous studies presented the binding affinity in agreement within a close range, as these findings (Radzuan *et al*., 2024; Zahra *et al*., 2024), validating the present study's reliability. By binding to the active site of the α-glucosidase, acarbose demonstrated its capacity to function as a competitive inhibitor (Figure 3.11A).

The same organizational homologue of α-glucosidase showing α-helices, β-strands, loops, and turns, active sites and the complete protein groups (Figure 3.9B) was subjected to docking (Figure 3.11B) with the inhibiting compounds identified from the plant's EA root extract (Table 3.3A). Multiple ligands docking by PyRx provided the binding affinities (Table 3.5). The same compound, Ligand 1A (4-[2,6-Dihydroxy-4-(6,7,8-trihydroxy-2-naphthyl) phenoxy]-3-hydroxy-7-(3,4,5-trihydroxyphenyl) naphthalene-1,2-dione) from EA root extract demonstrated the outstanding binding energy compared to other plant root phytochemicals docked as presented above (Figure 3.11B and 3.10B). The compound was bound to the enzyme by three interactions, as shown above. It was commonly validated that it attaches with the active site of the α-glucosidase via a single Pi-Anion interaction by Asp518; a single Pi-sigma interaction by Ala555; four Pi-alkyl interactions by Ala554, Arg527 and Ala555, which formed two of the bonds (Figure 3.11B).

© University of Venda

Furthermore, the chemical bonds with distant amino acid residues through Van der Waals interactions. Although these interactions had no hydrogen bonds. In comparison with the α-glucosidase positive inhibitor, altogether, this interaction has a total docking score of −10,2 kcal/mol, whereas the control binding energy was low at -7,8 kcal/mol (Table 3.5). The compound 4-[2,6-Dihydroxy-4-(6,7,8-trihydroxy-2-naphthyl) phenoxy]-3-hydroxy-7-(3,4,5-trihydroxyphenyl) naphthalene-1,2-dione can be regarded as a unique drug candidate because it showed that it could function as a competitive inhibitor by binding to the active site of the α-glucosidase with higher binding energy.

The same retrieved structural homolog of α-glucosidase (Figure 3.9B) was subjected to docking (Figure 3.11C) with the inhibiting compounds identified from the plant's EA stem extract (Table 3.3A). Multiple ligands docking by PyRx provided the binding affinities (Table 3.5). The same compound, Ligand 2A (3,5,6,7-tetrahydroxy-2-(3-methoxyphenyl)-8aH-chromen-8a-yl) from EA stem extract demonstrated the outstanding binding energy compared to other plant stem phytochemicals docked as presented above (Figures 3.10C and 3.11C). The compound was bound to the enzyme by six interactions as shown above. It was commonly confirmed to connect with the α-glucosidase's active region, creating three standard hydrogen bonds with amino acids Phe506, Lys418 and Asp409; two carbon-hydrogen bonds by Glu505 and Met502; three unfavourable Donor-Donor interactions by Arg456 and the amino acid residue Arg412 remarkably formed two of the bonds with different ligand hydrogen atoms; two Pi-sigma interaction by the same amino acid residue Thr415. Fascinatingly, the amino acid residue Phe414 registered two different interactions, namely Pi-Alkyl and Alkyl, as depicted above (Figure 3.11C). The substance is also linked with distant amino acid residues through Van der Waals interactions. The amino acid residues facilitating the protein-ligand complex's overall binding are Phe506, Lys418, and Asp409. In comparison with the α-glucosidase positive inhibitor, overall, a total docking score of -7.5 kcal/mol was attained by this interaction, whereas the control binding energy was high at -7,8 kcal/mol (Table 3.5). Although the compound 3,5,6,7-tetrahydroxy-2-(3-methoxyphenyl)-8aH-chromen-8a-yl, when docked against α-glucosidase, demonstrated a greater binding energy than the other stem phytochemicals, its ability to operate as a competitive inhibitor is less, as the binding energy is less than that of the positive control.

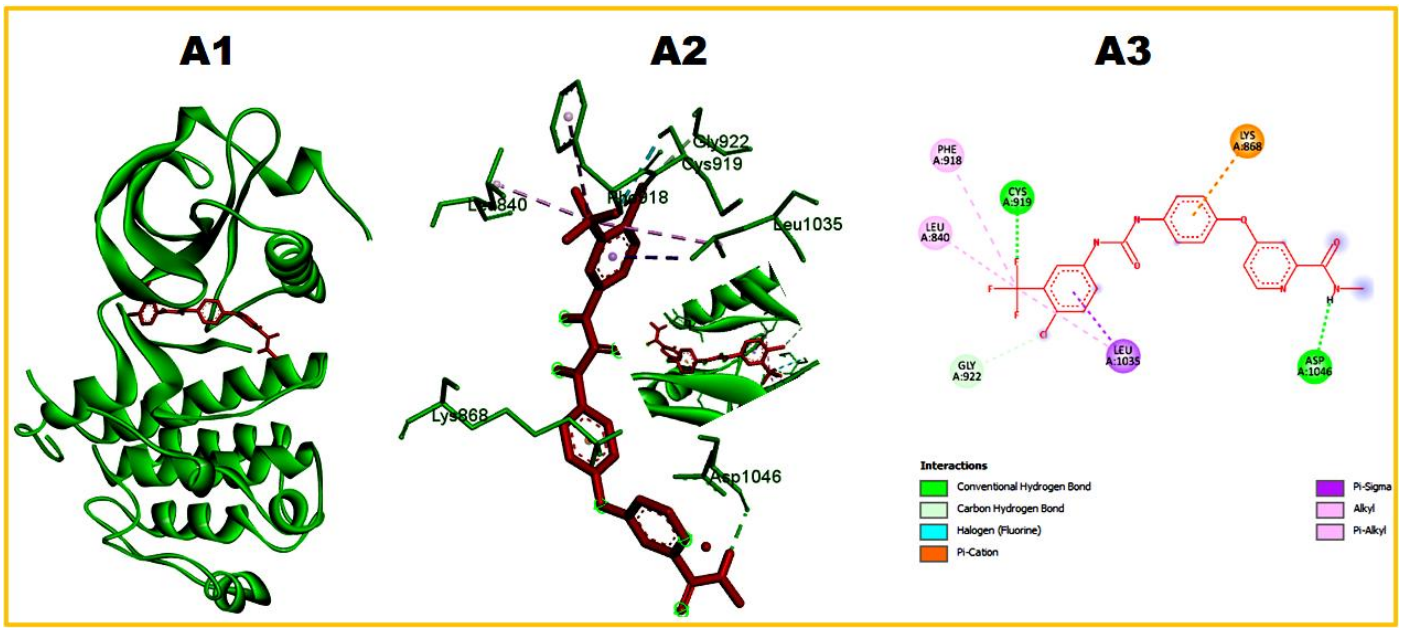
The retrieved α-glucosidase displaying α-helices, β-strands, loops, and turns, active sites and the whole protein groups (Figure 3.9B) was subjected to docking (Figure 3.11D) with the inhibiting compounds identified from the plant's EA leaf extract (Table 3.3A). Multiple ligands docking by PyRx provided the binding affinities (Table 3.5). The compound, Ligand 4A (2-[2-(2-prop-2-enoyloxyethynoxy)-4-[(E)-2-[4-(2-prop-2-enoyloxyethynoxy)-3-prop-2-enoylperoxyphenyl] ethenyl] phenoxy] ethynyl prop-2-enoate) from EA leaf extract demonstrated the outstanding binding energy compared to other plant leaf phytochemicals docked with as depicted above (Figure 3.11D). It was largely proven that it generates five conventional hydrogen bonds when it attaches to the α-glucosidase's active site with amino acids Arg608, Tyr360, Arg594, and the amino acids Val867 and Glu866 fascinatingly bond via the same ligand oxygen atom; furthermore, two carbon-

© University of Venda

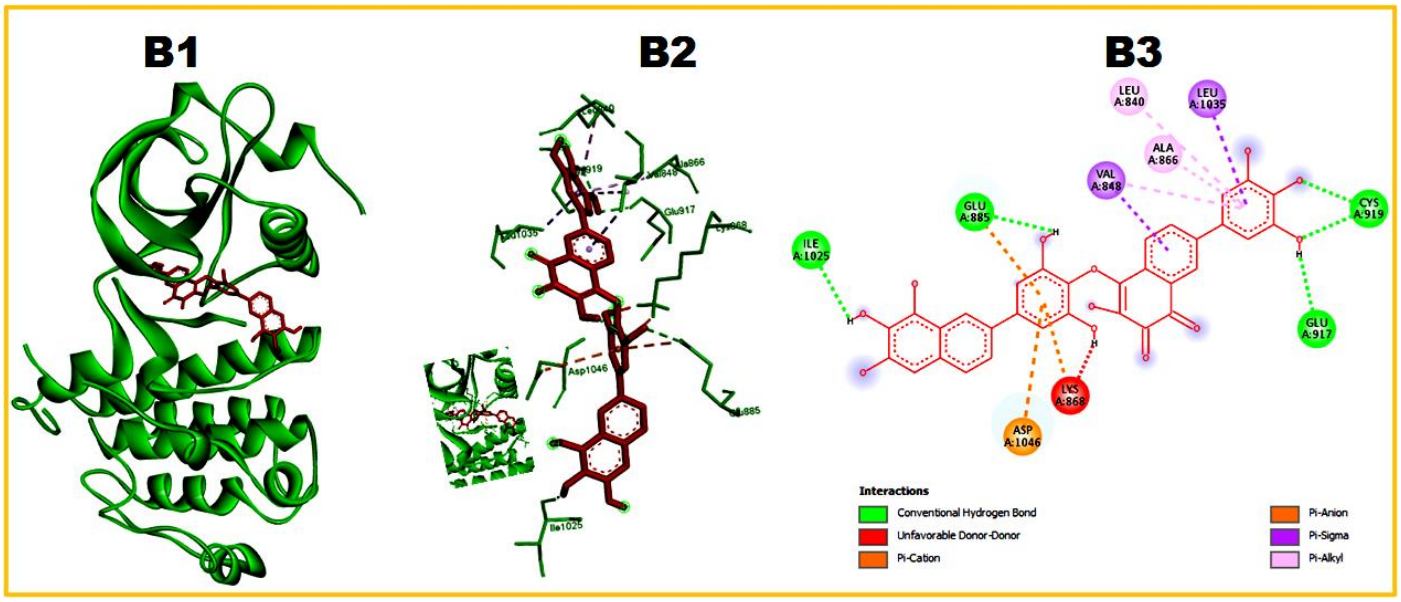
hydrogen bonds and Pi-Donor hydrogen bonds by same amino acid residues Gly359 and Tyr360; a single Pi-Pi T-shaped interaction by His584 and a single Pi-Alkyl by Arg608 (Figure 3.11D). The molecule also reacted with distant amino acid residues utilising Van der Waals interactions. The amino acid residues facilitating the protein-ligand complex's overall binding are Arg608, Tyr360, Arg594, Glu866 and Val867. In comparison with the α-glucosidase positive inhibitor, it registered a total docking score of −7,8 kcal/mol (Table 3.5). Although the compound, when docked against α-glucosidase, demonstrated a greater binding energy than the other leaf phytochemicals, its ability to operate as a competitive inhibitor is not quite impressive, as the binding energy is the same as that of the positive control shown above in Table 3.5.

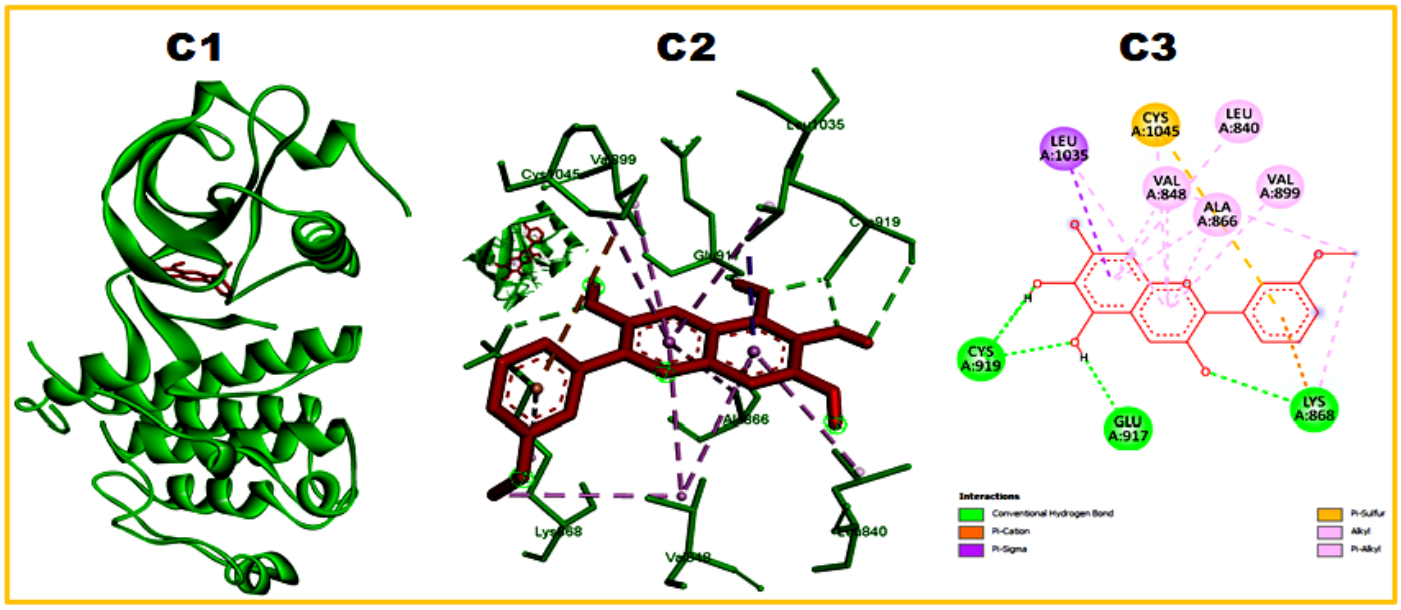
3.4.4.4. Selected identified compounds in EA extracts from different organs of *T. zeylanicum* docked against VEGFR2.

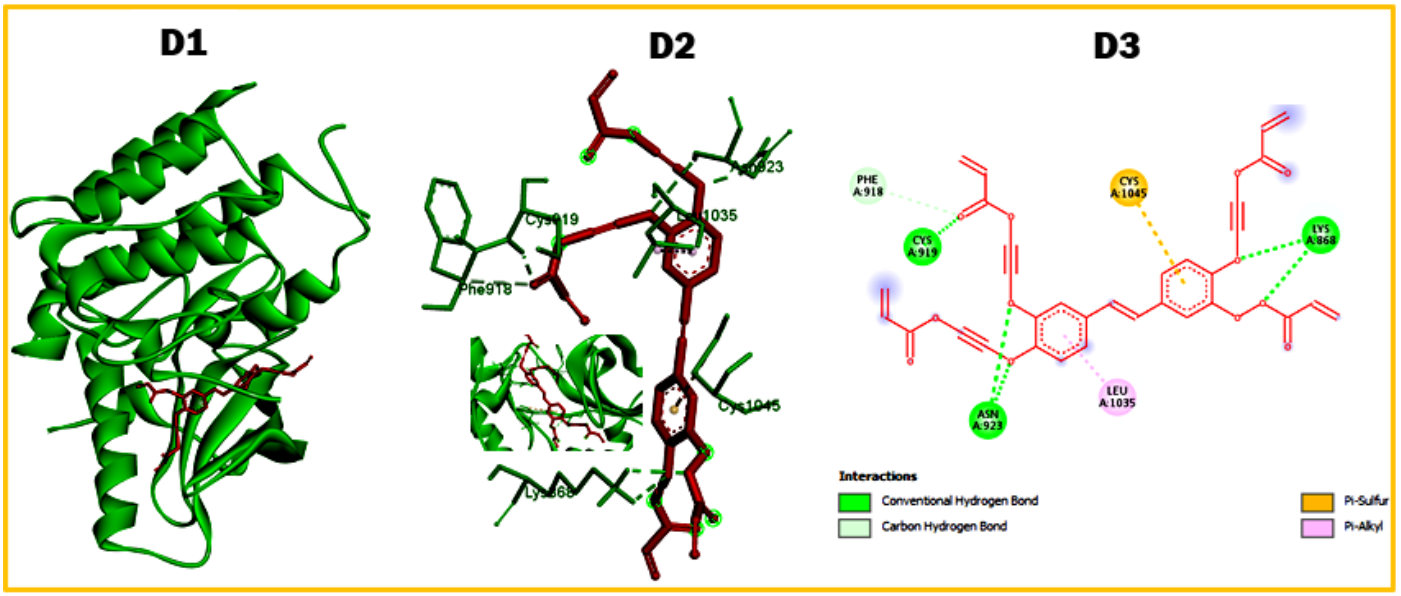
The VEGFR2 wound-associated kinase (Figure 3.9C) was also subjected to docking with its control sorafenib, as shown below (Figure 3.12A), and the inhibiting compounds identified from the plant's organ extracts (Table 3.3A). PyRx's docking of several ligands produced the binding affinities shown below in Table 3.6. The widely known VEGFR2 inhibitor sorafenib has been shown to attach to the active site by establishing just two conventional hydrogen bonds by amino acids, Cys919 and Asp1046; a single carbon-hydrogen bond by Gly922; Halogen (Fluorine); a single Pi-cation bond by Lys868; a single Pi-sigma bond by Leu1035 and interestingly the three amino acid residues Phe918, Leu840 and Leu1035 interacted with the inhibitor sorafenib and formed two different bonds namely, Alkyl and Pi-Alkyl bonds as shown below (Figure 3.12A). It also bonded with distant amino acid residues through Van der Waals interactions. The amino acid residues that facilitated the overall binding of the protein-ligand complex are Cys919 and Asp1046. The overall docking score for this connection is -8,1 kcal/mol (Table 3.6). Sorafenib thereby validated its capacity to function as a competitive inhibitor by binding to the active site of the VEGFR2 enzyme (Figure 3.12A).



© University of Venda







© University of Venda

Figure 3.12: Molecular docking of VEGFR2 against **(A) Sorafenib**, **(B) Ligand 1A, (C) Ligand 2A, and (D) Ligand 4A.** (A1–D1) depicts the active site of the VEGFR2, (A2–D2) demonstrate the zoomed-in interaction site enzyme and ligands; (A3–D3) display the interacting amino acid residues of the VEGFR2.

Table 3.6: The binding affinities of selected identified compounds in EA root, stem, and leaf extracts of *T. zeylanicum* with the highest binding affinity to the VEGFR2 and the interacting amino acid residues of the protein.

ligand	Ligand name/code and plant part extract	Molecular formula	Binding affinity (kcal/mol)	Rmsd /Ub	Rmsd /Lb	Interacting residues of the protein and their positions
Positive control	Sorafenib	$C_{21}H_{16}ClF_3N_4O_3$	-8,1	0	0	Cys919, Asp1046, Gly922, Lys868, Leu1035, Phe918, and Leu840
Ligand 1A	4-[2,6-Dihydroxy-4-(6,7,8-trihydroxy-2-naphthyl) phenoxy]-3-hydroxy-7-(3,4,5-trihydroxyphenyl) naphthalene-1,2-dione (EA root extract)	$C_{32}H_{20}O_{12}$	-9,6	0	0	Ile1025, Glu917, Glu885, Cys919, Lys868, Asp1046, Val848, Leu1035, Ala866, and Leu840
Ligand 2A	3,5,6,7-tetrahydroxy-2-(3-methoxyphenyl)-8aH-chromen-8a-yl (EA stem extract)	$C_{16}H_{13}O_6$	-7,0	0	0	Glu917, Cys919, Lys868, Leu1035, Cys1045, Val848, Ala866, Val899, and Leu840
Ligand 4A	2-[2-(2-prop-2-enoyloxyethynoxy)-4-[(E)-2-[4-(2-prop-2-enoyloxyethynoxy)-3-prop-2-enoylperoxyphenyl] ethenyl] phenoxy] ethynyl prop-2-enoate (EA leaf extract)	$C_{32}H_{20}O_{12}$	-7,1	0	0	Cys919, Asn923, Lys868, Phe918, Cys1045 and Leu1035
Ligand 6A	Capronor (EA root extract)	$C_{21}H_{28}O_2$	-8.4	0	0	Asp1046, Lys868, Leu840, Val848, Ala866, and Leu1035

© University of Venda

The retrieved structural homolog of VEGFR2 wound target protein depicting α-helices, β-strands, loops and turns, active sites and the whole protein groups (Figure 3.9C) was subjected to docking (Figure 3.12B) with the inhibiting compounds identified from the plant's EA root extract (Table 3.3A). Multiple ligands docking by PyRx provided the binding affinities (Table 3.6). The same compound, Ligand 1A (4-[2,6-Dihydroxy-4-(6,7,8-trihydroxy-2-naphthyl) phenoxy]-3-hydroxy-7-(3,4,5-trihydroxyphenyl) naphthalene-1,2-dione) from EA root extract demonstrated the outstanding binding energy compared to other plant root phytochemicals docked as depicted above (Figures 3.10B, 3.11B and 3.12B). As previously demonstrated above, the chemical and the enzyme established a connection via six distinct kinds of interactions. The establishment of four conventional hydrogen bonds with the α-glucosidase's active site through amino acids Ile1020, Glu917, Glu885, and two Cys919, generated by various ligand oxygen atoms, has been thoroughly outlined. Furthermore, it formed a single unfavourable Donor-Donor interaction by the same amino acid residue, Lys868. Fascinatingly, Asp1046, Glu858 and Lys868 interacted with the ligand via Pi-Cation and Pi-Sigma; additionally, it interacted via two Pi-Sigma interactions by Val848 and Leu1035; and three Pi-Alkyl interactions by Ala866, Leu840 and Val848 (Figure 3.12B). The substance additionally engaged with distant amino acid residues through Van der Waals interactions. The amino acid residues that facilitated the overall binding of the protein-ligand complex are Ile1025, Glu885, Glu917 and Cys919. This association had a total docking rating of -9.6 kcal/mol when compared to the VEGFR2 positive inhibitor, while the control binding energy was low at -8.1 kcal/mol (Table 3.6). The chemical 4-[2,6-Dihydroxy-4-(6,7,8-trihydroxy-2-naphthyl phenoxy]-3-hydroxy-7-(3,4,5-trihydroxyphenyl) naphthalene-1,2-dione can be regarded as a unique therapeutic candidate because it showed that it might function as a competitive inhibitor by binding to the active site of the VEGFR2 enzyme with a higher binding energy.

The same retrieved structural homolog of VEGFR2 wound target protein depicting α-helices, β-strands, loops and turns, active sites and the whole protein groups (Figure 3.9C) was subjected to docking (Figure 3.12C) with the inhibiting compounds identified from the plant's EA stem extract (Table 3.3A). Multiple ligands docking by PyRx provided the binding affinities (Table 3.6). The same compound, Ligand 2A (3,5,6,7-tetrahydroxy-2-(3-methoxyphenyl)-8aH-chromen-8a-yl) from EA stem extract demonstrated the outstanding binding energy compared to other plant stem phytochemicals docked as presented above (Figures 3.12C, 3.11C and 3.10C). The compound was bound to the enzyme by six various interactions as shown above. It was thoroughly established that it generates four conventional hydrogen bonds with the VEGFR2 enzyme's active site by amino acids Glu917, Lys868 and two Cys919; a single Pi-Cation by Lys868; a single Pi-Sigma by Leu1035; and a single Pi-Sulphur by Cys1045. Fascinatingly, the amino acid residues Leu1035, Val848, Ala866, Val899, Leu840, Cys1045 and Lys868 registered two different interactions, namely Pi-Alkyl and Alkyl, as depicted above (Figure 3.12C). The substance additionally engaged with distant amino acid residues through Van der Waals interactions. The amino acid residues that facilitated the overall binding of the protein-ligand complex are Cys919, Glu917 and Lys868.

© University of Venda

When compared to the α-glucosidase positive inhibitor, the overall docking grade for this connection is -7,0 kcal/mol, whereas the control binding energy was high at −8,1 kcal/mol (Table 3.6). Although the compound 3,5,6,7-tetrahydroxy-2-(3-methoxyphenyl)-8aH-chromen-8a-yl, when docked against VEGFR2 enzyme, demonstrated a greater binding energy than the other stem phytochemicals, its ability to operate as a competitive inhibitor is less, as the binding energy is less than that of the positive control.

The same retrieved structural homolog of VEGFR2 wound target protein depicting α-helices, β-strands, loops and turns, active sites and the whole protein groups (Figure 3.9C) was subjected to docking (Figure 3.12D) with the inhibiting compounds identified from the plant's EA leaf extract (Table 3.3A). Multiple ligands docking by PyRx provided the binding affinities (Table 3.6). The same compound, Ligand 4A (2-[2-(2-prop-2-enoyloxyethynoxy)-4-[(E)-2-[4-(2-prop-2-enoyloxyethynoxy)-3-prop-2-enoylperoxyphenyl] ethenyl] phenoxy] ethynyl prop-2-enoate) from EA leaf extract demonstrated the outstanding binding energy compared to other plant leaf phytochemicals docked with as presented above (Figure 3.12D and 3.11D). The compound was bound to the enzyme by four various interactions as shown above. It was thoroughly established that it generates five conventional hydrogen bonds with the VEGFR2 enzyme's active site by amino acids Cys919, two Asn923 from different ligand oxygen atoms and two Lys868 from different ligand oxygen atoms. It furthermore interacted via a single carbon-hydrogen bond by Phe918, a single Pi-Alkyl by Leu1035, and a single Pi-Sulphur by Cys1045, as depicted above (Figure 3.12D). The substance additionally engaged with distant amino acid residues through Van der Waals interactions. The amino acid residues that facilitated the overall binding of the protein-ligand complex are Cys919, Asn923, and Lys868. When compared to the α-glucosidase positive inhibitor, this interaction's overall docking grade was -7,1 kcal/mol, but the control binding strength, as shown in Table 3.6, was high at -8,1 kcal/mol. Although the compound, when docked against the VEGFR2, demonstrated greater binding energy than the other leaf phytochemicals, its ability to operate as a competitive inhibitor is less.

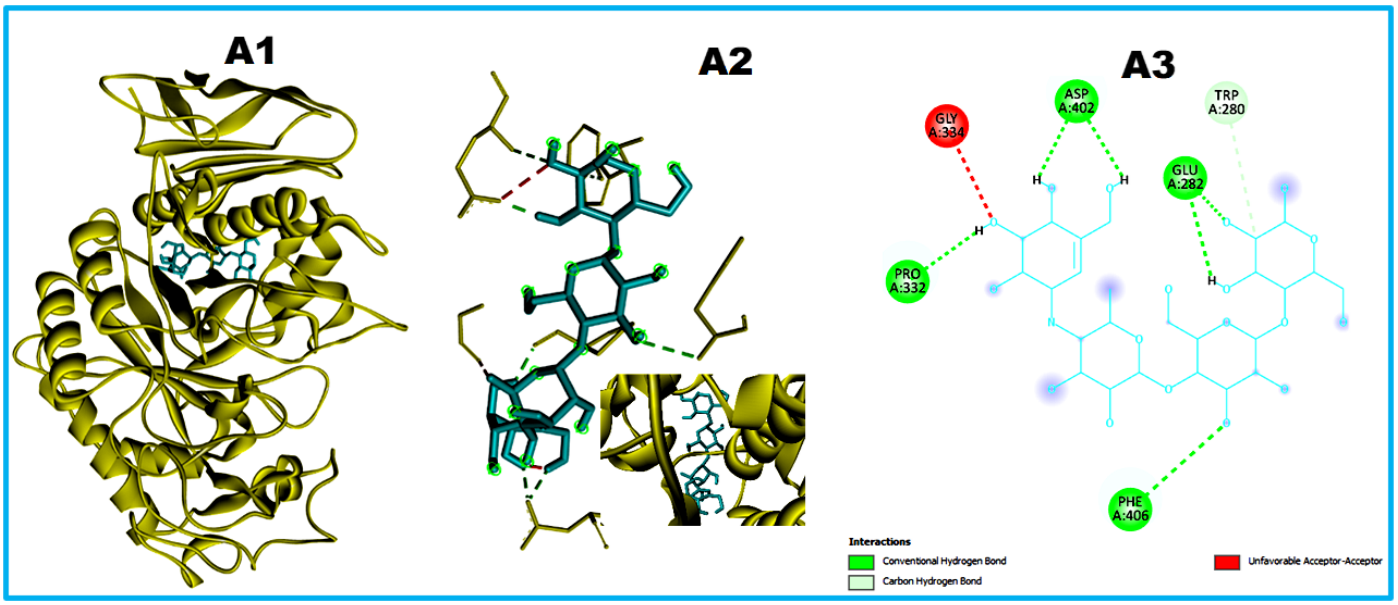
The EA root extract, Ligand 6A (Capronor) bound to VEGFR2 through conventional hydrogen bonds by Lys868, Asp1046, and Leu840, indicating some interaction with a polar or charged moiety. The lysine residue is positively charged, which may somehow involve interaction with a negatively polarized part of the ligand like an oxygen or hydroxyl group. The presence of aspartate, which is a negative charge, may involve a hydrogen donor group, for example (-OH group on the ligand). Such orientations work well to anchor the ligand in the binding pocket and add to the stability of the complex. Val848, Ala866, and Leu1035 are nonpolar, hydrophobic amino acids of the ligand, probably suggesting that the ligand has an appropriate hydrophobic area surface for hiding. These orientations help to stabilize the ligand in the binding pocket and minimize the extent to which the solvent interacts with these regions of reduced polarity. The involvement of both hydrophobic residues (leucine and valine) and polar/charged residues (lysine and aspartate) suggests that the binding pocket accommodates both polar and nonpolar regions of the ligand. The chemical also bonded with Van der Waals interactions with some distant amino acid residues.

© University of Venda

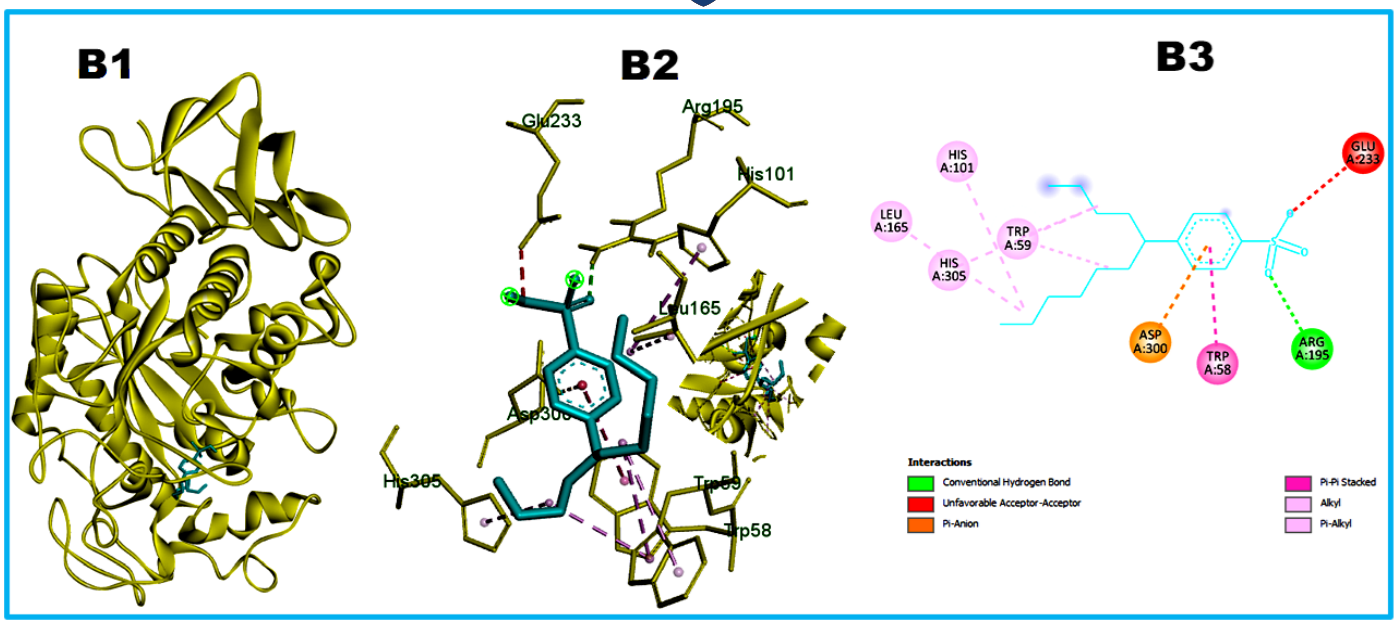
With the binding energy of -8.4 kcal/mol (Table 3.6), this ligand has great prospects of binding effectively to VEGFR2 compared to Sorafenib (-8.1 kcal/mol). A strong binding affinity may inhibit the enzyme activity, thus serving as a plausible inhibitor.

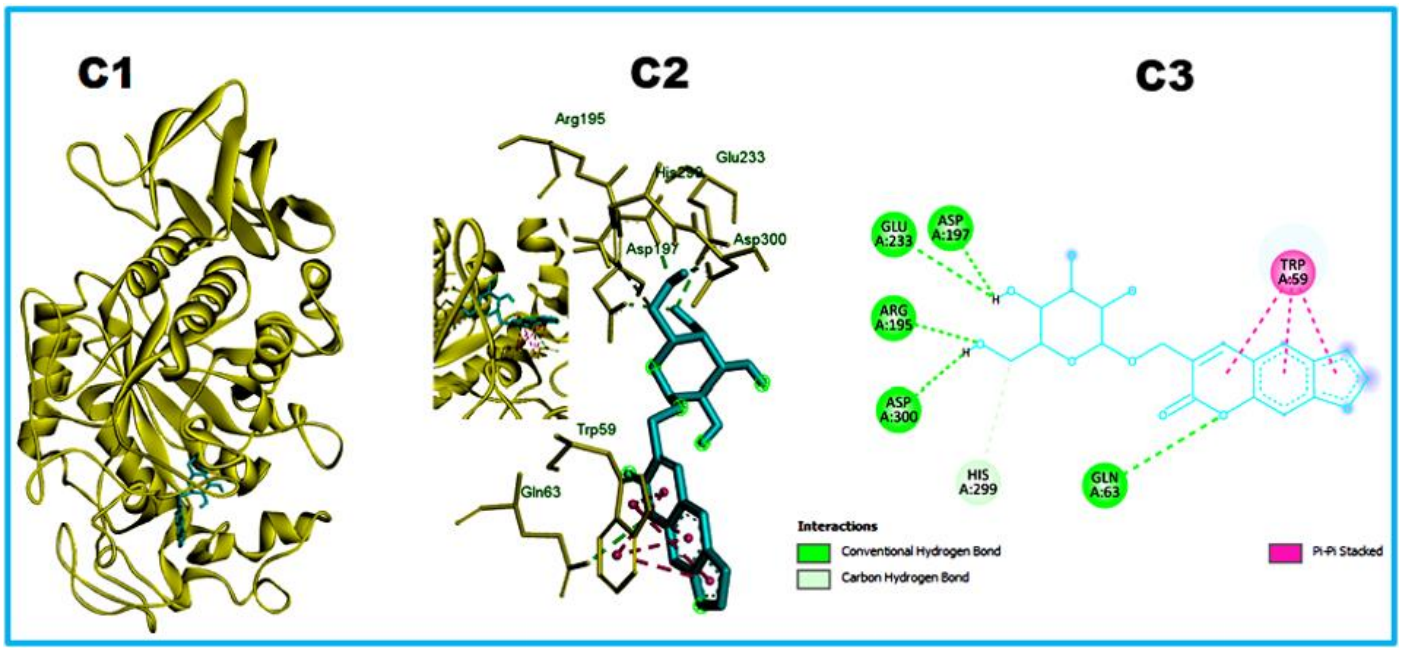
3.4.4.5. Selected identified compounds in ethanol extracts from different organs of *T. zeylanicum* docked against α-amylase.

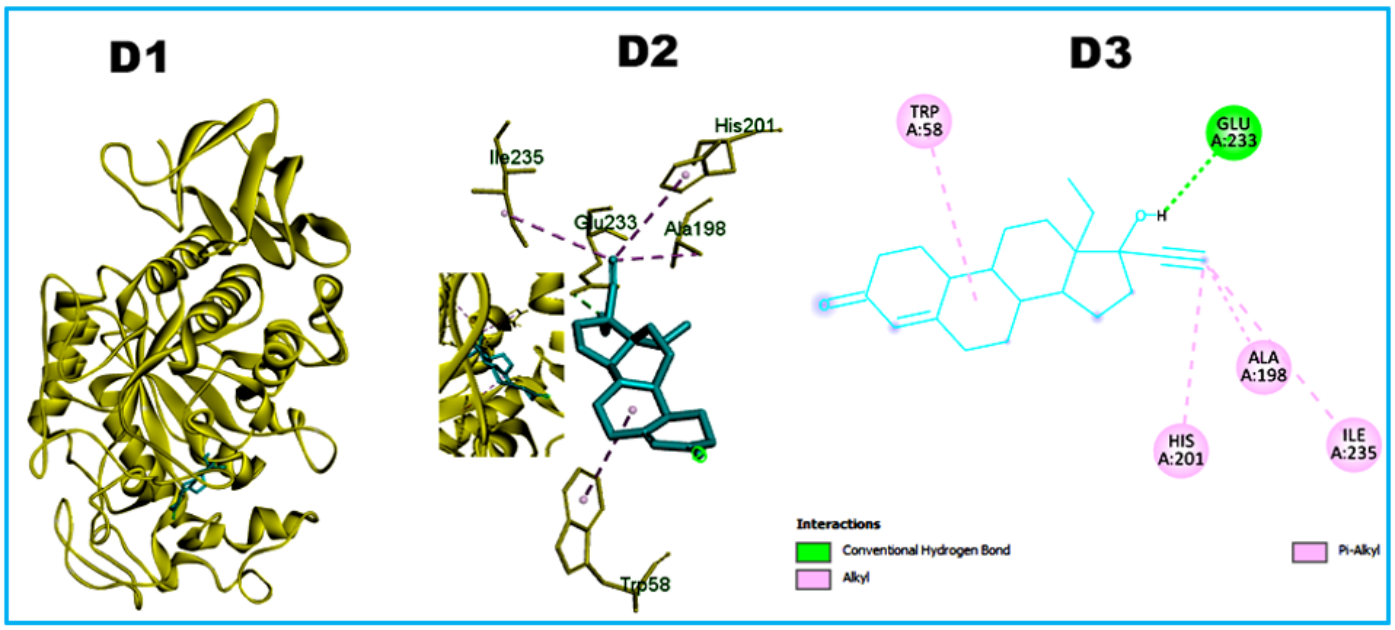
The retrieved structural homolog of α-amylase, depicting α-helices, β-strands, loops and turns, active sites and the whole protein groups (Figure 3.9A) was subjected to docking (Figure 3.13A) with acarbose and the inhibiting compounds identified from the plant's organ extracts (Table 3.3B). The interaction affinities were obtained by PyRx docking several ligands (Table 3.7). Acarbose, an established α-amylase inhibitor, has been shown to engage with the active site and establish six conventional hydrogen bonds with amino acids Pro332, Phe406, and remarkably the protein amino acid residues Asp402 and Glu282 interacted with the positive control acarbose and each generated two conventional hydrogen bonds from different ligand hydrogen atoms as shown in the first structure (Figure 3.13A); single carbon-hydrogen bond by Trp280; and a single unfavourable acceptor-acceptor bond by Glu334. The substance additionally engaged with distant amino acid residues through Van der Waals interactions. The amino acid residues that facilitated the overall binding of the protein-ligand complex are bound through conventional hydrogen bonds. Altogether, the overall docking score for the given interaction is −7.4 kcal/mol (Table 3.7). Additionally, these results correspond to the results that Radzuan *et al*. (2024) and Nada *et al*. (2024) previously reported. By binding to the α-amylase's active region, acarbose confirmed that it operates as a competitive inhibitor. Despite this study's high acarbose-α-amylase complex binding affinity consistent with the more recent studies stated above, in contrast to the previously published results (Zahra *et al*., 2024), the affinity is too low, whereas the findings reported by Baccari *et al*. (2024) were high. Remarkably, these conclusions are equivalent because the affinities fall within a narrow range, demonstrating the validity of the current investigation.



© University of Venda







© University of Venda

Figure 3.13: Molecular docking of **α-amylase** against **(A) Acarbose**, together with **(B) Ligand 7A, (C) Ligand 8A, and (D) Ligand 6A.** (A1–D1) depicts the active site of the α-amylase, (A2–D2) demonstrate the zoomed-in interaction site enzyme and ligands; (A3–D3) display the interacting amino acid residues of the α-amylase.

Table 3.7: The binding affinities of selected identified compounds in ethanol root, stem, and leaf extracts of *T. zeylanicum* with the highest binding affinity to the α-amylase and the interacting amino acid residues of the protein.

ligand	Ligand name/code and plant part	Molecular formula	Binding affinity (kcal/mol)	Rmsd /Ub	Rmsd /Ib	Interacting residues of the protein and their positions
Positive control	Acarbose	$C_{25}H_{43}NO_{18}$	-7,4	0	0	Pro332, Asp402, Glu282, Phe406, Gly334, and Trp280.
Ligand 7A	Geshoidin (ethanol root extract)	$C_{18}H_{18}O_9$	-8,7	0	0	Arg195, Glu233, Asp300, Trp58, Leu165, His101, Trp59, and His305
Ligand 8A	SCHEMBL6844198 (ethanol stem extract)	$C_{18}H_{18}O_9$	-8,5	0	0	Glu233, Asp197, Arg195, Asp300, Glu63, His299, and Trp59
Ligand 6A	Capronor (ethanol leaf extract)	$C_{21}H_{28}O_2$	-9,1	0	0	Glu233, Trp58, Ala198, His201, and Ile235
Ligand 6A	Capronor (ethanol root extract)	$C_{21}H_{28}O_2$	-8,3	0	0	Trp59, and Leu168
Ligand 9A	Trifolin (ethanol leaf extract)	$C_{21}H_{20}O_{11}$	-7,6	0	0	His305, Trp59, and His101

The retrieved α-amylase displaying α-helices, β-strands, loops, and turns, active sites and the entire protein groups (Figure 3.9A) was subjected to docking (Figure 3.13B) with the inhibiting compounds identified from the plant's ethanol root extract (Table 3.3B). Multiple ligands docking by PyRx provided the binding affinities (Table 3.7). The compound Ligand 7A (Geshoidin) from ethanol root extract demonstrated outstanding binding energy compared to other plant root phytochemicals docked. The compound was bound to the α-amylase by six various interactions as presented above. It was thoroughly established that it generates a single conventional hydrogen bond with the α-amylase's active site by amino acids Arg195; a single unfavourable Donor-Donor interaction by Glu233; a single Pi-Anion interaction by Asp300; a single Pi-Pi stacked interaction by Trp58. Remarkably, the four amino acid residues Leu165, His101, Trp59 and His305 registered two different interactions, namely Alkyl and Pi-Alkyl as depicted above (Figure 3.13B). The substance additionally engaged with distant amino acid residues through Van der Waals interactions. The amino acid residue that facilitated the overall binding of the protein-ligand complex is Arg195. In comparison with the α-amylase positive inhibitor α-amylase, altogether, the overall docking score for the given interaction is −8,7

© University of Venda

kcal/mol, whereas the control binding energy was low at -7,4 kcal/mol (Table 3.7). The molecule Geshoidin can be regarded as a potential therapeutic candidate because it showed that it might function as a competitive inhibitor by binding to the active site of the α-amylase with a higher binding energy. Interestingly, this compound has already been identified and reported in plant root using LC-qTOF-MS as also observed in the present study (Panara *et al*., 2022). It was characterized in previously reported studies (Muzila *et al*., 2010). Although this compound has been identified and characterised in previous studies, there are still no scientific in-silico studies proving the compound to have the ability to bind and inhibit the two enzyme markers for diabetes and the wound target protein. Hence, these *in-silico* inhibitory findings are novel.

The same retrieved α-amylase structural homolog depicting α-helices, β-strands, loops, and turns, active sites and the whole protein groups (Figure 3.9A) was subjected to docking (Figure 3.13C) with the inhibiting compounds identified from the plant's ethanol stem extract (Table 3.3B). Multiple ligands docking by PyRx provided the binding affinities (Table 3.7). The compound Ligand 8A (SCHEMBL6844198) from ethanol stem extract demonstrated outstanding binding energy compared to other plant stem phytochemicals docked. The compound was bound to the enzyme by three different interactions as presented above. It was thoroughly established that it generates five conventional hydrogen bonds with the α-amylase's active site by amino acids Glu233, Asp197, Arg195, Asp300 and Glu63. It also forms a single carbon-hydrogen bond by the same amino acid residue His299; and interestingly, the amino acid Trp59 interacts via three Pi-Pi stacked interactions (Figure 3.13C). The substance additionally engaged with distant amino acid residues through Van der Waals interactions. The amino acid residues that facilitated the overall binding of the protein-ligand complex are bound through conventional hydrogen bonds. In comparison with the α-amylase positive inhibitor, altogether, the docking score for the given interaction is −8,5 kcal/mol whereas the control binding energy was low at -7,4 kcal/mol (Table 3.7). The chemical SCHEMBL6844198 can be regarded as a potential therapeutic candidate because it established the ability to function as a competitive inhibitor by binding to the active site of the α-amylase (Figure 3.13C).

The same retrieved α-amylase structural homolog showing α-helices, β-strands, loops, and turns, active sites and the complete protein groups (Figure 3.9A) was subjected to docking (Figure 3.13D) with the inhibiting compounds identified from the plant's ethanol leaf extract (Table 3.3B). Multiple ligands docking by PyRx provided the binding affinities (Table 3.7). The compound Ligand 6A (Capronor) from ethanol leaf extract demonstrated outstanding binding energy compared to other plant leaf phytochemicals docked. The compound was bound to the enzyme by three various interactions as presented above. It was thoroughly established that it generates a single conventional hydrogen bond with the α-amylase's active site by amino acid Glu23. The amino acid residues remarkably formed an interaction with the ligand, resulting in two interactions, namely Alkyl and Pi-Alkyl (Figure 3.13D). Capronor additionally engaged with distant amino acid residues through Van der Waals interactions. The amino acid residue that facilitated the overall binding of the protein-ligand complex is Glu233.

© University of Venda

In comparison with the α-amylase positive inhibitor, altogether, the overall docking score for the given interaction is −9,1 kcal/mol, whereas the control binding energy was low at -7,4 kcal/mol (Table 3.7). The chemical Capronor attached itself to the active site of the α-amylase and showed that it could serve as a competitive inhibitor (Figure 3.13D). Hence, it can be considered a drug candidate. The most remarkable part of this compound is that it also has not been reported as two enzyme markers for diabetes and wound target protein inhibitors. Hence these *in-silico* findings are novel.

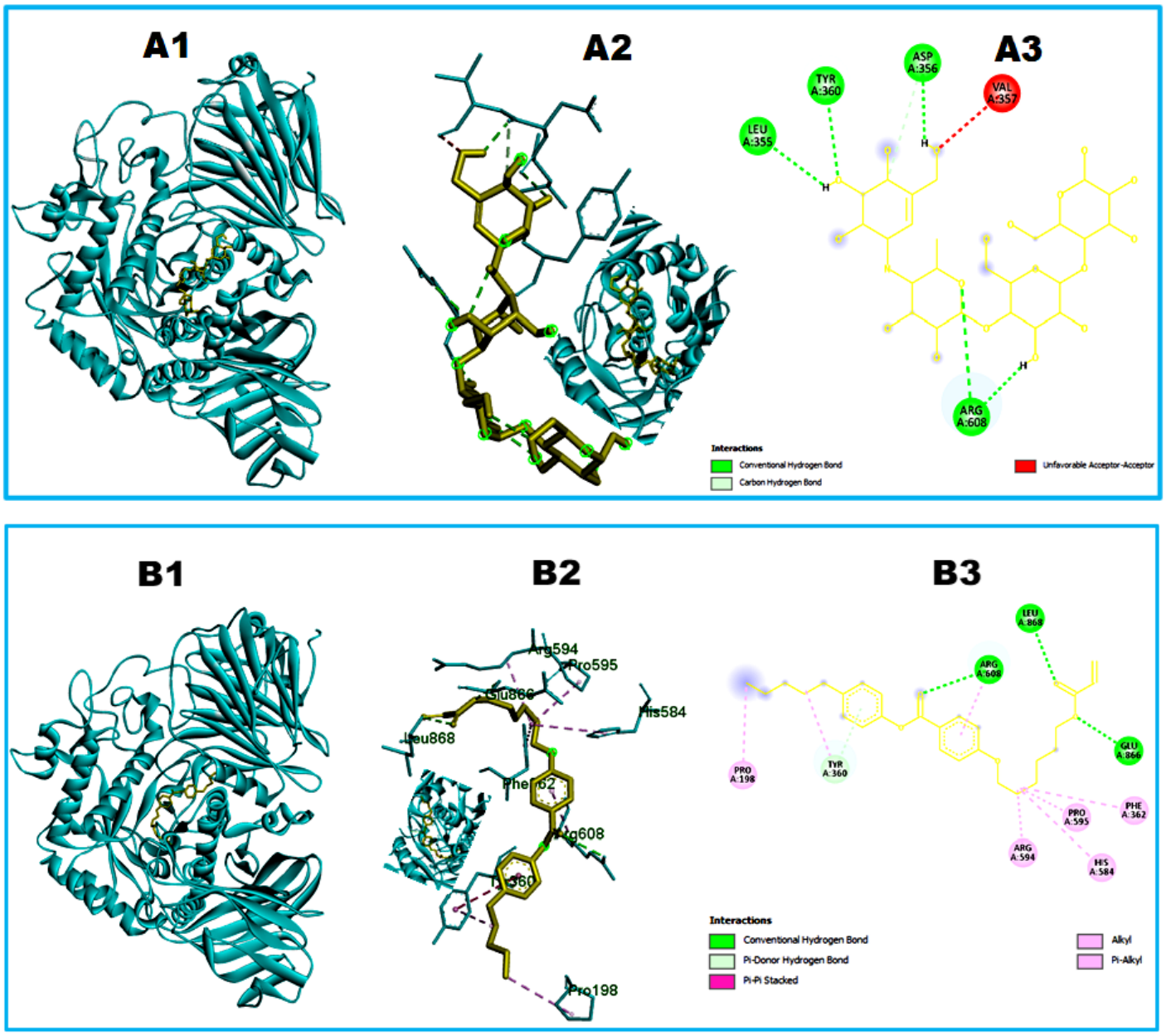
Ethanol root extract Ligand 6A (Capronor) was bound to pancreatic α-amylase via two types of interactions, Alkyl and Pi-Alkyl Interaction. The ligand forms alkyl and Pi-Alkyl Interactions with Leu168 and Trp59. Leucine is a nonpolar, hydrophobic amino acid, and this interaction suggests the ligand has a compatible hydrophobic region that fits well into the binding pocket. Tryptophan, being an aromatic and hydrophobic compound, engages in an interaction with hydrophobic and aromatic portions of ligands. This is an important interaction typically present in hydrophobic pockets and offers extra stability, especially in the presence of hydrophobic or aromatic functionalities. The binding pocket is mostly hydrophobic, with the involvement of hydrophobic residues, such as Leu168 and Trp59. The ligand's compatibility with this hydrophobic environment is a major contributor to the strong binding affinity. When compared to the α-amylase positive inhibitor, the overall docking grade for this connection is -8,3 kcal/mol, whereas the control binding energy was low at −7,4 kcal/mol (Table 3.7).

Ethanol leaf extract Ligand 9A (Trifolin) binds to α-amylase with a binding energy of -7.6 kcal/mol (Table 3.7), suggesting moderate to strong binding affinity. The key interactions include conventional and carbon-hydrogen bonding with His305 and Pi-Pi stacking with Trp59 and His101. The imidazole side chain of histidine (His305) allows it to act as both a hydrogen bond donor and acceptor. Trifolin acts on histidine in that regard with a hydroxyl or carbonyl group forming a standard hydrogen bond with the nitrogen atom of the imidazole ring of histidine. It is likely that this bond is vital in orienting and anchoring Trifolin within the binding pocket. Tryptophan (Trp59) is inert and typically undergoes Pi-Pi stacking interaction. Here Trifolin likely tangentially aligns its aromatic ring to that of the indole ring of tryptophan (forming a Pi-Pi stacking interaction), thereby contributing to stabilizing the developed complex. This interaction is of huge importance in binding pockets where aromatic residues are rich, and it is often observed in enzyme active sites or binding domains of receptors, which exhibit binding stability attributable to dispersion and hydrophobic forces acting in aggregates. These interactions imply that the ligand shows stable binding is what makes Trifolin stand as a candidate for further pharmacological exploration, particularly into antioxidant, anti-inflammatory, or anticancer therapy. Trifolin is a flavonoid, namely kaempferol 3-O-galactoside, which is normally obtained from several plants and is recognised for its activities due to its properties as an antioxidant, anti-inflammatory, and anti-cancerous substance. The flavonoid structure and binding to histidine residues suggest some antioxidant functionality since histidine participates in free radical reduction many times.

© University of Venda

3.4.4.6. Selected identified compounds in ethanol extracts from different organs of *T. zeylanicum* docked against α-glucosidase.

The α-glucosidase (Figure 3.9B) was also subjected to docking with the positive control acarbose and the inhibiting compounds identified from the ethanol plant organ extracts (Table 3.3B). The binding affinities were obtained by PyRx docking many ligands (Table 3.8). The widely recognized α-glucosidase inhibitor acarbose was typically confirmed to engage with the active site by generating five conventional hydrogen bonds by amino acids Tyr360, Asp356, and Leu355 and the amino acid residue Arg 608 generated two hydrogen bonds as it interacted with acarbose as depicted on the first structure (Figure 3.14A); a single carbon-hydrogen bond by amino acid Asp356 which interestingly again formed the conventional hydrogen bond as shown above; a single unfavourable acceptor-acceptor bond by Val357. The compound additionally engaged with distant amino acid residues through Van der Waals interactions.



© University of Venda

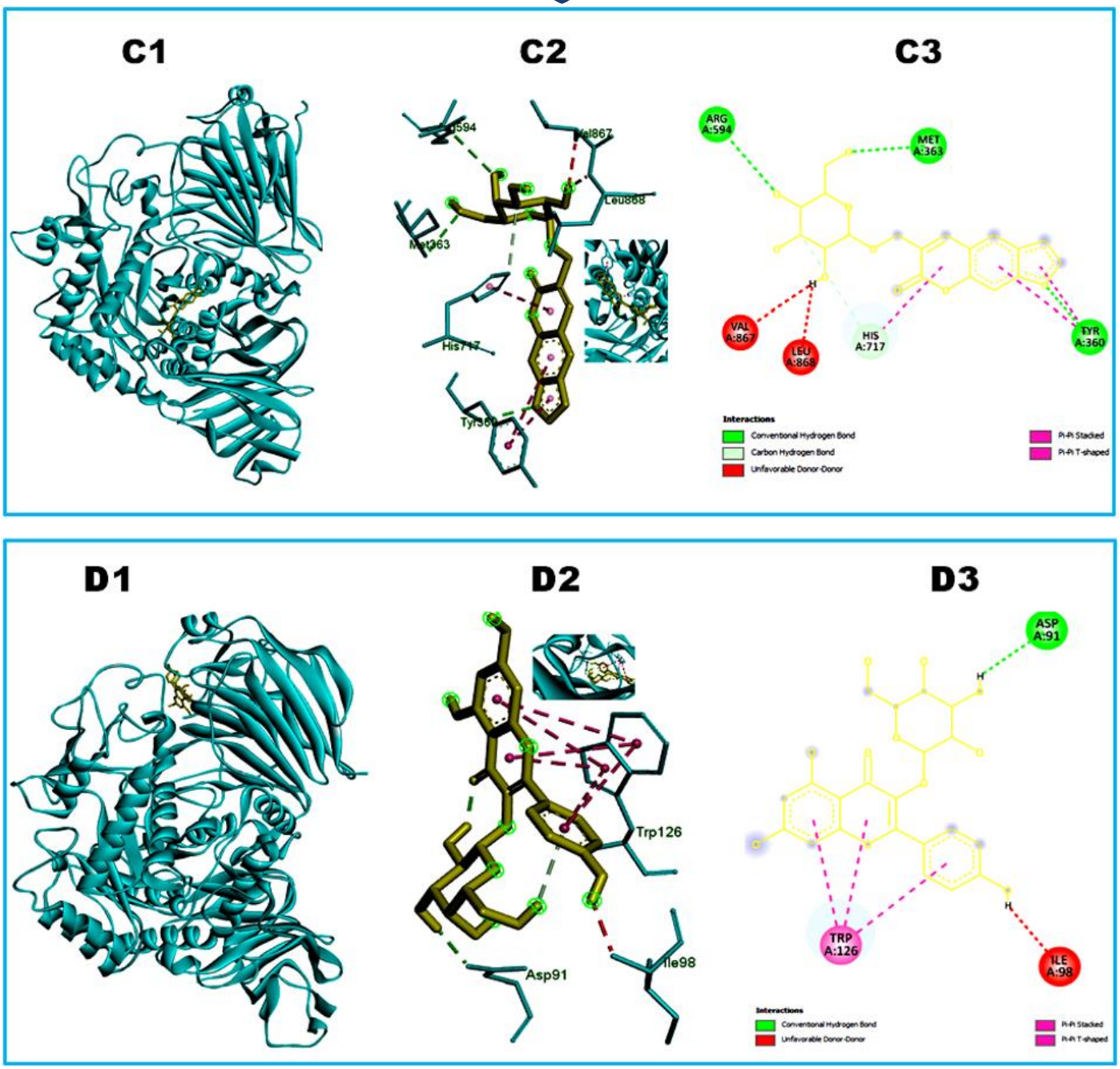


Figure 3.14: Molecular docking of **α-glucosidase** against **(A) Acarbose**, **(B) Ligand 10A, (C) Ligand 8A, and (D) Ligand 9A.** (A1–D1) depicts the active site of the α-glucosidase; (A2–D2) demonstrate the zoomed-in interaction site enzyme and ligands; (A3–D3) display the interacting amino acid residues of the α-glucosidase.

The amino acid residues facilitating the protein-ligand complex's overall binding are Leu355, Tyr360, Asp356 and Arg608. Altogether, the docking score for the given interaction is −7.5 kcal/mol (Table 3.8). Therefore, acarbose showed its ability to function as a competitive inhibitor by attaching to the active site of the α-glucosidase (Figure 3.14A). Previous studies (Radzuan *et al*., 2024; Zahra *et al*., 2024) confirmed the reliability of the current study by demonstrating the binding affinity in agreement within a narrow range (Figure 3.14A and Table 3.8).

© University of Venda

Table 3.8: The binding affinities of selected identified compounds in ethanol root, stem, and leaf extracts of *T. zeylanicum* with the highest binding affinity to the α-glucosidase and the interacting amino acid residues of the protein.

ligand	Ligand name/code and plant part extract	Molecular formula	Binding affinity (kcal/mol)	Rmsd /Ub	Rmsd /Ib	Interacting residues of the protein and their positions
Positive control	Acarbose	$C_{25}H_{43}NO_{18}$	-7,5	0	0	Leu355, Tyr360, Asp356, Val357, and Arg608
Ligand 10A	CID58879477 (ethanol root extract)	$C_{27}H_{33}O_5$	-7,8	0	0	Arg608, Leu868, Glu866, Tyr360, Pro198, Arg594, His584, Pro595 and Phe362.
Ligand 8A	SCHEMBL6844198 (ethanol stem extract)	$C_{18}H_{18}O_9$	-7,7	0	0	Arg594, Met363, Tyr360, His717, Val867 and Leu868.
Ligand 9A	Trifolin (ethanol leaf extract)	$C_{21}H_{20}O_{11}$	-7,6	0	0	Asp91, Ile98 and Trp126
Ligand 6A	Capronor (ethanol root extract)	$C_{21}H_{28}O_2$	-7,7	0	0	Trp126, Gln124, Pro125, Met122
Ligand 7A	Geshoidin (ethanol root extract)	$C_{18}H_{18}O_9$	-7,6	0	0	Val867, Leu868, and Arg594
Ligand 6A	Capronor (ethanol leaf extract)	$C_{21}H_{28}O_2$	-7,5	0	0	Asp91, Met122, and Trp126

The retrieved α-glucosidase showing α-helices, β-strands, loops, and turns, active sites and the whole protein groups (Figure 3.9B) was subjected to docking (Figure 3.14B) with the inhibiting compounds identified from the plant's ethanol root extract (Table 3.3B). Multiple ligands docking by PyRx provided the binding affinities (Table 3.8). The compound Ligand 10A (CID58879477) from ethanol root extract demonstrated outstanding binding energy compared to other plant root phytochemicals docked with as presented above. The compound was bound to the enzyme by five various interactions as shown above. It was thoroughly established that it generates three conventional hydrogen bonds with the α-glucosidase's active site by amino acids Arg608, Leu868 and Glu866; a single Pi-Donor hydrogen bond by Tyr360. CID58879477 further interacted via seven Alkyl and Pi-Alkyl interaction by amino acids Pro198, Tyr360, Arg608, interestingly the amino acids Arg594, His584, Pro959, and Phe362 alkyl and pi-alkyl interaction were formed from the same Carbon ligand atom (Figure 3.14B). The compound further interacted via Pi-Pi stacked interactions, of which the residues were not detectable, and Van der Waals interactions by amino acid residues at a distance. The amino acid residues that facilitated the overall binding of the protein-ligand complex are Arg608, Leu868, and Glu866. In comparison with the α-glucosidase positive inhibitor, altogether, the docking score for the given interaction is −7,8 kcal/mol whereas the control binding energy was low at -7,5 kcal/mol (Table 3.8).

© University of Venda

The chemical CID58879477 was attached to the active site of the α-glucosidase and showed that it could function as a competitive inhibitor with greater binding energy. Hence it can be considered a novel drug candidate.

The identical α-glucosidase structural homolog depicting α-helices, β-strands, loops, and turns, active sites and the entire protein groups (Figure 3.9B) was subjected to docking (Figure 3.14C) with the inhibiting compounds identified from the plant's ethanol stem extract (Table 3.3B). Multiple ligands docking by PyRx provided the binding affinities (Table 3.8). The same compound, Ligand 8A (SCHEMBL6844198) from ethanol stem extract demonstrated outstanding binding energy compared to other plant stem phytochemicals docked with as presented above (Figures 3.14C and 3.13C). The compound was bound to the enzyme by five different interactions, as shown above. It was thoroughly established that it generates three conventional hydrogen bonds with the α-glucosidase's active site by amino acids Arg594, Met363 and Tyr360; a single carbon-hydrogen bond by His717; two unfavourable Donor-Donor interactions by Val867 and Leu868. Fascinatingly, three Pi-Pi stacked, and Pi-Pi T-shaped interactions were formed by the amino acid residues His717 and two Tyr360, as depicted above (Figure 3.14C). The compound additionally interacted with distant amino acid residues through Van der Waals interactions. The amino acid residues facilitating the protein-ligand complex's overall binding are Arg594, Met363, and Tyr360. In comparison with the α-glucosidase positive inhibitor, thoroughly, the docking score for the given interaction is −7,7 kcal/mol, whereas the control binding energy was low at -7,5 kcal/mol (Table 3.8). The chemical SCHEMBL6844198 can be regarded as a unique drug candidate because it showed that it might function as a competitive inhibitor by connecting to the active site of the α-glucosidase with a higher binding energy.

The identical retrieved α-glucosidase structural homolog presenting α-helices, β-strands, loops, and turns, active sites and the complete protein groups (Figure 3.9B) was subjected to docking (Figure 3.14D) with the inhibiting compounds identified from the plant's ethanol leaf extract (Table 3.3B). Multiple ligands docking by PyRx provided the binding affinities (Table 3.8). The compound Ligand 9A (Trifolin) from ethanol leaf extract demonstrated outstanding binding energy compared to other plant leaf phytochemicals docked with, as depicted above. Trifolin compound was bound to the enzyme by four various interactions as shown above. It was established that it generates a single conventional hydrogen bond with the α-glucosidase's active site by amino acid Asp91, a single unfavourable Donor-Donor interaction by amino acid Ile98. The amino acid Trp126 was fascinatingly bound via Pi-Pi stacked and Pi-Pi T-shaped interaction. Furthermore, it registered three of the Pi-Pi stacked and Pi-Pi T-shaped interactions (Figure 3.14D). Trifolin further engaged with distant amino acid residues through Van der Waals interactions. The amino acid residue that facilitated the overall binding of the protein-ligand complex is Asp91. In comparison with the α-glucosidase positive inhibitor, the docking score for the given interaction is −7,6 kcal/mol whereas the control binding energy was low at -7,5 kcal/mol (Table 3.8). Although trifolin's competitive inhibitory properties have already been established (Makati *et al*., 2022), no investigation has tested it against diabetes enzyme indicators.

© University of Venda

By binding to the active site of the α-glucosidase with a higher binding energy, the molecule trifolin validated its function as a competitive inhibitor, as a result, it can be regarded as a novel therapeutic candidate.

Ethanol root extract Ligand 6A (Capronor) was bound to α-glucosidase via five types of interactions: conventional hydrogen bond by Trp126, Gln124 with the ligand, whereas Pro125 interacted via a carbon-hydrogen bond. Hydrogen bonds are strong, directional interactions that significantly stabilize ligand binding. Such interactions occur within the context of hydrogen atoms covalently bonded with electronegative species (oxygen, nitrogen) and lone-pair-containing electronegative atoms. The side chain of glutamine has an amide group which can form hydrogen bonds. It is likely interacting with the hydroxyl or keto groups of Capronor to stabilize the ligand in the binding pocket. Proline is unique because of its cyclic structure that confines its flexibility. In this case, however, its side chain does not participate directly in hydrogen bonding since it lacks a traditional hydrogen donor or acceptor, but it might be able to act through its backbone. So, this interaction may stabilize the protein's backbone conformation around the ligand. Pi-interactions are between aromatic rings of the ligand and non-polar groups of amino acids, involving Trp126 and Met122 (Pi-alkyl and Pi-sigma, respectively). These Pi interactions stabilize against hydrophobicity. The binding energy of -7.7 kcal/mol is an appraisal of the ligand's strength in binding with protein, (Table 3.8). Such binding energy in molecular docking, which is generally good, could also suggest that Capronor would, indeed, bind very well on the active site of the protein.

Another ethanol root extract, Ligand 7A (Geshoidin), binds to α-glucosidase with a binding energy of -7.6 kcal/mol, in comparison with the positive control, acarbose (-7.4 kcal/mol) indicating strong affinity and potential biological relevance (Table 3.8). The interaction involves conventional hydrogen bonds with Val867 and Leu868 and a pi-alkyl interaction with Arg594. These interactions indicate that Geshoidin could be a stable and possibly bioactive ligand; thus, it could be an attractive molecule for further pharmacological studies. Valine and Leucine are aliphatic amino acids that can be classified under chain-branched, hydropathy index scores being positive. They are not known to typically make hydrogen bonds since their side chain does not possess a hydrogen donor or acceptor. Here, however, the backbone amide or carbonyl group is likely to participate in hydrogen bonding, probably donating hydrogen to one of the oxygen atoms on Geshoidin (either hydroxyl or carbonyl). The arginine guanidinium group in most structures has been seen to adopt electrostatic interactions or hydrogen bonding. In this structure, it participates in a pi-alkyl interaction wherein one of the alkyl groups emanating from its side chain interacts with the aromatic ring of Geshoidin, thereby providing hydrophobic stabilization complementary to hydrogen bonds for overall ligand binding.

Ethanol leaf extract Ligand 6A (Capronor) interacts strongly with its target protein (α-glucosidase) with a docking score of -7.5 kcal/mol (Table 3.8), demonstrating a moderate binding affinity. Capronor interacts strongly with its target protein, forming key conventional hydrogen bonds with Asp91 and Alkyl and pi-alkyl interactions with Met122, and Trp126. As a result, Asp91 is acidic (aspartic acid), helping to provide a negatively charged environment.

© University of Venda

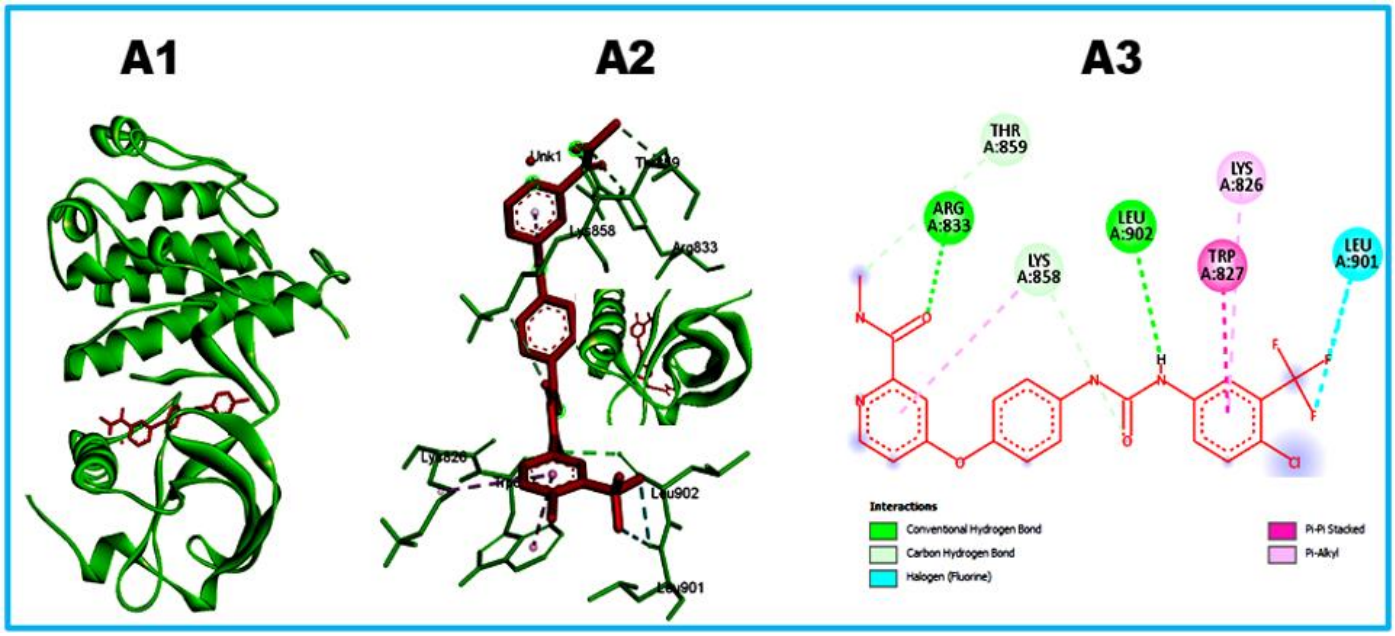
The carbonyl oxygen joins with Capronor via a hydrogen bond, which can either be a hydrogen donor or acceptor from Asp91. This is a strongly specific interaction that contributes significantly toward stabilizing ligand binding. Methionine (Met122), a hydrophobic amino acid with sulphur in it, here the alkyl group of Capronor interacts pi-alkyl with the side chain of Met122. The interactions, hydrophobic in nature, help position the ligand correctly within the binding pocket. Tryptophan 126 is an aromatic amino acid with a large pi-electron system. Capronor's aromatic or alkyl groups interact with the pi-electron cloud of Trp126 via pi-alkyl interactions. This interaction contributes to ligand stabilization and orientation in the hydrophobic pocket. This combination of polar (hydrogen bond) and non-polar (pi-alkyl) interactions ensures strong binding, specificity, and stability of the ligand in the active site.

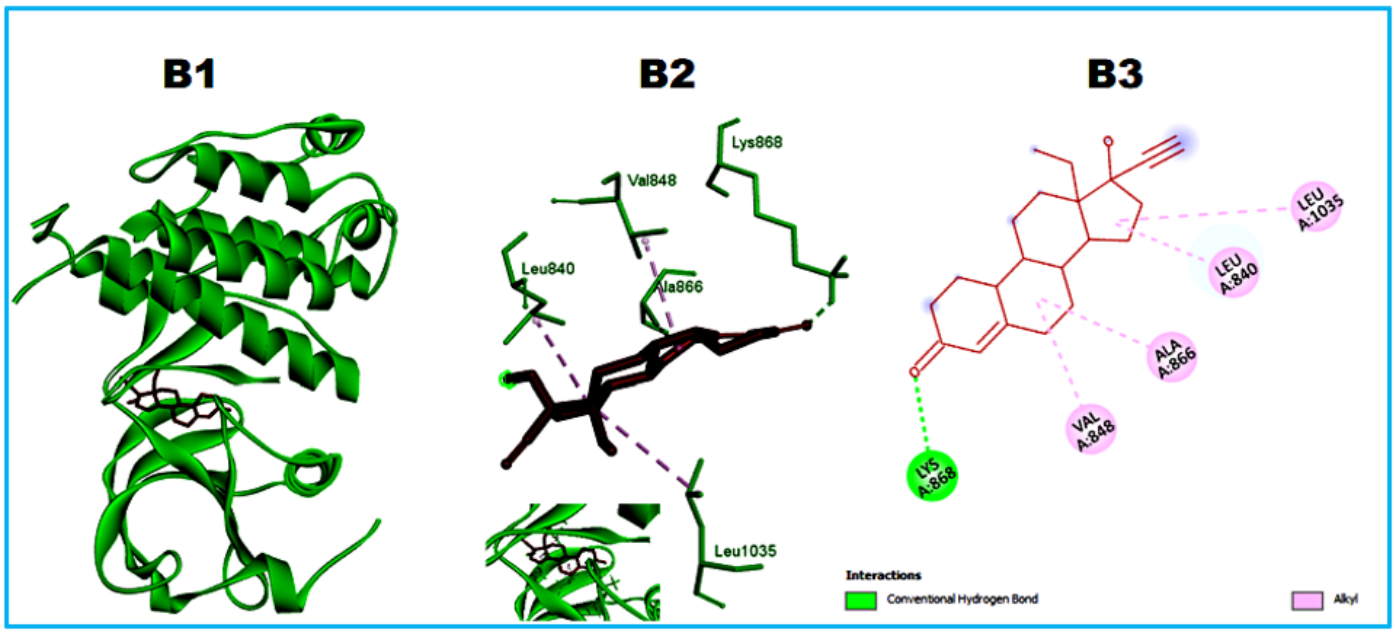
3.4.4.7. Selected identified compounds in ethanol extracts from different organs of *T. zeylanicum* docked against VEGFR2.

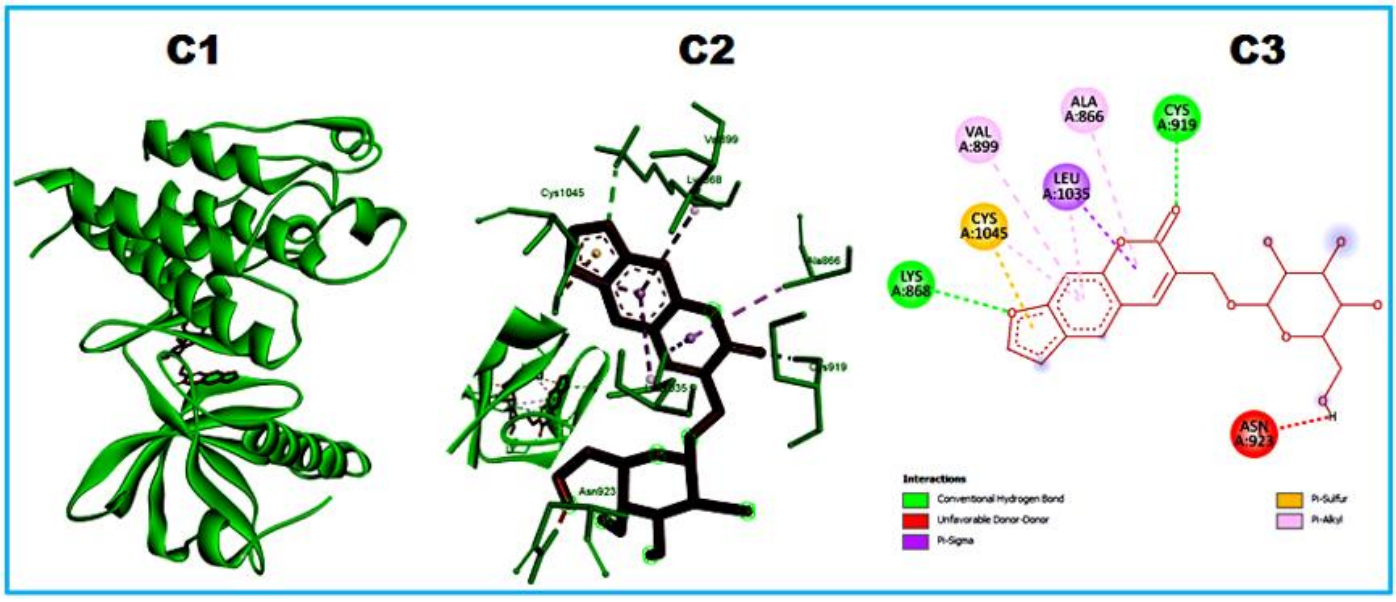
The VEGFR2 was also subjected to docking with its control sorafenib (Figures 3.15A and 3.9C) and the inhibiting compounds identified from the plant organ extract (Table 3.3B). The binding affinities were obtained by PyRx docking several ligands (Table 3.9). The widely recognized VEGFR2 inhibitor sorafenib was universally confirmed to bind with the active site by creating two conventional hydrogen bonds by amino acids, Arg833 and Leu902; two carbon-hydrogen bonds by Thr859 and Lys858; a single halogen (Fluorine) interaction by Leu901; a single Pi-Pi stacked interaction by Trp827 and two Pi-Alkyl interactions by Lys826 and Lys858 which remarkably further interacted by carbon hydrogen shown above (Figure 3.15A). The substance additionally engaged with distant amino acid residues through Van der Waals interactions. The amino acid residues that facilitated the overall binding of the protein-ligand complex are Arg833 and Leu902. Altogether, the docking score for the given interaction is −8,0 kcal/mol (Table 3.9).

The retrieved structural homolog of VEGFR2 wound target protein depicting α-helices, β-strands, loops and turns, active sites and the whole protein groups (Figure 3.9C) was subjected to docking (Figure 3.15B) with the inhibiting compounds identified from the plant's ethanol root extract (Table 3.3B). Multiple ligands docking by PyRx provided the binding affinities (Table 3.9). The compound Ligand 6A (Capronor) from ethanol root extract demonstrated outstanding binding energy compared to other plant root phytochemicals docked as depicted above. The compound was bound to the enzyme by two different interactions, as shown above. It was thoroughly established that it generates a single conventional hydrogen bond with the VEGFR2 enzyme's active site by an amino acid. Furthermore, it formed four Alkyl interactions by amino acids Val848, Ala868, Leu840 and Leu1035 (Figure 3.15B). The compound Capronor additionally engaged with distant amino acid residues through Van der Waals interactions.

© University of Venda







© University of Venda

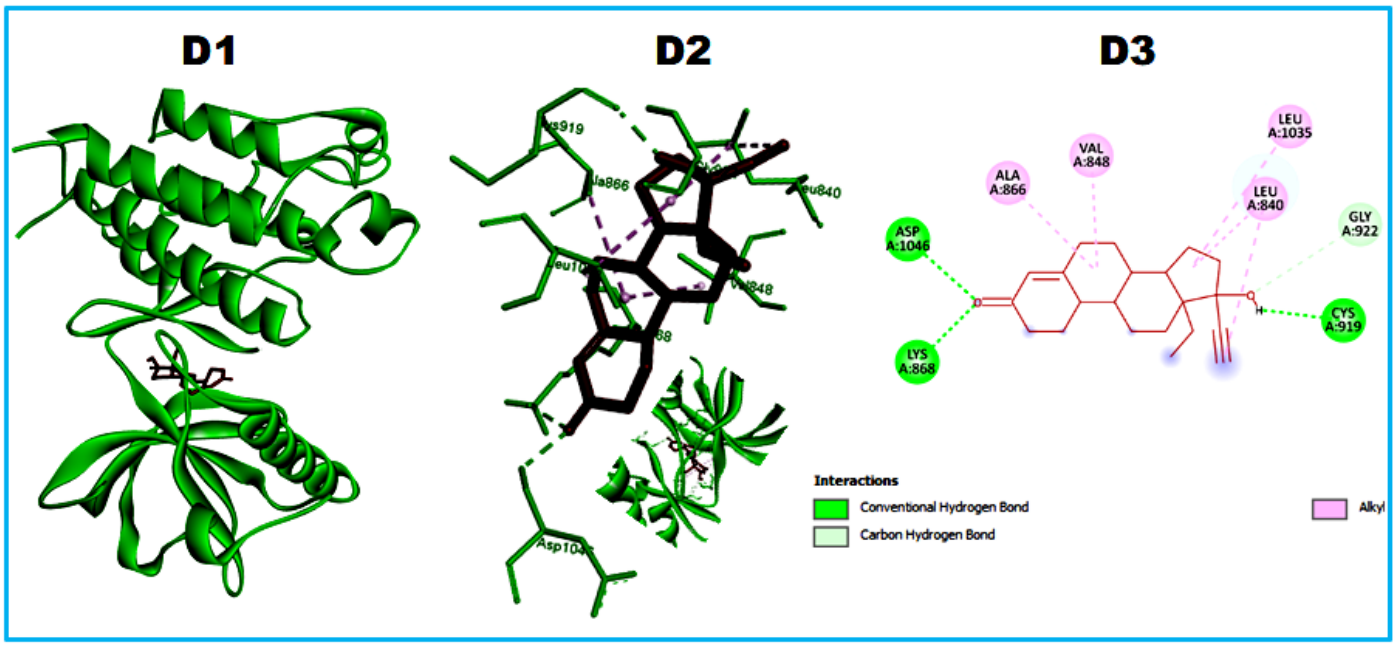


Figure 3.15: Molecular docking of **VEGFR2** against **(A) Sorafenib**, **(B) Ligand 6A, (C) Ligand 8A, and (D) Ligand 6A.** (A1–D1) depicts the active site of the VEGFR2, (A2–D2) demonstrate the zoomed-in interaction site enzyme and ligands (A3–D3) display the interacting amino acid residues of the VEGFR2.

Table 3.9: The binding affinities of selected identified compounds in ethanol root, stem, and leaf extracts of *T. zeylanicum* with the highest binding affinity to the VEGFR2 and the interacting amino acid residues of the protein.

ligand	Ligand name/code and plant part	Molecular formula	Binding affinity (kcal/mol)	Rmsd /Ub	Rmsd /lb	Interacting residues of the protein and their positions
Sorafenib	Positive control	$C_{21}H_{16}ClF_3N_4O_3$	-8,0	0	0	Arg833, Lys858, Leu902, Trp827, Leu901 and Lys826.
Ligand 6A	Capronor (ethanol root extract)	$C_{21}H_{28}O_2$	-8,4	0	0	Lys868, Val848, Ala868, Leu840, and Leu1035
Ligand 8A	SCHEMBL6844198 (ethanol stem extract)	$C_{18}H_{18}O_9$	-7,3	0	0	Lys868, Cys919, Asn923, Leu1035, Cys1045, Val899, and Ala866
Ligand 6A	Capronor (ethanol leaf extract)	$C_{21}H_{28}O_2$	-8,8	0	0	Asp1046, Lys868, Cys919, Gly922, Ala866, Val848, Leu1035 and Leu840

© University of Venda

The amino acid residue that facilitated the overall binding of the protein-ligand complex is Lys868 (Figure 3.15B). In comparison with the VEGFR2 positive inhibitor, altogether, the docking score for the given interaction is −8,4 kcal/mol, whereas the control binding energy was low at -8,0 kcal/mol (Table 3.9). By binding to the active site of the VEGFR2 enzyme with higher binding energy, the molecule Capronor showed that it could operate as a competitive inhibitor; as a result, it can be regarded as an exceptional therapeutic candidate.

The same retrieved structural homolog of VEGFR2 wound target protein depicting α-helices, β-strands, loops and turns, active sites and the whole protein groups (Figure 3.9C) was subjected to docking (Figure 3.15C) with the inhibiting compounds identified from the plant's ethanol stem extract (Table 3.3B). Multiple ligands docking by PyRx provided the binding affinities (Table 3.9). The same compound, Ligand 8A (SCHEMBL6844198), from ethanol stem extract demonstrated outstanding binding energy compared to other plant stem phytochemicals docked as presented above (Figures 3.15C, 3.14C and 3.13C). The compound was bound to the enzyme by five various interactions as shown above. It was thoroughly established that it generates two conventional hydrogen bonds with the VEGFR2 enzyme's active site by amino acids Lys868 and Cys919; a single Unfavourable Donor-Donor by amino acid Asn923; a single Pi-Sigma by Leu1035; a single Pi-sulphur by Cys1045 and four Pi-Alkyl interactions by amino acids Val899, Ala866, Cys1045 and Leu1035 as depicted above (Figure 3.15C). The compound SCHEMBL6844198 further engaged with distant amino acid residues through Van der Waals interactions. The amino acid residues facilitating the protein-ligand complex's overall binding are Lys868 and Cys919. In comparison with the α-glucosidase positive inhibitor, the docking score for the given interaction is −7,3 kcal/mol, whereas the control binding energy was high at −8,0 kcal/mol (Table 3.9). Although the compound SCHEMBL6844198, when docked against VEGFR2, demonstrated greater binding energy than the other stem phytochemicals, its ability to operate as a competitive inhibitor is less, as the binding energy is less than that of the positive control.

The identical retrieved structural homolog of VEGFR2 wound target protein depicting α-helices, β-strands, loops and turns, active sites and the whole protein groups (Figure 3.9C) was subjected to docking (Figure 3.15D) with the inhibiting compounds identified from the plant's ethanol plant leaf extract (Table 3.3B). Multiple ligands docking by PyRx provided the binding affinities (Table 3.9). The compound Ligand 6A (Capronor) from ethanol leaf extract demonstrated outstanding binding energy compared to other plant leaf phytochemicals docked with, as presented above. The compound was bound to the enzyme by four various interactions, as shown above. It was thoroughly established that it generates three conventional hydrogen bonds with the VEGFR2 enzyme's active site by amino acids Cys919, Asp1046 and Lys868 from the same ligand oxygen atom; a single carbon-hydrogen bond by amino acid Gly922; and five Alkyl interactions by amino acids Ala866, Val848, Leu1035 and two Leu840 as depicted above (Figure 3.15D). The compound Capronor further interacted with distant amino acid residues through Van der Waals interactions. The amino acid residues facilitating the protein-ligand complex's overall binding are Asp1046, Lys868, and Cys919.

© University of Venda

In comparison with the α-glucosidase positive inhibitor, altogether, the docking score for the given interaction is −8,8 kcal/mol, whereas the control binding energy was high at −8,0 kcal/mol (Table 3.9). The chemical Capronor can be regarded as a unique therapeutic candidate because it showed that it could serve as a competitive inhibitor by binding to the active site of the VEGFR2 enzyme with a higher binding energy.

3.4.4.8. The molecular docking summary

The study findings validated Ligand 1A from EA root extract as the potential inhibitor from *T. zeylanicum* EA extracts as it had an affinity for both diabetes enzyme markers and the wound-associated kinase as presented in Table 3.4, Table 3.5, and Table 3.6 and the corresponding figures (Figures 3.10B, 3.11B, and 3.12B). The findings demonstrated that ligand 1A from EA root extract has the potential to regulate the function of the α-amylase (Figure 3.10B and Table 3.4), hence it possibly regulates the breaking down of dietary carbohydrates such as starch into simple monosaccharides in the digestive system. Ligand 1A from EA root extract also showed activity against α-glucosidase function (Figure 3.11B and Table 3.5), indicating it could regulate the degradation of simple monosaccharides by α-glucosidases to glucose, which, on absorption, enters the bloodstream. The study findings are summarised in Table 3.10.

Table 3.10: Summary of selected identified compounds in studied plant extracts with good binding affinities against all three docked proteins.

Ligand	Molecular formula	Molecular name	Plant Part extract	α-amylase	α-glucosidase	VEGFR2
Ligand 1A	$C_{32}H_{20}O_{12}$	4-[2,6-Dihydroxy-4-(6,7,8-trihydroxy-2-naphthyl) phenoxy]-3-hydroxy-7-(3,4,5-trihydroxyphenyl) naphthalene-1,2-dione	EA root extract	✓	✓	✓
Ligand 8A	$C_{18}H_{18}O_9$	SCHEMBL6844198	Ethanol stem extract	✓	✓	
Ligand 6A	$C_{21}H_{28}O_2$	Capronor	Ethanol leaf extract	✓		✓

The compound's promising activity was remarkable as it displayed its ability to regulate the wound-associated protein (Figure 3.12B and Table 3.6) since it was previously reported by Greenhalgh (2003), that many people with diabetes develop wounds that are slow to heal, do not heal well, or never heal and sometimes, an opportunistic infection might develop (Yameny, 2024). As diabetes impairs how the body produces or responds to the insulin hormone, when blood glucose remains permanently high, it impairs the function of white blood cells (Yameny, 2024). Thus, when the white blood cells are unable to function correctly, the body is less able to fight bacteria and close open wounds (Greenhalgh, 2003). Uncontrolled diabetes may also affect circulation, causing blood to move more slowly, which makes it more difficult for the body to deliver nutrients to wounds. As a result, the injuries heal slowly or may not heal at all (Dinh *et al.*, 2011).

© University of Venda

Ligand 1A demonstrated the ability of diabetic wound healing properties, which can be achieved through the regulation of blood glucose levels. Hence, the body will probably be able to fight bacteria, and wounds will receive nutrients to heal quickly. The data is summarised above in Table 3.10. The findings are unique since no study has been conducted that shows molecular docking of Ligand 1A of the EA root extract of *T. zeylanicum.*

Ligand 8A from ethanol stem extract has the potential to regulate the function of the α-amylase (Figure 3.13C and Table 3.7), meaning it could possibly regulate the breaking down of dietary carbohydrates such as starch into simple monosaccharides in the digestive system. It also demonstrated its capability as it had activity against α-glucosidase function (Figure 3.14C and Table 3.8). Hence, it regulates the further degradation of simple monosaccharides by α-glucosidases to glucose, which, on absorption, enters the bloodstream. The findings demonstrated that although ligand 8A from ethanol stem extract has activity for the diabetes protein markers, it showed no activity to VEGFR2; therefore, this compound can inhibit diabetes formation. Ligand 6A from ethanol leaf extract has the potential to regulate the function of the α-amylase (Figure 3.13D and Table 3.7). Hence, it regulates the breaking down of dietary carbohydrates such as starch into simple monosaccharides in the digestive system. However, the compound did not have activity against α-glucosidase function; henceforth, it will not be able to regulate the further degradation of simple monosaccharides by α-glucosidases to glucose. Remarkably, the compound demonstrated the ability for diabetic wound healing (Figure 3.15D and Table 3.9) as the blood glucose levels can be regulated, possibly the body is likely to be able to fight bacteria, and wounds will receive nutrients to heal quickly.

3.4.5. Distribution of phytochemical compounds within the plant organs

The results below detail the profile of the phytochemical compounds from the root, stem and leaf of the plant extracted using two different solvents, EA and ethanol (Figure 3.16). The ethanol root extract contains a higher proportion of unidentified compounds, about 60%, compared to the EA root extract, with 50% (Figure 3.16 AB). This probably shows that ethanol is extracting a wider range of polar compounds (Lefebvre *et al*., 2021), of which most have still not been characterised. EA extracted 15% quinones and 10% Naphthols and derivatives in the root extract that are completely absent in the ethanol root extract. This, therefore, means that EA is a better solvent regarding the extraction of the specific compounds, which normally possess antioxidant and aromatic properties. This is because EA can form hydrogen bonds with some organic compounds and make them soluble (Kumar *et al*., 2023). On the other side, ethanol was able to extract 5% of each of the fatty acids and fatty alcohols in the root extract, which did not show up in the EA root extract (Figure 3.16 AB). These are important compounds in energy storage and structural functions (Kahwaji and White, 2021). While both ethanol and EA extracts contained benzenes and steroids, the EA root extract was richer in benzenes at 15%, with a similar extraction of steroids at 5% for both (Figure 3.16 AB). This, therefore, adds weight to the fact that the choice of solvent does determine, to a reasonable degree, its ability to extract some classes of compounds more than others, as shown below in Figure 3.16 AB.

© University of Venda

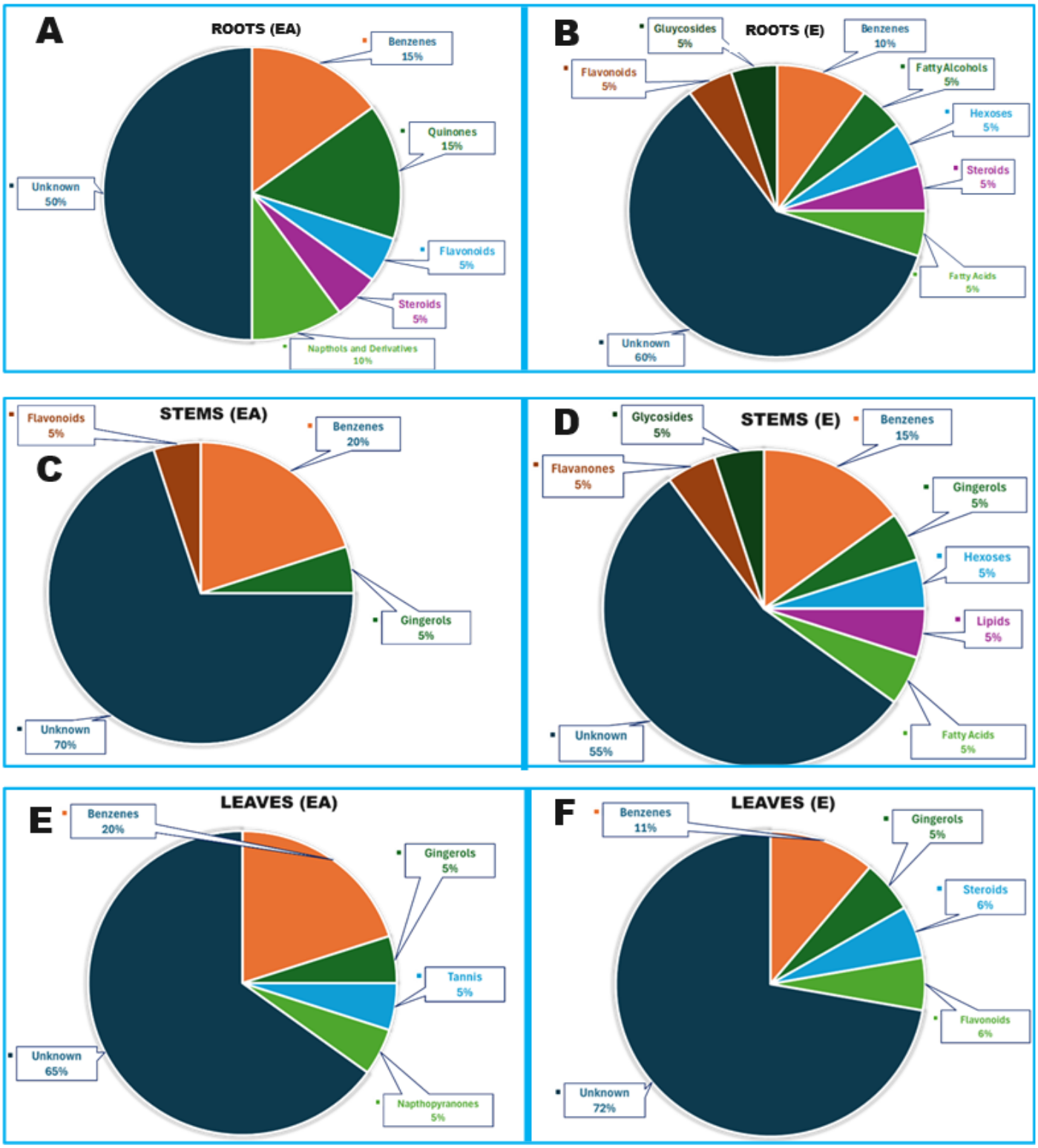


Figure 3.16: Metabolites relative abundance of EA and ethanol extracts from different organs of *T. zeylanicum*. **(A)** root, **(C)** stem, **(E)** leaf and ethanol **(B)** root, **(D)** stem, and **(F)** leaf extracts annotation and their distribution across the plant's organs. **EA** = EA and **E** = Ethanol.

Under stem, the EA extract is thus rich in benzene content of 20% (Figure 3.16 CD), which could mean that this is better regarding the extraction of aromatic hydrocarbons from EA stem extract. These may contribute something to the antioxidant properties of such compounds. EA is utilized to extract flavonoids and total phenolics because it is recognized to be non-toxic (Kumar *et al*., 2023).

© University of Venda

EA stem extract contains flavonoids and gingerols at 5%, both of which are good for their resultant antioxidant activity (Ghafoor *et al*., 2020; Tohma *et al*., 2017). However, most of the chemicals in the EA stem extract have not yet been identified, as it is 70% unknown or is just out of reach of detection (Figure 3.16 CD). A greater variety of chemical classes were represented in the ethanol stem extract, including benzenes (15%), gingerols (5%), flavonoids (5%), and the recently discovered class of hexoses (5%), glycosides (5%), lipids (5%), and fatty acids (5%) (Figure 3.16 CD). Ethanol, quite naturally, proves capable of simultaneously extracting both polar and non-polar compounds (Koffi *et al*., 2010). The ethanol stem extract indicates that the number of unknowns from research findings is lower at 55% (Figure 3.16 CD), meaning that ethanol extracts known bioactive compounds of a broader array from the stem than EA (Altemimi *et al*., 2017). Ethanol is an effective solvent for extracting a wide range of compounds because it is miscible with water and can dissolve both polar and nonpolar molecules (Lefebvre *et al*., 2021).

Under leaf extract, the content of benzene in the EA extract is higher (20%) than that of ethanol leaf extract (11%) (Figure 3.16 EF). This suggests that there exists a rich pool of aromatic hydrocarbon compounds that are possible to procure with EA (Szolar *et al*., 2002), which probably plays a significant role in the process of antioxidant activity (Tohma *et al*., 2017). Still, a considerable proportion (65%) remains an unexplored compound, suggesting that EA seems to have the potential to extract even more intricate or less common substances present in the leaf extract of *T. zeylanicum* (Figure 3.16 EF). Moreover, EA is also able to extract gingerols, tannins, and napthopyranones from leaf extract, which adds to the huge spectrum of bioactive compounds, though in very minimal amounts. EA is a well-known, semi-polar solvent that extracts the less-polar compounds such as benzenes and, perhaps, some phenolic compounds like gingerols (Didion *et al*., 2023). Although it cannot extract steroids and flavonoids in significant amounts, it greatly supports antioxidant actions by providing a good amount of benzene. These activities support the idea that EA can extract aromatic compounds from different organs of this plant, contributing to antioxidant abilities (Ghafoor *et al*., 2020; Szolar *et al*., 2002). However, its inadequacies in extracting sufficiently enormous quantities of steroids and flavonoids limit its use where these compounds are needed.

In general, ethanol leaf extract is characterized by the presence of steroids (6%) and flavonoids (6%), which are absent or less prominent in the EA leaf extract. Ethanol's polar nature likely explains its ability to extract these bioactive compounds, which are typically more soluble in polar solvents (Lezoul *et al*., 2020; Zainal-Abidin *et al*., 2017). Flavonoids are particularly important because of their extremely potent antioxidant and anti-inflammatory activities (Chagas *et al*., 2022). This implies that the ethanol extract is more likely to yield a product which possesses some degree of these activities. For the ethanol leaf extract, out of the total compounds that were investigated, 72% were found to be categorically unknown, slightly higher than 65% presented in the EA leaf extract. This means a significant amount of yet unknown or poorly characterised compounds were recovered by both solvents, and this should warrant further investigation.

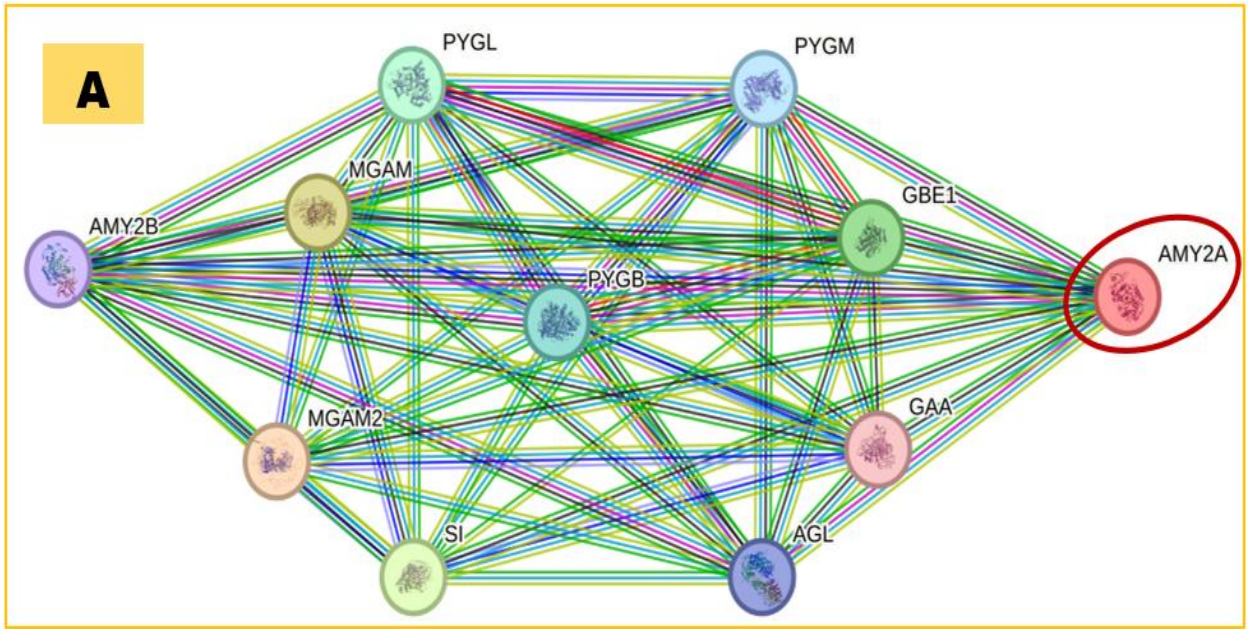
© University of Venda

A polar solvent, ethanol is commonly used to extract a multitude of bioactive compounds, especially those indicated by polar functional groups, including flavonoids and steroids (Abd Aziz *et al*., 2021). The presence of flavonoids and steroids in the ethanol extract makes it valuable for applications that require antioxidant agents (Ullah *et al*., 2020). Ethanol's ability to extract polar compounds makes it the preferred solvent for accessing a broader range of phytochemicals with diverse biological activities as depicted above in Figure 3.16.

3.4.6. Predicted biological protein-protein networks.

3.4.6.1. α-Amylase and α-glucosidase predicted biological protein-protein networks

Figures 3.17A and B were used to visualize the enzymes that are functionally and closely related to the two diabetes enzyme markers and whether they share the same enzyme network that could possibly be aiding in T2D. The network's edges' varied colours correspond to distinct kinds of evidence for the relationships, such as co-expression, experimental, and carefully chosen database entries. Due to these overlapping relations that bind the pancreatic α-amylase **(**AMY2A) and intestinal α-glucosidase **(**GAA) into countless metabolic pathways, any infraction in their activity would naively reflect upon some pathway of fundamental metabolic significance and could become a conduit to digestive health and metabolic disorders. This network illustrates all the important roles played by the pancreatic AMY2A and intestinal GAA in carbohydrate metabolism, where they interact substantially with other enzymes metabolising carbohydrates and breaking starch down (Szklarczyk *et al*., 2019). These insights are vital for developing an understanding of diseases related to carbohydrate metabolism and offer a guide to the formulation of therapeutic approaches for metabolic pathologies and blood sugar levels, as shown in Figures 3.17A and B.



© University of Venda

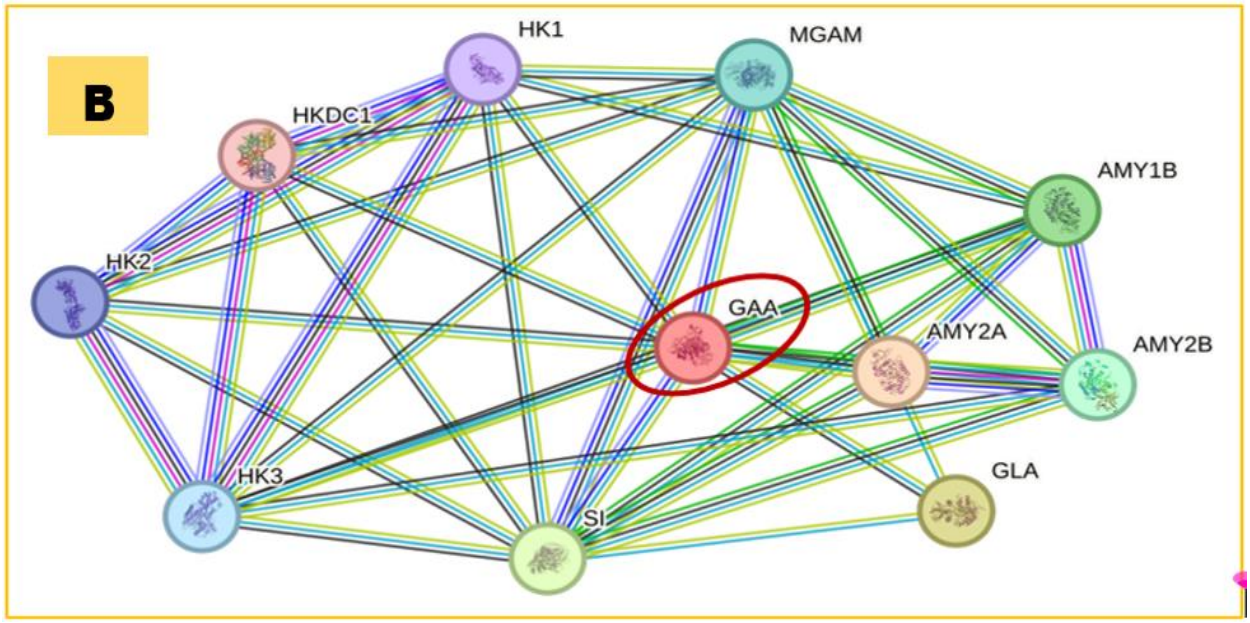


Figure 3.17: Protein-protein network focused on **(A)** the human pancreatic α-amylase (AMY2A) and **(B)** the intestinal α-glucosidase (GAA) and their networking enzymes. α-amylase (AMY1B, AMY2A and AMY2B), glycogen-related enzymes (PYGL, PYGM, GBE1), maltase glucoamylase (MGAM, MGAM2), intestinal α-glucosidase (GAA) and intestinal sucrase-isomaltose (SI). Both AMY2A and GAA in this network contain an array of proteins that pertain to carbohydrate metabolism.

In T2DM, insulin resistance and impaired glucose regulation lead to chronically elevated blood glucose levels (Ch'ng *et al*., 2019). This network (Figures 3.17A and B) highlights enzymes that participate in the metabolism of carbohydrates and glycogen, including α-amylase (AMY1B, AMY2A and AMY2B), glycogen-related enzymes (PYGL, PYGM, GBE1), maltase glucoamylase (MGAM, MGAM2), intestinal α-glucosidase (GAA) and intestinal sucrase-isomaltose (SI) (Mehraban *et al*., 2019). These enzymes are thought to have a direct impact on blood glucose homeostasis. α-Amylase (AMY1B, AMY2A and AMY2B) break down complex carbohydrates into simpler sugars, like maltose, which are further digested into simpler molecules (Kazeem *et al*., 2013; Vocadlo *et al*., 2008). These are further degraded by intestinal α-glucosidases (GAA) to glucose, which, on absorption, enters the bloodstream, contributing to blood sugar levels (Peyrot des Gachons and Breslin, 2016). The pancreas frequently produces more insulin in T2DM to make up for insulin resistance, which can increase the activity of α-amylases.

A quicker rise in glucose levels in the blood shortly after meals and a quicker breakdown of carbohydrates can result from increased amylase activity. Managing amylase and glucosidase activity may be one way to reduce the elevated postprandial glucose, which is a typical symptom of T2DM (DeFronzo, 2004; Sim *et al*., 2010). Glycogen-related enzymes known as glycogen phosphorylase (PYGL, PYGM) break down glycogen in the liver (PYGL) and muscle tissues (PYGM) (Migocka-Patrzałek and Elias, 2021), discharging glucose entering the bloodstream, particularly during periods of fasting or vigorous exercise (Ding *et al*., 2020).

© University of Venda

The insulin resistance underlying T2DM commonly impairs the control of hepatic glycogenolysis, leading to inappropriate glucose release by the liver into the blood when circulating glucose levels are already high, contributing to the characteristic elevated fasting blood glucose of T2DM (Llavero and Zugaza, 2014). GBE1 is expected to modulate the structure of glycogen by removing an outer shell so that glycogen becomes more soluble and more easily broken down. Disruption of the mechanism due to GBE1 gene mutation, the molecule's structure may change, altering glucose availability and ultimately causing glucose dysregulation in individuals with T2DM (Brereton *et al*., 2016). Intestinal α-glucosidase (GAA) plays an important role in the cleavage of glycogen in lysosomes, especially in tissues such as muscle. Its malfunction or disorderly degradation will produce tissue glycogen accumulation, which would adversely affect muscle function and possibly contribute to the resistance to insulin, even though it is less directly correlated with immediate blood glucose levels (Zhu *et al*., 2005). The lysosomal glycogen accumulation and degradation controlled by GAA have been linked to alterations in the energy metabolism of the cells, most commonly insulin resistance which is the hallmark of T2DM. The insulin resistance reduces the glucose uptake in muscle, leading to increases in blood sugar levels (Málaga *et al*., 2017).

The enzyme known as maltase glucoamylase (MGAM and MGAM2) proceeds to break down maltose, which is a byproduct of amylase activity, into glucose (Figures 3.17A and B). In the small intestine, this mechanism is essential for the absorption of glucose after consuming carbohydrates (Ren *et al*., 2011). Elevation or malfunctioning activity of MGAM might lead to greater glucose absorption, therefore raising postprandial blood glucose levels in T2DM patients (Xu *et al*., 2019). The increased sugar after meals continues to impact the pancreatic beta cells more severely, aggravating hyperglycaemia and possibly raising insulin requirements (Sim *et al*., 2008). Both amylase and glucosidase connect to intestinal sucrase-isomaltose (SI) (Figures 3.17A and B). These intestinal brush border enzymes can hydrolyse sucrose, maltose, maltotriose, and other α-1,6 and α-1,4 oligoglucans since they each contain two catalytic sites. SI is the most abundant in the human gut and is responsible for most α-glucosidase and sucrase activity (Ren *et al*., 2011; Sim *et al*., 2008). Because of this, and due to its implications in diabetes and other metabolic diseases, extensive discussions have been generated around it (Boudreau *et al*., 2002; Simsek *et al*., 2017). SI inhibition would further inhibit the uptake of glucose into the bloodstream and reduce postprandial hyperglycaemia (Mehraban *et al*., 2019).

3.4.6.2.VEGFR2 predicted biological protein-protein networks.

VEGFR2, responsible for wounds linked to T2DM, was examined in a network to determine its connection to enzymes related to the two diabetes markers (Figure 3.18). The goal was to find out if VEGFR2 was connected to the proximal diabetes enzyme indicators and if they shared an enzyme network that would aid in T2DM and wounds associated with it. The results did not support such a closer association, suggesting that although VEGFR2 contributes to T2DM-related wounds, it may not require assistance from the enzymes associated with the two diabetes enzyme indicators as presented in Figure 3.18.

© University of Venda

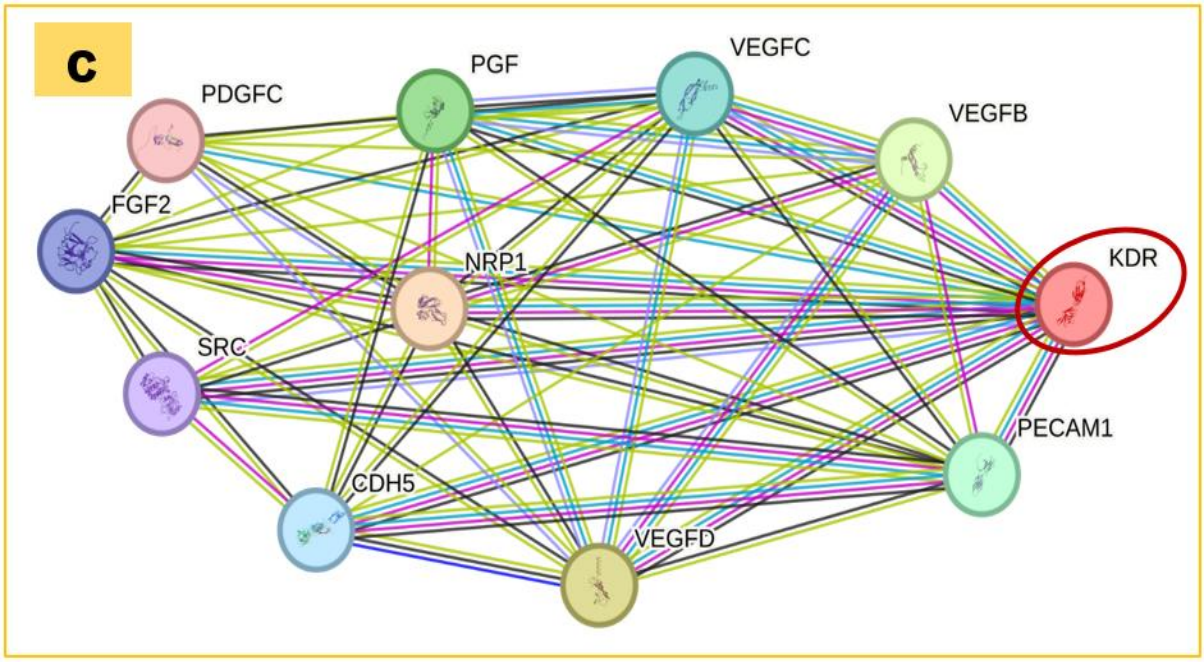


Figure 3.18: The protein-protein network centred around VEGFR2 (KDR) and its networking enzymes. Vascular Endothelial Growth Factors (VEGFB, VEGFC, VEGFD), Fibroblast Growth Factor 2 (FGF2), Neuropilin-1 (NRP1), Platelet and endothelial cell adhesion molecule 1 (PECAM1) and Platelet-derived Growth Factor C (PDGFC)

Vascular Endothelial Growth Factors (VEGFB, VEGFC, VEGFD) (Figure 3.18) are crucial for blood vessel development and regeneration (Carvalho *et al*., 2007; Ruszkowska *et al*., 2010), binding with VEGFR2 to trigger endothelial cell migration, proliferation, and survival, essential for wound healing according to Ruszkowska *et al*. (2010) and Wirostko *et al*. (2008). Bang *et al*. (2024) reported that diabetic wounds frequently have defective VEGF signalling, which results in inadequate angiogenesis and delayed healing. As Buraczynska *et al*. (2007) previously reported, chronically elevated blood glucose levels o in T2DM cause oxidative stress, vascular dysfunction, and inflammation, all of which hinder VEGF signalling and VEGFR2-mediated angiogenesis. As indicated by Bao *et al*. (2009), this network depicts the interaction of several growth factors, adhesion molecules, and signalling proteins to achieve angiogenesis and the healing process, which is often compromised in T2DM. In another study, this signalling pathway was found to be critical in the neovascularisation of oxygen-bearing blood vessels that perfuse a wound site (Florek *et al*., 2024).

Nevertheless, VEGF/VEGFR2 pathways are disrupted by high blood sugar in T2DM, reducing angiogenic potential (Liu *et al*., 2024; Silva *et al*., 2024). This clarifies the reason diabetic wounds often remain open for extended periods of time and are more susceptible to infection and ulceration (Buraczynska *et al*., 2007). T2DM affects growth hormones like Fibroblast Growth Factor 2 (FGF2) and Platelet-derived Growth Factor C (PDGFC) (Figure 3.18), which promote angiogenesis, proliferation, and cellular migration (Al-Mansoori *et al*., 2022; Li *et al*., 2022).

© University of Venda

VEGFR2 triggers endothelial cells, which in turn trigger FGF2 to promote the development and synthesis of new blood vessels (Larionov *et al*., 2024). Because PDGF and FGF regulate tissue repair and angiogenesis, abnormal PDGF and FGF signalling in T2DM patients leads to poor wound healing (Calvo *et al*., 2022; Cao *et al*., 2023; Hecking *et al*., 2022). T2DM causes modulations in growth factors relevant to wound healing, such as VEGF and FGF2 (Dai *et al*., 2021; Ornit and Itoh, 2015). Evidence shows that these growth factors are mainly reduced in diabetic wounds, thus dampening pathways mediated by VEGFR2 (Al-Mansoori *et al*., 2022).

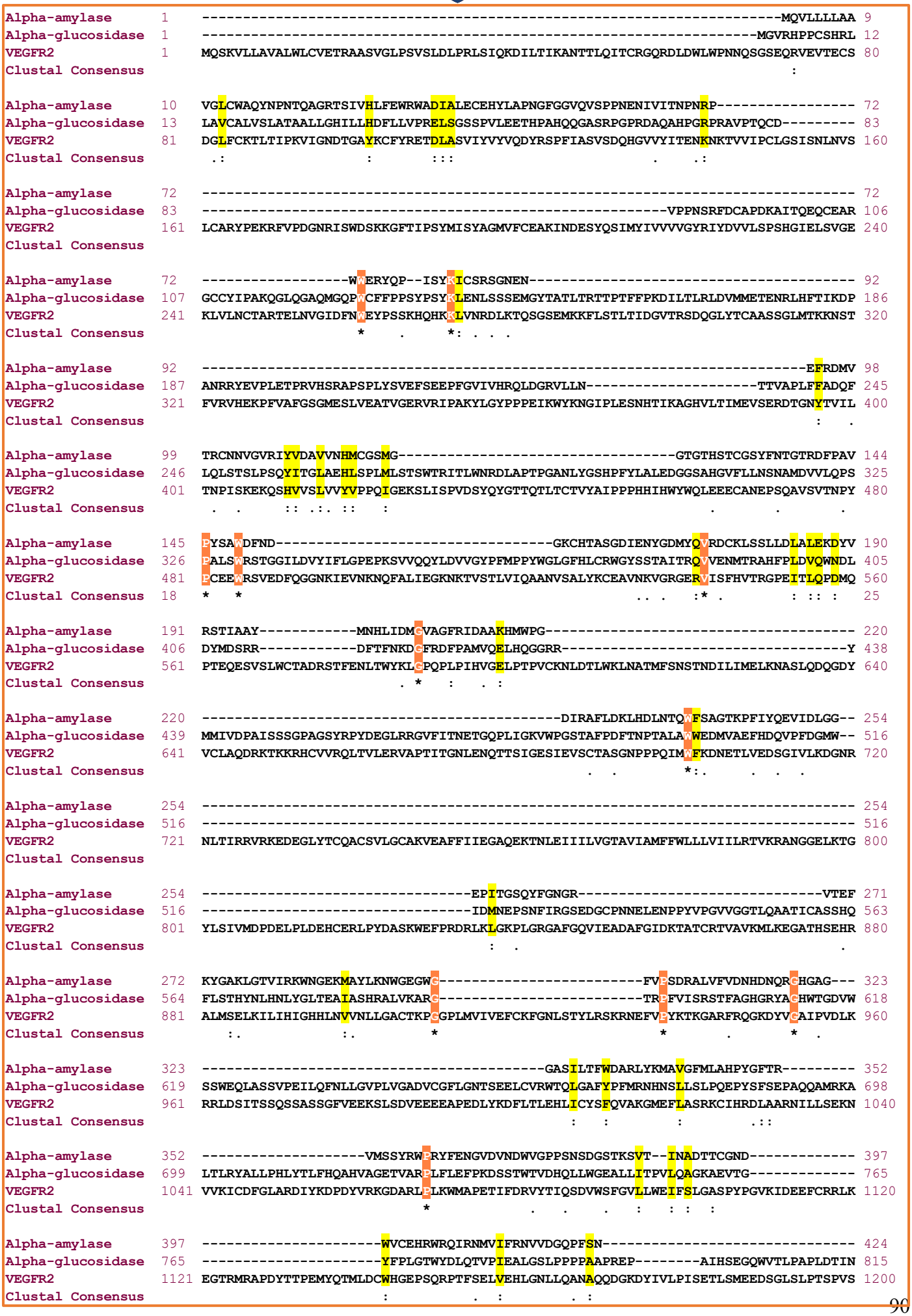
Neuropilin-1 (NRP1) (Figure 3.18), a co-receptor with VEGFR2 (Hsieh *et al*., 2008; Gelfand *et al*., 2014; Sharma *et al*., 2024), is known to increase downstream signalling and VEGF binding promoting angiogenesis (Ballmer-Hofer *et al*., 2011; Kofler and Simons, 2015; Sarabipour *et al*., 2024). Insufficient expression of NRP1 in diabetic tissues may block VEGFR2 signalling, resulting in poor blood vessel formation and wound-healing problems (Bondeva and Wolf, 2015; Liu *et al*., 2024). According to Raimondi (2014), targeting NRP1 in T2DM could enhance angiogenesis in diabetic wounds. Platelet and endothelial cell adhesion molecule 1 (PECAM1) (Figure 3.18) is involved in angiogenesis and stabilising endothelial junctions. It also aids in recruiting immune cells to repair sites (Bréchot *et al*., 2024; Li *et al*., 2024). Damage to PECAM1 function can impair wound healing in T2DM (Daniel and Van Buul, 2013).

3.4.7. α-Amylase, α-glucosidase and VEGFR2 Multiple sequence alignment

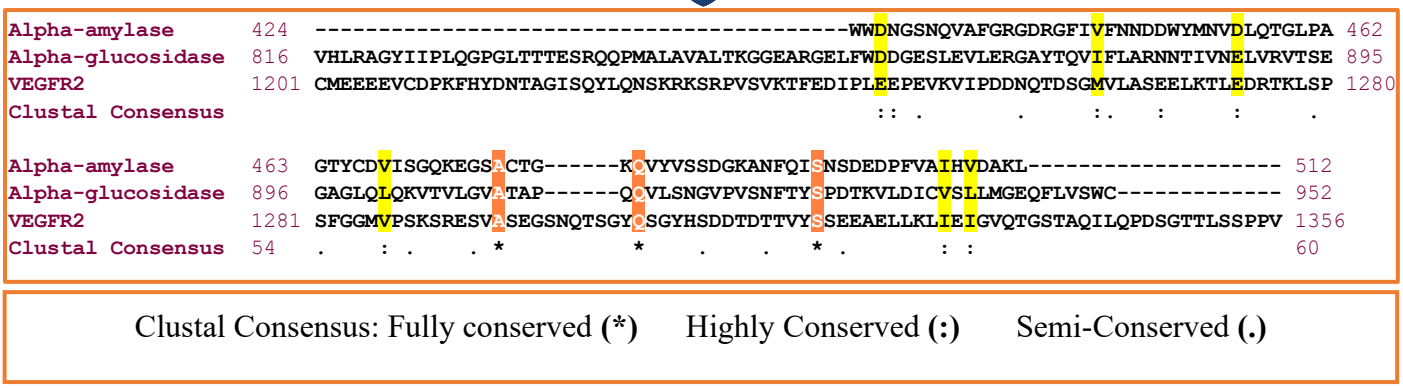
In this alignment (Figure 3.19), Orange colour-coded highlights indicate fully conserved sections, which are areas where amino acid residues are the same throughout the three sequences. Yellow colour-coded highlights indicate highly conserved sections. These conserved residues imply that the enzymes share structural or functionally significant areas (Figure 3.19). Gaps show areas where insertions or deletions have taken place over the course of evolution or where the sequences differ dramatically. In this study, multiple sequence alignment was done to check the conserved regions of the three proteins as they are all associated with the T2DM complications, whether the conserved regions play a role in the binding of the extracted compounds subjected to the binding pocket for inhibition purpose, and whether there are amino acid repeats or sequences that are conserved which can hence be hypothesised to play a functional role in T2DM formation and complications. The alignment is displayed below in Figure 3.19.

As expected, sequence alignment data demonstrated the α-amylase and α-glucosidase fully conserved regions, which can possibly support their role of digesting the carbohydrates and increasing the postprandial glucose level (Figure 3.19). Although the role of VEGFR2is not associated with dietary starch digestion, interestingly, sequence alignment data demonstrated a fully conserved residue at the same positions as α-amylase and α-glucosidase exhibited a fully conserved residue. This data can support the VEGFR2 role in causing T2DM-related wounds with extended research, as shown below (Figure 3.19).

© University of Venda



© University of Venda



Clustal Consensus: Fully conserved **(*)** Highly Conserved **(:)** Semi-Conserved **(.)**

Figure 3.19: Multiple sequence alignment display of human pancreatic α-amylase, intestinal α-glucosidase, and VEGRF2, all of which may have some relevance or closely linked to T2DM. VEGFR2 is responsible for T2DM-related wounds, while α-amylase and α-glucosidase are important targets for diabetic treatment since they are enzymes involved in glucose regulation and carbohydrate metabolism. The three proteins similarities and differences are emphasized by the sequence alignment.

3.5. Conclusion

Given that ethanol is miscible with water and can dissolve polar and nonpolar molecules (Lefebvre *et al*., 2021), it showed its potential to extract more bioactive chemicals from *T. zeylanicum* root, stem, and leaf extracts, exhibiting high percentage yields, with leaf extract presenting a superior yield (Figure 3.1). The relatively high amount of ethanol leaf extract agreed with the TLC chromatograms, wherein the ethanol leaf extract showcased more phytochemicals in comparison with the stem and root extracts (Figure 3.4B). The same trend was observed in EA plant extracts, wherein the extraction yields were extremely low, but a bit more in its leaf extract (Figure 3.4A). This, thus, validates the presence of phytochemicals in abundance within the leaf of this pla*nt.* The phytochemical screening of *T. zeylanicum* EA and ethanol leaf extracts further confirmed the presence of phytochemicals (phenols) with antidiabetic potentials and beneficial antioxidant activity (Table 3.1).

Compared with ethanol plant extract, the EA leaf extract of *T. zeylanicum* was identified as a promising natural antioxidant source, as detected by this study's qualitative and quantitative DPPH-scavenging tests (Figure 3.5A). The EA stem, root and leaf extracts showcased the highest percentage of DPPH inhibitions, with the leaf extract presenting the superior inhibition compared to ethanol extracts. Overall, in all EA and ethanol plant extracts, the leaf extract was the one with beneficial antioxidants (Figure 3.5A). The TPC further backed up the presence of the antioxidant compounds in the leaf. Phenolic content was higher in ethanol leaf extract (Figure 3.6B). The relatively high concentration in the leaf extract suggests that the leaf might be the richest source of phenolic compounds linked to high antioxidant action (Chen *et al*., 2020; Mazhar *et al*., 2022). With such a high concentration of phenolics, the ethanol leaf extract of *T. zeylanicum* is expected to have a powerful antioxidant property, hence adding substantial value to nutraceutical products and supplement formulations to reduce oxidative stress and promote general health (Chen *et al*., 2020).

© University of Venda

This strongly supports the traditional use of *T. zeylanicum* in medicine and the use of this plant to make products that promote health by combating oxidative stress and its associated diseases, such as diabetes and cancer. More research is needed for these plant extracts to fully elucidate their bioactive phytochemicals and provide substantial evidence to build effective natural antidiabetic and antioxidant therapies. Considering their antioxidants, the leaf of *T. zeylanicum* have great promise as natural antioxidants in other industries. Further work in identifying and quantifying the specific antioxidant compounds from these extracts would give a wholesome insight into the application of these extracts. The distribution of phenolic content in this plant's root, stem and leaf indicates the potential for various uses. Hence, the highest value extracts from EA and ethanolic leaf extract promise the best for application as anti-diabetic, nutraceutical, pharmaceutical, and cosmetic holdings on antioxidant formulations. Both EA and ethanolic leaf extract would be most promising for extracts rich in phenolics for anti-diabetic, nutraceutical, pharmaceutical, and cosmetic applications.

However, the ethanol and EA leaf extracts showcased superior antioxidant activity and total phenolic content. Among the selected identified compounds docked against two enzyme markers for diabetes (α-amylase and α-glucosidase) and one protein for wound development (VEGFR2), ligand 1A (4-[2,6-Dihydroxy-4-(6,7,8-trihydroxy-2-naphthyl) phenoxy]-3-hydroxy-7-(3,4,5-trihydroxyphenyl) naphthalene-1,2-dione) from root EA extract of *T. zeylanicum* showed the superior binding affinities when docked against α-amylase (-11,0 kcal/mol), α-glucosidase (-10,2 kcal/mol), and VEGFR2 (-9,6 kcal/mol) in comparison with acarbose (positive control) for α-amylase (-7.4 kcal/mol) and α-glucosidase (-7.8 kcal/mol), and sorafenib (positive control) for VEGFR2 (-8.1 kcal/mol) as inhibitors (Table 3.10). The *in-silico* findings in this study demonstrated that EA root extract of *T. zeylanicum* contains phytochemicals with anti-diabetic, wound healing, and antioxidant potentials, suggesting that root of this plant can serve as sources of phytochemicals with antidiabetic and wound healing properties (Table 3.10).

The molecular networking displayed that VEGFR2 is not associated with the human pancreatic α-amylases (AMY2A and AMY2B) or intestinal α-glucosidase (GAA), which are functionally closely related to each other as they contribute to the metabolism of carbohydrates along with the interacting enzymes that cause T2DM. α-Amylase, α-glucosidase, and VEGFR2 were all shown to have totally conserved areas in multiple sequence alignment data, which may indicate their function in wound formation and carbohydrate digestion, as diabetic patients are known to develop wounds associated with cancer, inflammation and oxidative stress.

3.6. Recommendations for the future studies

LC-qTOF-MS chromatograms obtained from 2 mg/mL plant extract did not show all possible compounds in the extracts used in this study. From this study, increasing the concentration of *T. zeylanicum* plant organ extracts from 2 mg/mL to 10 mg/mL was limited due to the breakdown of LC-qTOF-MS that was encountered during the laboratory work. It is recommended for future studies to increase the concentration of plant extract to 10 mg/mL to detect all compounds in these plant extracts.

© University of Venda

In addition to the fact that no *in-vitro* α-amylase and α-glucosidase inhibitory activity investigation was conducted in this study, it is also recommended for future studies to conduct an *in-vitro* α-amylase and α-glucosidase inhibitory activity for EA and ethanol extracts from different organs of *T. zeylanicum* to validate their antidiabetic potentials and to confirm the results from the molecular docking further, to evaluate the compound to inhibit the enzyme α-amylase α-glucosidase which plays a key role in breaking down carbohydrates and is often done to assess potential anti-diabetic properties by determining if a substance can slow down the absorption of glucose from food, potentially helping to manage blood sugar levels in diabetic individuals. Following molecular docking research, molecular dynamic simulation (MD) is recommended to study the molecular docking results further. MD can reveal subtle interactions like hydrogen bonds, hydrophobic contacts, and conformational changes that may not be fully captured by docking alone. By simulating the complex over time, MD can identify if the docked pose is stable and if the ligand maintains favourable interactions with the protein, helping to validate the initial docking predictions.

MD simulations can provide insights into the dynamic nature of the binding site, including conformational changes in the protein that may occur upon ligand binding. By studying the molecular movements within the complex, MD can help predict potential off-target interactions and identify potential issues related to drug stability or binding kinetics. Since this study did not test for cytotoxicity, it is highly recommended that the cytotoxicity of EA and ethanol extracts from leaf, root, and stem of *T. zeylanicum* be studied using the *in vivo* models, including animal and cell culture. It is crucial to conduct cytotoxicity of plant extracts to create awareness concerning plant extract consumption or inhalation.

© University of Venda

Chapter 4

4. List of References

This chapter summarises the detailed description of the source of information credited to the author via a citation, avoiding plagiarism, giving supporting evidence for the study ideas, arguments, and opinions, and allowing identification of the sources utilised.

4.1. References

Abd Aziz, N.A., Hasham, R., Sarmidi, M.R., Suhaimi, S.H. and Idris, M.K.H., 2021. A review on extraction techniques and therapeutic value of polar bioactives from Asian medicinal herbs: Case study on Orthosiphon aristatus, Eurycoma longifolia and Andrographis paniculata. *Saudi Pharmaceutical Journal*, *29*(2), pp.143-165. https://doi.org/10.1016/j.jsps.2020.12.016

Abdelgawad, A.A., El-Bassossy, T.A. and Ahmed, F.A., 2021. A review on phytochemical, pharmacological and ethnopharmacological aspects of genus Trichodesma. *Indian Journal of Natural Products and Resources (IJNPR) [Formerly Natural Product Radiance (NPR)]*, *12*(3), pp.333-347. 10.56042/ijnpr.v12i3.41693

Adarsh, A., Chettiyar, B., Kanthesh, B. and Raghu, N., 2020. Phytochemical screening and antimicrobial activity of "Cinnamon zeylanicum." *Int. J. Pharm. Res. Innov*, *13*, pp.22-33. 10.13140/RG.2.2.33937.04962

Adelakun, O.E., Oyelade, O.J., Ade-Omowaye, B.I.O., Adeyemi, I.A. and Van de Venter, M., 2009. Chemical composition and the antioxidative properties of Nigerian Okra Seed (Abelmoschus esculentus Moench) Flour. *Food and Chemical Toxicology*, *47*(6), pp.1123-1126. https://doi.org/10.1016/j.fct.2009.01.036

Ademiluyi, A.O. and Oboh, G., 2013. Soybean phenolic-rich extracts inhibit key-enzymes linked to T2DM (α-amylase and α-glucosidase) and hypertension (angiotensin I converting enzyme) *in-vitro*. *Experimental and toxicologic pathology*, *65*(3), pp.305-309. https://doi.org/10.1016/j.etp.2011.09.005

Adhikari, B., 2021. Roles of alkaloids from medicinal plants in the management of diabetes mellitus. *Journal of Chemistry*, *2021*(1), p.2691525. https://doi.org/10.1155/2021/2691525

Agarwal, P. and Gupta, R., 2016. A-amylase inhibition can treat diabetes mellitus. *Res. Rev. J. Med. Health Sci*, *5*(4), pp.1-8. Available from: https://www.researchgate.net/publication/312294768

Ahmad, S., 2013. An Old Disease, A New Insights. 10.1007/978-1-4614-5441-0

Ahmed, A.M., 2002. History of diabetes mellitus. *Saudi medical journal*, *23*(4), pp.373-378. Available from: https://www.researchgate.net/publication/336666069

Alamgir, A.N.M. and Alamgir, A.N.M., 2018. Methods of Qualitative and Quantitative Analysis of Plant Constituents. *Therapeutic Use of Medicinal Plants and their Extracts: Volume 2: Phytochemistry and Bioactive Compounds*, pp.721-804. https://doi.org/10.1007/978-3-319-92387-1_9

© University of Venda

Ali, M., Miao, L., Soudy, F.A., Darwish, D.B.E., Alrdahe, S.S., Alshehri, D., Benedito, V.A., Tadege, M., Wang, X. and Zhao, J., 2022. Overexpression of terpenoid biosynthesis genes modifies root growth and nodulation in soybean (Glycine max). *Cells*, *11*(17), p.2622. https://doi.org/10.3390/cells11172622

Ali, S., Khan, M.R., Irfanullah, Sajid, M. and Zahra, Z., 2018. Phytochemical investigation and antimicrobial appraisal of Parrotiopsis jacquemontiana (Decne) Rehder. *BMC complementary and alternative medicine*, *18*, pp.1-15. https://doi.org/10.1186/s12906-018-2114-z

Al-Mansoori, L., Al-Jaber, H., Prince, M.S. and Elrayess, M.A., 2022. Role of inflammatory cytokines, growth factors and adipokines in adipogenesis and insulin resistance. *Inflammation*, pp.1-14. https://doi.org/10.1007/s10753-021-01559-z

Al-Sanea, M.M., Chilingaryan, G., Abelyan, N., Sargsyan, A., Hovhannisyan, S., Gasparyan, H., Gevorgyan, S., Albogami, S., Ghoneim, M.M., Farag, A.K. and Mohamed, A.A., 2021. Identification of novel potential VEGFR-2 inhibitors using a combination of computational methods for drug discovery. *Life*, *11*(10), p.1070. https://doi.org/10.3390/life11101070

Altemimi, A., Lakhssassi, N., Baharlouei, A., Watson, D.G. and Lightfoot, D.A., 2017. Phytochemicals: Extraction, isolation, and identification of bioactive compounds from plant extracts. *Plants*, *6*(4), p.42. https://doi.org/10.3390/plants6040042

Archana, P., Samatha, T., Mahitha, B., Chamundeswari, C. and Ramaswamy, N., 2012. Preliminary phytochemical screening from leaf and seed extracts of Senna alata L. Roxb-an ethnomedicinalplant. Available from: https://www.researchgate.net/publication/308802406

Arya, V., Thakur, N., and Kashyap, C.P., 2012. Preliminary phytochemical analysis of the extracts of Psidium leaf. *Journal of Pharmacognosy and Phytochemistry*, *1*(1), pp.01-05. Available from: www.phytojournal.com

Ayoola, G.A., Ipav, S.S., Sofidiya, M.O., Adepoju-Bello, A.A., Coker, H.A. and Odugbemi, T.O., 2008. Phytochemical screening and free radical scavenging activities of the fruits and leaf of Allanblackia floribunda Oliv (Guttiferae). *International Journal of Health Research*, *1*(2), pp.87-93. 10.4314/ijhr.v1i2.47920

Azevedo, M. and Alla, S., 2008. Diabetes in sub-saharan Africa: kenya, mali, mozambique, Nigeria, South Africa, and Zambia. *International Journal of Diabetes in Developing Countries*, *28*(4), p.101. 10.4103/0973-3930.45268

Baccari, W., Saidi, I., Filali, I., Znati, M., Lazrag, H., Tounsi, M., Marchal, A., Waffo-Teguo, P. and Jannet, H.B., 2024. Semi-synthesis, α-amylase inhibition, and kinetic and molecular docking studies of arylidene-based sesquiterpene coumarins isolated from Ferula tunetana Pomel ex Batt. *RSC advances*, *14*(7), pp.4654-4665. 10.1039/D3RA07540K

© University of Venda

Ballmer-Hofer, K., Andersson, A.E., Ratcliffe, L.E. and Berger, P., 2011. Neuropilin-1 promotes VEGFR-2 trafficking through Rab11 vesicles thereby specifying signal output. *Blood, The Journal of the American Society of Hematology*, *118*(3), pp.816-826. https://doi.org/10.1182/blood-2011-01-328773

Bang, F.S., Leeberg, V., Ding, M., and Dreyer, C.H., 2024. The effect of VEGF stimulation in diabetic foot ulcers: A systematic review. *Wound Repair and Regeneration*. https://doi.org/10.1111/wrr.13171

Bao, P., Kodra, A., Tomic-Canic, M., Golinko, M.S., Ehrlich, H.P. and Brem, H., 2009. The role of vascular endothelial growth factor in wound healing. *Journal of Surgical Research*, *153*(2), pp.347-358. https://doi.org/10.1016/j.jss.2008.04.023

Barkey, A.R.B., Hussein, S.A., Alm-Eldeen, A.A.E., Hafez, Y.A. and Mohamed, A.M., 2017. Saponins and their potential role in diabetes mellitus. Diabetes Manag. 7 (1): 148–158. Available from: https://www.researchgate.net/publication/314209242

Bate-Smith, E.C. and Westall, R.G., 1950. Chromatographic behaviour and chemical structure I. Some naturally occuring phenolic substances. *Biochimica et Biophysica Acta*, *4*, pp.427-440. https://doi.org/10.1016/0006-3002(50)90049-7

Behl, T., Gupta, A., Albratty, M., Najmi, A., Meraya, A.M., Alhazmi, H.A., Anwer, M.K., Bhatia, S., and Bungau, S.G., 2022. Alkaloidal phytoconstituents for diabetes management: exploring the unrevealed potential. *Molecules*, *27*(18), p.5851. https://doi.org/10.3390/molecules27185851

Biradar, S.R. and Rachetti, B.D., 2013. Extraction of some secondary metabolites & Thin-layer chromatography from different organs of Centella asiatica L. (URB). *American Journal of Life Sciences*, *1*(6), pp.243-247. 10.11648/j.ajls.20130106.11

Bliss, M., 1993. The history of insulin. *Diabetes Care*, *16*(Supplement_3), pp.4-7. https://doi.org/10.2337/diacare.16.3.4

Bréchot, N., Rutault, A., Marangon, I. and Germain, S., 2024, March. Blood endothelium transition and phenotypic plasticity: A key regulator of integrity/permeability in response to ischemia. In *Seminars in Cell & Developmental Biology* (Vol. 155, pp. 16-22). Academic Press. https://doi.org/10.1016/j.semcdb.2023.07.004

Brereton, M.F., Rohm, M., Shimomura, K., Holland, C., Tornovsky-Babeay, S., Dadon, D., Iberl, M., Chibalina, M.V., Lee, S., Glaser, B. and Dor, Y., 2016. Hyperglycaemia induces metabolic dysfunction and glycogen accumulation in pancreatic β-cells. *Nature communications*, *7*(1), p.13496. https://doi.org/10.1038/ncomms13496

© University of Venda

Bnyan, R., Khan, I., Ehtezazi, T., Saleem, I., Gordon, S., O'Neill, F. and Roberts, M., 2019. Formulation and optimisation of novel transfersomes for sustained release of local anaesthetic. *Journal of Pharmacy and Pharmacology*, *71*(10), pp.1508-1519. https://doi.org/10.1111/jphp.13149

Bondeva, T. and Wolf, G., 2015. Role of neuropilin-1 in diabetic nephropathy. *Journal of clinical medicine*, *4*(6), pp.1293-1311. https://doi.org/10.3390/jcm4061293

Boudreau, F., Rings, E.H., van Wering, H.M., Kim, R.K., Swain, G.P., Krasinski, S.D., Moffett, J., Grand, R.J., Suh, E.R. and Traber, P.G., 2002. Hepatocyte nuclear factor-1α, GATA-4, and caudal related homeodomain protein Cdx2 interact functionally to modulate intestinal gene transcription: Implication for the developmental regulation of the sucrase-isomaltase gene. *Journal of Biological Chemistry*, *277*(35), pp.31909-31917. https://doi.org/10.1074/jbc.M204622200

Buraczynska, M., Ksiazek, P., Baranowicz-Gaszczyk, I. and Jozwiak, L., 2007. Association of the VEGF gene polymorphism with diabetic retinopathy in T2DM patients. *Nephrology dialysis transplantation*, *22*(3), pp.827-832. https://doi.org/10.1093/ndt/gfl641

Calvo, P.M., Hernández, R.G., de la Cruz, R.R. and Pastor, A.M., 2022. VEGF is an essential retrograde trophic factor for motoneurons. *Proceedings of the National Academy of Sciences*, *119*(26), p.e2202912119. https://doi.org/10.1073/pnas.2202912119

Cao, Z., Liu, Y., Wang, Y. and Leng, P., 2023. Research progress on the role of PDGF/PDGFR in T2DM. *Biomedicine & Pharmacotherapy*, *164*, p.114983. https://doi.org/10.1016/j.biopha.2023.114983

Carvalho, J.F., Blank, M. and Shoenfeld, Y., 2007. Vascular endothelial growth factor (VEGF) in autoimmune diseases. *Journal of clinical immunology*, *27*(3), pp.246-256. https://doi.org/10.1007/s10875-007-9083-1

Chagas, M.D.S.S., Behrens, M.D., Moragas-Tellis, C.J., Penedo, G.X., Silva, A.R. and Gonçalves-de-Albuquerque, C.F., 2022. Flavonols and flavones as potential anti-inflammatory, antioxidant, and antibacterial compounds. *Oxidative medicine and cellular longevity*, *2022*(1), p.9966750. https://doi.org/10.1155/2022/9966750

Chen, S.Y., Wang, G.Y., Lin, J.H. and Yen, G.C., 2020. Antioxidant and anti-inflammatory activities and bioactive compounds of the leaf of Trichodesma khasianum clarke. *Industrial crops and products*, *151*, p.112447. https://doi.org/10.1016/j.indcrop.2020.112447

Chidambaram, A.R. and Aruna, A., 2013. Pharmacognostic study and development of quality parameters of whole plants of trichodesma indicum (Linn.) R. Br. *Asian Journal of Pharmaceutical and Clinical Research*, pp.167-169. Available from: https://www.researchgate.net/publication/289652343

© University of Venda

Chrzanowska, E., Denisow, B., Ekiert, H., and Pietrzyk, Ł., 2024. Metabolites Obtained from Boraginaceae Plants as Potential Cosmetic Ingredients—A Review. *Molecules*, *29*(21), p.5088. https://doi.org/10.3390/molecules29215088

Ch'ng, L.Z., Barakatun-Nisak, M.Y., Zukiman, W.Z.H.W., Abas, F., and Wahab, N.A., 2019. Nutritional strategies in managing postmeal glucose for T2DM: A narrative review. *Diabetes & Metabolic Syndrome: Clinical Research & Reviews*, *13*(4), pp.2339-2345. https://doi.org/10.1016/j.dsx.2019.05.026

Dai, Q., Fan, X., Meng, X., Sun, S., Su, Y., Ling, X., Chen, X., Wang, K., Dai, X., Zhang, C. and Da, S., 2021. FGF21 promotes ischaemic angiogenesis and endothelial progenitor cells function under diabetic conditions in an AMPK/NAD+-dependent manner. *Journal of Cellular and Molecular Medicine*, *25*(6), pp.3091-3102. https://doi.org/10.1111/jcmm.16369

Dallakyan, S. and Olson, A.J., 2015. Small-molecule library screening by docking with PyRx. In *Chemical Biology* (pp. 243-250). Humana Press, New York, NY. https://doi.org/10.1007/978-1-4939-2269-7_19

Daniel, A.E. and Van Buul, J.D., 2013. Endothelial junction regulation: a prerequisite for leukocytes crossing the vessel wall. *Journal of innate immunity*, *5*(4), pp.324-335. https://doi.org/10.1159/000348828

Das, B.K., Al-Amin, M.M., Russel, S.M., Kabir, S., Bhattacherjee, R. and Hannan, J.M.A., 2014. Phytochemical screening and evaluation of analgesic activity of Oroxylum indicum. *Indian journal of pharmaceutical sciences*, *76*(6), p.571. PMCID: PMC4293694

Das, S.K., Dash, S., Thatoi, H. and Patra, J.K., 2020. *In-vitro* α-amylase and α-glucosidase Inhibition, Antioxidant, Anti-Inflammatory Activity and GC-MS Profiling of Avicennia alba Blume. *Combinatorial Chemistry & High Throughput Screening*, *23*(9), pp.945-954. https://doi.org/10.2174/1386207323666200428081748

DeFronzo, R.A., 2004. Pathogenesis of T2DM mellitus. *Medical Clinics*, *88*(4), pp.787-835. 10.1016/j.mcna.2004.04.013

Del Río, J.C., Rencoret, J., Gutiérrez, A., Lan, W., Kim, H. and Ralph, J., 2021. Lignin monomers derived from the flavonoid and hydroxystilbene biosynthetic pathways. *Recent advances in polyphenol research*, *7*, pp.177-206. https://doi.org/10.1002/9781119545958.ch7

Didion, Y.P., Tjalsma, T.G., Su, Z., Malankowska, M. and Pinelo, M., 2023. What is next? the greener future of solid liquid extraction of biobased compounds: Novel techniques and solvents overpower traditional ones. *Separation and Purification Technology*, *320*, p.124147. https://doi.org/10.1016/j.seppur.2023.124147

Ding, Y.J., Li, G.Y., Xu, C.D., Wu, Y., Zhou, Z.S., Wang, S.G. and Li, C., 2020. Regulatory functions of Nilaparvata lugens GSK-3 in energy and chitin metabolism. *Frontiers in Physiology*, *11*, p.518876. https://doi.org/10.3389/fphys.2020.518876

© University of Venda

Dinh, T., Elder, S. and Veves, A., 2011. Delayed wound healing in diabetes: Considering future treatments. *Diabetes Management*, *1*(5), p.509. 10.2217/dmt.11.44

Dona, A.C., Pages, G., Gilbert, R.G., and Kuchel, P.W., 2010. Digestion of starch: In vivo and *in-vitro* kinetic models used to characterise oligosaccharide or glucose release. *Carbohydrate Polymers*, *80*(3), pp.599-617. https://doi.org/10.1016/j.carbpol.2010.01.002

Dowarah, J. and Singh, V.P., 2020. Anti-diabetic drugs recent approaches and advancements. *Bioorganic & Medicinal Chemistry*, *28*(5), p.115263. https://doi.org/10.1016/j.bmc.2019.115263

Dührkop, K., Hufsky, F. and Böcker, S., 2014. Molecular formula identification using isotope pattern analysis and calculation of fragmentation trees. *Mass Spectrometry*, *3*(Special_Issue_2), pp. S0037-S0037. https://doi.org/10.5702/massspectrometry.S0037

Dührkop, K., Shen, H., Meusel, M., Rousu, J. and Böcker, S., 2015. Searching molecular structure databases with tandem mass spectra using CSI: FingerID. *Proceedings of the National Academy of Sciences*, *112*(41), pp.12580-12585. https://doi.org/10.1073/pnas.1509788112

DüZGüNES, N., 2003. Preparation and quantitation of small unilamellar liposomes and large unilamellar reverse-phase evaporation liposomes. *Methods in Enzymology*, *367*, pp.23-27. https://doi.org/10.1016/S0076-6879(03)67003-5

El Barky, A.R., Hussein, S.A., Alm-Eldeen, A.E., Hafez, Y.A. and Mohamed, T.M., 2017. Saponins and their potential role in diabetes mellitus. *Diabetes Manag*, *7*(1), pp.148-58. Available from: https://www.researchgate.net/publication/31420924

Florek, K., Mendyka, D. and Gomułka, K., 2024. Vascular Endothelial Growth Factor (VEGF) and Its Role in the Cardiovascular System. *Biomedicines*, *12*(5), p.1055. https://doi.org/10.3390/biomedicines12051055

Flores-Morales, V., Villasana-Ruíz, A.P., Garza-Veloz, I., González-Delgado, S., and Martinez-Fierro, M.L., 2023. Therapeutic effects of coumarins with different substitution patterns. *Molecules*, *28*(5), p.2413. https://doi.org/10.3390/molecules28052413

Gălbău, C.Ş., Irimie, M., Neculau, A.E., Dima, L., Pogačnik da Silva, L., Vârciu, M. and Badea, M., 2024. The Potential of Plant Extracts Used in Cosmetic Product Applications—Antioxidants Delivery and Mechanism of Actions. *Antioxidants*, *13*(11), p.1425. https://doi.org/10.3390/antiox13111425

Galiano, R.D., Tepper, O.M., Pelo, C.R., Bhatt, K.A., Callaghan, M., Bastidas, N., Bunting, S., Steinmetz, H.G. and Gurtner, G.C., 2004. Topical vascular endothelial growth factor accelerates diabetic wound healing through increased angiogenesis and by mobilizing and recruiting bone marrow-derived cells. *The American Journal of Pathology*, *164*(6), pp.1935-1947. https://doi.org/10.1016/S0002-9440(10)63754-6

© University of Venda

Gelfand, M.V., Hagan, N., Tata, A., Oh, W.J., Lacoste, B., Kang, K.T., Kopycinska, J., Bischoff, J., Wang, J.H. and Gu, C., 2014. Neuropilin-1 functions as a VEGFR2 co-receptor to guide developmental angiogenesis independent of ligand binding. *Elife*, *3*, p.e03720. https://doi.org/10.7554/eLife.03720

Greenhalgh, D.G., 2003. Wound healing and diabetes mellitus. *Clinics in Plastic Surgery*, *30*(1), pp.37-45. 10.1016/S0094-1298(02)00066-4

Ghafoor, K., Al Juhaimi, F., Özcan, M.M., Uslu, N., Babiker, E.E. and Ahmed, I.A.M., 2020. Total phenolics, total carotenoids, individual phenolics and antioxidant activity of ginger (Zingiber officinale) rhizome as affected by drying methods. *Lwt*, *126*, p.109354. https://doi.org/10.1016/j.lwt.2020.109354

Ghasemzadeh, A., Karbalaii, M.T., Jaafar, H.Z. and Rahmat, A., 2018. Phytochemical constituents, antioxidant activity, and antiproliferative properties of black, red, and brown rice bran. *Chemistry Central Journal*, *12*, pp.1-13. https://doi.org/10.1186/s13065-018-0382-9

Gujjeti, R.P. and Mamidala, E., 2013. Phytochemical screening and Thin-layer chromatographic studies of Aerva lanata root extract. *International Journal of Innovative Research in Science, Engineering and Technology*, *2*(10), pp.5725-5730. https://www.researchgate.net/publication/273693627

Gulcin, İ. and Alwasel, S.H., 2023. DPPH radical scavenging assay. *Processes*, *11*(8), p.2248. https://doi.org/10.3390/pr11082248

Gurib-Fakim, A., Gueho, J. and Sewraj-Bissoondoyal, M., 1997. The medicinal plants of Mauritius–part 1. *International Journal of Pharmacognosy*, *35*(4), pp.237-254. https://doi.org/10.1076/phbi.35.4.237.13313

Haller, M.J., Atkinson, M.A. and Schatz, D., 2005. Type 1 diabetes mellitus: etiology, presentation, and management. *Pediatric Clinics*, *52*(6), pp.1553-1578. 10.1016/j.pcl.2005.07.006

Hamissou, M., Smith, A.C., Carter Jr, R.E. and Triplett II, J.K., 2013. Antioxidative properties of bitter gourd (Momordica charantia) and zucchini (Cucurbita pepo). *Emirate Journal of Food Agriculture*, 25(9):641-647. https://doi.org/10.9755/ejfa.v25i9.15978

Hecking, I., Stegemann, L.N., Theis, V., Vorgerd, M., Matschke, V., Stahlke, S. and Theiss, C., 2022. Neuroprotective effects of VEGF in the enteric nervous system. *International Journal of Molecular Sciences*, *23*(12), p.6756. https://doi.org/10.3390/ijms23126756

Heinonen, M., Shen, H., Zamboni, N. and Rousu, J., 2012. Metabolite identification and molecular fingerprint prediction through machine learning. *Bioinformatics*, *28*(18), pp.2333-2341. https://doi.org/10.1093/bioinformatics/bts437

Hofmann, T., Schölkopf, B. and Smola, A.J., 2008. Kernel methods in machine learning. Ann. Statist. 36 (3) 1171 - 1220. https://doi.org/10.1214/009053607000000677

© University of Venda

Holmes, K., Roberts, O.L., Thomas, A.M., and Cross, M.J., 2007. Vascular endothelial growth factor receptor 2: structure, function, intracellular signalling, and therapeutic inhibition. *Cellular Signalling*, *19*(10), pp.2003-2012. https://doi.org/10.1016/j.cellsig.2007.01.640

Hsieh, S.H., Ying, N.W., Wu, M.H., Chiang, W.F., Hsu, C.L., Wong, T.Y., Jin, Y.T., Hong, T.M. and Chen, Y.L., 2008. Galectin-1, a novel ligand of neuropilin-1, activates VEGFR-2 signaling and modulates the migration of vascular endothelial cells. *Oncogene*, *27*(26), pp.3746-3753. https://doi.org/10.1038/sj.onc.1211029

Hyde, M.A., Wursten, B.T. and Ballings, P., 2013. Flora of Zimbabwe: Location Details: Mukuvisi Woodland.

Hyde, M.A., Wursten, B.T. and Ballings, P., 2013. Flora of Zimbabwe: Species information: Kirkia acuminata.

Ibrahim, S.R., Mohamed, G.A., Abdel-Latif, M.M., El-Messery, S.M., Al Musayeib, N.M., and Shehata, I.A., 2015. Minutaside A, new α-amylase inhibitor flavonol glucoside from Tagetes minuta: Antidiabetic, antioxidant, and molecular modeling studies. *Starch-Stärke*, *67*(11-12), pp.976-984. https://doi.org/10.1002/star.201500068

Iqbal, E., Salim, K.A. and Lim, L.B., 2015. Phytochemical screening, total phenolics and antioxidant activities of bark and leaf extracts of Goniothalamus velutinus (Airy Shaw) from Brunei Darussalam. *Journal of King Saud University-Science*, *27*(3), pp.224-232. https://doi.org/10.1016/j.jksus.2015.02.003

Joshi, B., Pandya, D. and Mankad, A., 2018. Comparative study of phytochemical screening and antibacterial activity of Curcuma longa (L.) and Curcuma aromatica (Salib.). *J. Med. Plants*, *6*, pp.145-148. Available from: https://www.researchgate.net/publication/351512673

Kabrun, N., Buhring, H.J., Choi, K., Ullrich, A., Risau, W. and Keller, G., 1990. Flk-1 expression defines a population of early embryonic hematopoietic precursors. *Development*, *124*(10), pp.2039-2048. https://doi.org/10.1242/dev.124.10.2039

Kahn, C.R., 1994. Insulin action, diabetogenes, and the cause of type II diabetes. *Diabetes*, *43*(8), pp.1066-1085. https://doi.org/10.2337/diab.43.8.1066

Kahwaji, S. and White, M.A., 2021. Organic phase change materials for thermal energy storage: influence of molecular structure on properties. *Molecules*, *26*(21), p.6635. https://doi.org/10.3390/molecules26216635

Kajal, K., Panda, A.K., Bhat, J., Chakraborty, D., Bose, S., Bhattacharjee, P., Sarkar, T., Chatterjee, S., Kar, S.K. and Sa, G., 2019. Andrographolide binds to ATP-binding pocket of VEGFR2 to impede VEGFA-mediated tumor-angiogenesis. *Scientific Reports*, *9*(1), p.4073. https://doi.org/10.1038/s41598-019-40626-2

© University of Venda

Kalpoutzakis, E., Chatzimitakos, T., Athanasiadis, V., Mitakou, S., Aligiannis, N., Bozinou, E., Gortzi, O., Skaltsounis, L.A. and Lalas, S.I., 2023. Determination of the total phenolics content and antioxidant activity of extracts from organs of plants from the Greek Island of Crete. *Plants*, *12*(5), p.1092. https://doi.org/10.3390/plants12051092

Kancherla, N., Dhakshinamoothi, A., Chitra, K. and Komaram, R.B., 2019. Preliminary analysis of phytoconstituents and evaluation of anthelminthic property of Cayratia auriculata (*in-vitro*). *Maedica*, *14*(4), p.350. 10.26574/maedica.2019.14.4.350

Kang, D., Pang, X., Lian, W., Xu, L., Wang, J., Jia, H., Zhang, B., Liu, A.L. and Du, G.H., 2018. Discovery of VEGFR2 inhibitors by integrating naïve Bayesian classification, molecular docking, and drug screening approaches. *RSC Advances*, *8*(10), pp.5286-5297. 10.1039/C7RA12259D

Karvonen, M., Pitkäniemi, M., Pitkäniemi, J., Kohtamäki, K., Tajima, N. and Tuomilehto, J., 1997. Sex difference in the incidence of insulin-dependent diabetes mellitus: an analysis of the recent epidemiological data. *Diabetes/Metabolism Reviews*, *13*(4), pp.275-291. https://doi.org/10.1002/(SICI)1099-0895(199712)13:4≤275::AID-DMR197>3.0.CO;2-V

Katsarou, A., Gudbjörnsdottir, S., Rawshani, A., Dabelea, D., Bonifacio, E., Anderson, B.J., Jacobsen, L.M., Schatz, D.A., and Lernmark, Å., 2017. Type 1 diabetes mellitus. *Nature Reviews Disease primers*, *3*(1), pp.1-17. https://doi.org/10.1038/nrdp.2017.16

Kazeem, M.I., Ogunbiyi, J.V. and Ashafa, A.O., 2013. *In-vitro* studies on the inhibition of α-amylase and α-glucosidase by leaf extracts of Picralima nitida (Stapf). *Tropical Journal of Pharmaceutical Research*, *12*(5), pp.719-725. https://doi.org/10.4314/tjpr.v12i5.9

Kerbel, R. and Folkman, J., 2002. Clinical translation of angiogenesis inhibitors. *Nature Reviews Cancer*, *2*(10), pp.727-739. https://doi.org/10.1038/nrc905

Khanam, Z., Wen, C.S. and Bhat, I.U.H., 2015. Phytochemical screening and antimicrobial activity of root and stem extracts of wild Eurycoma longifolia Jack (Tongkat Ali). *Journal of King Saud University-Science*, *27*(1), pp.23-30. https://doi.org/10.1016/j.jksus.2014.04.006

Kim, S., Chen, J., Cheng, T., Gindulyte, A., He, J., He, S., Li, Q., Shoemaker, B.A., Thiessen, P.A., Yu, B. and Zaslavsky, L., 2021. PubChem in 2021: new data content and improved web interfaces. *Nucleic Acids Research*, *49*(D1), pp. D1388-D1395. https://doi.org/10.1093/nar/gkaa971

Koffi, E., Sea, T., Dodehe, Y. and Soro, S., 2010. Effect of solvent type on extraction of polyphenols from twenty-three Ivorian plants. Available from: https://www.researchgate.net/publication/313163469

Kofler, N.M. and Simons, M., 2015. Angiogenesis versus arteriogenesis: neuropilin 1 modulation of VEGF signaling. *F1000prime reports*, *7*. 10.12703/P7-26

© University of Venda

Kumar, A., P, N., Kumar, M., Jose, A., Tomer, V., Oz, E., Proestos, C., Zeng, M., Elobeid, T., K, S. and Oz, F., 2023. Major phytochemicals: recent advances in health benefits and extraction method. *Molecules*, *28*(2), p.887. https://doi.org/10.3390/molecules28020887

Kumar, B., Vijayakumar, M., Govindarajan, R. and Pushpangadan, P., 2007. Ethnopharmacological approaches to wound healing—exploring medicinal plants of India. *Journal of Ethnopharmacology*, *114*(2), pp.103-113. https://doi.org/10.1016/j.jep.2007.08.010

Kumar, N. and Goel, N., 2019. Phenolic acids: Natural versatile molecules with promising therapeutic applications. *Biotechnology reports*, *24*, p.e00370. https://doi.org/10.1016/j.btre.2019.e00370

Larionov, A., Hammer, C.M., Fiedler, K. and Filgueira, L., 2024. Dynamics of Endothelial Cell Diversity and Plasticity in Health and Disease. *Cells*, *13*(15), p.1276. https://doi.org/10.3390/cells13151276

Lefebvre, T., Destandau, E. and Lesellier, E., 2021. Selective extraction of bioactive compounds from plants using recent extraction techniques: A review. *Journal of Chromatography A*, *1635*, p.461770. https://doi.org/10.1016/j.chroma.2020.461770

Le Thi, V.A., Nguyen, N.L., Nguyen, Q.H., Van Dong, Q., Do, T.Y. and Nguyen T, K.O., 2021. Phytochemical Screening and Potential Antibacterial Activity of Defatted and Nondefatted Methanolic Extracts of Xao Tam Phan (Paramignya trimera (Oliv.) Guillaum) Peels against Multidrug-Resistant Bacteria. *Scientifica*, *2021*(1), p.4233615. https://doi.org/10.1155/2021/4233615

Lezoul, N.E.H., Belkadi, M., Habibi, F. and Guillén, F., 2020. Extraction processes with several solvents on total bioactive compounds in different organs of three medicinal plants. *Molecules*, *25*(20), p.4672. https://doi.org/10.3390/molecules25204672

Li, H., Wang, R., Xu, P., Yuan, C., Huang, M. and Jiang, L., 2024. Elucidating the molecular basis of PECAM-1 and Tie2 interaction from binding dynamics and complex formation. *Biochemical and Biophysical Research Communications*, *735*, p.150484. https://doi.org/10.1016/j.bbrc.2024.150484

Li, M., Chi, X., Wang, Y., Setrerrahmane, S., Xie, W. and Xu, H., 2022. Trends in insulin resistance: insights into mechanisms and therapeutic strategy. *Signal transduction and targeted therapy*, *7*(1), p.216. https://doi.org/10.1038/s41392-022-01073-0

Liu, T., Zhang, J., Chang, F., Sun, M., He, J. and Ai, D., 2024. Role of endothelial Raptor in abnormal arteriogenesis after lower limb ischaemia in T2DM. *Cardiovascular Research*, *120*(10), pp.1218-1234. https://doi.org/10.1093/cvr/cvae105

Llavero, F. and Zugaza, J.L., 2024. The importance of muscle glycogen phosphorylase in glial cells function. *Biochemical Society Transactions*, p. BST20231058. https://doi.org/10.1042/BST20231058

© University of Venda

Makati, A.C., Ananda, A.N., Putri, J.A., Amellia, S.F. and Setiawan, B., 2022. Molecular docking of ethanol extracts of katuk leaf (Sauropus androgynus) on functional proteins of severe acute respiratory syndrome coronavirus 2. *South African Journal of Botany*, *149*, pp.1-5. https://doi.org/10.1016/j.sajb.2022.04.044

Málaga, D.R., Brusius-Facchin, A.C., Michelin-Tirelli, K., Félix, T.M., Schulte, J., Pereira, J., Neto, E.C., Filho, C.S. and Giugliani, R., 2017. Pseudo deficiency of intestinal α-glucosidase: a challenge in the newborn screening for Pompediseases. *Genet. Mol. Res.*, *16*, p.16039844. http://dx.doi.org/10.4238/gmr16039844

Malik, S., Brudzyńska, P., Khan, M.R., Sytar, O., Makhzoum, A. and Sionkowska, A., 2023. Natural plant-derived compounds in food and cosmetics: A paradigm of shikonin and its derivatives. *Materials*, *16*(12), p.4377. https://doi.org/10.3390/ma16124377

Matsumoto, K. and Yokoyama, S.I., 2012. Induction of uncoupling protein-1 and-3 in brown adipose tissue by kaki-tannin in type 2 diabetic NSY/Hos mice. *Food and chemical toxicology*, *50*(2), pp.184-190. https://doi.org/10.1016/j.fct.2011.10.067

Mazhar, M., Afzal, M. and Naveed, M., 2022. Phytochemical Profiling, Biological Activities, and *In-silico* Virtual Screening of Bioactive Compounds of Trichodesma Indicum (L) R. Br. Extracts. *ChemistrySelect*, *7*(46), p.e202203821. https://doi.org/10.1002/slct.202203821

Mekonnen, A., Atlabachew, M. and Kassie, B., 2018. Investigation of antioxidant and antimicrobial activities of Euclea schimperi leaf extracts. *Chemical and Biological Technologies in Agriculture*, *5*, pp.1-12. https://doi.org/10.1186/s40538-018-0128-x

Mehraban, M.H., Motovali-Bashi, M. and Ghasemi, Y., 2019. MiR-26a and miR-26b downregulate the expression of sucrase-isomaltase enzyme: a new chapter in diabetes treatment. *Biochemical and Biophysical Research Communications*, *519*(1), pp.192-197. https://doi.org/10.1016/j.bbrc.2019.08.138

Metwally, N.S., Mohamed, A.M. and ELSharabasy, F.S., 2012. Chemical constituents of the Egyptian Plant Anabasis articulata (Forssk) Moq and its antidiabetic effects on rats with streptozotocin-induced diabetic hepatopathy. *Journal of Applied Pharmaceutical Science*, (Issue), pp.54-65. https://dx.doi.org/10.7324/JAPS.2012.2403

Migocka-Patrzałek, M. and Elias, M., 2021. Muscle glycogen phosphorylase and its functional partners in health and disease. *Cells*, *10*(4), p.883. https://doi.org/10.3390/cells10040883

Miller, G.L., 1959. Use of dinitrosalicylic acid reagent for determination of reducing sugar. *Analytical Chemistry*, *31*(3), pp.426-428. https://doi.org/10.1021/ac60147a030

Modi, S.J. and Kulkarni, V.M., 2019. Vascular endothelial growth factor receptor (VEGFR-2)/KDR inhibitors: medicinal chemistry perspective. *Medicine in Drug Discovery*, *2*, p.100009. https://doi.org/10.1016/j.medidd.2019.100009

© University of Venda

Mohamed, J., Nafizah, A.N., Zariyantey, A.H. and Budin, S., 2016. Mechanisms of diabetes-induced liver damage: the role of oxidative stress and inflammation. *Sultan Qaboos University Medical Journal*, *16*(2), p.e132. 10.18295/squmj.2016.16.02.002

Morris, G.M., Huey, R., Lindstrom, W., Sanner, M.F., Belew, R.K., Goodsell, D.S. and Olson, A.J., 2009. AutoDock4 and AutoDockTools4: Automated docking with selective receptor flexibility. *Journal of Computational Chemistry*, *30*(16), pp.2785-2791. https://doi.org/10.1002/jcc.21256

Mosti, S. and Selvi, F., 2007. Trichodesma cinereum Mosti & Selvi (Boraginaceae), a new species from Oman. *Candollea*, *62*(2), pp.205-210. Available from: https://www.researchgate.net/publication/290749389

Muzila, A., Msagati, T.A., Abegaz, B. and Nindi, M.M., 2010. Characterization of Geshodin-metal complexation by electrospray-mass spectrometry. In *11th NAPRECA Symposium, Book of Proceedings* (pp. 35-44).

Mwambyale, T., 2021. Phytochemical, antioxidant activity and toxicity evaluation of medicinal plants commonly used for asthma management in Malawi (Doctoral dissertation, Kamuzu University of Health Sciences). http://nkhokwe.kuhes.ac.mw/handle/20.500.12845/652

Nada, A.A., Metwally, A.M., Asaad, A.M., Celik, I., Ibrahim, R.S. and Eldin, S.M.S., 2024. Synergistic effect of potential α-amylase inhibitors from Egyptian propolis with acarbose using *in-silico* and *in-vitro* combination analysis. *BMC Complementary Medicine and Therapies*, *24*(1), p.65. https://doi.org/10.1186/s12906-024-04348-x

Narendra, K., Joshi, D.S., Prasad, M.S., Reddi, K.R., Swathi, J., Sowjanya, K.M. and Satya, A.K., 2015. *In-vitro* and in vivo anti-inflammatory efficiency of *Trichodesma indicum* (l.) Leaf extracts. *Journal of Pharmaceutical and Scientific Innovation*, *4*(6), pp.319-323. 10.7897/2277-4572.04670

Ngonda, F., 2013. In-vitro Antioxidant Activity and Free Radical Scavenging Potential of root of Malawian Trichodesma zeylanicumm (burm. f.). *Asian Journal of Biomedical and Pharmaceutical Sciences*, *3*(20), p.21. https://doi.org/10.15272/AJBPS.V3I20.266

Ngonda, F., 2014. Evaluation of the wound healing potential of Trichodesma zeylanicum (Burm. f.) formulation in excision wounds in albino rats. *Annual Research & Review in Biology*, pp.828-839. https://doi.org/10.9734/ARRB/2014/6741

Nguyen, N.M.P., Le, T.T., Vissenaekens, H., Gonzales, G.B., Van Camp, J., Smagghe, G. and Raes, K., 2019. *In-vitro* antioxidant activity and phenolic profiles of tropical fruit by-products. *International Journal of Food Science & Technology*, *54*(4), pp.1169-1178. https://doi.org/10.1111/ijfs.14093

© University of Venda

Oboh, G., Ogunsuyi, O.B., Ogunbadejo, M.D. and Adefegha, S.A., 2016. Influence of gallic acid on α-amylase and α-glucosidase inhibitory properties of acarbose. *Journal of Food and Drug Analysis*, *24*(3), pp.627-634. https://doi.org/10.1016/j.jfda.2016.03.003

Oishi, Y., Sakamoto, T., Udagawa, H., Taniguchi, H., Kobayashi-Hattori, K., Ozawa, Y. and Takita, T., 2007. Inhibition of increases in blood glucose and serum neutral fat by Momordica charantia saponin fraction. *Bioscience, biotechnology, and biochemistry*, *71*(3), pp.735-740. https://doi.org/10.1271/bbb.60570

Olokoba, A.B., Obateru, O.A. and Olokoba, L.B., 2012. T2DM mellitus: a review of current trends. *Oman Medical Journal*, *27*(4), p.269. 10.5001/omj.2012.68

Ornitz, D.M. and Itoh, N., 2015. The fibroblast growth factor signaling pathway. *Wiley Interdisciplinary Reviews: Developmental Biology*, *4*(3), pp.215-266. https://doi.org/10.1002/wdev.176

Oyedemi, S.O., Bradley, G., and Afolayan, A.J., 2010. In-vitro and-vivo antioxidant activities of aqueous extract of Strychnos henningsii Gilg. *Afr J Pharm Pharmacol*, *4*(2), pp.70-78. https://doi.org/10.5897/AJPP.9000176

O'Kelly, J. and Sargeant, K., 1961. Supinine from seeds of trichodesma zeylanicum, RBR. *Journal of the Chemical Society*, (JAN), p.484.

Ozioma, E.O.J. and Chinwe, O.A.N., 2019. Herbal medicines in African traditional medicine. *Herbal medicine*, *10*, pp.191-214. https://doi.org/10.5772/INTECHOPEN.80348

Panara, A., Aalizadeh, R. and Thomaidis, N.S., 2022. Chemical characterisation of Pelargonium sidoides root based on LC-QToF-MS non-target screening strategies. *Phytochemical Analysis*, *33*(1), pp.40-56. https://doi.org/10.1002/pca.3059

Pandey, A. and Tripathi, S., 2014. Concept of standardization, extraction and pre phytochemical screening strategies for herbal drug. *Journal of Pharmacognosy and Phytochemistry*, *2*(5), pp.115-119. https://api.semanticscholar.org/CorpusID:29496193

Paschou, S.A., Papadopoulou-Marketou, N., Chrousos, G.P. and Kanaka-Gantenbein, C., 2018. On type 1 diabetes mellitus pathogenesis. *Endocrine Connections*, *7*(1), pp. R38-R46. https://doi.org/10.1530/EC-17-0347

Patlak, M., 2002. New weapons to combat an ancient disease: treating diabetes. *The FASEB Journal*, *16*(14), pp.1853e-1853e. http://dx.doi.org/10.1096/fasebj.16.14.1853e

Petterson, C.C., Dahlquist, G.G., Gyürüs, E., Green, A. and Soltész, G., 2009. Incidence trends for childhood type 1 diabetes in Europe during 1989–2003 and predicted new cases 2005–20: a multicentre prospective registration study. *The Lancet*, *373*(9680), pp.2027-2033. 10.1016/S0140-6736(09)60568-7

© University of Venda

Peyrot des Gachons, C. and Breslin, P.A., 2016. Salivary amylase: digestion and metabolic syndrome. *Current Diabetes Reports*, *16*(10), pp.1-7. https://doi.org/10.1007/s11892-016-0794-7

Pooja, S. and Vidyasagar, G.M., 2016. Phytochemical screening for secondary metabolites of Opuntia dillenii Haw. *Journal of Medicinal Plants Studies*, *4*(5), pp.39-43. https://api.semanticscholar.org/CorpusID:217960657

Prabhakar, P.K. and Batiha, G.E.S., 2024. Potential Therapeutic Targets for the management of Diabetes Mellitus Type 2. *Current Medicinal Chemistry*, *31*(21), pp.3167-3181. https://doi.org/10.2174/0929867330666230501172557

Radzuan, S.N.M., Phongphane, L., Bakar, M.H.A., Omar, M.T.C., Shahril, N.S.N., Supratman, U., Harneti, D., Wahab, H.A. and Azmi, M.N., 2024. Synthesis, biological activities, and evaluation molecular docking-dynamics studies of new phenylisoxazole quinoxalin-2-amine hybrids as potential α-amylase and α-glucosidase inhibitors. *RSC advances*, *14*(11), pp.7684-7698. 10.1039/D3RA08642A

Rai, S., Acharya-Siwakoti, E., Kafle, A., Devkota, H.P. and Bhattarai, A., 2021. Plant-derived saponins: a review of their surfactant properties and applications. *Sci*, *3*(4), p.44. https://doi.org/10.3390/sci3040044

Raimondi, C., 2014. Neuropilin-1 enforces extracellular matrix signalling via ABL1 to promote angiogenesis. *Biochemical Society Transactions*, *42*(5), pp.1429-1434. https://doi.org/10.1042/BST20140141

Ramabulana, A.T., Petras, D., Madala, N.E. and Tugizimana, F., 2021. Metabolomics and molecular networking to characterize the chemical space of four Momordica plant species. *Metabolites*, *11*(11), p.763. https://doi.org/10.3390/metabo11110763

Ranđelović, S. and Bipat, R., 2021. A review of coumarins and coumarin-related compounds for their potential antidiabetic effect. *Clinical Medicine Insights: Endocrinology and Diabetes*, *14*, p.11795514211042023. https://doi.org/10.1177/11795514211042023

Re, R., Pellegrini, N., Proteggente, A., Pannala, A., Yang, M. and Rice-Evans, C., 1999. Antioxidant activity applying an improved ABTS radical cation decolourization assay. *Free Radical Biology and Medicine*, *26*(9-10), pp.1231-1237. https://doi.org/10.1016/S0891-5849(98)00315-3

Ren, L., Cao, X., Geng, P., Bai, F. and Bai, G., 2011. Study of the inhibition of two human maltase-glucoamylases catalytic domains by different α-glucosidase inhibitors. *Carbohydrate research*, *346*(17), pp.2688-2692. https://doi.org/10.1016/j.carres.2011.09.012

Ren, L., Qin, X., Cao, X., Wang, L., Bai, F., Bai, G. and Shen, Y., 2011. Structural insight into substrate specificity of human intestinal maltase-glucoamylase. *Protein & cell*, *2*, pp.827-836. https://doi.org/10.1007/s13238-011-1105-3

© University of Venda

Retief, E., 2002. The genus Trichodesma (Boraginaceae: Boraginoideae) in southern Africa. *Bothalia*, *32*(2), pp.151-166. https://doi.org/10.4102/abc.v32i2.479

Ripsin, C.M., Kang, H. and Urban, R.J., 2009. Management of blood glucose in T2DM mellitus. *American Family Physician*, *79*(1), pp.29-36. https://api.semanticscholar.org/CorpusID:13444258

Robertson, R.P., 1995. Antagonist: diabetes and insulin resistance--philosophy, science, and the multiplier hypothesis. *Journal of Laboratory and Clinical Medicine*, *125*(5), pp.560-564. https://api.semanticscholar.org/CorpusID:28904021

Ruszkowska, B., Koprowska, E., Rość, D., Pater, A. and Odrowąż-Sypniewska, G., 2010. The role of VEGF in T2DM. *Medical and Biological Sciences*, *2*, p.13. https://doi.org/10.1038/eye.2010.86

Saboo, S.S., Tapadiya, G.G. and Khadabadi, S.S., 2013. Antimicrobial potential of tropical plant Trichodesma indicum and Trichodesma sedgwickianum. *Research Journal of Microbiology*, *8*(1), p.63. https://scialert.net/abstract/?doi=jm.2013.63.69

Saboo, S.S., Tapadiya, G.G., Lamale, J.J. and Khadabadi, S.S., 2014. Phytochemical screening and antioxidant, antimitotic, and antiproliferative activities of Trichodesma indicum shoot. *Ancient Science of Life*, *34*(2), pp.113-118. https://doi.org/10.4103/0257-7941.153480

Sales, P.M., Souza, P.M., Simeoni, L.A., Magalhães, P.O. and Silveira, D., 2012. α-Amylase inhibitors: a review of raw material and isolated compounds from plant source. *Journal of Pharmacy & Pharmaceutical Sciences*, *15*(1), pp.141-183. https://doi.org/10.18433/j35s3k

Salimi, A., Lim, J.H., Jang, J.H. and Lee, J.Y., 2022. The use of machine learning modeling, virtual screening, molecular docking, and molecular dynamics simulations to identify potential VEGFR2 kinase inhibitors. *Scientific Reports*, *12*(1), p.18825. https://doi.org/10.1038/s41598-022-22992-6

Sarabipour, S., Kinghorn, K., Quigley, K.M., Kovacs-Kasa, A., Annex, B.H., Bautch, V.L. and Mac Gabhann, F., 2024. Impact of ligand binding on VEGFR1, VEGFR2, and NRP1 localization in human endothelial cells. *bioRxiv*, pp.2024-09. https://doi.org/10.1101/2024.09.29.615728

Shandukani, P.D., Tshidino, S.C., Masoko, P. and Moganedi, K.M., 2018. Antibacterial activity and in situ efficacy of Bidens pilosa Linn and Dichrostachys cinerea Wight et Arn extracts against common diarrhoea-causing waterborne bacteria. *BMC complementary and alternative medicine*, *18*(1), pp.1-10. https://doi.org/10.1186/s12906-018-2230-9

Sharma, R.A., Singh, B., Singh, D. and Chandrawat, P., 2009. Ethnomedicinal, pharmacological properties and chemistry of some medicinal plants of Boraginaceae in India. *J Med Plant Res*, *3*(13), pp.1153-75. https://api.semanticscholar.org/CorpusID:86642059

© University of Venda

Sharma, S., Ehrlich, M., Zhang, M., Blobe, G.C. and Henis, Y.I., 2024. NRP1 interacts with endoglin and VEGFR2 to modulate VEGF signaling and endothelial cell sprouting. *Communications Biology*, *7*(1), p.112. https://doi.org/10.1038/s42003-024-05798-2

Shen, H., Dührkop, K., Böcker, S. and Rousu, J., 2014. Metabolite identification through multiple kernels learning on fragmentation trees. *Bioinformatics*, *30*(12), pp. i157-i164. https://doi.org/10.1093/bioinformatics/btu275

Sieniawska, E., 2015. Activities of tannins–from *in-vitro* studies to clinical trials. *Natural Product Communications*, *10*(11), p.1934578X1501001118. https://doi.org/10.1177/1934578X1501001118

Silva, D.R., Aguiar, G., Luís, C., Soares, R. and Coelho, P., 2024. Vascular Dysfunction in Adipose Tissue: Its Impact on T2DM and Cancer. *Revista Portuguesa de Diabetes*, *19*(2), pp.53-59.

Sim, L., Jayakanthan, K., Mohan, S., Nasi, R., Johnston, B.D., Pinto, B.M. and Rose, D.R., 2010. New glucosidase inhibitors from an ayurvedic herbal treatment for T2DM: structures and inhibition of human intestinal maltase-glucoamylase with compounds from Salacia reticulata. *Biochemistry*, *49*(3), pp.443-451. https://doi.org/10.1021/bi9016457

Sim, L., Quezada-Calvillo, R., Sterchi, E.E., Nichols, B.L. and Rose, D.R., 2008. Human intestinal maltase–glucoamylase: crystal structure of the N-terminal catalytic subunit and basis of inhibition and substrate specificity. *Journal of Molecular Biology*, *375*(3), pp.782-792. https://doi.org/10.1016/j.jmb.2007.10.069

Simsek, M., Quezada-Calvillo, R., Nichols, B.L. and Hamaker, B.R., 2017. Phenolic compounds increase the transcription of mouse intestinal maltase-glucoamylase and sucrase-isomaltase. *Food & function*, *8*(5), pp.1915-1924. https://doi.org/10.1039/C7FO00015D

Singleton, V.L. and Rossi, J.A., 1965. Colourimetry of total phenolics with phosphomolybdic-phosphotungstic acid reagents. *American Journal of Enology and Viticulture*, *16*(3), pp.144-158. https://doi.org/10.5344/ajev.1965.16.3.144

Skehan, P., Storeng, R., Scudiero, D., Monks, A., McMahon, J., Vistica, D., Warren, J.T., Bokesch, H., Kenney, S., and Boyd, M.R., 1990. New colourimetric cytotoxicity assay for anticancer-drug screening. *JNCI: Journal of the National Cancer Institute*, *82*(13), pp.1107-1112. https://doi.org/10.1093/jnci/82.13.1107

Song, D., Zhao, J., Deng, W., Liao, Y., Hong, X. and Hou, J., 2018. Tannic acid inhibits NLRP3 inflammasome-mediated IL-1β production via blocking NF-κB signaling in macrophages. *Biochemical and biophysical research communications*, *503*(4), pp.3078-3085. https://doi.org/10.1016/j.bbrc.2018.08.096

Sun, C., Zhao, C., Guven, E.C., Paoli, P., Simal-Gandara, J., Ramkumar, K.M., Wang, S., Buleu, F., Pah, A., Turi, V. and Damian, G., 2020. Dietary polyphenols as antidiabetic agents: Advances and opportunities. *Food Frontiers*, *1*(1), pp.18-44. https://doi.org/10.1002/fft2.15

© University of Venda

Sykłowska-Baranek, K., Gaweł, M., Kuźma, Ł., Wileńska, B., Kawka, M., Jeziorek, M., Graikou, K., Chinou, I., Szyszko, E., Stępień, P. and Zakrzewski, P., 2023. Rindera graeca (A. DC.) Boiss. & Heldr. (Boraginaceae) *In-vitro* Cultures Targeting Lithospermic Acid B and Rosmarinic Acid Production. *Molecules*, *28*(12), p.4880. https://doi.org/10.3390/molecules28124880

Szklarczyk, D., Gable, A.L., Lyon, D., Junge, A., Wyder, S., Huerta-Cepas, J., Simonovic, M., Doncheva, N.T., Morris, J.H., Bork, P., and Jensen, L.J., 2019. STRING v11: protein–protein association networks with increased coverage, supporting functional discovery in genome-wide experimental datasets. *Nucleic acids research*, *47*(D1), pp. D607-D613. https://doi.org/10.1093/nar/gky1131

Szklarczyk, D., Nastou, K., Koutrouli, M., Kirsch, R., Mehryary, F., Hachilif, R., Hu, D., Peluso, M.E., Huang, Q., Fang, T., and Doncheva, N.T., 2025. The STRING database in 2025: protein networks with directionality of regulation. *Nucleic Acids Research*, *53*(D1), pp. D730-D737. https://doi.org/10.1093/nar/gkae1113

Szolar, O.H., Rost, H., Braun, R., and Loibner, A.P., 2002. Analysis of polycyclic aromatic hydrocarbons in soil: minimizing sample pretreatment using automated Soxhlet with EA as extraction solvent. *Analytical Chemistry*, *74*(10), pp.2379-2385. https://doi.org/10.1021/ac015739l

Tan, H.M., Leong, K.H., Song, J., Mohd Sufian, N.S.F., Mohd Hazli, U.H.A., Chew, L.Y. and Kong, K.W., 2020. Antioxidant and LC-QToF-MS/MS analysis of polyphenols in polar and non-polar extracts from Strobilanthes crispus and Clinacanthus nutans. *International Food Research Journal*, *27*(5). http://eprints.um.edu.my/id/eprint/36385

Tang, D., Chen, Q.B., Xin, X.L. and Aisa, H.A., 2017. Anti-diabetic effect of three new norditerpenoid alkaloids *in-vitro* and potential mechanism via PI3K/Akt signaling pathway. *Biomedicine & Pharmacotherapy*, *87*, pp.145-152. https://doi.org/10.1016/j.biopha.2016.12.058

Tepal, P., 2016. Phytochemical screening, total flavonoid, and phenolic content assays of various solvent extracts of tepal of Musa paradisiaca. *Malaysian Journal of Analytical Sciences*, *20*(5), pp.1181-1190. http://dx.doi.org/10.17576/mjas-2016-2005-25

Tian, F., Zhang, X., Tong, Y., Yi, Y., Zhang, S., Li, L., Sun, P., Lin, L. and Ding, J., 2005. PE, a new sulfated saponin from sea cucumber, exhibits anti-angiogenic and anti-tumor activities *in-vitro* and in vivo. *Cancer biology & therapy*, *4*(8), pp.874-882. https://doi.org/10.4161/cbt.4.8.1917

Tohma, H., Gülçin, İ., Bursal, E., Gören, A.C., Alwasel, S.H. and Köksal, E., 2017. Antioxidant activity and phenolic compounds of ginger (Zingiber officinale Rosc.) determined by HPLC-QTOF-MS /MS. *Journal of food measurement and characterization*, *11*, pp.556-566. https://doi.org/10.1007/s11694-016-9423-z

© University of Venda

Tshidino, S.C. and Montsho, N., 2017. Antioxidant and hepatoprotective potentials of Bauhinia variegata seeds against ferric chloride-induced lipid peroxidation in chicken liver homogenate. *African Journal of Traditional, Complementary and Alternative Medicines*, *14*(5), pp.219-230. 10.21010/ajtcam.v14i5.25

Ullah, A., Munir, S., Badshah, S.L., Khan, N., Ghani, L., Poulson, B.G., Emwas, A.H. and Jaremko, M., 2020. Important flavonoids and their role as a therapeutic agent. *Molecules*, *25*(22), p.5243. https://doi.org/10.3390/molecules25225243

Vailhé, B., Vittet, D. and Feige, J.J., 2001. *In-vitro* models of vasculogenesis and angiogenesis. *Laboratory Investigation*, *81*(4), pp.439-452. https://doi.org/10.1038/labinvest.3780252

Vasistha, P., Singh, P.P., Srivastava, D., Johny, L. and Shukla, S., 2025. Effector proteins of Funneliformis mosseae BR221: unravelling plant-fungal interactions through reference-based transcriptome analysis, *in-vitro* validation, and protein–protein docking studies. *BMC genomics*, *26*(1), p.42. https://doi.org/10.1186/s12864-024-10918-7

Vocadlo, D.J. and Davies, G.J., 2008. Mechanistic insights into glycosidase chemistry. *Current Opinion in Chemical Biology*, *12*(5), pp.539-555. https://doi.org/10.1016/j.cbpa.2008.05.010

Wang, X., Li, R. and Zhao, H., 2024. Enhancing angiogenesis: innovative drug delivery system to facilitate diabetic wound healing. *Biomedicine & Pharmacotherapy*, *170*, p.116035. https://doi.org/10.1016/j.biopha.2023.116035

Wang, M., Carver, J.J., Phelan, V.V., Sanchez, L.M., Garg, N., Peng, Y., Nguyen, D.D., Watrous, J., Kapono, C.A., Luzzatto-Knaan, T. and Porto, C., 2016. Sharing and community curation of mass spectrometry data with Global Natural Products Social Molecular Networking. *Nature Biotechnology*, *34*(8), pp.828-837. https://doi.org/10.1038/nbt.3597

Wirostko, B., Wong, T.Y. and Simó, R., 2008. Vascular endothelial growth factor and diabetic complications. *Progress in retinal and eye research*, *27*(6), pp.608-621. https://doi.org/10.1016/j.preteyeres.2008.09.002

Xia, Y., Song, X., Li, D., Ye, T., Xu, Y., Lin, H., Meng, N., Li, G., Deng, S., Zhang, S. and Liu, L., 2014. YLT192, a novel, orally active bioavailable inhibitor of VEGFR2 signalling with potent antiangiogenic activity and antitumor efficacy in preclinical models. *Scientific Reports*, *4*(1), p.6031. https://doi.org/10.1038/srep06031

Xiao, J., 2022. Recent advances in dietary flavonoids for management of T2DM. *Current Opinion in Food Science*, *44*, p.100806. https://doi.org/10.1016/j.cofs.2022.01.002

© University of Venda

Xu, S., Feng, Y. and Zhao, S., 2019. Proteins with evolutionarily hypervariable domains are associated with immune response and better survival of basal-like breast cancer patients. *Computational and structural biotechnology journal*, *17*, pp.430-440. https://doi.org/10.1016/j.csbj.2019.03.008

Yameny, A.A., 2024. Diabetes Mellitus Overview 2024. *Journal of Bioscience and Applied Research*, *10*(3), pp.641-645. 10.21608/jbaar.2024.382794

Yurchenko, E.A., Kolesnikova, S.A., Lyakhova, E.G., Menchinskaya, E.S., Pislyagin, E.A., Chingizova, E.A. and Aminin, D.L., 2020. Lanostane triterpenoid metabolites from a Penares sp. marine sponge protect neuro-2a cells against paraquat neurotoxicity. *Molecules*, *25*(22), p.5397. https://doi.org/10.3390/molecules25225397

Zainal-Abidin, M.H., Hayyan, M., Hayyan, A., and Jayakumar, N.S., 2017. New horizons in the extraction of bioactive compounds using deep eutectic solvents: A review. *Analytica chimica acta*, *979*, pp.1-23. https://doi.org/10.1016/j.aca.2017.05.012

Zahra, S., Zaib, S. and Khan, I., 2024. Identification of isobenzofuranone derivatives as promising antidiabetic agents: Synthesis, *in-vitro* and in vivo inhibition of α-glucosidase and α-amylase, computational docking analysis and molecular dynamics simulations. *International Journal of Biological Macromolecules*, *259*, p.129241. https://doi.org/10.1016/j.ijbiomac.2024.129241

Zhang, J., Durham, J. and Cong, Q., 2024. Revolutionizing protein–protein interaction prediction with deep learning. *Current Opinion in Structural Biology*, *85*, p.102775. https://doi.org/10.1016/j.sbi.2024.102775

Zhu, Y., Dong, Y., Qian, X., Cui, F., Guo, Q., Zhou, X., Wang, Y., Zhang, Y. and Xiong, Z., 2012. Effect of superfine grinding on antidiabetic activity of bitter melon powder. *International journal of molecular sciences*, *13*(11), pp.14203-14218. https://doi.org/10.3390/ijms131114203

Zhu, Y., Li, X., Mcvie-Wylie, A., Jiang, C., Thurberg, B.L., Raben, N., Mattaliano, R.J., and Cheng, S.H., 2005. Carbohydrate-remodelled intestinal α-glucosidase with higher affinity for the cation-independent mannose 6-phosphate receptor demonstrates improved delivery to muscles of Pompe mice. *Biochemical Journal*, *389*(3), pp.619-628. https://doi.org/10.1042/BJ20050364

Zimmet, P., 2001. Alberti KG, Shaw J. Global and societal implications of the diabetes epidemic. *Nature*, *414*, pp.782-787. https://doi.org/10.1038/414782a

Zulkifli, K.S., Abdullah, N., Abdullah, A., Aziman, N. and Kamarudin, W.S.S.W., 2012. Phytochemical screening and activities of hydrophilic and lipophilic antioxidant of some fruit peels. *Malaysian Journal of Analytical Sciences*, *16*(3), pp.3. Available from: https://www.researchgate.net/publication/286516607

© University of Venda